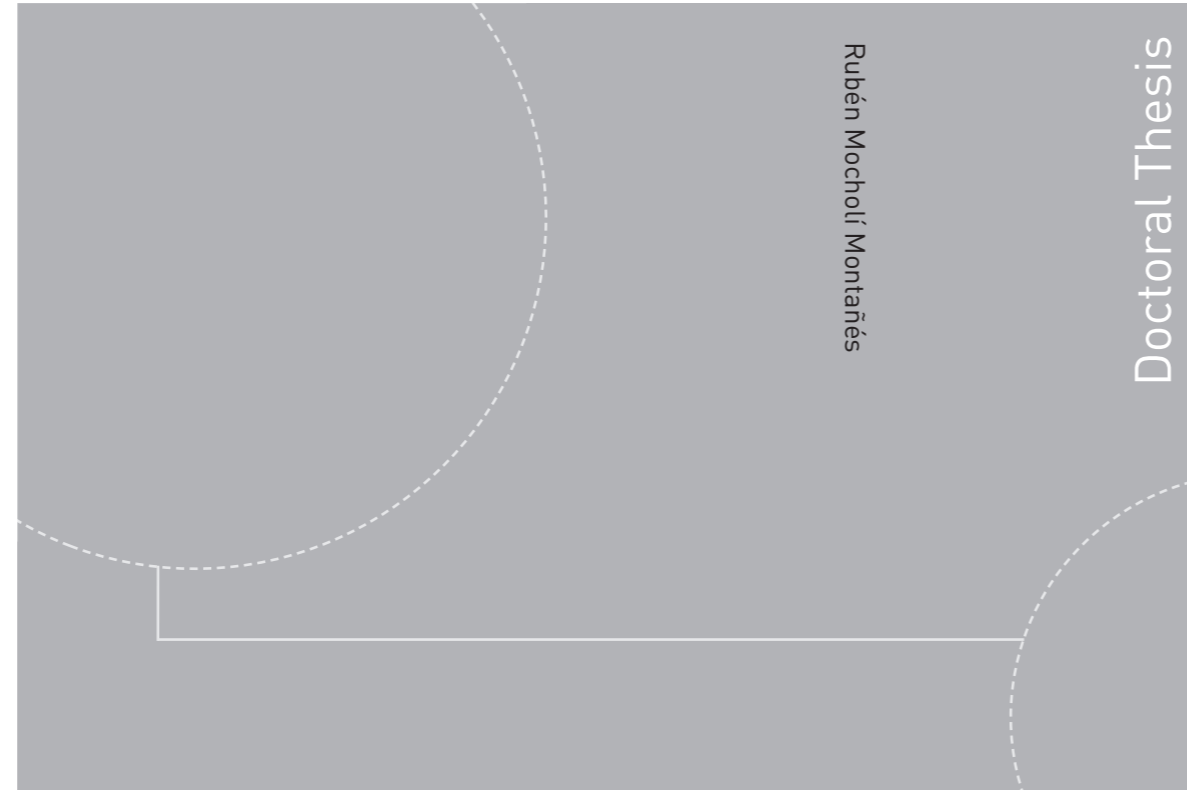


ISBN 978-82-326-3126-1 (printed version)
ISBN 978-82-326-3127-8 (electronic version)
ISSN 1503-8181



Doctoral theses at NTNU, 2018:168

Rubén Mocholí Montañés

Transient performance of combined cycle power plant with absorption based post-combustion CO₂ capture: dynamic simulations and pilot plant testing

Doctoral theses at NTNU, 2018:168

NTNU
Norwegian University of
Science and Technology
Faculty of Engineering
Department of Energy and Process Engineering

 **NTNU**
Norwegian University of
Science and Technology

 NTNU

 **NTNU**
Norwegian University of
Science and Technology

Rubén Mocholí Montañés

Transient performance of combined cycle power plant with absorption based post-combustion CO₂ capture: dynamic simulations and pilot plant testing

Thesis for the degree of Philosophiae Doctor

Trondheim, June 2018

Norwegian University of Science and Technology
Faculty of Engineering
Department of Energy and Process Engineering



Norwegian University of
Science and Technology

NTNU

Norwegian University of Science and Technology

Thesis for the degree of Philosophiae Doctor

Faculty of Engineering

Department of Energy and Process Engineering

© Rubén Mocholí Montañés

ISBN 978-82-326-3126-1 (printed version)

ISBN 978-82-326-3127-8 (electronic version)

ISSN 1503-8181

Doctoral theses at NTNU, 2018:168



Printed by Skipnes Kommunikasjon as

Preface

The thesis is submitted in partial fulfillment of the requirements for the degree of philosophiae doctor (Ph.D.) at the Norwegian University of Science and Technology (NTNU). The work was carried out at the Department of Energy and Process Engineering at the Faculty of Engineering, with Associate Professor Lars Olof Nord as main supervisor. Professor Magnus Korpås from Department of Electric Power Engineering at NTNU was co-supervisor. The research was funded by the Department of Energy and Process Engineering at NTNU.

Abstract

The thesis presents transient performance analysis of chemical absorption processes for reducing CO₂ emissions from natural gas combined cycle power plants (NGCCs), which can contribute to reduce greenhouse gas emissions to the atmosphere and mitigate climate change. Objectives focused on understanding process dynamics of NGCC with post-combustion CO₂ capture (PCC) with an amine based chemical absorption process. Contributions comprised development and validation of high fidelity dynamic process models and evaluation of process dynamics of commercial scale NGCC with PCC power plant, including analysis of the performance of decentralized control structures for PCC units. In addition, experimental transient testing was conducted at a large-scale state-of-the-art pilot plant for the evaluation of control structures applied to the chemical absorption process. Additional contributions included design of validation cases for dynamic process models of chemical absorption processes. The main methods employed were dynamic modeling and simulation and experimental transient testing. The thesis results include five peer-review research articles.

High efficiency thermal power plants using novel solutions for operational flexibility improvements and CO₂ emission reductions will be needed now and in the future to balance the variable renewable energy within decarbonized power systems. Carbon capture and storage (CCS) technologies can significantly reduce the carbon intensity of thermal power plants. The carbon intensity of state-of-the-art combined cycle power plants is around 365 g CO₂/kWh, while for NGCC with PCC it is calculated to be around 50 g CO₂/kWh. A 600 MW NGCC with PCC was designed and evaluated. The process configuration selected included one heavy-duty gas turbine and a triple-pressure reheat heat recovery steam generator in the combined cycle power plant, and a chemical absorption post-combustion CO₂ capture unit with 30 wt% MEA as chemical solvent. The resulting net LHV electric efficiency of the integrated process was 52.8% and the specific reboiler duty at design point was 3.73 MJ/kgCO₂.

In order to identify scenarios for flexible operation of thermal power plants with CCS, a study on power markets and technical requirements was conducted. Technical grid requirements and frameworks for power units to provide ancillary services and bidding in balancing markets in four different power areas in EU were identified. In order to assess the transient performance of the NGCC with PCC, it was required to develop high fidelity physical dynamic process models. The selected tool for dynamic process modeling was the open physical modeling language Modelica. The focus of the study was to evaluate flexible operation of the chemical absorption process when integrated with power plant operations, with focus on power plant load variations.

A detailed literature review proved necessary to validate dynamic process models of post-combustion chemical absorption of CO₂ with large-scale pilot plant data for flue gas with low CO₂ content characteristic of GT flue gas. However, the availability of suitable data sets for validation was scarce. Therefore, a set of validation cases for dynamic process model of the post-combustion CO₂ capture process with chemical absorption using 30 wt% MEA was designed with data from operations of the large-scale amine plant at Technology Centre Mongstad. The plant can capture 80 ton CO₂/day when operated

with flue gas with a CO₂ content of around 3.7 vol%. The data consisted of ten data sets representing a wide range of steady-state operating conditions with a slipstream of flue gas from a natural gas fueled power plant. The data included three transient tests for dynamic process model validation under transient conditions representing the main disturbances applied to the process. The validation results of a dynamic process model of the pilot plant showed capabilities of dynamic process modeling applied to large-scale experimental tests of the chemical absorption process with aqueous MEA. The validation of the thermal power plant model was conducted with steady-state design and off-design data from simulations. The software-to-software validation showed the proper implementation and development of the dynamic process model of the thermal power plant.

The evaluation of process dynamics of a state-of-the-art PCC pilot plant was done via dynamic process model simulations and experimental transient testing. Results showed that, when the plant was operated at part load, it took a longer time to stabilize the main process variables in response to open-loop step changes in the main inputs of the process, namely solvent flow rate, flue gas flow rate and reboiler duty. Circulation times and solvent hold-up distribution through the equipment of the chemical absorption process showed to be a key aspect for process dynamics. It was found that the desorption rate stabilized faster than the absorption rate for set-point step changes in solvent flow rate and reboiler duty.

An evaluation of performance of decentralized control structures of the PCC pilot plant was done via dynamic process model simulations. Simulation results showed that the best performance was obtained with the control structure in which capture rate is controlled by manipulating reboiler duty, and stripper bottom temperature controlled by manipulating solvent flow rate. Experimental transient tests for fast load change scenarios were conducted at the pilot plant. Testing results revealed that the process can reject fast disturbances in flue gas flow rate and could bring the process towards desired off-design steady-state conditions within 60 min by means of decentralized control structures. These tests provided empirical evidence at large-scale that combined cycle power plants with post-combustion CO₂ capture can keep similar operational procedures as equivalent unabated power plants, considering fast load changes driven by GT load change. However, fast and large changes in solvent flow rate as a control measure can cause instabilities due to the interaction between the stripper temperature and the capture rate control loops.

The transient performance of NGCC with PCC was studied by co-simulating and linking the dynamic process model of the power plant and the dynamic process model of the scaled-up PCC unit. Tests on load change driven by changes in GT load were conducted for variable ramp rates and for different control structures in the PCC unit. Based on these simulations, it was concluded that the addition of the PCC unit to the NGCC plant should not impose any constraint on, or problem for, stable power plant operation under scheduled load changes, even for aggressive ramp rates. The control structure where liquid-to-gas ratio in the absorber column was kept constant and reboiler temperature controlled by the steam throttle valve, showed similar part-load off-design performance as found in control structures with controlled capture rate. This control structure resulted in relatively faster total stabilization time of the steam turbine power output and CO₂ product flow rate.

Areas for future work include: i) studying the transient performance of the system with higher levels of process integration; ii) assessment of transient performance of PCC with other chemical solvents; iii) development of reduced order models for faster numerical solution of dynamic process model simulations; iv) economic evaluation of flexible operation strategies including lifetime reduction due to thermal stresses in critical components of the process; v) optimization of start-up sequence of the integrated processes.

Acknowledgements

I want to express my gratitude to my main supervisor Prof. Lars O. Nord. Thanks for always giving good advice and directions towards the Ph.D. project. Your door was always open for me when I needed, and your suggestions kept me motivated and challenged. I am very proud of being your first PhD student.

I would like to thank my co-supervisor Prof. Magnus Korpås for introducing me to his research group at Department of Electric Power Engineering at NTNU. Your advice and discussions were very valuable, especially at the beginning of this Ph.D. project. Thanks to Dr. Rohan Dutta for our discussions on dynamic process modeling and simulation at the early stages of my Ph.D. studies. Thanks to Prof. Olav Bolland for discussions on the project topics.

It was a great pleasure to visit the Combustion and Carbon Capture Technologies research group at Division of Energy Technology at Chalmers University of Technology during my Ph.D. studies. I would like to thank Prof. Fredrik Normann and Prof. Filip Johnsson for our collaborative work. My stays at Chalmers helped me to continue motivated and focus. It will be great to work with you in the future. How great it was to work with Dr. Stefanía Ósk Gardarsdóttir! Thanks for all the meetings, discussions and good work. It was very interesting to re-discover the Swedish *midsonmar* from an Icelandic perspective and all the good hikes after work in Gothenburg and Trondheim.

Thanks to the staff and researchers at Technology Centre Mongstad in Norway (TCM). Special thanks to Espen S. Hamborg for his efforts on developing our collaboration, and for allowing us to conduct research at the amine plant at TCM. A very special mention goes to Dr. Nina Enaasen Flø! It was very rewarding to work with you. Thanks for always addressing questions and discussions with a very positive attitude and enthusiasm, all combined with an extremely professional approach to work.

It was great to share this adventure with many Ph.D. candidates, colleagues and friends, at the Energy and Process Engineering Department at NTNU. Just going for a run, to the gym, taking a coffee or going for lunch together was invaluable. Thanks to all of you for creating such a great working environment. A special mention to Luca, thanks for being such an interesting officemate! Your advice as more senior Ph.D. candidate and eventually Postdoc was very helpful. Thanks for continue opening me the door of the corridor (or even the building) those late office days when I forgot my keycard inside the office! Specially in cold winter days. Well, and for all the fun together. It was great to experience the Ph.D. journey at the same time as Shareq. I am sure that our friendship will endure. Yes, we all know that "winter is coming", but life continues. Thanks to all the master students I had the pleasure to co-supervise during my Ph.D. studies: Benjamin, Inés, Magnus, Mikael, Elise and Jairo. Your questions helped me to stay sharp and focus.

Join me in a loud applause dedicated to the administration staff at Department of Energy and Process Engineering (EPT) at NTNU. More in general, to all the people that makes working at EPT such a dream! Special mention to the EPTraining program organizers. All the squash, cross-country skiing and running sessions were amazing platforms that forced me to be in good shape and join colleagues in a more relaxed context. It was a lot of fun to participate for three years in a row at St. Olavsloppet!

I am so grateful to the amazing country of Norway and how great it was to live in Trondheim. As a Mediterranean born and raised, it was a delicious experience to live surrounded by forest, northern lights, a fiord and a great deal of snow. But all of that would have meant nothing without the company of all the very good friends that I had the pleasure to make. Borja, Anxo, Raquel, María, Mi Chi, Rodrigo, Manolo, Manuel, Juan, Inés, Roberto, Giorgia, Jairo, Juan and Marta. You made me feel at home! Thanks to all of you for sharing so many good moments with me. I also want to thank all my friends from Valencia. The fact that we stay friends after all these years abroad means that our friendship is well grounded. Your visits, seeing you in Spain and traveling during holidays helped me to relax from my Ph.D. studies.

¡Qué suerte tengo de tener una familia tan genial! Muchísimas gracias a mis padres, Toni y María Ángeles, por todo el amor y paciencia que me demuestran cada día. Gracias por darme todo lo que estaba de vuestra mano para garantizarme una buena educación, y especialmente por apoyarme en mis decisiones. Nada de lo que he conseguido en mi vida hubiera sido posible sin vosotros. Gracias a Sergi, estoy orgulloso de ser tu hermano. Muchas gracias a mi familia, todas nuestras reuniones, comidas, cenas, meriendas, etc... en Valencia, me hacen sentir muy feliz en casa.

Finally, I would like to dedicate all my efforts and work towards this Ph.D. thesis to the memory of my grandfather, Antonio Luis Mocholí Puchades. The impact of his example and role in my life was, and still is, immense. *T'estime iaio.*

Rubén Mocholí Montañés

Gothenburg, Sweden, 6th May 2018

Contents

| | |
|--|------------|
| Preface | i |
| Abstract | iii |
| Acknowledgements | vii |
| 1 Introduction | 1 |
| 1.1 Background and motivation | 1 |
| 1.2 Objectives | 3 |
| 1.3 Contributions | 3 |
| 1.4 Thesis structure | 4 |
| 1.5 Publications and scientific dissemination | 5 |
| 1.5.1 Publications included in the thesis | 5 |
| 1.5.2 Other publications | 6 |
| 1.5.3 Conference and seminar presentations | 8 |
| 2 Technical background | 9 |
| 2.1 Climate change and CCS | 9 |
| 2.2 The balancing problem | 11 |
| 2.2.1 Operational flexibility in the power sector | 11 |
| 2.2.2 Operational flexibility of thermal power plants | 12 |
| 2.3 Combined cycle power plants with CCS | 14 |
| 2.3.1 Gas and steam turbine combined cycles | 14 |
| 2.3.2 Post-combustion CO ₂ capture | 14 |
| 2.3.3 Process integration | 16 |
| 2.3.4 Operational flexibility of NGCC with PCC | 18 |
| 2.4 Dynamic process modeling and simulation | 20 |
| 2.4.1 Steady-state and transient operation of systems | 20 |
| 2.4.2 Modeling paradigm | 22 |
| 3 Methodology | 25 |
| 3.1 Identifying operational requirements for thermal power plants with CCS . . | 25 |
| 3.2 Modeling of combined cycle power plant with PCC | 25 |
| 3.2.1 Dynamic process modeling of combined cycle | 31 |
| 3.2.2 Dynamic process modeling of chemical absorption process for CO ₂ capture | 38 |
| 3.3 Dynamic process model validation | 40 |

| | | |
|----------|---|-----------|
| 3.4 | Pilot plant testing at Technology Centre Mongstad | 42 |
| 3.4.1 | Pilot plant description | 44 |
| 3.4.2 | Selection of experimental data for dynamic process model development and validation | 46 |
| 3.4.3 | Transient testing at Technology Centre Mongstad | 59 |
| 3.5 | Selection and evaluation of control structures and transient performance . . | 63 |
| 3.5.1 | Control structures for the PCC process | 63 |
| 3.5.2 | Evaluation of transient performance | 68 |
| 3.5.3 | Evaluation of control structures | 69 |
| 4 | Results and discussions | 71 |
| 4.1 | Identifying operational requirements for flexible power plant with CCS in future energy systems | 71 |
| 4.2 | Dynamic process model validation | 72 |
| 4.3 | Transient response of the chemical absorption process | 75 |
| 4.4 | Evaluation of transient performance of decentralized control structures . . . | 81 |
| 4.5 | Transient performance of commercial scale natural gas combined cycle power plant with post-combustion CO ₂ capture | 84 |
| 5 | Conclusions and future work | 87 |
| 5.1 | Conclusions | 87 |
| 5.2 | Future work | 90 |
| | Bibliography | 91 |
| | A Papers | 99 |

List of Figures

| | | |
|------|---|----|
| 2.1 | Methods for CO ₂ separation from thermal power plants | 9 |
| 2.2 | Simple process flow sheet for chemical absorption process of CO ₂ | 15 |
| 2.3 | Drawing on power plant integration and power system integration | 18 |
| 2.4 | Steady-state, off-design and transient performance | 21 |
| 3.1 | Methodology for dynamic process model development of combined cycle power plant with post-combustion CO ₂ capture | 27 |
| 3.2 | Process flow diagram of the NGCC power plant integrated with post-combustion CO ₂ capture | 28 |
| 3.3 | GT off-design data for Mitsubishi JAC 701 | 33 |
| 3.4 | GT transient simulation of exhaust based on equilibrium quasi-static models | 34 |
| 3.5 | Dymola implementation of Heat exchanger recuperator model | 36 |
| 3.6 | Dymola implementation of HRSG | 39 |
| 3.7 | Amine pilot plant at Technology Centre Mongstad | 45 |
| 3.8 | Flow diagram amine pilot plant at Technology Centre Mongstad | 47 |
| 3.9 | Methodology for data selection for dynamic process model validation at TCM DA amine pilot plant | 48 |
| 3.10 | Absorber temperature profile sensors | 56 |
| 3.11 | Stripper temperature profile sensors | 57 |
| 3.12 | Simulations for open-loop testing planing | 61 |
| 3.13 | Transient reponse for different controller tuning for the simulated model of the TCM DA amine plant. Rich solvent flowrate and capture rate. | 64 |
| 3.14 | Transient reponse for different controller tuning for the simulated model of the TCM DA amine plant. Reboiler duty and stripper bottom temperature. | 65 |
| 4.1 | Dispatch simulation results | 72 |
| 4.2 | Parity plots of lean CO ₂ loading and CO ₂ product flow rate | 74 |
| 4.3 | Validation of temperature profiles absorber and stripper columns | 74 |
| 4.4 | Validation of output trajectories of chemical absorption process | 76 |
| 4.5 | Total stabilization times of transient response of process variables at different loads of chemical absorption process | 78 |
| 4.6 | Open loop transient trajectories of the PCC unit of a combined cycle power plant operated at 60% GT load | 79 |
| 4.7 | Open loop tests at Technology Centre Mongstad: transient response of capture rates | 81 |
| 4.8 | Transient performance of combined cycle power plant with PCC unit: different control structures | 83 |

| | | |
|-----|--|----|
| 4.9 | Transient performance of combined cycle power plant with PCC unit: variable ramp rates | 85 |
|-----|--|----|

List of Tables

| | | |
|-----|--|----|
| 3.1 | Dynamic process models structure of Modelica models | 30 |
| 3.2 | Dynamic process simulation of Modelica models | 31 |
| 3.3 | Absorber column TCM DA materials and geometry | 46 |
| 3.4 | Stripper column TCM DA materials and geometry | 48 |
| 3.5 | Steady-state cases data presented in paper II | 54 |
| 3.6 | Steady-state cases data presented in paper II | 55 |
| 3.7 | Controller tuning parameters for capture rate | 63 |
| 3.8 | Control structures and nomenclature employed in papers II, III and V . . . | 68 |

List of Abbreviations

| | |
|-----------------|--|
| CCS | Carbon Capture and Storage |
| DAE | System of Differential and Algebraic equations |
| DCC | Direct Contact Cooler |
| EGR | Exhaust Gas Recirculation |
| FMI | Functional Mockup Interface |
| FMU | Functional Mockup Unit |
| FVM | Finite Volume Method |
| FT | Flow Transmitter |
| FTIR | Fourier Transform Infrared |
| GA | Gas Analyzer |
| GC | Gas Chromatograph |
| GT | Gas Turbine |
| HP | High Pressure |
| IP | Intermediate Pressure |
| IGCC | Integrated Gasification Combined Cycle |
| LP | Low Pressure |
| MEA | Monoethanolamine |
| NDIR | Non-dispersive Infrared |
| P&ID | Piping and Instrumentation Diagram |
| PCC | Post-combustion CO ₂ Capture |
| R&D | Research and Development |
| TSO | Transmission System Operator |
| TPM | Throughput Manipulator |
| TCM DA | CO ₂ Technology Centre Mongstad |
| VRE | Variable Renewable Energy Sources |
| VSR | Variable Stripper Regeneration |

List of Symbols

| | |
|---------------------|---|
| CO_2 | Carbon dioxide |
| CH_4 | Methane |
| N_2O | Nitrose oxide |
| A_{heat} | Heat transfer area [W] |
| C_{eff} | Calibration factor for enhancement factor |
| d_{hyd} | Hydraulic diameter [m] |
| F_a | Tube arrangement factor |
| F_{gas} | Flue gas volumetric flow rate [Sm^3/hr] |
| F_{rich} | Rich solvent mass flow rate [kg/hr] |
| F_{lean} | Lean solvent mass flow rate [kg/hr] |
| F_{prod} | CO_2 rich product mass flow rate [kg/hr] |
| F_{steam} | Reboiler steam mass flow rate [kg/hr] |
| h | enthalpy [kJ/kg] |
| K_s | Stodola's flow area coefficient |
| L_{lean} | Lean solvent loading [mol/mol] |
| L_{rich} | Rich solvent loading [mol/mol] |
| N_{eq} | Number of equations |
| N_{pa} | Number of parameters |
| N_s | Number of states |
| N_{un} | Number of unknowns |
| N_{va} | Number of variables |
| Nu | Nusselt number |
| p_{cond} | Reboiler condensate pressure [barg] |
| p_{fg} | Flue gas supply pressure [barg] |
| $p_{\text{la,dis}}$ | Lean amine pump discharge pressure [barg] |
| $p_{\text{ra,dis}}$ | Rich amine pump discharge pressure [barg] |
| $p_{\text{ra,in}}$ | Rich amine pump intake pressure [barg] |
| p_{steam} | Steam supply pressure [barg] |
| p_{stop} | Stripper overhead pressure [barg] |
| p_{str} | Stripper pressure [barg] |
| L/G | Liquid to gas ratio in absorber column [kg/kg] |
| Q | Heat transfer [W] |
| Q_{reb} | Reboiler duty [kW] |
| $T_{\text{abs,in}}$ | Lean amine supply temperature to absorber [$^{\circ}\text{C}$] |
| $T_{\text{abs,o}}$ | Rich amine return temperature [$^{\circ}\text{C}$] |
| $T_{\text{a,i}}$ | Temperature absorber column at intermediate height [$^{\circ}\text{C}$] |

| | |
|---------------------|---|
| T_{cond} | Reboiler condensate temperature [°C] |
| T_{cond} | Overhead condenser temperature [°C] |
| T_{fg} | Temperature of flue gas [°C] |
| T_{fluid} | Fluid temperature [°C] |
| $T_{\text{str,in}}$ | Rich amine supply temperature to stripper [°C] |
| $T_{\text{str,o}}$ | Lean amine return temperature from stripper [°C] |
| T_{la} | Temperature lean solvent to lean amine cooler [°C] |
| T_{str} | Stripper bottom temperature [°C] |
| T_{reb} | Reboiler solution temperature [°C] |
| T_{steam} | Steam reboiler supply temperature [°C] |
| T_{stop} | Stripper overhead temperature [°C] |
| T_{wall} | Wall temperature [°C] |
| t_{sim} | Simulation time [s] |
| t_{CPU} | Simulation time [s] |
| P_{el} | Electrical power output [W] |
| P_{mech} | Mechanical power [W] |
| α_{g} | Heat transfer coefficient gas side [W/m ² K] |
| α_{s} | Heat transfer coefficient steam side [W/m ² K] |
| β | Baumann's factor |
| η | Efficiency |
| λ | Thermal conductivity [W/mK] |
| ρ | Density [kg/m ³] |

Chapter 1

Introduction

1.1 Background and motivation

Anthropogenic greenhouse gas emissions have raised substantially since the pre-industrial era, and that has led to increased atmospheric concentrations of carbon dioxide CO₂, methane CH₄ and nitrose oxide N₂O. Anthropogenic greenhouse gas emissions are considered the main factor contributing to accelerate global warming during the 20th century (IPCC, 2014). The European Union is committed towards a future energy system with reduced greenhouse gas emissions to 80-95% below 1990 levels by 2050. According to the European Commission, a secure, competitive and decarbonized energy system in 2050 is possible (European Commission, 2012). In decarbonized scenarios, electricity will play an increased role, together with renewable energy sources. Investment models to identify the most cost-effective route towards a decarbonized European power system have been developed by the Zero Emissions Platform. Their results show the requirement of an energy mix combining hydro, wind and solar power, together with a progressive introduction, between 2030 and 2050, of lignite, coal, gas and biomass power plants with Carbon Capture and Storage (CCS) (Zero Emissions Platform, 2013). Nevertheless, the mentioned target will exert intensive pressure on energy systems.

In the particular context of the power system, an expected and promoted higher penetration of variable renewable energy sources (VRE) such as wind and solar, will accentuate the challenge of power system balancing. Fluctuations in net load, i.e. the demand curve after subtracting the power generation by variable renewables, are expected to be more frequent and have stronger uncertainty impacts (IEA, 2012). Therefore, deployment of new power market design, system operation principles, grid extensions and flexible resources are being considered in order to enhance the flexibility of power systems and ensuring security of supply. With the high penetration of solar and wind power, reduction in load or increase of renewable production can be handled by different means, such as demand side management and response, energy storage facilities, grid reinforcement, part load operation of thermal units, stopping thermal units or wind curtailment. Under scenarios with high penetration of VRE, thermal power units with high start-up costs and high minimum load (base load units) will be less utilized. However, there still will be a need for capacity to supply the net load during times with poor wind and solar conditions (Chalmers, 2014). Therefore, within power systems with high penetration of VRE there will be a need for flexible fossil fueled (e.g. coal and natural gas) thermal power plants with low CO₂ emissions. This means, high efficiency thermal power plants using novel

solutions for operational flexibility improvements and CO₂ emission reductions will be needed now and in the future to balance the variable renewable energy in the power system.

In recent years, there has been an increased concern of the role that power generation with CCS might have in future power systems with high penetration of VRE. Thermal power plants equipped with CO₂ capture systems might be operated as mid-merit plants due to new power market conditions. Increasing interest has grown in the field of operational flexibility of thermal power plants with carbon sequestration technologies. A report from IEAGHG summarizes several aspects of operational flexibility of different power plant technologies with and without CCS (IEAGHG, 2012). In addition, the Carbon Capture and Storage 2014 update (Boot-Handford et al., 2014) concluded that:

“The financial case for CCS requires that it operates in a flexible manner, load-following ability is extremely important to the long-term economics”.

Post-combustion CO₂ capture (PCC) from fossil-fueled power plants using aqueous monoethanolamine (MEA) solvent is often considered as a mature technology. The addition of process equipment for CO₂ capture increases the complexity and cost of the plant, and imposes a reduction in net power plant output and therefore a lower efficiency. This is mainly due to the energy required to operate the post-combustion plant, which is provided by steam from the steam turbine (to feed the reboiler duty), electrical power for auxiliaries, and shafts of the blower, compressor train and pumps. Process integration between the power plant and the post-combustion capture plant can reduce the capture penalty, at the expense of increasing the complexity of the plant. There is a need to study the flexible operation of thermal power plants with CCS, and its process feasibility and controllability during transient performance for different events such as start-up, load changes and shut-down. The scarcity of existing large scale thermal power plants with CCS and published transient performance data of such plants, claims for an interest within the research community of the development of dynamic process simulation models (Bui et al., 2014) that can assist on developing the learning curve for flexible operation of thermal power plants with CCS. Such process models must be validated against pilot plant data to the furthest extent possible, in order to obtain trustworthy and meaningful results. In addition, transient testing in pilot plants can provide data for dynamic process model validation and experience on flexible operation of PCC systems.

When considering the full-integrated power plant and post-combustion capture process, the limiting factor for transient performance will be the capture plant, since it has a slower response. There is a need to understand the performance of such plants during transient operation. Several technical challenges remain in order to make this technology attractive (Jordal et al., 2012):

“Understanding part load operation and behavior of a power plant with integrated post-combustion capture of CO₂”.

“Understanding the dynamic interaction between the capture process unit and the power plant

during start-up, load change and shut-down”.

1.2 Objectives

New knowledge within this Ph.D. work was on understanding part load operation and behavior as well as the dynamic performance of natural gas combined cycle power plants with post-combustion CO₂ capture (PCC) based on chemical absorption process. In order to achieve the main objective of this Ph.D. work, the following subtasks are presented:

- Identification of operational requirements for flexible CCS power plants in power systems with high penetration of renewables.
- Development of a high fidelity physical dynamic process model of a combined cycle power plant with post-combustion CO₂ capture in the open physical modeling language Modelica.
- Dynamic process model validation.
- Evaluate the transient performance of the post-combustion CO₂ capture process with MEA via dynamic process model simulation and pilot plant testing.
- Selection of control structures for the PCC unit.
- Evaluate the performance of decentralized control structures of the PCC unit at a pilot plant via dynamic process modeling and transient testing.
- Evaluate the performance of decentralized control structures for the PCC unit when integrated with the combined cycle power plant via dynamic process model simulation.

1.3 Contributions

The main contributions contained in this Ph.D. thesis can be summarized to:

- Identification of operational requirements for flexible CCS power plants in future energy systems within the European power system.
- Design of validation cases for dynamic process model of the post-combustion CO₂ capture process with chemical absorption using MEA. The data consisted of ten data sets representing a wide range of steady-state operating conditions with flue gas from a natural gas fueled thermal power plant. The data included three transient tests for dynamic process model validation under transient conditions representing the main disturbances applied to the process.
- Validation of dynamic process models of the power plant and post-combustion CO₂ capture process in Modelica language.

- Evaluation of process dynamics of a state-of-the-art PCC pilot plant. The evaluation was done via dynamic process model simulation and via transient testing at the pilot plant.
- Implementation and evaluation of transient performance of decentralized control structures applied to the PCC process at a state-of-the-art PCC pilot plant. The evaluation was done via dynamic process model simulation and via transient testing at the pilot plant.
- Development of dynamic process models for a three-pressure reheat (3PRH) natural gas combined cycle power plant with post-combustion CO₂ capture in Modelica language.
- Evaluation of process dynamics of the PCC unit of combined cycle power plant at commercial scale, via dynamic process model simulation.
- Evaluation of decentralized control structures applied to the PCC process when it is scaled-up and integrated to a commercial scale combined cycle power plant.
- Evaluation of the transient performance of a combined cycle power plant with PCC for fast load changes and variable ramp rates.

1.4 Thesis structure

This Ph.D. thesis is structured in five chapters and a collection of five research papers. Chapter 1 includes an introduction to the area of research and motivation of the work, followed by a description of objectives, contributions and exposition of research results of this Ph.D. work. The research is presented in scientific publications in international journals and also was disseminated in international conferences, seminars and technical meetings. Chapter 2 includes the technical background exposing the potential role of CCS that can significantly contribute to climate change mitigation, with focus on the power sector. In addition, the balancing problem and the need for flexible thermal power plants are described. Furthermore, different aspects of the natural gas combined cycle power plant with post-combustion CO₂ capture and its operational flexibility are exposed. This chapter also includes a description of the modeling paradigm employed in this work. Chapter 3 describes the methodologies employed in order to assess the objectives of the thesis. Chapter 4 includes a summary of the results and findings of the research papers presented in this thesis and discussions. Finally, the main conclusions of this Ph.D. thesis are exposed and further work is proposed in Chapter 5. The research papers subject to evaluation in this Ph.D. thesis are presented in Appendix A.

1.5 Publications and scientific dissemination

1.5.1 Publications included in the thesis

The following list of publications, I to V, are included in the appendix A of this thesis and are subject to evaluation. All publications went through a peer-review process. Publications I and IV are part of conference proceedings on international conferences, while papers II, III and V were published in international journals. Rubén M. Montañés is the principal author of the five publications and the corresponding author. The contribution by the co-authors of the publication is explained for each of the papers included in the thesis.

Paper I. International conference proceedings, first author, peer-review

Rubén M. Montañés, Magnus Korpås, Lars O. Nord, Stefan Jaehnert, Identifying operational requirements for flexible CCS power plant in future energy systems, *Energy Procedia*, January 2016; 86, pp. 22-31.

Rubén M. Montañés conducted the research and review on technical requirements and wrote the paper. Magnus Korpås reviewed the manuscript and participated in discussions. Lars O. Nord reviewed the manuscript; participated in discussions; and supervised the work. Stephan Jaehnert participated in discussions and provided the simulation results from the day-ahead multi-area power market simulator.

Paper II. International journal publication, first author, peer-review

Rubén M. Montañés, Nina E. Flø, Lars O. Nord, Dynamic process model validation and control of the amine plant at CO₂ Technology Centre Mongstad, *Energies*, October 2017; 10, 1527.

Rubén M. Montañés contributed to the selection of experimental data; processed the experimental data; developed the dynamic process models; carried out the calibration, validation and simulation of the dynamic process models; defined and carried out the case studies; analyzed the results; and wrote the manuscript. Nina E. Flø contributed to the experimental data selection; contributed to the critical analysis of the results; and reviewed the manuscript. Lars O. Nord contributed to the critical analysis of the results; reviewed the manuscript; and supervised the work.

Paper III. International journal publication, first author, peer-review

Rubén M. Montañés, Nina E. Flø, Lars O. Nord, Experimental results of transient testing at the amine plant at Technology Centre Mongstad: open-loop responses and performance of decentralized control structures for load changes, *International Journal of Greenhouse Gas Control Technologies*, June 2018; 73, pp. 42-59.

Rubén M. Montañés defined the case studies; conducted the test planning; conducted dynamic process simulations to prepare the test matrix; proposed the test matrix; post-processed the experimental data; analyzed the results; and wrote the manuscript. Nina E. Flø contributed to the development of the test matrix; contributed to the critical analysis of the results; and reviewed the manuscript. Lars O. Nord contributed to the critical analysis of the results; reviewed the manuscript; and supervised the work. The three co-authors were present at Technology Centre Mongstad during the transient tests on July 2017.

Paper IV. International conference proceedings, first author, peer-review

Rubén M. Montañés and Lars O. Nord, Dynamic Simulations of the Post-combustion CO₂ Capture System of a Combined Cycle Power Plant, *Proceedings of the 12th International Modelica Conference, Prague, Czech Republic, May 15-17, 2017*, Issue 132, pp. 111-119.

Rubén M. Montañés developed the dynamic process models; defined the objectives of the analysis; conducted dynamic process simulations; post-processed the simulation results; analyzed the results; and wrote the manuscript. Lars O. Nord contributed to the critical analysis of the results; reviewed the manuscript; and supervised the work.

Paper V. International journal publication, first author, peer-review

Rubén M. Montañés, Stefania Osk Gardarsdottir, Fredrik Normann, Filip Johnsson, Lars O. Nord, Demonstrating load change transient performance of a commercial scale natural gas combined cycle power plant with post-combustion CO₂ capture, *International Journal of Greenhouse Gas Control Technologies*, August 2017; 63, pp. 158-174.

Rubén M. Montañés developed the dynamic process models of the combined cycle power plant and the post-combustion CO₂ capture system; implemented and selected the control structures; conducted the simulations of Modelica models; post-processed the simulation results; analyzed the results and wrote the manuscript. Stefania Osk Gardarsdottir participated in discussions; provided the design data of the PCC unit in Aspen Plus; and reviewed the manuscript. Fredrik Normann participated in discussions and reviewed the manuscript. Filip Johnsson participated in discussions. Lars O. Nord participated in discussions; provided the plant design with Thermoflow Inc.; reviewed the manuscript; and supervised the work.

1.5.2 Other publications

The following list of publications are research articles included in journal publications or conference proceedings. Those are not included in the thesis because they are out of the scope of the project or because they overlap with some of the content included in the list

of publications in Appendix A.

Paper VI. International journal publication, first author, peer-review

Rubén M. Montañés, Johan Windahl, Jens Pålsson, Marcus Thern, Dynamic modeling of a parabolic trough solar thermal power plant with thermal storage using Modelica, *Heat Transfer Engineering*, January 2018; 39, Issue 3, pp. 277-292.

Paper VII. International journal publication, coauthor, peer-review

Stefania Osk Gardarsdottir, Rubén M. Montañés, Fredrik Normann, Lars O. Nord, Filip Johnsson, Effects of CO₂-Absorption Control Strategies on the Dynamic Performance of a Supercritical Pulverized-Coal-Fired Power Plant. *Industrial & Engineering Chemistry Research*, March 2017; 56 (15), pp. 4415-4430.

Paper VIII. Conference proceedings, first author, non peer-review

Rubén M. Montañés, Nina E. Flø, Rohan Dutta, Lars O. Nord, Olav Bolland, Dynamic process model development and validation with transient plant data collected from an MEA test campaign at the CO₂ Technology Center Mongstad, *Energy Procedia*, July 2017; 114, pp. 1538-1550.

Paper IX. International journal publication, coauthor, peer-review

Inés Encabo Cáceres, Rubén M. Montañés, Lars O. Nord, Flexible operation of combined cycle gas turbine power plants with supplementary firing, *Journal of Power Technologies*, Accepted 2017.

Paper X. Conference proceedings, coauthor, peer-review

Jairo Rua Pazos, Rubén M. Montañés, Luca Riboldi, Lars O. Nord, Dynamic modeling and simulation of an offshore combined heat and power (CHP) plant, *Proceedings of the 58th Conference on Simulation and Modelling (SIMS 58)*, Reykjavik, Iceland, September 2017; 138, pp. 241-250.

Paper XI. International journal publication, coauthor, peer-review

Lars O. Nord and Rubén M. Montañés, Compact steam bottoming cycles: model validation with plant data and evaluation of control strategies for fast load changes, *Submitted. Applied Thermal Engineering*.

1.5.3 Conference and seminar presentations

This section includes a list of presentations conducted in international conferences and seminars. These are presented in chronological order, and include two presentations in seminars (A and D), five presentations in international conferences (B, C, E, F and H) and two presentations at the COMPACTS project technical meetings (G and I). All the presentations were on oral format, but presentation E which consisted of a poster presentation.

A. Dynamic process simulation of decarbonized thermal power generation. *PhD Seminar, Department of Electric Power Engineering NTNU-Norwegian University of Science and Technology*. Trondheim, Norway, April 2015.

B. Dynamic simulation of combined cycle power plant with post-combustion CO₂ capture. *The 8th Trondheim Conference on CO₂ Capture, Transport and Storage*. Trondheim, Norway, June 2015.

C. Identifying operational requirements for flexible CCS power plants in future energy systems. *The 8th Trondheim Conference on CO₂ Capture, Transport and Storage*. Trondheim, Norway, June 2015.

D. CO₂ Capture at Technology Center Mongstad: Validation of a dynamic process model of the amine plant at CO₂ Technology Center Mongstad. *Climit PhD Seminar*, Hamar, Norway, October 2016.

E. Dynamic process model development and validation with transient plant data collected from an MEA test campaign at the CO₂ Technology Center Mongstad. *13th International Conference on Greenhouse Gas Control Technologies*, Lausanne, Switzerland, November 2016.

F. Dynamic Simulations of the Post-Combustion CO₂ Capture System of a Combined Cycle Power Plant. *12th International Modelica Conference*, Prague, Czech Republic, May 2017.

G. Dynamic and steady-state simulations of steam bottoming cycle for offshore oil and gas installation. *COMPACTS Technical Meeting number 6*, Trondheim, Norway, May 2017.

H. Power plant dynamics with post-combustion CO₂ capture – A comparison between a supercritical coal fired power plant and a natural gas combined cycle power plant. *The 9th Trondheim conference on CO₂ capture, transport and storage*, Trondheim, Norway, June 2017.

I. Dynamic and steady-state simulations of steam bottoming cycle for offshore oil and gas installation. *COMPACTS Technical Meeting number 7*, Trondheim, Norway, December 2017.

Chapter 2

Technical background

2.1 Climate change and CCS

Atmospheric concentrations of CO₂ have increased by 40% relative to pre-industrial levels, primarily from fossil fuel emissions, and there is unequivocal base evidence that it is one of the major drivers of climate change (IPCC, 2013)(IPCC, 2014). Limiting climate change would require maintained and substantial reductions of anthropogenic greenhouse gas (GHG) emissions during the next decades and near zero GHG emissions by the end of the 21st century (IPCC, 2014). Therefore there is a need to find the right pathways towards sustainable energy systems and implementing low-carbon technologies in order to meet energy access and air quality targets (IEA, 2015b). The challenge should be addressed considering the increased primary energy demand with a population that is expected to grow from 7.4 billion in 2017 to 9 billion by 2040. In any case, it is expected that coal and natural gas, together with renewables, will play an important role in power generation by 2040 (IEA, 2015b).

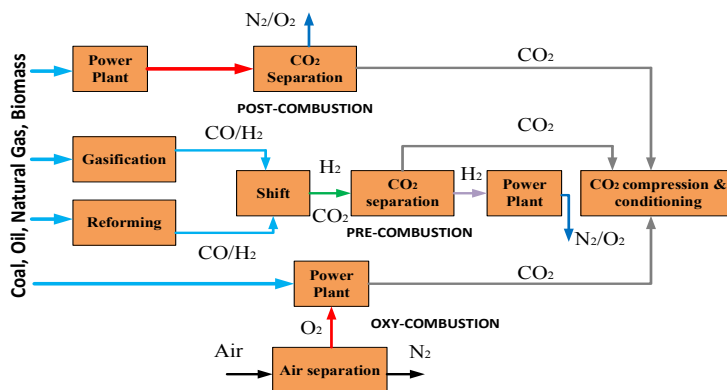


FIGURE 2.1: Methods for separation of CO₂ from thermal power plants using fossil fuels: post-combustion, pre-combustion and oxy-combustion.

Carbon capture and storage (CCS) is a group of technologies that can significantly reduce the CO₂ emissions from thermal power plants in the power sector. In addition, CCS is the only available technology to achieve deep CO₂ emission reductions in other industrial processes including iron and steel manufacturing, refining, petrochemical, pulp and paper, and cement manufacturing (IEA, 2016b). According to modeling from the International Energy Agency (IEA), CCS could provide 13% cumulative CO₂ emission reductions in a 2°C scenario, which account to 6 billion tonnes of CO₂. That would be following end-use fuel and electricity efficiency (38%) and renewables (30%) (IEA, 2015a).

The concept of CO₂ capture and storage consists of a group of the methods for capturing and permanently storing CO₂ that would have been emitted to the atmosphere and contributed to global climate change. As shown in Figure 2.1, there are three main methods for capturing CO₂ from fossil fueled thermal power plants:

- **Post-combustion.** The fossil fuel or biomass is combusted with air and the exhaust gasses are treated to selectively separate the CO₂ from the rest of the components in the exhaust gas. The rich CO₂ stream is sent for compression and conditioning.
- **Pre-combustion.** The main idea is to convert the heating value of the fuel into heating value of H₂. The fuel molecule is split into H₂ and CO (syngas) by partial oxidation. CO₂ and H₂ are obtained in the presence of steam and the CO₂ is afterwards separated from the H₂. The H₂ is used as fuel in the power plant.
- **Oxy-combustion.** Air is replaced by O₂ as oxidizer for combustion. In the ideal case the exhaust gas consists only of CO₂ and H₂O. Water is removed from the exhaust gas by condensation. It requires a source of oxygen, which is generally provided by air separation.

To be consistent with a 2°C climate pathway, the carbon intensity in the power sector should achieve a global average of 100 kg CO₂/MWh by 2040 (IEA, 2017). While the carbon intensity of sub-critical coal fired power plants are at the high end of the carbon intensity scale with around 955 kg CO₂/MWh, supercritical coal fired power plants can already provide a significant reduction in emissions due to their higher fuel efficiency and lower carbon intensity of around 755 kg CO₂/MWh, by simply replacing subcritical coal fired power plants at the end of their lifetime with supercritical technology. However, these technologies are above today's average of 540 kg CO₂/MWh (IEA, 2017). Natural gas combined cycle power plants are regarded as low carbon alternatives today with a carbon intensity of 400 kg CO₂/MWh, however in the mid-to-long term it might be required to further decarbonize natural gas combined cycle power plants by building new power plants with CCS or retrofitting existing units with post-combustion CO₂ capture, obtaining around 50 kg CO₂/MWh (Adams and Dowell, 2016), and enlarging the lifetime of existing units. Boundary Dam, the first coal fired power plant with post-combustion CO₂ capture and storage of CO₂ combined with enhanced oil recovery (EOR) in Canada, has proven that CCS can significantly reduce the carbon intensity of coal fired units with a facility that can capture 1.3 million tonnes CO₂ per year with a carbon intensity of around 130 kg CO₂/MWh. In the lower end of the carbon intensity scale, wide deployment

of renewables such as wind and solar can significantly reduce the carbon intensity and decarbonize the power sector.

According to the Global CCS Institute (*Global CCS Institute*), there are 21 large-scale CCS integrated projects (>800 000 tonnes CO₂ stored per year for coal power plants and >400 000 tonnes CO₂ stored per year for other industrial processes) operating or under construction in 2017. Most of the projects are dedicated to industrial separation and the main storage option is EOR. When it comes to thermal power plants, the post-combustion CO₂ capture method with chemical absorption is the most developed and commercially available technology for near-term deployment of CCS. It has been technically proven at commercial scale in coal-fired power plants at Boundary Dam in Canada (Singh and Stéphanne, 2014), and at Petra Nova project in Texas, USA (*W.A. Parish Post-Combustion CO₂ Capture and Sequestration Project*). However, the IEA highlights that the CCS technology deployment is not on track with the 2 °C climate pathway. If all the projects at large-scale that are being considered to be build were successful, it would mean that by 2025 the annually captured CO₂ would be below 70 Mt, which is around 15% of the expected deployment in the 2 °C scenario by 2025 (IEA, 2016a).

Due to the highly important role of renewables towards a low carbon economy and the incentives towards deployment of renewables, CCS should be seen as a tool that complements the deployment of renewables towards achieving climate change targets. Within this regard, the Carbon Capture and Storage Update (Boot-Handford et al., 2014) concludes that the financial case for CCS requires that it operates in a flexible manner.

2.2 The balancing problem

2.2.1 Operational flexibility in the power sector

Flexibility in the power system refers to the extent to which the power system can vary electricity production or consumption in response to variability, expected or not (IEA, 2012). Variability has traditionally been driven by variability of electricity demand. The system needed to adapt its generation patterns to balance the variability in power demand, and this balance was traditionally provided by cycling thermal power units (IEA, 2012). However, with the higher penetrations of variable renewable energy sources (VRE), variability is added to the generation side of the power system.

Variable renewable energy sources mainly refer to wind turbines and solar photovoltaic (PV). These are variable in nature since their output is dependent on weather conditions such as suitable wind speeds and suitable levels of solar irradiation. The net load curve is defined as the demand curve minus the production by variable renewables. The demand curve presents a regular pattern, following daily variations that correlate with human activity for electricity consumption. However, the net load follows a pattern with larger variability requirements. Some clashing effects between power demand and VRE production lead to increased needs for flexibility to be provided by the rest of the power system actuators. For example, the VRE output could decrease while the demand increases towards the early hours of the day, causing a sharp increase in net load. On the

other hand, the demand decreases towards the end of the day while production by VRE could increase, creating even a negative net load.

It is important to mention that balancing at power system level can be provided by different flexible resources within the system, including dispatchable power plants, demand side management and response, energy storage facilities and interconnection with adjacent markets (Chalmers, 2014). Another option is curtailment of VRE. Balancing in the power system needs to be provided at different time scales, and it implies the coordination of power market operation, system operation and grid hardware in combination with the flexible resources employed to balance the variability of net load and contingencies within the power system. Three main time scales are considered for the balancing problem in the power system, to make sure that there is balance between supply and demand at all time scales:

- ms to s: voltage and frequency control (stability).
- min to hour: scheduled production meets demand and electricity production meets the load (balancing).
- Weeks to seasons: production and transmission capacity to meet the demand the whole year (adequacy).

The requirements for flexibility in a power system depend on various aspects which include the energy mix, capacity (size of the system) and the penetration of renewables. More ramping and flexibility is required in smaller power systems and systems with higher penetrations of VRE (Huber, Dimkova, and Hamacher, 2014). In addition, higher penetration of renewables result in different impacts on daily operation of power systems (Brouwer et al., 2013): increased demand for reserves, displacement of thermal power units in the merit order, efficiency of thermal power generation and wind curtailment. The increased penetrations of variable renewable energy sources within Europe have impacted the operational patterns of fossil-fueled thermal power plants, with strong decreases in average full load hours since 2006 and decreased energy efficiency (Groot, Crijns-Graus, and Harmsen, 2017).

In power systems with large shares of variable renewables, it might be needed to have installed capacity of thermal power plants providing regulation capacity (variable power output for balancing) and back-up capacity for the periods of time in which poor wind and solar conditions reduce power output from VREs (Chalmers, 2014)(Gonzalez-Salazar, Kirsten, and Prchlik, 2018). These aspects increase the need for flexible thermal power plants.

2.2.2 Operational flexibility of thermal power plants

Current and future thermal power plants, initially designed for base load, should be operated on a load following basis. Considering aspects of operational flexibility in the design of thermal power plants is becoming an important design criterion. Thermal power plants need to cycle (on and off) and to provide fast rump-up and ramp-down more frequently, and more cost-effectively and rapidly (Gonzalez-Salazar, Kirsten, and Prchlik,

2018). The characteristics of operational flexibility of thermal power plants vary from technology to technology and types of fuel. Key aspects of operational flexibility of thermal power plants can be summarized as follows (SIEMENS AG, 2011):

- **Part load efficiency.** A thermal power plant within power markets with high penetration of VREs, might be operated at part load during a significant amount of its lifetime. In addition, it should be capable to be operated over its full operational load range. Therefore, design and operation philosophies for high part load efficiency are of importance. That improves the operational efficiency, reduces fuel consumption and CO₂ emissions.
- **Low minimum compliant load (turndown).** For cyclic operation it is of importance that the plant can be operated at as low load as possible. This increases the operational window of the power plant. However, minimum compliant load is normally constrained by part load emissions, which should be compliant with regulations. Normally high NO_x or CO formation at part load are the limiting factors for gas turbine based power plants.
- **High cycling capability.** Frequent start-up and shut-down, load change and fast load ramps, low start-up emissions, and high start-up reliability. Fast load ramps and reserve capacity are of importance for grid stabilization services.
- **Start-up times.** High start-up efficiency or short start-up times are desired features in thermal power plants. Minimizing start-up costs and times can help to provide power on demand and be more competitive in the day-ahead power market.

A recent review work by Gonzalez-Salazar et al. evaluates state-of-the-art technologies for gas and coal-fired conventional thermal power plants (Gonzalez-Salazar, Kirsten, and Prchlik, 2018). Their review work shows that combined cycles (NGCCs) are more efficient (average LHV efficiency for NGCC at 58%) than for coal plants (average LHV efficiency range from 31% to 43% depending on technology) at full load and minimum compliant load. However, the efficiency range is larger and minimum compliant load is higher for gas based power plants (40-50% of full load for heavy duty gas turbines) than for coal fired power plants (10-20% of full load, although it can be very high for some technologies reaching 60-70 % of full load). An exception is aeroderivative GTs (10-20% of full load). It is expected that NGCC could reduce the value to 30% of full load in the future.

Ramp rates are higher in gas power plants than coal fired power plants. Defining the ramp rate as the rate of change in %/min of power plant load from minimum compliant load to full load, Gonzalez-Salazar et al. (Gonzalez-Salazar, Kirsten, and Prchlik, 2018) states that combined cycle power plants ramp rates are 5.4 %/min on average and are expected to double in the future.

The cyclic operation of thermal power plants have impacts on the thermal power plant unit, since cycling has a degenerative effect on power plants. During ramp-up or down, or during start-up or shut-down of the unit various components of the power plant are subject to large temperature and pressure stresses (NREL, 2012). These stresses reduce the lifetime of components of the thermal power plant due to combined effects of creep and

thermal fatigue (EPRI, 2001). Cyclic operation can potentially provide larger income in the short term for the power plant, but the reduction in equipment lifetime will incur additional costs associated with maintenance and availability (Stoppato et al., 2012). In addition, cycling results in degraded performance and higher emissions over time (NREL, 2012).

2.3 Combined cycle power plants with CCS

2.3.1 Gas and steam turbine combined cycles

A basic principle to increase the efficiency of a thermodynamic cycle is to add heat at a high temperature and reject heat at low temperature. This is the principle behind combined cycles, which combine a thermodynamic cycle with high temperature heat addition (such as the Brayton cycle with gas turbine) and a thermodynamic cycle with lower temperature of heat addition and also low temperature of heat rejection (like the steam Rankine cycle). In combined cycles with gas and steam turbines, the remaining hot gas from the gas turbine exhaust is as a heat source to produce the steam in a bottoming steam cycle by means of a heat recovery steam generator (HRSG) (Kehlhofer et al., 2009). The basic thermodynamic principles of thermodynamic cycles and heat engines can be found in basic thermodynamics books (Moran et al., 2012). For a good overview of the technology the reader is encouraged to read the book by Kehlhofer et al. (Kehlhofer et al., 2009).

Natural gas combined cycle power plants have moderate capital costs, short construction times, and high efficiency and flexibility (IEAGHG, 2012). State-of-the art large-scale natural gas combined cycle power plants with three-pressure reheat configurations (3PRH) have recently reached lower heating value (LHV) fuel efficiencies of above 60% by different vendors. This LHV fuel efficiency is higher than most efficient coal-based power plants with up to 47% LHV fuel efficiency. In addition, at 350-450 kgCO₂/MWh, combined cycle power plants are less carbon intense than their coal-based counterparts at 750-1000 kgCO₂/MWh (IEA, 2017). As of today, combined cycle power plants represent a mature technology that is part of the generation capacity of power systems throughout the world. In addition, combined cycle power plants show better operational flexibility characteristics than coal fired thermal power plants (Gonzalez-Salazar, Kirsten, and Prchlik, 2018). This may lead to implementation of combined cycle natural gas-fueled power plants in the transition towards future low-carbon energy systems in different areas of the world.

2.3.2 Post-combustion CO₂ capture

The post-combustion route towards CO₂ capture from thermal power plants englobes a group of process and technologies that have in common that CO₂ is selectively separated from the rest of the components of the flue gas after combustion has occurred in the power

plant. Comparing with the other technologies like membranes, it is clear that the post-combustion route with chemical absorption is the most mature method and the technology most likely to be implemented in the near future (Wang et al., 2017)(Boot-Handford et al., 2014). In the following, a description of the chemical absorption process of CO₂ is presented. A similar description was included in paper IV (Montañés and Nord, 2017). For details on the process the reader is referred to dedicated literature.

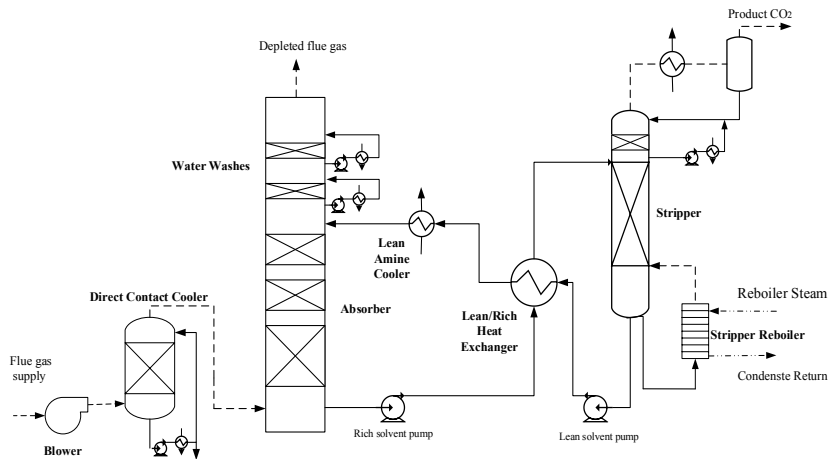


FIGURE 2.2: Simple process flow sheet of chemical absorption process for post-combustion CO₂ capture.

Figure 2.2 shows the process flow sheet for the simple absorber-desorber chemical absorption process. The process of CO₂ capture by chemical absorption is a two-step regenerative process; one involves the absorption of CO₂ into a solvent, while the other involves the desorption or stripping of CO₂ from the solvent and the regeneration of the solvent. The process conditions change in the absorption and desorption process, being main changes temperature and pressure, and also solvent concentrations and pH. In addition, the volumetric flow in the absorber is larger than in the stripper, as well as the fluid composition differs significantly. The absorption process is exothermic while the desorption process is endothermic. For absorption, low temperature and high partial pressure of CO₂ are desired, while for desorption, high temperature and low partial pressure of CO₂ are desired.

When the process is utilized for flue gas treatment from a power plant, the exhaust gases are normally cooled down in a direct contact cooler (DCC), that reduces the flue gas temperature and the water content. A fan overcomes the gas pressure drop in the absorber, which is operated slightly above atmospheric pressure, and at around 40 °C; refer to Figure 2.2. In the absorber column, the exhaust gas flowing upwards meets the chemical solvent flowing downwards. Packing material allows having a thin film of liquid with high surface contact area for heat and mass transfer between the gas and liquid phases,

and the exothermal chemical absorption process. Depleted flue gas leaves the absorber at the top through a stack, normally after flowing through a water wash section that allows keeping the water mass balance of the process and reduces chemical solvent emissions due to solvent droplets or solvent vapor carry over. The rich solvent, i.e., solvent with a lot of bounded CO_2 , accumulates in the absorber sump and is then pumped towards the top of the stripper. An intermediate heat exchanger allows for heat integration between the absorber and stripper columns. The rich solvent is heated up by the lean solvent coming from the stripper bottom and then enters the stripper at the top of the column. This heat integration allows reducing reboiler and cooling duties. A mixing tank allows for accumulation of the solvent at different operating conditions of the plant. The location of the mixing tanks differs from plant to plant, and the most common location is in the recycle loop. At some pilot plants the absorber sump can have the function of mixing tank.

The desorption process normally occurs at around 100 to 130 °C. Steam supplied from the power plant provides the reboiler duty required to regenerate the solvent (endothermal desorption process), and to generate the stripping vapors flowing upwards in the stripper column, consisting mainly of H_2O and CO_2 . The regenerated lean solvent is sent to the absorber inlet via the heat exchanger and a lean amine cooler that controls the temperature of the solvent at the inlet of the absorber to around 40 °C. At the top of the stripper there is a condenser and a cooler where the solvent and steam condenses. The condensate is recycled to the column. The product CO_2 rich flow at the top of the stripper is compressed for transport and storage purposes.

Most of the published work on chemical absorption of CO_2 from thermal power plants have been carried out with 30 wt% MEA as chemical solvent. The typical specific reboiler duty for capturing 90% of CO_2 with MEA is around 3.5 MJ/kg CO_2 captured (Boot-Handford et al., 2014). Several efforts in research are being done in order to develop solvents and process configurations that can reduce the required regeneration energy, and hence reduce the efficiency penalty associated with the regeneration stage of the process when integrated with the power plant (Rochelle, 2009). An interesting non-proprietary option is the chemical absorption process with concentrated aqueous piperazine with a lower heat requirement of 2.6 MJ/kg CO_2 , which also allows higher temperature of regeneration of 150 °C without significant thermal degradation, has less volatility than MEA and is not corrosive to stainless steel (Rochelle et al., 2011).

2.3.3 Process integration

The thermal power plant and the chemical absorption process of CO_2 are not independent units. Low levels of process integration would consist of the basic retrofit case, in which flue gas from the exhaust of the HRSG must be sent to the PCC unit for gas separation and a steam extraction from the power plant is utilized to feed the reboiler of the chemical absorption process, together with electrical power to drive the auxiliary and cooling systems of the PCC unit and compressor train. This results in an efficiency penalty of the power plant with CCS compared with a reference NGCC power plant without CCS. Jordal et al. reviewed published work on power plant designs and the respective efficiency penalty

of NGCC with PCC based on MEA solvent and a capture rate of 90% (Jordal et al., 2012), with different configurations and heat integration options between the power plant and the PCC unit. The typical efficiency of base case NGCC (without CCS) varies from 56.3% to 59.4%, while the efficiency for the corresponding designs with integrated PCC unit varies from 47.9% to 51.8%. The efficiency penalty due to CO₂ capture ranges from 6.2%-point to 9.6%-point, and specific reboiler duty varies from 3.4 MJ/kg CO₂ to 4.04 MJ/kg CO₂ (Jordal et al., 2012). By increasing levels of process integration, the efficiency penalty of CO₂ capture can be reduced. For combined cycle power plants with post-combustion CO₂ capture several process integration alternatives have been studied and proposed.

Some work in the literature has put emphasis on design of the PCC unit and increasing the level of process integration within the different components of the PCC unit itself to reduce the specific reboiler duty (SRD). Several process configurations have been proposed. They include absorber inter-cooling, solvent split-flow to stripper, and lean vapor recompression (Amrollahi et al., 2012)(Amrollahi, Ertesvåg, and Bolland, 2011). Amrollahi et al. find that with the modified chemical absorption process configuration with a combination of lean vapor recompression with absorber inter-cooling, the specific reboiler duty can be reduced from the base case chemical absorption process configuration with 3.7 MJ/kg CO₂ down to 2.7 MJ/kg CO₂ (Amrollahi et al., 2012).

In addition, a technique called exhaust gas recirculation (EGR) is studied in the literature (Finkenrath et al., 2007)(Sipöcz and Tobiesen, 2012)(Luo, Wang, and Chen, 2015)(Alcaráz-Calderon et al., 2017). The principle consists of recirculating a fraction of the CO₂ rich mass flow in order to increase the CO₂ concentration of the exhaust gas from the GT. That results in smaller equipment size in the PCC unit, which can lead to significant reduction in capital and operational costs (Sipöcz and Tobiesen, 2012). Another means of increasing CO₂ concentration in the exhaust gas is by including supplementary firing in the HRSG (Díaz et al., 2016), which utilizes excess oxygen from lean combustion in the GT to burn more fuel in HRSG integrated burners. That allows producing more steam in the HRSG and increasing CO₂ concentration in the exhaust gas.

Higher levels of heat integration between the power plant and the PCC unit are studied in (Chinn et al., 2005)(Jonshagen, Sammak, and Genrup, 2011)(Jordal et al., 2012). Jonshagen et al. evaluated the benefits of coupling the economizer and reboiler in a specially designed NGCC, with the main finding being that utilizing this concept similar efficiency of the NGCC with PCC can be obtained with one-pressure level (drum) in the HRSG as with three-pressure levels (three drums)(Jonshagen, Sammak, and Genrup, 2011). Chinn et al. suggest partial integration of the reboiler duty within the HRSG (Chinn et al., 2005).

The coupling between the thermal power plant and the chemical absorption process occurs both at steady-state and during transient operations. In this Ph.D. thesis the focus was on dynamic performance and control of the integrated power plant with PCC. This first attempt was done for the process integration method suggested by (Biyouki, 2014), with a three-pressure reheat configuration in the NGCC and the basic absorber-desorber process in the PCC with two absorbers and one stripper unit as proposed by Jordal et al. (Jordal et al., 2012). Steam is partly extracted from the IP-LP crossover. For further details refer to Section 3.2 and paper V.

2.3.4 Operational flexibility of NGCC with PCC

Thermal power plant operation is tightly coupled to the operation of the power system and power markets. As discussed in Section 2.2.2, thermal power plants within power systems with high penetration of renewables are being operated in cycling mode (Gonzalez-Salazar, Kirsten, and Prchlik, 2018). This causes dynamic interactions between power plant and the power system (Welfonder, 1999). From a power system perspective, the thermal power plant can be seen as an actuator to balance the variabilities in net load and to provide ancillary services for frequency control (Rebours et al., 2007).

As illustrated in Figure 2.3, thermal power plants with post-combustion CO₂ capture are integrated systems, in which thermal integration and recirculations of flows of matter between the power plant and the chemical absorption process are of importance in order to reduce the efficiency penalty due to CO₂ capture; refer to Section 2.3.3. Therefore, the power plant and the chemical process operation are coupled under steady-state and transient conditions. Work by Boot-Handford et al. concludes that CCS thermal power plants need to be flexible, and that load following capability of these systems is of paramount importance for the long term economics (Boot-Handford et al., 2014). Operational flexibility of thermal power plants with CCS has become an important area of research within the CCS community (IEAGHG, 2012).

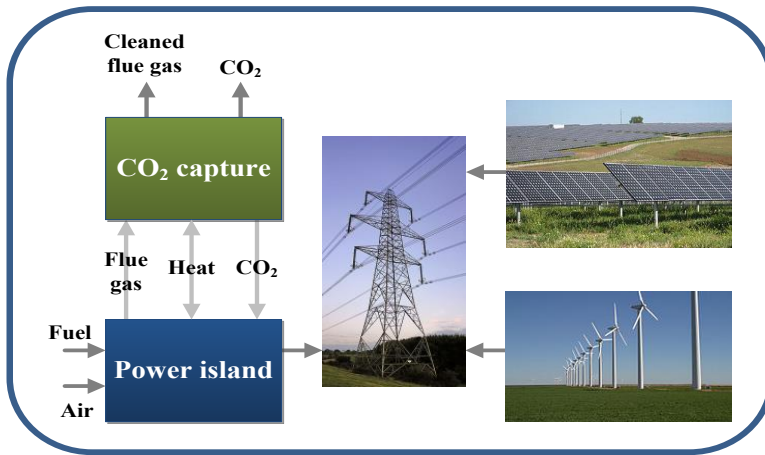


FIGURE 2.3: Thermal power plant with post-combustion CO₂ capture integrated in a power system.

Several research articles have assessed the steady-state part load performance of natural gas combined cycle power plants with chemical absorption CO₂ capture using 30% MEA as chemical solvent, and for different power plant designs. Jordal et al. studied the part load performance of NGCC with 3PRH configuration with a PCC unit with 2 absorber columns in parallel and 1 stripper column. Their study concludes that there is

enough steam available at the intermediate pressure and low pressure (IP-LP) crossover to feed the reboiler duty at part loads down to 40% GT load to keep 90% capture rate at part load. Their study shows that reference unabated NGCC power plant has a reduction of LHV efficiency from 58% at design load of 100% GT load to 50% LHV efficiency at 40% GT load, while their design with PCC unit presents a LHV efficiency of 50% at design load down to 42% at 40% GT load (Jordal et al., 2012). This means that the capture penalty in %-points is close to constant at full load and at part load. Rezazadeh et al. (Rezazadeh et al., 2015) include an study of the part load performance of the NGCC with PCC with a similar process configuration and integration. Their study includes operability aspects of the PCC unit at part loads. Their work shows an increased specific reboiler duty at part load operation to keep a capture rate of 90%. Their main results show that at 60% GT load there is a risk of under-wetting in the absorber column due to reduced solvent flow to keep CO₂ capture rate at 90%. Under-wetting can result in poor mass transfer in packed segments, due to uneven flow distribution within the packing (Rezazadeh et al., 2015). They also highlight that there are other aspects that can affect the operability of the PCC unit at low loads, such as the increase in O₂ concentration which can result in enhanced thermal degradation of the solvent and corrosion issues (IEAGHG, 2012). The work by Vaccarelli et al. (Vaccarelli et al., 2016) showed the steady-state part load performance of the NGCC with PCC for different HRSG configurations, and other works have assessed steady-state off-design performance of the system for NGCC with PCC including EGR (Alcaráz-Calderon et al., 2017)(Adams and Dowell, 2016).

Several strategies have been proposed to provide flexibility with thermal power plants with CCS. The main idea is to change the power output of the power plant by changing the operating conditions of the integrated process. The goal is to obtain flexible operational strategies that can be utilized by power plant owners in order to increase profitability and in turn provide flexibility to the power system. The four main strategies proposed can be summarized as follows (IEAGHG, 2012):

- Varying the CO₂ capture rate, depending on electricity prices and CO₂ costs.
- Turning on and off the CO₂ capture unit or exhaust gas by-pass (Gibbins and Crane, 2004). When by-passing the exhaust gas to the capture unit, the power plant operates with partial or no CO₂ capture, by venting part of the gas directly to the atmosphere. That allows reduction of the energy required for solvent regeneration, and the steam can be utilized to produce power in the steam turbine.
- Providing solvent storage to decouple plant operation (boiler or GT) from the CO₂ capture (Gibbins and Crane, 2004). The CO₂ capture rate is kept constant and solvent is stored in tanks (lean and rich). In this way, the regeneration energy is shifted towards times when electricity prices are low.
- Allowing the power plant to increase or decrease load, following its own ramp up or down rates.

A study on flexible operation of coal- and gas-CCS power plants by Mechleri et al. (Mechleri, Fennell, and Dowell, 2017) showed that the option of exhaust gas by-pass is

highly dependent on CO₂ emissions costs, and therefore it is only profitable in scenarios when carbon prices are very low. The viability of solvent storage is highly dependent on the capital expenditure to build the infrastructure to store the solvent, and might also be profitable in scenarios where CO₂ costs are relatively high (Versteeg et al., 2013). Another option called variable stripper regeneration (VSR) (Dowell and Shah, 2015), consisting of varying the amount of steam sent to the reboiler, and utilizing that steam to produce additional power. In other words, decreasing solvent regeneration when electricity prices are low and increasing when electricity prices are high. The key limitation for this option is the availability of steam from the power plant. CO₂ is stored within the chemical solvent, and is regenerated when electricity prices are low. However, the profitability of this option depends on the compromise between the peak electricity prices (characteristic of power markets with high penetration of renewables) and the CO₂ prices.

The chemical absorption process is characterized by slow process dynamics, i.e. it takes hours to stabilize the process when a large disturbance is applied. However, the thermal power plant load change is generally considered relatively fast, in the order of a few minutes. The focus in this Ph.D. work has been on the assessment of time dependent performance of the system when the power plant increases or decreases load with fast ramp rates, as required in power systems with high penetration of renewables (Gonzalez-Salazar, Kirsten, and Prchlik, 2018). When including the power plant in the analysis, several recent works have highlighted the need for studies on the transient performance of the power plant with integrated PCC by linked dynamic process models (Adams and Dowell, 2016)(IEAGHG, 2016)(He and Ricardez-Sandoval, 2016)(Mechleri, Fennell, and Dowell, 2017), since these works did not include the process dynamics of the power plant in their analyses. In addition to not including power plant process dynamics, the study by (Mechleri, Fennell, and Dowell, 2017) is limited to very slow ramp rates on the thermal power plant load for their base case. In addition, most of the work published on process dynamics and has focused on the PCC unit, and mostly for coal fired power plants (Bui et al., 2014), with limited validation of the dynamic process models. For a literature review on dynamic process model validation of the chemical absorption process refer to paper II in this thesis. In addition, transient testing at a demonstration scale post-combustion CO₂ capture plant provides empirical evidence on the observations gained via dynamic process simulation on transient performance of the process, as well as gives insight into practical implementation of flexible operational strategies that go beyond the output from the simulations.

2.4 Dynamic process modeling and simulation

2.4.1 Steady-state and transient operation of systems

In a power plant or any industrial process, relevant process variables for the operation of the unit are measured. Figure 2.4 shows the evolution over time of a generic process variable. This process variable could be any process variable monitored or calculated at the plant: a pressure, a temperature, a composition, power output, heat duty, etc. In continuous processes under normal operation it would be typical to observe a constant

value of most process variables, the actual value is dynamic, and the average over time of the actual value is what we call steady-state values. Note that some processes perform with intrinsic dynamics such as batch processes.

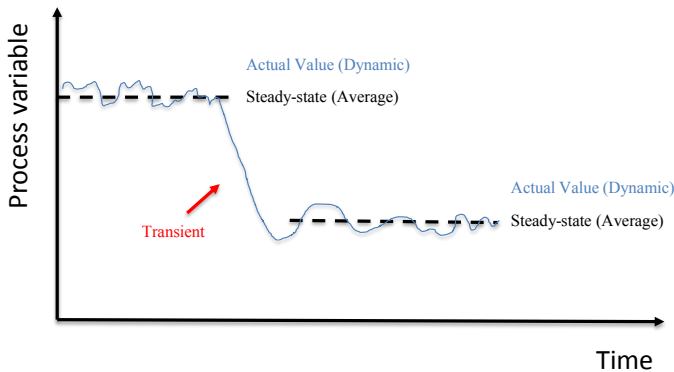


FIGURE 2.4: Generic process variable trajectory over time in an industrial plant: steady-state and transient trajectory.

Instrumentation and control are normally required to have safe and stable operation of the process and a regulatory control layer for consistent inventory control is implemented at the plant to avoid excessive drifting of some process variables from target set-points. That ensures stable operation of the process. The process can be operated close to its design conditions, but it might also be operated at different loads or under ambient conditions far from design specifications. This is normally called off-design operation. In thermal power plants, typical steady-state off-design conditions are driven by variations in ambient conditions (temperature, pressure, humidity) since the performance of thermal engines is greatly affected by ambient conditions (Kehlhofer et al., 2009). In addition, off-design operating conditions are obtained when the plant is operated at part-load or when employing strategies for flexible operation of the process.

When the load of the plant is changed, the process variables will evolve over time, describing an output trajectory and eventually reach steady-state again. The so called floating variables will reach a different steady-state value than the initial one, if the process can be brought to new operating conditions and reach stabilization. Other transient events that drive transient performance of the process besides load changes include start-up/shut-down sequences, failures or equipment trips and changes in the process upstream or downstream.

The dynamic process models are developed for a purpose of application, and they should describe the steady-state behaviour (off-design) and process dynamics (output trajectories) considering the time scales and physical phenomena of the transient events

of interest. The main applications of dynamic process modeling applied to the chemical absorption process include:

- Understand transient performance of the CO₂ capture plant.
- Study various transient events for flexible plant operation.
- Develop plantwide control strategies.
- Understand dynamic interactions between the capture plant and the power plant, and other components of the CCS chain.
- Utilize for real plant operations: Operator training and decision support tool.
- Implement within optimal control strategies, such as model predictive control (MPC) (Skogestad and Postlethwaite, 2006).

2.4.2 Modeling paradigm

There are several tools that enable the development of dynamic process models and allow to conduct dynamic simulations of thermal power plants (Alobaid et al., 2017) and for the chemical absorption process. These include ProTRAX[®] (*ProTRAX, Trax LLC, Energy Solutions, Lynchburg, VA.*), Aspen HYSYS[®] (*Aspen HYSYS, 2018*), Unisim[®] (*Unisim, Honeywell*), Apros (*Apros, Process Simulation Software, Fortum Power Solutions, Fortum, Finland*), gPROMS[®] (*gPROMS, Process Systems Enterprise*). A generic tool is Matlab Simulink (*Matlab Simulink, Mathworks, Natick, MA*), which is widely applied in transient simulation and control of dynamic systems. In recent years, a modeling language called Modelica has been used by academia and industry for modeling and simulation of the transient performance of thermal power plants.

In this work, the tool employed to develop the dynamic process models was the Modelica language within Dymola simulation environment. Modelica is an object-oriented and open physical modeling language developed by the non-profit Modelica Association (*Modelica and the Modelica Association*). The Modelica language enables the development of systems of differential and algebraic equations that represent the physical phenomena of multi-domain systems (Fritzson, 2003). In addition, Modelica is a-causal and equation-oriented, which allows a component to be utilized in different contexts and a model to be used in different studies.

Multi-domain engineering means that Modelica can simulate systems from different engineering fields in the same tool. That helps to develop high fidelity models of different fields of engineering, such as, in this case thermo-hydraulic models of thermal power plants and the CO₂ absorption process of the chemical engineering domain. This feature, together with the Modelica modeling flexibility and capabilities to work with the source code, were the main reasons behind selecting Modelica/Dymola as the tool to develop the dynamic process models in this thesis. In other words, Modelica is a powerful tool that enables the development of high fidelity physical models of complex integrated systems.

Physical models means that the models developed are based on physical principles, such as energy, mass and momentum balances in thermodynamic systems. Typical principles in process models separate the typical equipment in process systems in two main types: large systems and small systems.

- In large systems, storage of energy and mass is considered important from the system level perspective. These equipments include tanks, reactors, and some heat exchangers. When considering system's level modeling, these models are described as volume type models. Volume type models are described as large, with well-mixed homogeneous properties. In these models, storage of mass and energy are considered in the balance equations which result in systems of differential equations.
- For small systems, storage of mass and energy is negligible, those include valves, pumps, compressors, and some heat exchangers. From a system's level modeling perspective, these are described by flow type models. In flow type models volumes are negligible and the models describe resistances. The models describe large gradients of properties over short distances. The resulting system of equations are algebraic and often non-linear. These models normally define the relations between driving forces and flows.

Publications and applications of Modelica technology in the modeling and simulation of thermal power plants are available in the literature. In addition, there are several open-source libraries available for modeling thermal power plants, such as ThermoPower, ClaRa, ThermoSysPro, and SiemensPower. In the Master Thesis work by Gule (Gule, 2016), a comparison of these open-source libraries is presented. However, in this work a commercial library was chosen for developing the thermal power plant model. ThermalPower (*Modelon Thermal Power Library*) developed by Modelon AB. The Modelica language has been employed to model coal fired power plants (Huebel et al., 2014)(Chen, Zhou, and Bollas, 2017)(Hübel et al., 2017), combined-cycle power plants (Benato, Stoppato, and Mirandola, 2015), nuclear power plants (Cammi et al., 2011) and concentrated solar thermal power plants (Hefni, 2014)(Montañés et al., 2018). Other works include the modeling of integrated gasification combined cycle (IGCC) power plants (Casella and Colonna, 2012). Recent works include the integration of thermal power plants with CCS from natural gas combined cycle power plant (Montañés et al., 2017a) and from coal fired power plants (Wellner, Marx-Schubach, and Schmitz, 2016)(Garðarsdóttir et al., 2017). The works with Modelica technology include methodologies for life-time reduction estimation for components due to thermal stresses induced by flexible operation of thermal power plants (Benato, Stoppato, and Mirandola, 2015)(Hübel et al., 2017), and new methodologies for implementing transient operation as a design criteria in organic Rankine cycles (Pierobon et al., 2014).

Despite of the widespread application of Modelica in several engineering fields, such as, the automotive industry or thermal power plant applications, the application of Modelica in the process industry is still limited. The library utilized in this work, was the GasLiquidContactors library (*Modelon Gas Liquid Contactors Library*), also provided by Modelon AB. Publications of the chemical absorption process with Modelica technology

include the works by (Prölß et al., 2011)(Garðarsdóttir et al., 2015)(Haar et al., 2017)(Montañés, Flø, and Nord, 2017). The publications included in this thesis regarding dynamic simulations of the chemical absorption process contribute to the application of Modelica technology in the process industry. The transient estimation and analysis of state-of-the-art thermal power plants, such as, 3PRH combined cycle power plant, is complicated. The full solution of the resulting system of equations is a challenging task, since developing these high-fidelity models require large amount of model development hours, the knowledge of multi-engineering disciplines and programming tools (Can Gülen and Kim, 2013). The development and validation of these models is normally complicated due to the steep learning curves to dominate the tool and understand the system.

Chapter 3

Methodology

3.1 Identifying operational requirements for thermal power plants with CCS

Results from a day-ahead multi-area power market simulator (EMPS) used for the TWENTIES EU project were utilized in paper I (Montañés et al., 2016). These results were used to illustrate wind power production and the market-based electric generation dispatch of three different thermal power plants in the Nordic and Continental Europe region.

The European Commission has stated the goal of integrating European power markets for making efficient use of energy across national borders. The Network Codes, developed by the European Network of Transmission System Operators for Electricity (ENTSO-E) (ENTSOE, 2012), are meant to overcome the challenge of integrating VRE into the future pan-European power system by 2030. These network codes describe regulations that power system participants will have to follow in the European system. They include power system operation, market related codes, and grid connection codes. The technical requirements that can be found in these codes are described as general guidelines. Since each power system has its own flexibility requirements (IEA, 2012), there is room for decision to be made at national level and local transmission system operators (TSO)s can define specific requirements within the frameworks defined by ENTSO-E.

With the purpose of identifying the technical requirements for grid connection of thermal power plants in current and future power systems, the grid codes of four selected European countries were studied. In addition, requirements for power plants to be able to bid in balancing markets are exposed in Table 1 of paper I. The selected countries were Spain, Germany, Great Britain (GB), and Denmark, since these are areas of interest when it comes to flexibility and renewable energy production.

3.2 Modeling of combined cycle power plant with PCC

The methodology to develop the dynamic process models of the combined cycle power plant with post-combustion CO₂ capture was based on three main steps: i) defining the process configuration and design of the process; ii) developing dynamic process models in Modelica; iii) dynamic process simulations of the linked dynamic process models. Figure 3.1 summarizes the three steps and presents the software tools employed for design

of the combined cycle power plant configuration with post-combustion CO₂ capture and the tools to develop the dynamic process models and carry out simulations and post-processing of simulation results.

i) Defining the process configuration and design of the process

The process was designed with the aim of obtaining a combined cycle power plant with PCC with the process integration method presented by (Biyouki, 2014). The reason behind selecting this process configuration was to conduct a first assessment of the dynamic performance of NGCC with PCC with detail dynamic process models of the power plant, therefore a process configuration with relative low levels of process integration was selected for the first approach. The resulting system is a three pressure reheat combined cycle power plant with post-combustion CO₂ capture presented in paper V. The flow sheet of the full power plant (without compression stages) is presented in Figure 3.2. The gas turbine selected was the Mitsubishi 701 JAC, burning 100 vol% CH₄ and with an exhaust gas flow of 887 kg/s and an exhaust CO₂ concentration of 4.33 vol% at design point of 100% GT load at ISO ambient conditions of 1.013 bar and 15 °C.

The configuration consists of a three-pressure reheat combined cycle power plant and a post-combustion CO₂ capture unit with two absorbers and one stripper column, as suggested by (Jordal et al., 2012). The power plant has a net power output of 613 MW (452 MW from the GT and 161 MW from the steam turbine) and an LHV efficiency of 52.8% with CCS. The three pressure levels heat recovery steam generator at design conditions was a 145/30/3.69 bar configuration with 591 °C live steam and reheat temperature. The tool employed for design of the process flow sheet and sizing of equipment of the combined cycle was GT PRO (*Thermoflow Inc.*). This tool was selected because it is widely used in industry for design of gas turbine based power plants, and allows to obtain detail sizing of components, including equipment size, geometry, materials and fluid inventories. This is required for the detailed parameterization of dynamic process models. In addition, the tool allows to carry out off-design steady-state simulations which can be seen as reference performance data of combined cycle power plants (Jordal et al., 2012). In addition, the steady-state off-design data was useful for validation of the steady-state off-design performance of the dynamic process model; refer to Section 3.3.

The post-combustion CO₂ capture system had two absorber columns (16.3 m in diameter and 23.2 m height) and one stripper column (9.7 m diameter and 10 m height), and utilizes 30% aqueous MEA as chemical solvent. The tool employed for detailed design and sizing of the post-combustion CO₂ capture system was Aspen Plus (*Aspen Plus V8.6. 2014*).

Process integration of the system was based on the methodology developed in (Biyouki, 2014). The resulting steam mass flow extraction from the power plant to feed the reboiler of the PCC unit consisted at design point of:

- Steam from the IP/LP crossover of the steam turbine (3.7 bar), 71% of total steam to reboiler mass flow rate.
- Steam from LP superheater, 14% of total steam to reboiler mass flow rate.

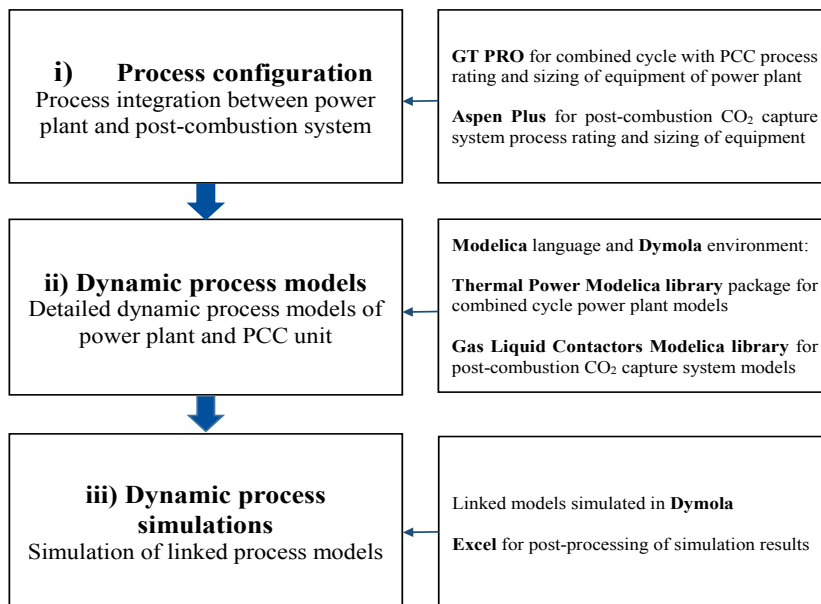


FIGURE 3.1: Methodology steps and software tools employed for the development of the design of the power plant with post-combustion CO₂ capture and the development of the dynamic process models of the integrated system.

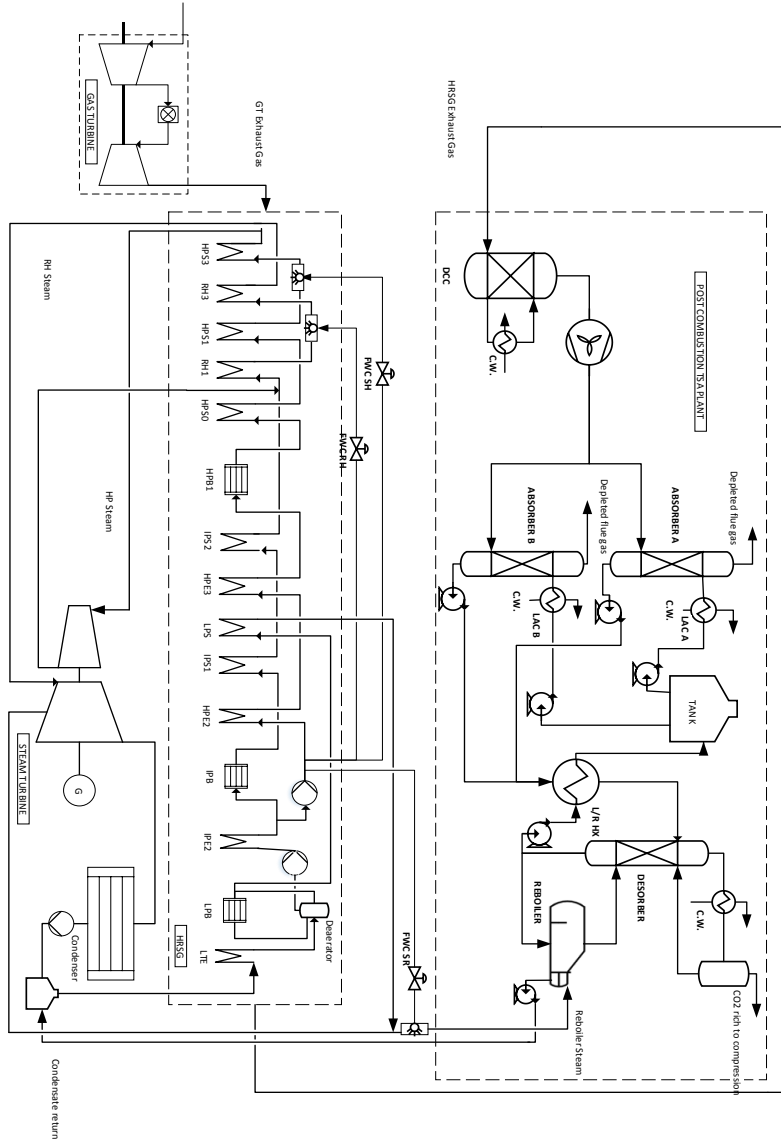


FIGURE 3.2: Process flow diagram of the NGCC power plant integrated with post-combustion CO₂ capture; modified from paper V. Note that in Figure 1 of paper V the gas turbine location was not correct. It has been modified in this figure. Note that in Figure 4 of paper V the direction of exhaust gas flow was also incorrect.

- Steam from HP water extraction for temperature control, 15% of total steam to reboiler mass flow rate.

The resulting specific reboiler duty at design point was 3.73 MJ/kgCO₂. Further details on the design of the process can be found in paper V.

ii) Development of dynamic process models

The dynamic process models of the power plant configuration in Figure 3.2 were developed by means of the Modelica language (*Modelica and the Modelica Association*) and the Dymola process simulation environment (*Dymola systems engineering*). The thermo-hydraulic models of the power plant steam cycle were obtained from a commercial library called Thermal Power Library (*Modelon Thermal Power Library*). The library contains base models of power plant components such as recuperators in HRSG, drums, feedwater heaters, steam expansion sections, condenser, deaerator, pumps, valves, flow resistances and regulation elements (including PIDs, blocks, multipliers and ramps). These sub-models from the library were used as a base to develop the dynamic process model of the steam cycle. The sub-models were parameterized, modified and combined to model the power plant steam cycle. The main purpose of application was estimating load change transient performance of the power plant. Further details on the dynamic process models of the power plant are explained in Section 3.2.1 and paper V.

The dynamic process model of the post-combustion CO₂ capture system configuration were developed by means of Modelica language with Dymola environment. The chemical absorption process models were obtained from a library called Gas Liquid Contactors (*Modelon Gas Liquid Contactors Library*). The library contains process sub-models of the post-combustion CO₂ capture process with MEA, including absorber column models, stripper column models, reboiler, internal heat exchanger, condensers, transport delay pipe models, pumps, valves, flow resistances and regulation elements. For further details on the development of the dynamic process model refer to paper V. The dynamic process model of the PCC unit in paper V was calibrated against the design data obtained from Aspen Plus simulations, with a similar methodology as explained in Section 3.4.2. In addition, this model was employed in paper IV for the analysis of the open-loop performance of the PCC system at different power plant loads. The dynamic process model was validated with experimental data in paper II; refer to Section 3.4.2.

iii) Dynamic process model simulations

The simulations of the integrated dynamic process model of the plant were conducted in Dymola simulation environment, and results were exported to Excel as .csv files for post-processing. The dynamic process models employed and developed in this Ph.D. thesis resulted in complex DAE systems which are solved numerically by Dymola by means of a selected numerical method, in this case the DASSL numerical method. These models represent physical phenomena of the equipment and the interactions between different subsystems under transient operation due to disturbances applied to the process. The resulting systems of equations are relatively large and require a significant computational

TABLE 3.1: Dynamic process models structure for process models employed in this thesis. The indicators presented are number of equations (N_{eq}), number of unknowns (N_{un}), number of states (N_s), number of parameters (N_{pa}), and number of variables (N_{va}).

| Dynamic process model | N_{eq} | N_{un} | N_s | N_{pa} | N_{va} |
|--------------------------------|----------|----------|-------|----------|----------|
| TCM amine plant | 13931 | 13931 | 343 | 31361 | 11783 |
| PCC unit of the NGCC plant | 29851 | 29851 | 740 | 69726 | 25116 |
| Combined cycle power plant | 26248 | 26248 | 400 | 10456 | 24396 |
| Integrated NGCC with PCC model | 56219 | 56219 | 1141 | 80217 | 49613 |

effort which results in relatively slow simulations for each transient test. In Table 3.1 and Table 3.2 an overview of the size of the resulting system of equations and the required CPU simulation times is presented. The time needed to solve the system of differential equations is dependent on the events simulated and simulation setup. The simulation statistics are presented here to give the reader an overview of the complexity of the formulation in hand, and not to perform a detailed analysis of the numerical performance of the models or on model verification. The simulations presented in Table 3.1 and Table 3.2 are for the following events:

- **TCM amine plant model:** open-loop transient response to step change of 10% solvent flow rate.
- **PCC unit of the NGCC plant:** open-loop transient response to step change of 10% solvent flow rate.
- **Combined cycle power plant model:** GT deloading of combined cycle power plant transient event from 100% to 85% GT load with a ramp rate of 2.5%/min.
- **Integrated NGCC with PCC model:** GT deloading of combined cycle power plant transient event from 100% to 85% GT load with a ramp rate of 2.5%/min and L/G ratio control structure in PCC unit.

It can be seen that physical models of combined cycle power plants and PCC units in Modelica/Dymola results in large systems of equations that require long CPU times to be computed, ranging from the order of a few minutes to 6-8 hours. Therefore performing simulations of the process can result in a tedious process that requires a significant amount of time employed only in conducting the simulations. In this work CPU time was not a constraint and it was not the objective of this work to obtain fast simulations. However, there are applications in which simulation time can be of importance, for example for optimization or model predictive control (MPC). Efforts should be done to develop reduced order models with faster simulations without significantly compromising the accuracy of model predictions.

TABLE 3.2: CPU and simulation times for process models employed in this thesis. Simulations were carried out with DASSL solver, with tolerance 10^{-4} .

| Dynamic process model | t_{sim} (s) | t_{CPU} (s) |
|--------------------------------|----------------------|----------------------|
| TCM amine plant | 40000 | 81.3 |
| PCC unit of the NGCC plant | 40000 | 246 |
| Combined cycle power plant | 40000 | 884 |
| Integrated NGCC with PCC model | 100000 | 22900 (6.36 h) |

3.2.1 Dynamic process modeling of combined cycle

Gas turbine model

Gas turbines are to be considered as compact engines built from different subcomponents, including compressor, combustion chamber and turbine. The formulation for calculating simple gas turbine cycles can be found in literature for gas turbine theory (Saravanamutto et al., 2009) and fundamentals of thermodynamics (Moran et al., 2012). The calculations are based on energy and mass balances over components of the system and concepts of isentropic or politropic efficiencies for compressor and turbine components. These calculations allow to calculate optimal design point for gas turbines knowing the process configuration, power plant load and ambient conditions (pressure and temperature), power demand, design conditions and maximum firing temperature. As described in (Saravanamutto et al., 2009), the performance of the individual components of a gas turbine, such as, compressors and turbine components can be obtained based on previous design experience by manufacturers or by performance tests.

For a given gas turbine cycle configuration, the performance of the integrated engine is limited by the balanced performance of the different units, which impose restrictions on the operating points for the different components. Chapter 9 in (Saravanamutto et al., 2009) describes the calculation of the equilibrium running points, lines and diagrams over a compressor map for steady-state off-design performance of gas turbines based on equilibrium principles of compatibility of flow, work and rotational speed between components, to form the named matching calculations. These calculations are based on compressor and turbine characteristics. These allow engineers to understand the basic thermodynamics and fluidmechanics behind off-design performance of gas turbine, and these physical models allow to calculate the off-design performance of the unit for different loads.

Knowledge of the transient performance of gas turbines can be useful when designing the gas turbine control system, specially when designing new gas turbines concepts where there is no previous experience or significant amount of testing hours on transient performance. Dynamic process models are based on off-design performance models by the additon of characteristic curves that can be tuned afterwards in the development phase of the engine, and used for control purposes. It is normally done by assuming flow compatibility in the off-design models. Note that this is a good assumption if considering fast pressure dynamics for fast transients (Saravanamutto et al., 2009). These models

are normally developed by including phenomena of rotor dynamics and acceleration of the rotor due to the related increase of net torque with increased fuel flow, and resulting change in rotational speed. Such transient effects are of importance for rotor stability and frequency control problems (Glover, Sarma, and Overbye, 2012), which are normally associated with fast transients in the order of a few seconds. Can Gülen and Kim (Can Gülen and Kim, 2013) included a literature review of commercial software for combined cycle power plants, and emphasize that transient gas turbine modeling and simulation in the literature are normally limited to the study of governor controls via the block diagram approach (Rowen, 1983). In addition, Shin et al. found that for fast load changes in gas turbine combined cycles, the GT load stabilizes within 5 seconds (Shin et al., 2002) for a step load change of 100 to 90%, and other process variables of the GT also stabilize within a few seconds, which is significantly faster compared to process variables of the steam cycle, which is in the order of a few minutes (Shin et al., 2002).

The dynamic process models in this work focus on the performance of the steam cycle for transient load changes. Therefore it is of importance to capture the process dynamics within the minutes time scales, and focus on the bottoming steam cycle transient performance. The gas turbine models are employed here to define the dynamic boundary conditions for the exhaust gas from the GT outlet to the heat recovery steam generator, and the quasi-static performance of the gas turbine for load changes is assumed. Note that when the quasi-static assumption for transient performance is assumed, the GT system is considered in equilibrium at each point in time, and that the transient performance is a succession of steady off-design results (Dechamps, 1994). The exhaust mass flow rate of the gas turbine and the exhaust temperature of the gas turbine were defined as disturbances to the steam cycle dynamic process model. The exhaust characteristics were based on simulations from validated gas turbine models from GTPRO (*Thermoflow Inc.*). The calculations were obtained for the selected GT (in this case Mitsubishi 701 JAC) with ISO ambient conditions of 15 °C and 1 atm; refer to paper V. The focus was on steady-state part load off-design, and not on aspects of off-design GT performance due to varying ambient conditions such as ambient temperature, pressure or humidity. The models from Thermoflex are based and developed on performance data from GT manufacturers and considering simplified physical models including turbine and compressor maps. GT controllers try to keep constant TIT, which is normally achieved by controlling the turbine exhaust temperature (TET) to a target value that will keep TIT constant, since TIT cannot be measured in modern GTs (*Thermoflow Inc.*).

Simulations of the off-design performance of the selected GT at different GT loads are conducted to obtain the equilibrium off-design performance points for GT composition, exhaust temperature and exhaust mass flow rate; refer to Figure 3.3a and Figure 3.3b. The exhaust characteristics for a given GT will depend on the GT controls, and will differ for different GT technologies. However, a common trend is to observe a reduction in exhaust mass flow rate and it is desired to obtain high TIT for high GT efficiency while high TET is desired for good heat recovery in the HRSG and high efficiency of the steam cycle. The variability in exhaust gas composition was not considered for simulations in this work, because for the range of GT loads tested it was found rather small. CO₂ composition ranged from 4.33 vol% to 4.17 vol%; refer to Figure 3.3b. This assumption should be

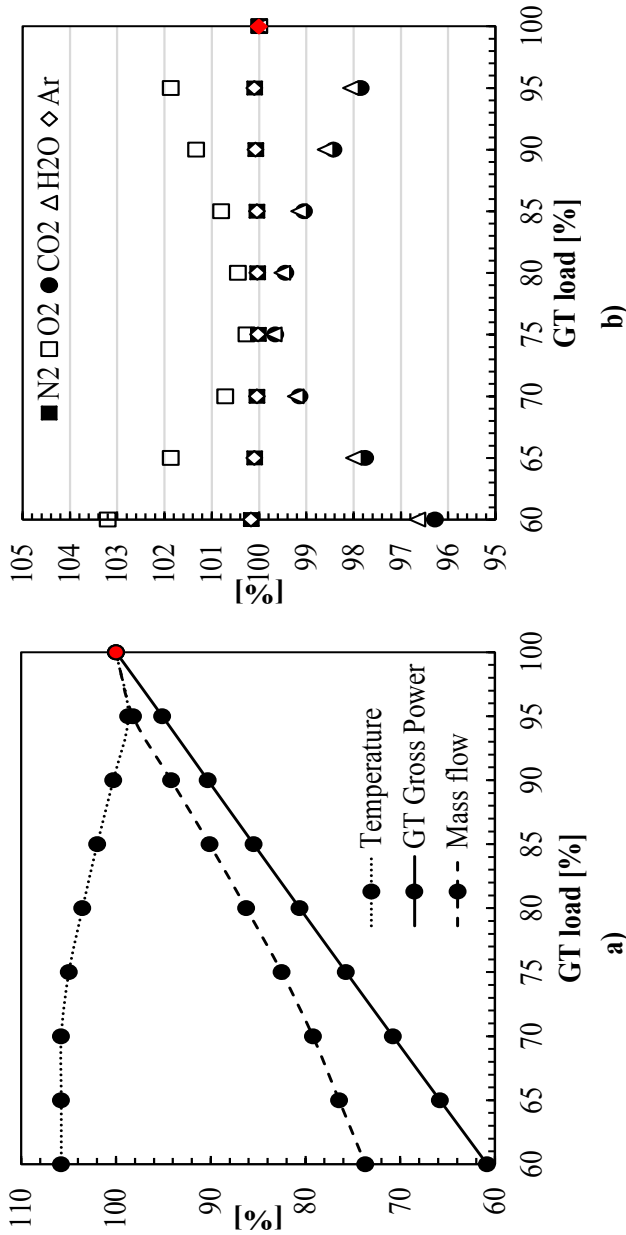


FIGURE 3.3: Off-design simulation results for the Mitsubishi JAC 701 gas turbine from 100% to 60% GT load. The values shown as a percentage of the design value, which is marked in red. a) Exhaust mass flow rate, exhaust temperature and GT gross power as a percentage value of the design value (887.1 kg/s, 451.8 MW, 632 °C). b) Exhaust gas composition at turbine exhaust for different GT loads. Values as percentage of design value for composition (73.97 vol% N₂, 11.25 vol% O₂, 4.33 vol% CO₂, 9.56 vol% H₂O and 0.89 vol% Ar).

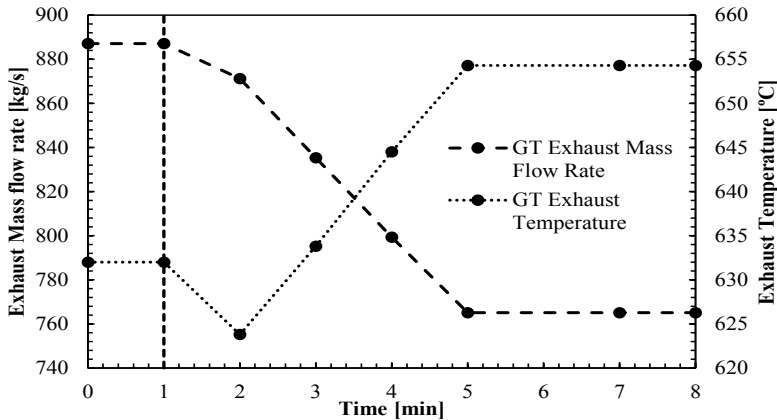


FIGURE 3.4: Transient simulation of exhaust mass flow for Mitsubishi JAC 701 gas turbine from 100% to 80% GT load in 4 min (5% GT load reduction per minute).

revised if the models were to be run at lower GT loads where exhaust gas compositions change more significantly compared to the design point.

Assuming a GT load change ramp rate, the disturbance applied on the boundary conditions of the heat recovery steam generator was defined. Intermediate points between the reference off-design steady-state points were obtained by linear interpolation. This was implemented with time series data table blocks in Dymola. Figure 3.4 shows the evolution of GT exhaust mass flow rate over time for a ramp rate of 5%/min and a GT load change from 100% to 80%. This trajectory for GT load change is comparable to the load change transient data for a heavy duty gas turbine presented by Kim et al. (Kim et al., 2000).

Steam turbine model

In this work, an approach to steam turbine modeling based on section rather than detailed models of steam turbine stages was selected. This approach is common in system level modeling. The sections considered were HP, IP and LP steam turbine sections, with one steam extraction from the IP/LP crossover. The steam turbine section models are quasi-static models, with static mass balance for the expansion within one section. Considering that the main focus of modeling was load change transient estimation of combined cycles during power plant online operation, the rotordynamics and thermal inertia phenomena of the steam turbine were disregarded, as in the modeling approach by (Shin et al., 2002) and (Benato, Stoppato, and Mirandola, 2015). Other modeling approaches might be required if start-up procedure of the steam turbine is to be simulated (Birnbaum et al.,

2009).

The model consists of a constant dry step isentropic efficiency for all sections and the calculation of mechanical power based on energy balance over each turbine section; refer to Eq. 3.1 and Eq. 3.3. Note that at part load operation of the steam turbine, the pressure drop in the last stages (LP section) will change, leading to a change in dry isentropic efficiency. However, constant dry isentropic efficiency was assumed for dynamic process simulations. The generator model is a simplified model in which the power supply is equal to the power demand, meaning that the rotating frequency is constant. A constant generator and mechanical efficiency $\eta_{\text{mech-el}}$ of 0.99 was applied. The condensing section LP dry efficiency was corrected by the Baumann's formula in Eq. 3.2, where x_m is the steam quality and β is the Baumann factor that varies from 0.4 to 0.9 (Bolland, 2014), and was set to 0.8 based on calibration process with reference software data.

$$\eta_{\text{dry,is}} = \frac{h_i - h_o}{h_i - h_{o,\text{is}}} \quad (3.1)$$

$$\eta_{\text{wet,is}} = \eta_{\text{dry,is}} - \beta(1 - x_m) \quad (3.2)$$

$$P_{\text{mech},i} = \dot{m}_{\text{steam}}(h_i - h_o) \quad (3.3)$$

$$P_{\text{el}} = \eta_{\text{mech-el}} P_{\text{mech}} \quad (3.4)$$

$$K_t = \frac{\dot{m}_n}{\sqrt{p_{i,n} \rho_{i,n} \left(1 - \left(\frac{p_{o,n}}{p_{i,n}}\right)^2\right)}} \quad (3.5)$$

$$\dot{m}_t = K_t \sqrt{p_i \rho_i \left(1 - \left(\frac{p_o}{p_i}\right)^2\right)} \quad (3.6)$$

For off-design calculations, the flow characteristics is defined by Stodola's law of cones, refer to Eq. 3.5 and Eq. 3.6, where K_t is the flow area coefficient, and n , i and o stand for nominal, inlet and outlet, respectively.

Heat recovery steam generator model

During load change transient events, the main inertia to the process for load changes is added by the heat recovery steam generator of the combined cycle power plant (Shin et al., 2002). The heat recovery steam generator is composed of different heat exchanger recuperator components (economizers, evaporators and superheaters) and cylindrical drums. Auxiliary components for operation of the HRSG include variable speed pumps and valves, including control valves for drum level control and feedwater cooling of superheated and reheated steam streams. The recuperators consist of tube bundles in which the exhaust gas heats up the water/steam circulating within the tubes. Details on the dynamic process model of the heat recovery steam generator developed in this work can

be found in paper V. The paper includes a description of the heat exchanger recuperator models, and further details on the formulation for thermohydraulic models implemented in Modelica can be found in (Tummescheit, 2002). Details on formulation for heat exchanger modeling in the object-oriented based language Modelica based on the Finite Volume Method (FVM) can be found in (Schiavo and Casella, 2007). In the following a summary of the heat exchanger recuperator model from TPL (*Modelon Thermal Power Library*) is presented.

The recuperator model consisted of a shell and tube heat exchanger with gas on primary side (shell), single or two-phase medium on secondary side (tube) and a wall model. Figure 3.5 shows the dymola implementation of the recuperator model, with main subcomponents being gas side flow model, metal wall model and water/steam side model.

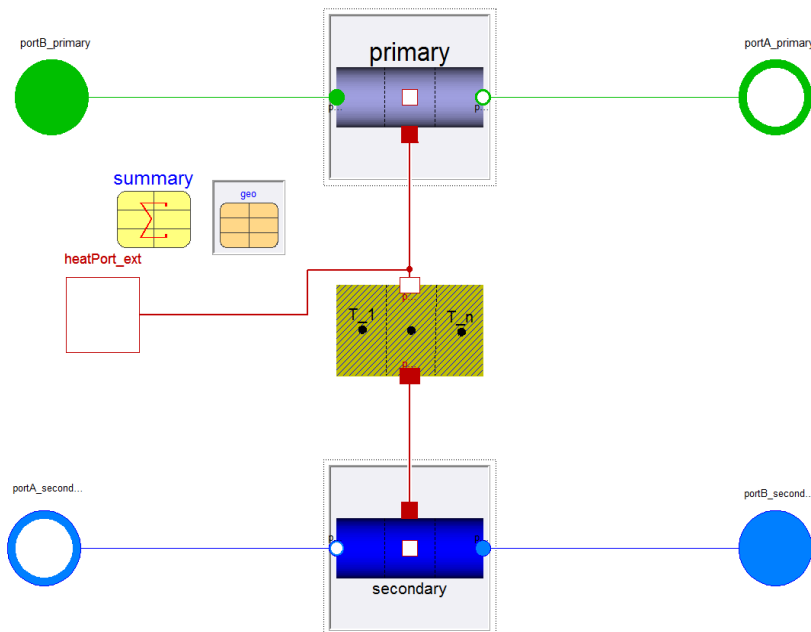


FIGURE 3.5: Heat exchanger dynamic process model, as seen in the Dymola modeling object-oriented display window with ThermalPower library (*Modelon Thermal Power Library*). The process model consists of base models for piping hot side (primary), piping cold side (secondary) and heat transfer wall.

The piping models are based on the finite volume method.

A discretized 1-D pipe model with lumped pressure was employed for the gas side. Static mass, mass-fraction, and energy balance equations are discretised in n volume segments with the finite volume method. Static mass and energy balances can be assumed on

the gas side because at high gas velocities the exhaust gas exchanges significantly more heat than it accumulates (Dechamps, 1994). The state variables were n temperatures, one pressure p (lumped) and mass fractions. In order to calculate the heat transfer coefficient for each volume, a convective heat transfer correlation for gas flow over tube bundles α_g is utilized; refer to Eq. 3.7, where d_{hyd} is the hydraulic diameter of the pipe, F_a is a tube arrangement factor, and λ is the thermal conductivity of the gas. The Nusselt number Nu_o for each volume is calculated by Reynolds dependent correlations from (*VDI-Värmeatlas, 9th edition, section Gg* 1997). The pressure drop model is lumped at the outlet.

$$\alpha_g = \frac{F_a Nu_o \lambda}{d_{hyd}} \quad (3.7)$$

For the one phase and two-phase flow in water/steam side pipe, a similar modeling approach is considered. In this case dynamic energy and mass balances are considered. The general mass balance is presented in Eq. 3.8, where p is pressure, h is the specific enthalpy and ρ is density. The general energy balance is shown in Eq. 3.9. Note that in the model, the energy and mass balances are also discretized in the longitudinal direction of the pipe in n volumes. Large discretization (number of volumes n) will increase the number of states of the system, increasing the complexity of the resulting system of equations and contributing to slower simulations in terms of CPU time of the final model. In general, large number of volumes gives more accurate results with less need for calibration of the model heat transfer correlations, and is normally desired for large recuperators with large temperature drops from inlet to outlet ports in a heat exchanger side. A default number employed for most heat exchangers was four, which was increased for large heat exchangers to up to ten volumes such as in the intermediate pressure economizer.

$$\frac{dm}{dt} = V \left(\frac{d\rho}{dh} \frac{dh}{dt} + \frac{d\rho}{dp} \frac{dp}{dt} \right) \quad (3.8)$$

$$V\rho \frac{dh}{dt} = \dot{m}_{in}h_{in} - \dot{m}_{out}h_{out} + V \frac{dp}{dt} + Q \quad (3.9)$$

The radial heat transfer is calculated with Eq. 3.11. For the steam/water side a heat transfer correlation has been considered for estimating convective heat transfer coefficient for superheaters, α_s , for 1-phase, see Eq. 3.10. A similar formulation is employed for the economizer. Reynolds number dependent correlations from (*VDI-Värmeatlas, 9th edition, section Gg* 1997) are utilized to calculate mean Nusselt number Nu_m .

$$\alpha_s = \frac{Nu_m \lambda}{d_{hyd}} \quad (3.10)$$

$$Q = \alpha_s A_{heat} (T_{wall} - T_{fluid}) \quad (3.11)$$

A common modeling approach for two-phase flow in system level simulations is to assume that the boiling process is reduced to the saturated boiling regime (Hoppe, Gottelt, and Wischhusen, 2017). For the two-phase flow in the boiler section, a constant heat transfer coefficient for the cold side of 120 kW/m²K was considered. The solid wall model

is utilized for considering transient conductive heat transfer where the heat capacity is lumped at the center of the wall. Note that other wall formulations allow to calculate the temperature gradients within the walls, by discretizations of the wall in the radial direction, for estimation of thermal stresses and lifetime reduction of equipment due to thermomechanical fatigue phenomena (Benato, Stoppato, and Mirandola, 2015).

The drum models formulation and validation can be found in Casella et al. (Casella and Leva, 2003), and details on drum dynamics and implementation within Modelica thermohydraulic libraries can be found in the work by Eborn (Eborn, 2001).

The dynamic process model of the three pressure level horizontal heat recovery steam generator was built by parameterizing, testing and calibrating each of the unit models separately (recuperators, deaerator, valves, pumps and drums). Controllers were added to each subsection of the system while developing the full HRSG model by joining step-by-step different subsections of the HRSG. This method, called step-by-step approach is explained in detail for the post-combustion CO₂ capture model in Section 3.4.2. Figure 3.6 shows the Dymola implementation of the heat recovery steam generators. The green ports represent the flue gas source and sink ports (physical interfaces) for the flue gas, while the blue ports are physical ports for i) output: low pressure superheated steam, intermediate reheat steam and high pressure superheated steam, high pressure water extraction from high pressure water line for feed water cooling of low pressure steam ii) inputs: feedwater from condenser and condensate return, and intermediate pressure steam to reheaters.

The HRSG model includes a process control unit which was designed in an integrated manner. It means that a control unit model was built with interfaces for control measurements and control action signals. There, the decentralized control structure for HRSG operation and consistent inventory control was implemented. The control loops included three-element controllers for drum level control, pressure control of the deaerator, and temperature desuperheating for superheated steam and reheated steam. The control strategy implemented for HRSG operation at different loads was sliding pressure operation mode, which is the common method of operation of HRSG units in combined cycle power plants from mid-to-high loads (Kehlhofer et al., 2009). Further details on control loops of the steam cycle and regulatory control layer are presented in paper V.

3.2.2 Dynamic process modeling of chemical absorption process for CO₂ capture

The dynamic process models of the chemical absorption process were obtained from GLC library (*Modelon Gas Liquid Contactors Library*). Paper II includes a literature review on dynamic process models and validation work presented in the literature. The main reason for selecting Modelica/Dymola for the PCC unit dynamic process models was to be capable of linking the dynamic process model of the power plant with the dynamic process model of the post-combustion CO₂ capture system in the same tool (Dymola) for co-simulation of the integrated system models within the same simulation environment. The dynamic process models employed were based on the two-film theory for heat and mass transfer phenomena in the absorber and stripper column, with thermodynamic

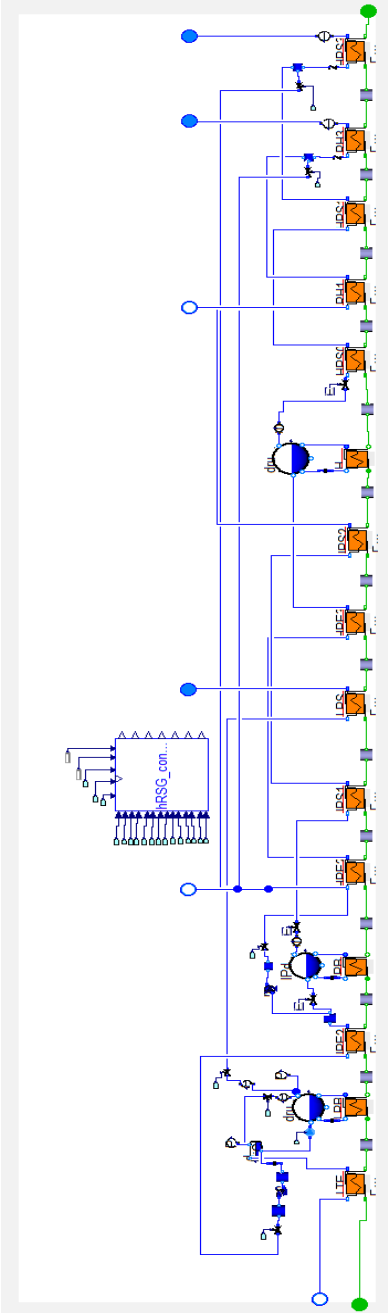


FIGURE 3.6: Dymola implementation of the three-pressure reheat heat recovery steam generator model. The model includes dynamic process models of four economizers, six superheaters, two reheaters, 3 level drums and one deaerator. Pumps and control valves for drum level control are included, as well as two valves for superheated and reheated steam temperature control.

equilibrium at the gas-liquid interface. Interface mass transfer in packed sections was modeled with a rate-based approach with enhancement factor, which takes into account the mass transfer due to chemical reactions. The dynamic process models were validated with large scale experimental data from Technology Centre Mongstad in paper II, and details on the models were presented in the paper. For further details refer to publications from the model developers (Pröhl et al., 2011)(Akesson et al., 2012).

3.3 Dynamic process model validation

Model validation is a complicated task. A model is developed for a given purpose, to capture physical phenomena that occurs at specific time and spatial scales. Therefore, it is of importance to define the application and objective of modeling and simulations of the model to understand the needs for validation. The key with model validation is to define a set of reference data that represents the performance of the real world. With dynamic process models, we want to capture both the steady-state phenomena (steady-state off-design performance and process variability in the presence of disturbances) and the process dynamics at the time scales of the transient events of interest of the study. Therefore, it is key to design validation cases that will test the main process steady-state variation and dynamics. With validation, the model is simulated and its capability to represent the performance of the real system is tested (Cellier, 1991).

The concept of model validation is sometimes confused or used interchangeably with model verification. Generally speaking, model validation tries to assess the capability of the resulting system of equations to represent the behaviour of the real system, while model verification tries to assess the validity of the coded mathematical model in a given modeling language to represent the reference mathematical model. In general the tasks are to answer the following questions (Tummescheit, 2002):

- **Model validation** Am I solving the right system of equations? Does my model correspond to the real system?
- **Model verification** Am I solving the system of equations right? Have I implemented the mathematical model in the modeling language right?

When employing dynamic process models included in libraries, one assumes that the models have been intensively verified by the model suppliers. This is sometimes considered as an added value of using commercial libraries, since they have been further verified and tested than open source libraries. However, models developed within libraries are normally flexible in their modeling objective and applications (Tummescheit, 2002), i.e. there is flexibility available to the modeller to select a set of assumptions for the given application since the model contained in the library does not represent any specific real system. Therefore, it is difficult for library developers to ensure the validity of dynamic process models for a wide range of applications. Even when employing dynamic process models included in libraries, the modeller should still carry out validation for its own objective and application.

The task of adapting model parameters to obtain a better match between model simulation outputs and reference data is called calibration. Model calibration is often needed when developing process models. The process of model calibration of physical models that result in non-linear systems of algebraic and differential equations is often approached by hand-tuning of selected model parameters by a process based on trial and error or on physical insight. The process of parameter tuning is often unavoidable when dealing with complex high fidelity physical models (Tummescheit, 2002). On another note, the need for model calibration and the presence of uncertain parameters in a process model is sometimes considered a big challenge when scaling up technology and when employing process models for design calculations of equipment at larger scales than the reference data for model validation. Generally speaking, the accuracy required for a process model that is to be employed in control design is lower than that for process design.

Deviations between model predictions and the experimental data are because the model is a simplified representation of reality. The perfect model simply does not exist. In addition, there is uncertainty related to the validity of the experimental data, which is based on instrumentation that need to be calibrated and certain process conditions need to be achieved for ensuring the suitability of the data sets. Uncertainties related to experimental data are mainly due to instrument bias error and the precision error associated with reading variability for same operating conditions.

Another challenge related to dynamic process model validation is the availability of experimental data for process model validation purposes. This is related to the lack of published transient experimental data from commercial scale power plants and PCC processes. The data is normally considered as proprietary and is rarely published from commercial facilities and industrial actors, at least to the extent of detail needed for process model validations. An alternative to using experimental data is to use process simulation softwares with process models that have been validated with experimental data. Simulations from these models can be employed to assess the validity of process models, in a method sometimes called software-to-software validation.

In order to assess the validity of the process models employed in this work, the following method was employed. First, the capability of the process models to predict the steady-state operating conditions was evaluated. If calibration was required, models were calibrated against design process conditions of the reference data. Simulations were compared with model outputs by calculating absolute percentage errors (*AP*) with Eq. 3.12 and mean absolute percentage errors (*MAP*) with Eq. 3.13. Note that x refers to the process variable, n to the number of steady-state data cases, subscript s refers to the steady-state value predicted from simulation of the process model and subscript r to the reference steady-state value.

$$AP = 100 \left| \frac{x_s - x_r}{x_r} \right| \quad (3.12)$$

$$MAP = 100 \sum_{i=1}^n \left| \frac{x_{s,i} - x_{r,i}}{x_{r,i}} \right| \quad (3.13)$$

Once the dynamic process model is validated for steady-state off-design conditions, validation transient test cases were employed to validate dynamic process models. This is normally done by applying set-point step changes in main inputs of the process (reference pilot plant or reference process model) and logging the output trajectories from the reference system. Then, the same disturbance was applied to the dynamic process model to be validated by means of input trajectories or step changes. Output trajectories of interest for validation were plotted in graphs and the capability of the dynamic process model to predict the trends was assessed. Trends here mean the capability to reproduce dead times and stabilization times observed at the real experimental facility or the reference model, and result in similar trajectories.

Validation of dynamic process models included in this work was considered separately for the different subsystems. In paper II, process models in Modelica language for the post-combustion CO₂ capture process with chemical absorption and 30 wt% aqueous MEA was validated with experimental data from Technology Centre Mongstad, with steady-state and transient plant data; refer to Section 3.4. In paper V results from the validation of the Modelica model for the 3PRH configuration developed are presented. The steady-state data for various off-design GT load operating conditions of the combined cycle were obtained with simulations from GT PRO (*Thermoflow Inc.*). This tool is developed with experimental data from various industrial facilities and is considered as reliable models representing state-of-the-art performance of power cycles based on gas turbine. GT PRO (*Thermoflow Inc.*) has been employed in the literature for steady-state off-design analyses of thermal power plants with post-combustion CO₂ capture with chemical absorption (Jordal et al., 2012)(Rezazadeh et al., 2015). In addition to this work, dynamic process models of a combined cycle power plant for off-shore oil and gas installations based on once-through boiler technology were validated with a software-to-software approach. The Modelica process models were validated for both steady-state and transient data cases generated with GT PRO; refer to paper XI. The results of paper XI include validation of reference steady-state off-design models with industrial power plant data, which provides confidence in the use of GT PRO simulations as a reference for steady-state off-design performance of GT based thermal power plants.

3.4 Pilot plant testing at Technology Centre Mongstad

The Technology Centre Mongstad (TCM DA) is considered the world's largest technology centre dedicated to testing and improving CO₂ capture technologies. The test centre is located next to the Statoil's refinery Mongstad in Norway. TCM DA is a joint venture of different companies, currently: Gassnova (representing the Norwegian State), Statoil, Shell and Total. The facility contains two pilot plants for post-combustion CO₂ capture and available site for potentially installing other capture facilities. Currently there is an amine plant designed by Aker Solutions and a chilled ammonia process plant designed by Alstom (now General Electric).

The main objectives of the TCM DA facility include to reduce technical, environmental and financial risk associated with full-scale CO₂ capture (Koeijer et al., 2009). The facility is built in a flexible manner so that the pilot plants can treat a variety of flue gas

compositions in terms of CO₂ content. The pilot plants can treat a slipstream of flue gas coming from the residue fluid catalytic cracker of the refinery with a CO₂ content of around 13 vol%, typical of flue gas from coal-fired power plants; and a slipstream of flue gas with around 3.5 vol% CO₂ from the cogeneration Statoil's combined heat and power plant (CHP) that supplies heat and power to the refinery. In addition, when the plant is configured with the CHP stripper, a stream of CO₂ rich product flow could be recirculated and hence intermediate compositions of flue gas CO₂ vol% could be tested. That would represent flue gas compositions found in different applications from other industrial sources or even on power plant process configurations with exhaust gas recirculation (EGR) (Gjernes et al., 2017). This provides with capabilities of testing the performance of the process and a variety of solvents (proprietary or non-proprietary) for a wide range of flue gas compositions representing different industrial applications of the CO₂ chemical absorption process with amines at demonstration scale.

Together with the size, it is the capability of the test centre to operate the process with a slipstream of flue gas coming directly from a natural gas fueled combined cycle power plant what makes this facility more unique compared to other test centres throughout the world, since the rest can test the process for flue gas coming from coal fired power plants. According to data from the Global CCS Institute (*Global CCS Institute*) there are five test centres focusing on capture technologies including TCM DA: the National Carbon Capture Centre (NCCC) in the US (*National Carbon Capture Centre NCCC*); CSIRO's Post Combustion Capture Centre (PCC) in Australia (*CSIRO PCC*); Shand Carbon Capture Test Facility (CCTF) in Canada (*Saskpower Shand Carbon Capture Test Facility*); and UKCCSRC Pilot-scale Advanced Capture Technology (PACT) in the United Kingdom (*UKCCSRC Pilot-scale Advanced Capture Technology (PACT)*).

Among the different activities conducted at TCM DA, one of them is the performance of MEA campaigns in the chemical absorption plant. The main purpose of the MEA campaigns is to develop knowledge of the process at demonstration scale when utilizing the non-proprietary chemical solvent aqueous monoethanolamine (MEA) and the scientific dissemination of some of the data generated during the MEA campaigns. In other words, to produce data and information that can be relevant to the realization of full-scale CO₂ capture (*The Third MEA Campaign at the CO₂ Technology Centre Mongstad*). The amine plant came on-line in 2012 and first operational results were presented by (Andersson et al., 2013). A first MEA campaign (MEA1) was conducted from December 2013 to February 2014, with the main objectives of generating results from the CHP plant operations with CO₂ capture and developing an independently verified TCM DA amine plant base case with CHP flue gas (around 3.5 vol% CO₂) with 30 wt% aqueous MEA solvent system (Brigman et al., 2014)(Thimsen et al., 2014)(Hamborg et al., 2014). A second MEA campaign (MEA2) was conducted from July to October 2015 with the main objectives including the verification of mass balances and the revision of the verified baseline (Gjernes et al., 2017)(Faramarzi et al., 2017). In addition, a third MEA campaign (MEA3) was conducted mainly during summer 2017 (*The Third MEA Campaign at the CO₂ Technology Centre Mongstad*). During the MEA3 test campaign objectives included the development of control schemes and the impact of dynamic operations.

In the context of this Ph.D. project a collaborative framework was developed in order

to utilize and disseminate sets of data generated during MEA2, and to propose a set of transient tests that were conducted during July 2017 in MEA3. Data from MEA2 was selected, processed and employed for dynamic process model development and validation purposes. That work led to publications included in Paper II (Montañés, Flø, and Nord, 2017) and Paper VII (Montañés et al., 2017b) as well as scientific dissemination in presentations D and E (refer to Section 1.5.3). In Section 3.4.2, the methodology is explained and complementary information to paper II is presented. In addition, two sets of 48 hours of testing were suggested and performed at the amine plant at TCM DA during MEA3 test campaign, consisting on dynamic operation of the process and implementation of decentralized control structures. These results are presented in paper III (Montañés, Flø, and Nord, 2018). Section 3.4.3 shows the methodology followed for the proposal of tests and complementary information to the work conducted within this Ph.D. thesis in the context of the MEA3 test campaign.

3.4.1 Pilot plant description

The amine pilot plant installed at Technology Centre Mongstad has the capacity to capture 80 ton CO₂/day (29200 ton CO₂/year) with a flue gas volumetric flow capacity in the absorber column of around 60000 Sm³/hr. A picture with a view of the amine plant installed at TCM DA is shown in Figure 3.7. In addition, a simplified flow diagram of the amine plant at TCM DA is shown in Figure 3.8. The pilot plant has two stripper columns to accommodate the different CO₂ concentrations of flue gas coming from the catalytic cracker or from the CHP plant. In this section the pilot plant is described for the process configuration that treats CHP flue gas.

The power plant located next to the TCM DA and the Statoil refinery is a combined heat and power plant. The process configuration consists of two gas turbines which feed with exhaust gas to two heat recovery steam generators (HRSGs), which generate the process steam for the refinery and the steam for one steam turbine. The power plant has a capacity of around 280 MW_{el} of electricity and 350 MW_{th} of heat. The GTs are two GE 9001E and the typical composition contains around 3.5-3.7 vol% CO₂. At full volumetric flow capacity of the absorber column, a slipstream of around 3% of the total exhaust gas mass flow rate generated by the GTs is fed to the amine pilot plant at TCM DA with a flue gas blower. The blower has variable speed drives that allow the manipulation of mass flow rate sent to the inlet of the absorber column. The flue gas volumetric flow rate at the inlet of the absorber can be specified by means of the set-point of a PI feedback flow cascade controller; refer to FT1 in Figure 3.8. The flue gas is cooled down in the direct contact cooler (DCC), where the flue gas flows upwards while it meets a countercurrent stream of cooling water. The flue gas leaves the DCC saturated with water at the desired temperature. Then it is conducted towards the inlet of the absorber column. The CHP DCC consists of a packing material of Koch Glitsch Flexipack 3X with a cross-section of 3 m diameter and 3.1 m of height, and 16 m total height (Hamborg et al., 2014).

The absorber column consists of a 64 m absorber column. The column has a total of 24 m of absorber packing material divided in three packed sections: 12 m at the bottom, 6 m in the middle and 6 meters at the top. In addition, at the top of the absorber column there



FIGURE 3.7: Amine pilot plant at Technology Centre Mongstad. Image obtained from (*The Third MEA Campaign at the CO₂ Technology Centre Mongstad*). To the right the direct contact coolers. In the centre the absorber column (64-m-height) and to the left the two stripper columns.

are two waterwash packing sections (3 m and 3 m) that allow reducing solvent emissions and control the water mass balance of the plant. The absorber packing material consists of Koch Glitsch Flexipac 2X and has rectangular cross-section. The water wash sections consist of Koch Glitsch Flexipac 2Y HC. Table 3.3 shows data on the absorber column materials and geometry. It is possible to change the total packing height of the column by injecting all the mass flow of solvent at different heights by opening and closing the feed valves at different column heights, i.e. resulting in 12 m, 18 m or 24 m of packing height; refer to Figure 3.8. The chemical solvent is collected in the absorber sump at the bottom of the absorber column, and it acts as an integrated buffer tank during pilot plant operations. Liquid re-distributors, collectors and mesh mist eliminators are located at different locations along the absorber column (Hamborg et al., 2014). The depleted flue gas leaves the absorber column through the stack located at the top of the column.

The pilot plant has two main solvent circulation pumps with variable speed, the rich amine pump located downstream of the absorber sump and the lean amine pump located downstream of the stripper sump. An integration heat exchanger is placed in between the stripper and absorber column, in which the main stream of lean amine flow coming from the stripper sump heats up the main rich solvent stream. This helps to recover heat from the lean stream. It is a plate-and-frame heat exchanger with a total heat transfer area of 308 m². In addition, an amine cooler allows to control the lean solvent temperature at the fed to the inlet of the absorber column, by a stream of cooling water. It has a total heat transfer area of 78.8 m².

The CHP stripper column with reboiler and overhead condenser system allows the

TABLE 3.3: Direct contact cooler and absorber column of TCM DA amine plant: materials and geometry.

| Direct contact cooler | |
|---|-----------------------------|
| Column diameter [m] | 3 |
| Packing height [m] | 3.1 |
| Total height [m] | 16 |
| Packing material | Koch Glitsch Flexipack 3X |
| Absorber column | |
| Column Cross Sectional Area [m ²] | 3,55x2 |
| Packing height (12+6+6) [m] | 24 |
| Water Wash section height (3+3) [m] | 6 |
| Absorber packing type | Koch Glitsch Flexipac 2X |
| Absorber Washer packing type | Koch Glitsch Flexipac 2Y HC |

process of CO₂ recovering and to return the lean solvent flow towards the absorption section of the process. It consists of a column with a total of 30 m height and a diameter of 1.3 m. The packing material consists of Koch Glitsch Flexipack 2X structure stainless steel of 8 m height. In the upper section of the stripper column a water wash section with Koch Glitsch Flexipac 2Y HC structured stainless-steel packing material of 1.6 m of height. A liquid collector, re-distributor and mesh mist eliminator are located at different heights of the stripper column. A thermosifon steam-driven reboiler is located at the bottom of the stripper column. It has a size of 142 m² total heat transfer area. It allows to generate the stripping vapors and to regenerate the solvent. Lean amine accumulates in the stripper sump. A reflux drum, condenser and pumps are utilized to dry the CO₂ product coming from the overhead condenser. Data on materials and geometry of stripper column, reboiler, lean-rich heat exchanger and amine cooler are summarized in Table 3.4.

3.4.2 Selection of experimental data for dynamic process model development and validation

Data generated during the MEA2 test campaign at the amine plant at Technology Centre Mongstad was employed for dynamic process model validation purposes. The main steps of the methodology followed are presented in Figure 3.9 and described in this section.

I. Study of P&IDs and engineering drawings

The first step involved the detailed study of the P&IDs and the engineering drawings of the amine pilot plant at Technology Centre Mongstad. Piping and instrumentation diagrams (P&IDs) are common diagrams employed in the process industry to describe the main piping, equipment and vessels in the process flow, together with the instrumentation and controllers. The engineering drawings define the requirements and specifications

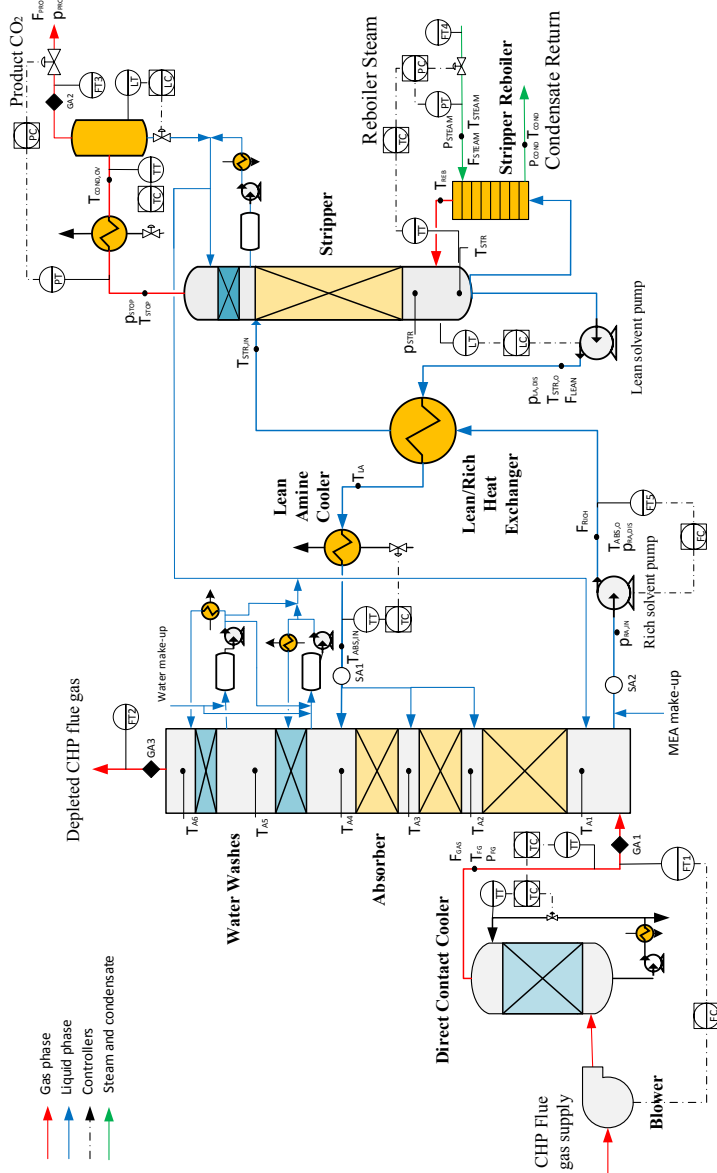


FIGURE 3.8: Flow diagram of the amine pilot plant at Technology Centre Mongstad when configured for CHP flue gas, obtained from (Montañés, Flø, and Nord, 2017).

TABLE 3.4: CHP stripper, reboiler and heat exchangers at the amine plant at Technology Centre Mongstad: materials and geometry.

| Stripper column | |
|--|-----------------------------|
| Column diameter [m] | 1.3 |
| Packing height [m] | 8 |
| Water Wash section height [m] | 1.6 |
| Total height [m] | 30 |
| Stripper packing type | Koch Glitsch Flexipac 2X |
| Stripper Washer packing type | Koch Glitsch Flexipac 2Y HC |
| Reboiler | |
| Total heat transfer area [m ²] | 142 |
| Material | SS 316L |
| Lean/Rich heat exchanger | |
| Total heat transfer area [m ²] | 308 |
| Material | SS 316L |
| Lean amine cooler | |
| Total heat transfer area [m ²] | 78.8 |
| Material | Titanium |

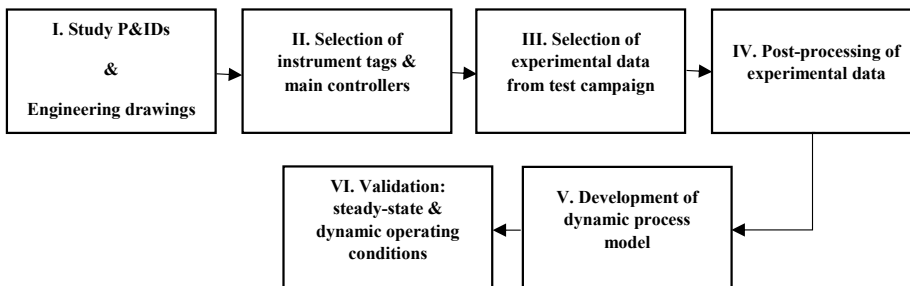


FIGURE 3.9: Methodology followed for data selection and dynamic process model development and validation with data from MEA campaigns at the amine plant at CO₂ Technology Centre Mongstad.

for the equipment at the pilot plant. The study of the P&IDs allowed to identify the main components of the system and to develop a simplified process flow sheet as the one in Figure 3.8. The actual pilot plant is more complex and contains several subsystems which might not be operated under normal operation (for example the carbon filter or the reclaiming unit) or that are not important from a dynamic process modeling perspective (passive safety controllers or valves for start-up or shut-down sequences). These are not included in the simplified flow diagram. In addition, the study of P&IDs allowed to understand the process configuration when the pilot plant is employing CHP flue gas (CHP stripper) and to identify the size, geometry and materials of different equipment, as presented in Table 3.3 and Table 3.4.

II. Selection of instrument tags and main controllers

The amine pilot plant at TCM is designed and operated for R&D purposes. This implies that the pilot plant is fully equipped with instruments for detailed evaluation and analysis of the process. Andersson et al. reported that the pilot plant is equipped with more than 1000 instruments (Andersson et al., 2013). This also involves the multiplicity of instruments for same process variables. An example of that is the gas analyzers for flue gas composition located at the inlet of the absorber column (GA1 in Figure 3.8), at the outlet of the absorber column (depleted flue gas GA3 in Figure 3.8) and rich product CO₂ flow; refer to GA2 Figure 3.8. As described in Faramarzi et al. there are multiple instruments for measuring the flue gas composition at the amine plant at the ground level instrument house (Faramarzi et al., 2017). These include non dispersive infrared units (NDIR), Fourier transform infrared (FTIR) and gas chromatographs (GC). These can measure the flue gas compositions in a near simultaneous fashion at the three locations and with the three methods. Measuring gas composition at different locations is a desired feature during dynamic operations of the process. Initially all the tags were selected and acquired, and then the instrumentation was selected based on published work from TCM DA such as (Faramarzi et al., 2017) and (Gjernes et al., 2017) or by conversations with TCM DA staff. In this work, at first a list of tags was suggested for data acquisition. The list contains around 300 tags, involving process variables of the process including (Montañés et al., 2017b):

- Gas analyzers at the inlet of the absorber, outlet of the absorber, and CO₂ rich to stack.
- Main liquid and gas flow rates.
- Main process temperatures, including absorber and stripper temperatures.
- Pressures and pressure drops at different components of the plant.
- Online solvent analysis measurements include pH, density and conductivity, at the inlet and outlet of the absorber (lean and rich solvent).
- Liquid hold-ups distribution at different components of the plant.

- Main active controller set-points and tuning parameters.

As described in Section 3.5.1, the main function of the regulatory control layer of a chemical plant is to stabilize the process and provide smooth operation (Skogestad and Postlethwaite, 2006). Basically the main objectives are to keep measured values at desired setpoints and to avoid excessive drifting of process variables in the presence of disturbances. It is a bottom layer in the hierarchy, and it is normally a decentralized control structure which can include cascaded control loops; refer to Section 3.5.1. The regulatory control layer normally involves the control of inventories (pressures and levels) and the control of temperatures and specification of flows. The main controllers of the regulatory control layer at TCM DA are shown in Figure 3.8. Following the methodology described by Aske and Skogestad on consistent inventory control (Aske and Skogestad, 2009), the rich solvent mass flow rate can be considered a throughput manipulator (TPM) that defines the solvent flow network, since the setpoint of rich solvent flow rate is specified manually by the operator in the control room thanks to the FT5 controller; refer to Figure 3.8. The lean solvent flow rate is then automatically manipulated by the stripper level feedback controller. The flue gas volumetric flow rate is specified by means of the cascade controller FT1, and a temperature cascade controller allows to control the temperature of the flue gas fed to the absorber column T_{FG} by means of the DCC system. In addition, the stripper overhead pressure can be controlled with a feedback control loop that manipulates the product CO₂ valve opening and the condensing temperature of the overhead condenser can be specified with the setpoint of the respective controllers. The lean amine temperature at the inlet of the absorber column is also specified with a feedback controller that manipulates a flow of cooling water in the lean amine cooler. In addition, stripper bottom temperature T_{STR} measured at the stripper sump, can be controlled by means of a cascaded controller in which the steam pressure is specified. The steam pressure correlates quite well with the steam mass flow rate and it is normally used by operators to manipulate the reboiler duty of the plant.

III. Selection of experimental data from test campaign

The data presented in paper II for dynamic process model validation was obtained from tests conducted at the amine plant of TCM DA with CHP flue gas operations during the test campaign MEA2. For steady-state dynamic process model validation, the objective is to find suitable sets of data that represent a wide range of steady-state operating conditions of the process. The steady-state data was logged with the IP21 system at TCM DA. Data was logged and data files were generated with data points every 30 seconds from the data acquisition system. Note that the time scales of operation that were of interests from a dynamic perspective were in the order of min-hours, so there was no need to generate data files for shorter time steps. Steady-state data sets involved periods of around 4-8 hours of steady-state operation. The data logged were the ones mentioned in point II of this methodology.

During MEA2, test series were conducted with parameter variations in terms of absorber packing, stripper bottom temperature and solvent flow rate, resulting in different capture rates ranging from 84.7% to 68.1%, when the plant was operated with CHP flue

gas and full flue gas volumetric flow rate capacity in the absorber column. These data sets correspond to tests 1 to 5 in paper II. As presented by Gjernes et al. (Gjernes et al., 2017), one of the objectives of MEA2 was to develop the so called u-curves (SRD vs T_{STR}) and (SRD vs L_{lean}), in which optimal conditions of the process (in terms of specific reboiler duty), for a given flue gas volumetric capacity and for a specified capture rate target (of 85%) are researched. For that, the stripper bottom temperature is specified (changed for creating different points) and the solvent flow rate is modified (tuned) to achieve the desired target capture rate. From these tests, tests 6 to 10 in Table 3 of paper II were selected. That would represent a variability in terms of L/G ratio in the absorber column and stripper bottom temperature for same target CO_2 capture rate (85%) and flue gas capacity of around $47000 \text{ Sm}^3/\text{hr}$. The reported minimum specific reboiler duty at the pilot plant with 30% aq. MEA, CHP flue gas and 85% capture rate is 3.60 MJ/kgCO_2 at $47000 \text{ Sm}^3/\text{hr}$ flue gas volumetric flow rate capacity (Gjernes et al., 2017) and 3.62 MJ/kgCO_2 with $59000 \text{ Sm}^3/\text{hr}$ flue gas flow rate capacity (Faramarzi et al., 2017). Therefore, the resulting sets of steady-state data represented a wide range of steady-state operating conditions in terms of: flue gas volumetric flow rate, L/G ratio in absorber column (or solvent flow rate), packing height, stripper bottom temperature T_{STR} and CO_2 capture rate. In addition, detailed distribution of solvent inventory though the plant was logged at steady-state process conditions and presented in paper II.

For dynamic process model validation, sets of transient data representing the main dynamics of the process are required. The open-loop step-change method is desired because it reduces data variability and allows the study of the effect of a disturbance/input change to the process on the rest of process variables, and also facilitates the task of dynamic process model validation. Transient tests were obtained from the MEA2 test campaign and presented in paper II for dynamic process model validation. The tests included changes in flue gas volumetric flow rate: ramp-down and ramp-up, solvent flow rate ramp-down and step-changes in steam pressure (reboiler duty).

IV. Post-processing of experimental data

A way for assessing the validity of industrial experimental data in thermodynamic and chemical systems is the use of data reconciliation methods. In this work a detailed data reconciliation method was not employed, however several measures were taken in order to reduce random errors in the data. The instrumentation quality is normally considered by: i) accuracy or bias error, which is the error associated between the measurement reading and the true value; or ii) the precision error which is associated with the variability of the instrument reading when process conditions do not change (random error). While in practise, data reconciliation methods focus on reducing the bias error, there are ways of reducing the random error, for example by carrying out time average of measurement readings. In this work the steady-state data presented in paper II and expanded (including more data) in this section was calculated based on 1 hour steady-state operating data for each of the steady-state cases presented. This helps to reduce the random error associated with measurements reading. In addition, CO_2 mass balance was checked during the data selection process during the steady-state performance of the plant with the selected

method presented in Gjernes et al. (Gjernes et al., 2017). Note that Gjernes et al. considers satisfactory CO₂ mass balance during steady-state operation of the process being close to 100% during the verification test series conducted during MEA2 (Gjernes et al., 2017). When a variable was giving non realistic values for a certain period of time, the averaged value during the previous 10 minutes of operation was given for that period of time. In addition, each of the process variables were plotted before calculating steady-state values. This allowed to identify failures in measurement readings due to recalibration of the instruments or data transfer stochastic errors. For example, a temperature measurement within the absorber column was giving constantly zero measurement reading, it was discarded from the averaged values in the radial plane.

The data logged was post-processed and prepared for dynamic process model validation purposes. The steady-state values of the process variables and calculated values were obtained by a time average of the variable during 1 hour of steady-state operation (with data points generated in data files every 30 seconds). The sets of data were presented in paper II, consisting of ten steady-state cases. A more complete set of steady-state data with more process variables than the one presented in paper II is presented in Table 3.5 and Table 3.6. Refer to Figure 3.8 to identify the location of the process variables included in the tables. It should be noted here that these sets of steady-state data were selected from the MEA2 campaign at TCM DA, and calculated with 1 hour of steady-state operation, which differ from the comprehensive data sets for baseline operating conditions in Hamborg et al. (Hamborg et al., 2014) and Faramarzi et al. (Faramarzi et al., 2017), which included third party verification protocols and larger number of operating hours.

Reboiler duty Q_{reb} was calculated considering the steam and condensate reboiler properties of enthalpy and steam mass flow rate, as expressed in Equation 3.14. Note that it has been reported in the literature (Bui et al., 2016) that the calculation of reboiler duty as in Equation 3.14 does not truly represent the regeneration energy due to effects from external factors such as fluctuating ambient temperature and heat losses through non-insulated pipes and equipment. However, it was decided to use this calculation method to be consistent with previous work at TCM DA (Hamborg et al., 2014)(Faramarzi et al., 2017)(Gjernes et al., 2017). The actual regeneration duty could be calculated considering the CO₂ desorption energy, sensible heat that brings the CO₂ absorbent to the reboiler solution temperature and the required heat to evaporate the water which is equivalent to latent heat of water condensation at the condenser (Bui et al., 2016).

$$Q_{reb} = \left(h(T_{steam}, p_{steam}) - h_{sat}(p_{steam}) \right) F_{steam} \quad (3.14)$$

The composition measurements shown in Table 3.5 were measured at GA1 and GA3 with the gas chromatographs gas analyzers, which report wet values of composition; refer to Figure 3.8. At the inlet of the absorber column $y_{i,in}$ for supply flue gas at GA1 and for depleted flue gas at the outlet of the absorber column $y_{i,dep}$ at GA3.

The temperature profiles within the absorber column packed segments were used for dynamic process model validation. The temperature profiles at TCM DA absorber column can be measured both in the axial and radial directions. Figure 3.10 shows the distribution of temperature measurements within absorber packing segments in the absorber column. The absorber has multiple temperature measurements in the same radial plane at

a given axial position within the column absorber packing material. There is a total of 96 temperature measurements within packing segments in the absorber column, with four temperature measurements distributed within the radial plane per meter of absorber column. Some of the measurements within the same radial plane are closer to the geometric center of the absorber packing, while others are closer to the wall, which leads to different readings in temperature measurements within a given radial plane. Note that the models employed for dynamic process modeling of the heat and mass transfer phenomena within the absorber column are based on the two-film theory approach with discretization in n volumes in the axial direction. Therefore, in order to generate the temperature profiles, averaged values of the four measurements readings at each axial position were employed. This means that each of the data points in the Figure 3.10 are averaged over time during steady-state conditions (1 hour of steady-state), of the averaged 4 temperature measurements radially distributed within the absorber column at the given axial position of the column. The temperature profiles along the absorber column shown in Figure 3.10 are for Case 1 and Case 6 in Table 3.5 and Table 3.6, and were employed for dynamic process model validation in paper II. One temperature sensor was not working during these tests and was giving a zero value of the measurement, therefore the reading of that value was discarded during calculation of temperature profiles.

The temperature profiles at TCM DA stripper column were also utilized for dynamic process model validation. At the pilot plant, as for the absorber column, these can be measured both in the axial and radial directions. Figure 3.11 shows the distribution of temperature measurements within the stripper packing segment in the stripper column. There is a total of 28 temperature measurements within packing segments in the absorber column, with four temperature measurements distributed within the radial plane per meter of absorber column. Some of the measurements are located closer to the center and some others closer to the wall. This means that each of the data points in the Figure 3.11 are averaged over time during steady-state conditions, of the averaged 4 temperature measurements radially distributed within the stripper column at the given axial position of the column. The temperature profiles along the stripper column shown in Figure 3.10 are for Case 1 and Case 6 in Table 3.5 and Table 3.6, and were employed for dynamic process model validation in paper II.

V. Development of dynamic process model

The dynamic process models of process equipment for the chemical absorption process with MEA were obtained from the GasLiquidContactors library (*Modelon Gas Liquid Contactors Library*). The dynamic process models are described in paper II. The dynamic process model of TCM DA amine plant was developed following a step-by-step approach. The process plant was divided in three main subsections:

- Absorber column with sump and rich pump.
- Lean rich heat exchanger and amine cooler.
- Stripper column with overhead condenser, reboiler and lean amine pump.

TABLE 3.5: I. Steady-state data at the amine pilot plant at TCM DA with 30 wt% aqueous MEA during test campaign MEA2. The data includes a more complete set of process variables than the one presented in paper II (Montañés, Flo, and Nord, 2017). The process variables names refer to the ones in Figure 3.8.

| Process variable | Case 1 | Case 2 | Case 3 | Case 4 | Case 5 | Case 6 | Case 7 | Case 8 | Case 9 | Case 10 |
|------------------------------------|---------|---------|---------|---------|---------|---------|---------|---------|---------|---------|
| F_{gas} (Sm ³ /hr) | 59461 | 59468 | 59442 | 59499 | 59544 | 46973 | 46973 | 46973 | 46973 | 46973 |
| F_{rich} (kg/hr) | 62388 | 62301 | 61988 | 55808 | 62057 | 73998 | 62996 | 58005 | 45851 | 41247 |
| Q_{reb} (kW) | 3417 | 3159 | 2664 | 2397 | 3056 | 2745 | 2669 | 2667 | 2659 | 2682 |
| $y_{CO_2,in}$ (vol%) | 3.64 | 3.61 | 3.59 | 3.58 | 3.59 | 3.60 | 3.62 | 3.62 | 3.62 | 3.62 |
| $y_{O_2,in}$ (vol%) | 15.52 | 15.54 | 15.55 | 15.46 | 15.35 | 15.30 | 15.48 | 15.49 | 15.51 | 15.52 |
| $y_{H_2O,in}$ (vol%) | 3.98 | 3.92 | 3.93 | 4.01 | 4.22 | 3.80 | 3.36 | 3.46 | 3.52 | 3.43 |
| $y_{N_2,in}$ (vol%) | 79.09 | 79.02 | 78.85 | 78.57 | 78.20 | 78.18 | 78.88 | 78.94 | 79.06 | 78.96 |
| L_{lean} (mol/mol) | 0.280 | 0.294 | 0.333 | 0.341 | 0.314 | 0.342 | 0.329 | 0.310 | 0.260 | 0.229 |
| L_{rich} (mol/mol) | 0.490 | 0.485 | 0.498 | 0.500 | 0.495 | 0.475 | 0.488 | 0.486 | 0.493 | 0.491 |
| F_{prod} (kg/hr) | 3412.8 | 3192.3 | 2714.7 | 2458.8 | 3013.5 | 2651.9 | 2658.8 | 2695.5 | 2763.5 | 2729.2 |
| L/G ratio (kg/kg) | 0.89 | 0.89 | 0.89 | 0.80 | 0.89 | 1.34 | 1.14 | 1.05 | 0.83 | 0.75 |
| T_g (°C) | 30.3 | 30.2 | 30.6 | 30.5 | 31.3 | 29.2 | 27.6 | 27.9 | 28.1 | 27.6 |
| p_g (barg) | 0.046 | 0.046 | 0.046 | 0.046 | 0.047 | 0.031 | 0.030 | 0.030 | 0.029 | 0.029 |
| $y_{CO_2,dep}$ (vol%) | 0.54 | 0.61 | 1.14 | 1.39 | 0.88 | 0.56 | 0.56 | 0.52 | 0.45 | 0.53 |
| $y_{O_2,dep}$ (vol%) | 15.81 | 15.81 | 15.71 | 15.57 | 15.55 | 15.57 | 15.74 | 15.82 | 15.85 | 15.80 |
| $y_{H_2O,dep}$ (vol%) | 4.52 | 4.41 | 4.42 | 4.50 | 4.82 | 4.20 | 3.86 | 3.84 | 3.88 | 3.86 |
| F_{lean} (kg/hr) | 59190.8 | 59194.7 | 59200.8 | 53100.5 | 59001.4 | 71102.0 | 59940.5 | 55779.4 | 42871.2 | 38563.0 |
| $T_{abs,t}$ (°C) | 36.8 | 36.8 | 36.8 | 36.8 | 36.8 | 36.8 | 36.8 | 36.8 | 36.8 | 36.7 |
| ρ_{lean} (kg/m ³) | 1073.8 | 1078.5 | 1089.0 | 1089.3 | 1083.2 | 1091.1 | 1086.7 | 1082.1 | 1068.4 | 1062.0 |
| $T_{abs,o}$ (°C) | 34.2 | 35.0 | 34.6 | 34.3 | 35.6 | 34.2 | 32.1 | 32.2 | 32.2 | 31.6 |
| $T_{a,1}$ (°C) | 33.9 | 35.1 | 34.7 | 34.1 | 35.5 | 35.6 | 33.2 | 32.9 | 31.3 | 30.5 |
| $T_{a,2}$ (°C) | 40.4 | 48.4 | 44.1 | 41.1 | 46.2 | 45.7 | 41.6 | 40.7 | 37.3 | 34.9 |
| $T_{a,3}$ (°C) | 47.3 | 49.4 | 47.1 | 45.6 | 48.5 | 51.0 | 48.1 | 47.6 | 45.1 | 42.6 |
| $T_{a,4}$ (°C) | 40.3 | 40.1 | 38.8 | 37.8 | 39.1 | 36.4 | 36.9 | 38.3 | 39.8 | 38.4 |
| $T_{a,5}$ (°C) | 38.7 | 39.1 | 37.0 | 35.8 | 38.5 | 36.7 | 36.5 | 37.0 | 37.4 | 36.8 |
| $T_{a,6}$ (°C) | 31.5 | 31.3 | 31.3 | 31.6 | 32.8 | 29.8 | 28.9 | 28.9 | 29.0 | 29.0 |

TABLE 3.6: II. Steady-state data at the amine pilot plant at TCM DA with 30 wt% aqueous MEA during test campaign MEA2. The data includes a more complete set of process variables than the one presented in paper II Montañés, Flø, and Nord, 2017. The process variables names refer to the ones in Figure 3.8.

| Process variable | Case 1 | Case 2 | Case 3 | Case 4 | Case 5 | Case 6 | Case 7 | Case 8 | Case 9 | Case 10 |
|------------------------------------|--------|--------|--------|--------|--------|--------|--------|--------|--------|---------|
| T_{la} (°C) | 43.3 | 44.3 | 43.7 | 43.0 | 44.7 | 43.4 | 41.2 | 41.1 | 40.4 | 39.5 |
| $T_{str,in}$ (°C) | 110.5 | 110.6 | 108.6 | 108.5 | 109.7 | 106.4 | 107.7 | 108.7 | 111.4 | 112.1 |
| T_{stro} (°C) | 120.8 | 120.9 | 118.9 | 118.5 | 119.9 | 116.5 | 118.0 | 118.8 | 120.9 | 121.5 |
| ρ_{rich} (kg/m ³) | 1124.4 | 1126.7 | 1128.5 | 1129.3 | 1126.9 | 1123.5 | 1126.9 | 1125.5 | 1126.2 | 1125.9 |
| F_{steam} (kg/hr) | 5379.9 | 5344.3 | 4368.4 | 3899.5 | 4947.1 | 4453.9 | 4325.1 | 4329.8 | 4314.4 | 4334.7 |
| T_{steam} (°C) | 153.5 | 153.2 | 152.5 | 146.9 | 159.6 | 150.3 | 151.6 | 152.4 | 152.9 | 157.5 |
| p_{steam} (barg) | 2.05 | 2.09 | 1.82 | 1.71 | 1.967 | 1.73 | 1.75 | 1.76 | 1.85 | 1.85 |
| T_{cond} (°C) | 132.8 | 133.4 | 130.6 | 129.4 | 131.9 | 129.1 | 129.6 | 129.8 | 131.0 | 131.1 |
| p_{cond} (barg) | 1.96 | 2.02 | 1.75 | 1.65 | 1.88 | 1.66 | 1.68 | 1.69 | 1.78 | 1.79 |
| p_{stop} (barg) | 0.903 | 0.904 | 0.913 | 0.909 | 0.905 | 0.908 | 0.906 | 0.908 | 0.905 | 0.904 |
| T_{stop} (°C) | 96.1 | 96.8 | 94.9 | 94.5 | 96.0 | 94.1 | 94.4 | 94.9 | 96.2 | 97.3 |
| $T_{cond,ov}$ (°C) | 19.5 | 20.6 | 20.4 | 20.4 | 19.9 | 20.5 | 20.6 | 20.1 | 20.0 | 20.4 |
| T_{str} (°C) | 120.9 | 121.1 | 119.1 | 118.9 | 120.1 | 116.6 | 118.3 | 119.1 | 121.4 | 121.8 |
| T_{reb} (°C) | 125.2 | 125.6 | 123.9 | 123.5 | 124.6 | 122.5 | 123.3 | 123.6 | 124.5 | 124.6 |
| p_{prod} (barg) | 0.017 | 0.017 | 0.017 | 0.017 | 0.017 | 0.0115 | 0.0117 | 0.0119 | 0.0112 | 0.0119 |
| p_{str} (barg) | 0.950 | 0.950 | 0.950 | 0.949 | 0.949 | 0.950 | 0.949 | 0.949 | 0.950 | 0.950 |
| $p_{ra,dis}$ (barg) | 6.73 | 6.69 | 6.61 | 6.02 | 6.58 | 6.32 | 5.68 | 5.39 | 6.28 | 6.13 |
| $p_{ra,in}$ (barg) | 0.450 | 0.451 | 0.454 | 0.460 | 0.453 | 0.347 | 0.364 | 0.376 | 0.393 | 0.393 |
| $p_{la,dis}$ (barg) | 7.27 | 7.09 | 7.09 | 6.28 | 5.30 | 6.56 | 5.93 | 5.73 | 5.26 | 6.83 |

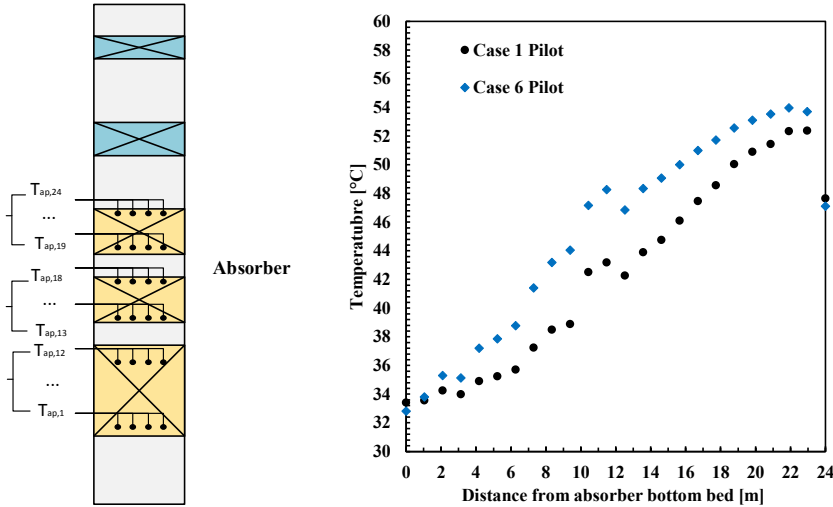


FIGURE 3.10: Temperature sensors distribution within absorber packing segments at the absorber column at CO₂ Technology Centre Monstad amine pilot plant. There are four temperature sensors (elements) per meter of absorber column packed segments. This results in 12 elements in the 12 m bottom packing with temperatures from T_{ap1} to T_{ap12} ; 6 temperature elements in the 6 m middle packing segment with temperatures from T_{ap13} to T_{ap18} ; and 6 temperature elements in the 6 m top packing segment with temperatures from T_{ap19} to T_{ap24} .

The models of the different subsections were developed separately by initializing, parameterizing, calibrating and testing each of the submodels. In addition, proper boundary conditions were specified for each of the submodels. Data parameterization involved the selection of flow media, materials and geometries of different equipment. In addition, initial values were given considering the reference data for process model calibration. In this case, the steady-state operating conditions from case 1 in paper II were utilized as reference data for model development and calibration, and for specifying the boundary conditions of the submodels. This process conditions were selected because they represent close to design conditions (full volumetric flow rate capacity of the absorber column with target CO₂ capture rate of 85%), and it also corresponds with the baseline case presented by Faramarzi et al. (Faramarzi et al., 2017).

For the absorber column subsection, the main tuner for model calibration was a pre-multiplying factor for enhancement factor; refer to paper II. The model was tested by carrying out simulations and comparing the outputs from the simulation of the dynamic process model under final and stable steady-state operating conditions and the reference

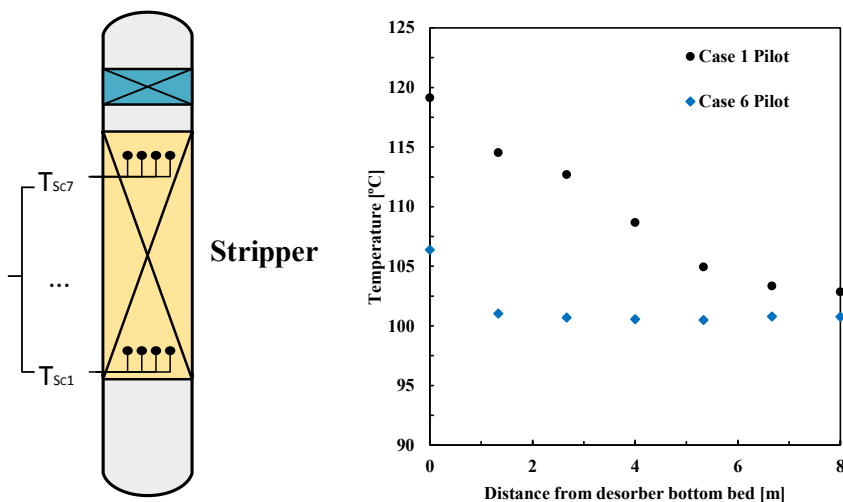


FIGURE 3.11: Temperature sensors distribution within stripper packing segments in the CHP stripper column at CO₂ Technology Centre Monstad amine pilot plant. There are four temperature sensors (elements) per meter of stripper column packed segment. This results in 7 elements in the 8 m packing with temperatures from T_{sc1} to T_{sc7} .

data. The process variables checked included CO₂ absorption rate, rich loading, absorber temperature profile and pressure drop. By modifying C_{ef} the model was fine tuned to get a good compromise between model outputs and reference data.

The lean-rich heat exchanger was modeled with the ϵ -number of transfer units approach; refer to literature on heat exchanger modeling for detailed formulation (Shah and Sekulić, 2003). It was necessary to fine tune the overall heat transfer coefficient by a pre-multiplying factor in order to match the four terminal temperatures in the lean-rich heat exchanger. So again, an iterative process on model tuning was employed. It was found during dynamic process model validation with transient plant data that it was required to add pure transport property delay models within piping to properly predict dead times within the recycle loops. These models were included with lumped volume for heat exchanger piping and piping of lean and rich solvent with data from TCM amine plant. The resulting dead time is equivalent to the residence time within the pipes.

The stripper column with reboiler and overhead condenser subsection was also tested separately. The main tuner for model calibration was a pre-multiplying factor for enhancement factor. The model was tested by carrying out simulations and comparing the outputs from the simulation of the dynamic process model under final and stable

steady-state operating conditions and the reference data. The process variables checked included CO₂ desorption rate, lean loading, stripper temperature profile, stripper bottom temperature and pressure drop. By modifying C_{ef} the model was fine tuned to get a good compromise between model outputs and reference data.

The step-by-step approach allows to isolate different parts of the system model and reduces the propagation of deviations in prediction from some process submodels to other process submodels. The subcomponents of the system are then joint to develop the final dynamic process model of the amine plant at TCM, also implementing the equivalent regulatory control layer of the process and closing and tuning control loops for stabilization of liquid levels and process variables. In addition, it is of importance for dynamic process simulation results to properly parameterize and implement the solvent inventory (hold-up) distribution within the process.

VI. Validation: Steady-state and dynamic operating conditions

The methodology presented in Section 3.3 was employed. Simulations of the dynamic process model were conducted in Dymola software. Simulated results in Dymola (*Dymola systems engineering*) were then exported to Microsoft Excel environment and plotted against the experimental data. Note that in paper VIII another tool was employed. The dynamic process model of TCM DA amine plant was exported as a Functional Mockup Unit (FMU) via the Functional Mockup Interface (FMI) technology export capabilities of Dymola. Then the FMU was imported and simulated in a Microsoft Excel Add In. That allowed to carry out batch simulations (for the different steady-state cases) and automatize a spreadsheet or dynamic process model validation.

The calibrated model against the Case 1 steady-state operating conditions in Table 3.5 and Table 3.6 was then simulated for the different process conditions in cases 1 to 10. In paper II the deviations between the process experimental data and the predictions by the dynamic process model were calculated for steady-state operating conditions, by means of absolute percentage errors and mean absolute percentage errors. The main process variables considered were rich loading L_{rich} , lean loading L_{lean} , CO₂ product flow F_{prod} , specific reboiler duty SRD and stripper bottom temperature T_{STR} . Details on the results can be found in paper II.

In addition, dynamic process model validation of the model with transient plant data was conducted. In the work, input trajectories were employed for dynamic process model validation purposes. The input trajectories measured at the pilot plant in terms of i) flue gas volumetric flow rate F_{gas} , ii) solvent mass flow rate F_{rich} and iii) reboiler duty Q_{rebr} were utilized as time series inputs/disturbances to the dynamic process model. The transient response of the dynamic process model was plotted together with the measured transient responses of the pilot plant during the transient tests. Refer to paper II for details on the results. The dynamic process model was employed for carry out two test studies at this plant scale: open-loop step responses and performance of decentralized control structures; refer to paper II. In addition, the dynamic process model was employed for preparing the test matrixes and the dynamic tests during MEA3 testing presented in paper III.

3.4.3 Transient testing at Technology Centre Mongstad

During MEA3 testing at Technology Centre Mongstad two sets of 48 hours of testing were employed for dynamic testing. The tests were conducted during the week of 17 to 23 July 2017. One set of tests was dedicated to open-loop testing while others to the evaluation of performance of decentralized control structures. The results from the tests are presented in paper III. The tests were prepared by simulating the process conditions by means of the validated dynamic process model; refer to Section 3.4.2. The initial steady-state conditions for the tests were selected to have the process being operated at full load (flue gas volumetric flow of $60000 \text{ Sm}^3/\text{hr}$) with close to optimal operating conditions with a CO_2 capture rate of 85%, which would correspond with the baseline process conditions presented by Faramarzi et al. (Faramarzi et al., 2017).

The advantages of carrying out simulations to prepare tests are multiple. It allows to plan properly the desired process conditions and do an estimation of required times for each test. In addition, it helps to illustrate and explain the purpose of the tests to the plant operating staff and process engineers working at the plant, before the tests are conducted. It can also assist on doing a preliminary analysis of the process performance to select the most interesting tests to be conducted at the plant. In addition, it can help to provide a starting point for tuning of controllers if there is not time to do controller tuning at the process plant.

There were several challenges associated with planning the tests at the amine pilot plant. First of all, the desired process conditions can be different than the ones achievable at the process plant during the process planning. It happened that during a significant amount of time of the testing week from 17 to 23 July 2017 the fuel utilized at the gas turbines of the upstream CHP power plant at Mongstad contained refinery gas, which lead to higher CO_2 concentration than expected (ca. 4.1 vol% CO_2 instead of ca. 3.6 vol% CO_2). That lead to different resulting process conditions at the beginning of the tests. In addition, each set of 48 hours of testing was conducted during two days in a row. During a 24-hour period, engineers are available 8 hours at the facility. This means that only during those 8 hours significant disturbances could be applied to the plant, while smaller disturbances could be applied during the rest of the hours. In addition, shift between operators were happening during different part of the tests. Other challenges related to process operating conditions are related to the difficulty to predict the total solvent inventory of the process, and that is of importance for transient performance of the process, specially when doing tuning of controllers based on dynamic process simulation.

Therefore the methodology followed the steps of i) defining the objectives of the transient tests; ii) developing the test matrix with support of the dynamic process model; iii) proposal of test matrix for open-loop testing and decentralized control structures; iv) attending at the pilot plant during tests; v) post-processing of experimental results and analysis.

Planning of open-loop tests with dynamic process simulation

The purpose of the dynamic tests was to investigate the transient performance of the amine PCC pilot plant by implementing open-loop set-point changes. The idea with

open-loop transient testing is to change one input/disturbance to the process at a time, in order to observe the transient response of important process variables to the disturbances applied. This approach helps to minimize the impact of control on the transient response of the process, so that the main process dynamics can be studied and explained. It also reduces data variability; refer to Section 3.5.2. The main input selected for this analysis was the rich solvent flow rate change and the flue gas volumetric flow rate. It was done for different flue gas capacities (100% and 78% F_{gas}) and different L/G ratios of the plant.

Figure 3.12 shows the results of the open-loop tests applied to the dynamic process model of the amine plant. The vertical line shown at time 1 hour shows the beginning of the tests. Flue gas flow rate and solvent flow rate are considered the main input/disturbances; refer to Figure 3.12a. Six tests were conducted, and results of the tests applied to the amine plant are presented in paper III. In addition, Figure 3.12b shows the simulation results for CO₂ absorbed and CO₂ desorbed and Figure 3.12c shows the transient results for CO₂ lean loading and CO₂ rich loading.

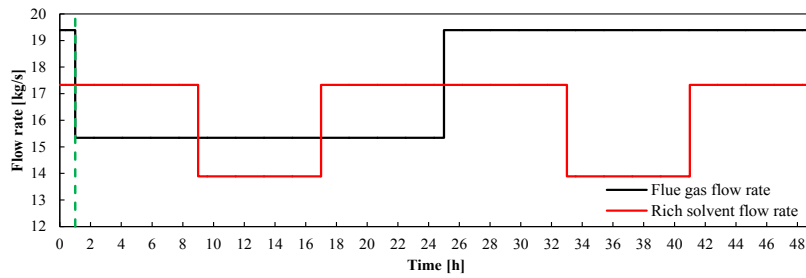
During the open-loop at the pilot plant it became clear that the regulatory control layer of the amine pilot plant at TCM was tuned conservatively with slow responses. The main purposes of previous testing during MEA1 and MEA2 was on steady-state performance of the process, for example to find u-curves or establishing baselines for plant operation with aqueous monoethanolamine (Gjernes et al., 2017). This could be observed for the very slow closed-loop response of the flow cascade controllers for flue gas volumetric flow rate (FT1 in Figure 3.8) and rich solvent flow rate FT5 in Figure 3.8. Even if the set-point of FT1 and FT5 was changed in a step manner, the resulting measured changes in flow rate was slower and with oscillations over the final set-point. This is due to the tuning parameters of the PI controllers implemented in the regulatory control layer for the cascade flow controllers. There was no time to fine tune these controllers before conducting the transient tests presented in this work.

Planning of decentralized control structure tests with dynamic process model simulation

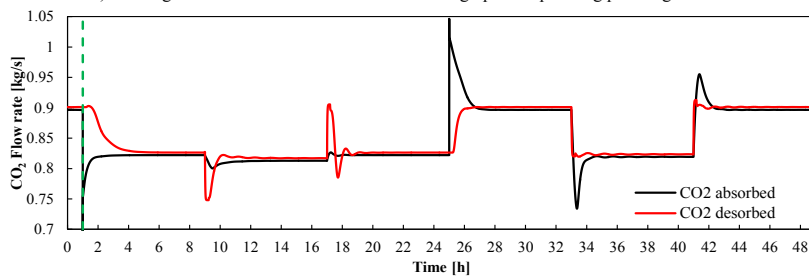
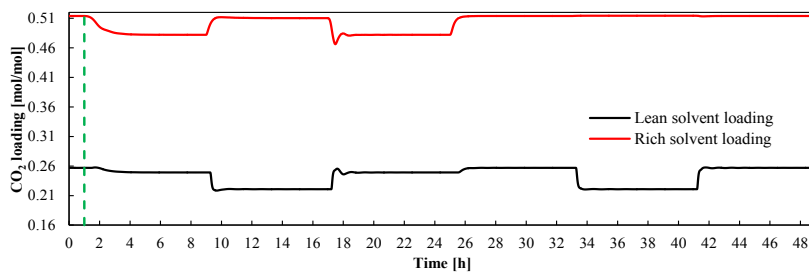
The purpose of this study was to analyze the performance of decentralized control structures of the TCM DA amine plant, during load changes of the power plant. This was performed at TCM by changing the flue gas volumetric flow rate with the blower (upstream DCC), at a given rate of change. The rate of change (ramp rate) was defined in order to represent realistic operation of the power plant. It consisted of 10%/min load reduction (refer to paper III for details on ramp rate and magnitude of the load change). The plant was initially operated at steady-state under baseline conditions of MEA-2. Flue gas volumetric flow rate was ramped down and up.

Two decentralized control structures were tested. Control structure A was tested during the initial 24 hours of testing for flue gas volumetric flow ramp down and ramp up, while control structure B was tested from test hour 24 to test hour 48 for flue gas volumetric flow ramp down and up. The tests were simulated with a validated dynamic process model.

The key manipulated variables (MVs) were (i) mass flow rate of rich solvent and (ii)



a) Flue gas flow rate and solvent flow rate during open-loop testing planning simulations.

b) CO₂ absorbed and CO₂ desorbed during open-loop testing planning simulations.c) Lean and rich CO₂ loadings during open-loop testing planning simulations.FIGURE 3.12: Dynamic process simulations for open-loop testing planning at the amine plant at CO₂ Technology Centre Mongstad.

steam to reboiler. The controlled variables (CVs) were (i) CO₂ capture rate; (ii) stripper bottom temperature; and (iii) liquid-to-gas ratio in the absorber column.

- **Control structure A:** implemented from 0 h to 24 h of testing. The main pairings consist of: i) mass flow rate of rich solvent (MV) to control *L/G* ratio in absorber column. Note: This is implemented by ramping down (and up) solvent mass flow rate to a new set-point, that will keep the *L/G* ratio constant at steady-state conditions. Solvent flow rate is ramped down and up simultaneously as the flue gas flow rate is ramped down and up. ii) steam mass flow rate (MV) to control stripper bottom temperature.
- **Control structure B:** implemented from hour 24 to hour 48 of testing. The main pairings consist of: i) mass flow rate of rich solvent (MV) to control CO₂ capture rate (refer to Eq. 3.15). Note: This control loop had to be added in the plant control system. ii) steam mass flow rate (MV) to control stripper bottom temperature.

For these tests to be conducted, it was needed to include one additional control loop in control structure B (capture rate controller), to the typical control structure utilized at the amine plant. The controller for stripper bottom temperature is not normally activated, and the steam flow rate is manually changed by the operators by changing the steam pressure set-point. Since there was limited time for preliminary tests to tune the capture rate controller, it was decided to utilize the validated dynamic process model to provide preliminary values for feedback controller tuning. Capture rate was defined with Method 1 in Faramarzi et al. (Faramarzi et al., 2017). The capture rate was calculated for the controller as the ratio between product CO₂ flow rate and the CO₂ supply flow rate, as in Eq. 3.15:

$$Cap_a = \frac{CO_2 product}{CO_2 supply} \quad (3.15)$$

The idea was to use the set-point of the rich pump mass flow rate (which is already on cascade control with FT1 in Figure 3.8) as a manipulated variable to control the calculated Cap_a . This means that there was a series cascade controller:

- **Slave:** pump speed to control rich solvent flow rate.
- **Master:** set-point of rich solvent flow rate of FT1 controller to control Cap_a .

The controller was tuned using the SIMC tuning rules (Skogestad and Postlethwaite, 2006) and simulations with the validated dynamic process model. An open-loop step change of 10% in solvent flow rate was done applied to the dynamic process model, and based on the open-loop response in the control variable Cap_a , the tuning parameters were calculated considering the following formulas 3.16, 3.17 and 3.18, where θ is the dead time, y is the response of Cap_a , u is the input (F_{rich} rich solvent flow rate), τ_1 is the time from which the process variable y starts to respond until it reaches $y_o + \Delta y * (1-1/e)$. The subscript f stands for final while the subscript o stands for initial. The controller tuning

TABLE 3.7: Calculated tuning parameters for controller Cap_a . Resulting controller values for tight, middle, smooth and conservative values of tuning parameter τ_c

| Tuning parameters | Tight | Middle | Smooth | Conservative |
|-------------------|-------|--------|--------|--------------|
| τ_c (min) | 5 | 10 | 15 | 25 |
| K_c [%/%] | 0.4 | 0.2 | 0.14 | 0.08 |
| τ_I (min) | 8 | 8 | 8 | 8 |

parameters are K_c and τ_I . Note that τ_c denotes the desired closed-loop time constant, which has to be decided.

$$K = \frac{\Delta y}{\Delta u} = \frac{y_f - y_o}{u_f - u_o} \quad (3.16)$$

$$K_c = \frac{1}{K} \cdot \frac{\tau_I}{\theta + \tau_c} \quad (3.17)$$

$$\tau_I = \min\{\tau_I, 4 \cdot (\tau_c + \theta)\} \quad (3.18)$$

From open-loop testing responses to set-point change in solvent flow rate at the amine pilot plant, it was observed a time constant of 3-5 min in the actual response of solvent flow change to the set-point change. This is the slave controller in this cascade (inner). Normally, it is desired to have a good time scale separation in terms of closed-loop time constant between slave and master (this is basically τ_c in the outer controller that is being used as a tuning parameter). A rule of thumb is a larger value by a factor of at least five (Skogestad and Postlethwaite, 2006). Therefore, it was decided to start with a value of τ_c of 15-25 min. The Table 3.7 shows the resulting values for proportional and integral tuning values K_c [%/%] and τ_I min.

Figure 3.13 and Figure 3.14 show the responses of controlled variables and manipulated variables to disturbances in flue gas flow rate for the following scenario: at time $t = 0$, flue gas flow rate is ramped down from 100 % volumetric flow capacity (60000 Sm³/hr) to 80% (47000 Sm³/hr), in 2 minutes. At time $t = 480$ min, the flue gas flow rate is ramped up to 100 % capacity in 2 minutes. The responses are shown for the controllers in Table 3.7 with tight, middle and smooth controller tuning. This shows the effects of the controller tuning on the responses of the process to the described disturbances.

3.5 Selection and evaluation of control structures and transient performance

3.5.1 Control structures for the PCC process

Decentralized control structures of the chemical absorption process were selected from previous studies in the literature to test them at the pilot plant at Technology Centre

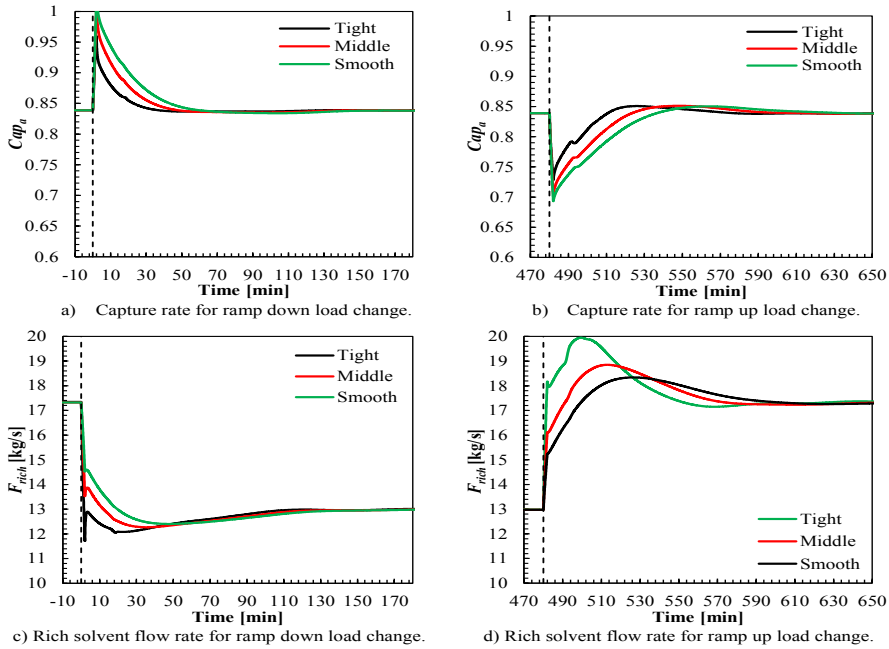


FIGURE 3.13: Response of controlled variables Cap and input rich solvent flow rate F_{rich} , for disturbance in flue gas volumetric flow rate. Different curves are obtained from different tuning parameters of the capture rate controller as presented in Table 3.7.

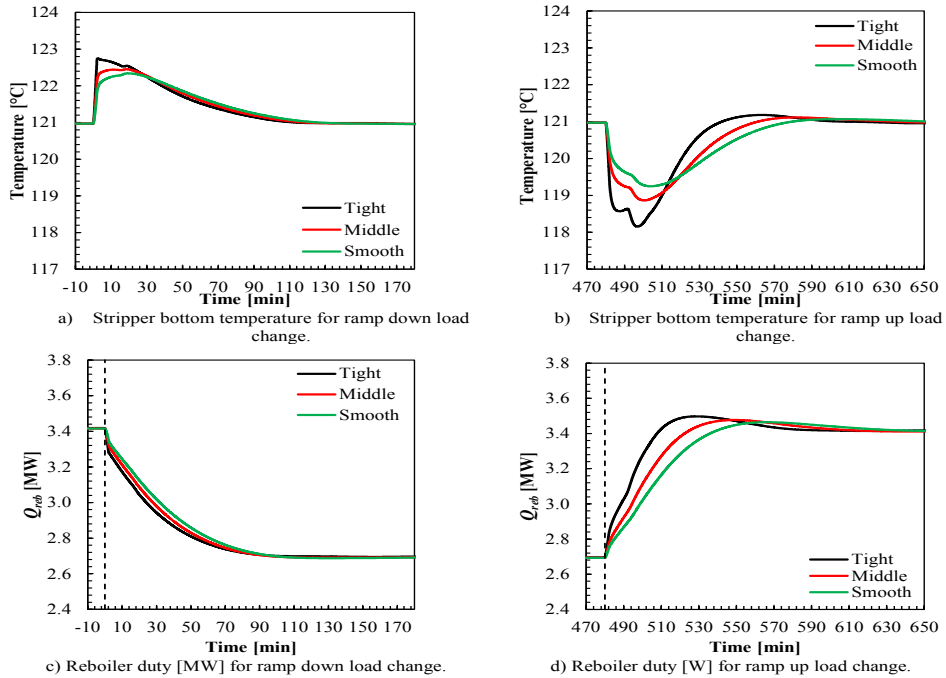


FIGURE 3.14: Response of controlled variables stripper bottom temperature T_{STR} and input reboiler duty Q_{reb} , for disturbance in flue gas volumetric flow rate. Different curves are obtained from different tuning parameters of the capture rate controller as presented in Table 3.7.

Mongstad, via a case study with dynamic process model simulations in paper II and via experimental transient testing in paper III. In addition, the performance of the control structures was evaluated with the scaled-up process integrated with the NGCC power plant in paper V. The control structures to study were selected based on previous works available in the literature. In paper V the control structure of the combined cycle power plant was explained.

The control system of a process plant is normally designed in a hierarchical manner (Kehlhofer et al., 2009)(Skogestad and Postlethwaite, 2006). As described in paper V, the control layer of a chemical and a power plant can be divided in two main layers, the supervisory control layer and the regulatory control layer:

- Supervisory control layer: It takes care of control variables which are of importance from an overall point of view in the longer time scale. It is a slower upper layer that acts on the set-points of the regulatory control layer or remaining degrees of freedom. This layer is in charge of supervising load changes.
- Regulatory control layer: It takes care of stabilizing drifting variables under fast disturbances and keeps these variables close to their set-points in the fast timescale. Stabilization means that the process does not drift away from acceptable operating conditions under disturbances. In practice, it implies controlling temperatures, pressures, and levels. In addition, it is of importance to have a consistent inventory control layer (Aske and Skogestad, 2009).

Rules for consistent inventory control (Aske and Skogestad, 2009) were applied when designing the regulatory control layer of the chemical absorption process in paper V. In paper II an equivalent control layer was implemented in the dynamic process model of the amine pilot plant at TCM. The location of the throughput manipulator (TPM) of the plant needs to be selected. In the amine plant at TCM it is the rich solvent mass flow rate set-point that defines the solvent flow network, while the lean solvent mass flow rate is on level control of the stripper sump. The common way of operation of the chemical process at the amine pilot plant is to change the set-point of rich solvent mass flow rate during parametric testing. The location of the TPM in the rich solvent flow rate follows from that the absorber sump at TCM also has the function of surge tank. However, in the PCC unit of the NGCC power plant in paper V the TPMs were located as the lean solvent flow rate at the inlet of the absorber column, since the surge tank was located in between the lean amine cooler and the lean rich heat exchanger in the recycle loop. The main pairings of the regulatory control layer of the amine pilot plant at TCM are shown in Figure 3.8. For the PCC unit of the NGCC power plant these are shown in Figure 5 of paper V.

The supervisory control layer for the absorption-desorption process has two main degrees of freedom: the solvent mass flow rate and reboiler duty. The degrees of freedom are employed to control different process variables, depending on the operational strategy of the plant. Based on a literature study, the following control structures were selected for evaluation. Panahi and Skogestad (Panahi and Skogestad, 2011)(Panahi and Skogestad, 2012) carried out a plantwide control design procedure based on self-optimizing control theory (Skogestad and Postlethwaite, 2006) for the CO₂ capture process with chemical

absorption. The study concluded that the main self-optimizing control variables of the process for economic performance under off-design operating conditions were keeping the capture rate constant Cap and a temperature within the stripper column. In this work Cap and stripper bottom temperature T_{str} were selected as controlled variables. In addition, control structures in which keeping capture rate constant was not an operational objective were studied. These include keeping constant L/G ratio via feedforward control or ratio control, and keeping the solvent flow rate constant at off-design conditions. By combinations of the degrees of freedom or manipulated variables (MV) and the controlled variables (CV) the following control structures were studied. The nomenclature employed here corresponds with the nomenclature in paper V. In Table 3.8 an explanation of how the control structures were implemented in papers II, III and V is presented. All control structures were tested in paper V, while a selection of control structures were tested in papers II and paper III. The feedback control loops were tuned by means of the SIMC tuning rules (Skogestad and Postlethwaite, 2006).

- Control structure A uses solvent flow rate F_{solv} to control capture ratio at the top of the absorber Cap defined by the ratio between absorption rate in the absorber column and the CO_2 supply to the column. In addition, reboiler duty (or steam mass flow rate) is employed to control the stripper bottom temperature. This control structure was employed in previous dynamic simulation studies including (Panahi and Skogestad, 2012)(Nittaya et al., 2014), showing a fast response and capability to reject disturbances.
- Control structure B uses F_{solv} to control the solvent temperature at the stripper bottom T_{str} , and reboiler duty to control capture ratio at the absorber. Note that changes in reboiler duty result in a large change in solvent lean CO_2 loading (large relative change RC). A similar version was suggested by Panahi and Skogestad (Panahi and Skogestad, 2012), where it was found that this control structure showed similar dynamic behavior, in response to disturbances in flue gas flow rate, compared with a model predictive control scheme (MPC).
- Control structure C keeps solvent flow rate constant at off-design operating conditions of the plant. The changes in solvent flow rate result in large disturbances to the plant due to circulation times and total stabilization times of the main process variables of the chemical absorption process. It was decided to keep it constant for this control structure. In addition, steam flow rate is employed to control stripper bottom temperature T_{str} via feedback control.
- Control structure D utilizes solvent flow rate F_{solv} to control the mass based L/G ratio in the absorber column at the same value as that in the close-to-design-point operating conditions. This control loop is implemented via ratio control. In addition, reboiler duty is manipulated to control T_{str} . The control structure leads to different final steady-state operating conditions when ramping down the plant load than the other alternatives.
- Control structure E utilizes solvent flow rate F_{solv} to control the mass based L/G ratio in the absorber column at the same value as that in the close-to-design-point

TABLE 3.8: Pairings for control structures A to F employed in papers II, III and V. The nomenclature employed can be mixed in the different papers. How those correspond to the nomenclature in this section is explained in this table.

| Control structure | Pairings MV-CV | Paper II | Paper III | Paper V |
|-------------------|---|----------|-----------|---------|
| A | F_{solv} - Cap and Q_{reb} - T_{str} | A | B | A |
| B | F_{solv} - T_{str} and Q_{reb} - Cap | B | - | B |
| C | Constant F_{solv} and Q_{reb} - T_{str} | - | - | C |
| D | F_{solv} - L/G and Q_{reb} - T_{str} | C | A | D |
| E | F_{solv} - L/G and F_{steam} - F_{steam}/F_{solv} | - | - | E |

operating conditions. This is implemented via ratio control. In addition, the steam flow rate is ramped down keeping the ratio between steam flow rate F_{steam} and solvent flow rate F_{solv} constant as suggested by (Ceccarelli et al., 2014).

3.5.2 Evaluation of transient performance

A common approach to evaluate the transient performance of a dynamic system is by implementing open-loop step changes in main inputs/disturbances to the process. During open-loop testing, step changes are applied in set-points of some inputs or disturbances to the plant or dynamic process model, and the transient response of the process variables of the system are monitored or outputs from simulations are calculated. This approach helps to characterize and analyze the transient response of the process and contributes to generate suitable data sets that can be utilized for dynamic process model validation when applied to pilot or actual plants. The open-loop tests are desired since they minimize data variability and also allow to identify the effects that one input or disturbance to the plant have on important process variables of the process. In addition, the influence of the control loops of the advanced control layer of the chemical plant on the resulting transient performance is reduced. In this work, key transient open-loop performance characteristics were obtained by calculating dead times θ , settling times t_s , rise times t_r and total stabilization times t_{sta} :

- Dead time θ describes how long it takes before a process variable begins to respond to a change in the process input. With begins to respond it is meant that the trajectory of the process variable moves out of the band defined by the initial steady-state value of the process variable y_0 , and a $\pm 1\%$ change in the process variable Δy , i.e.: $-0.01 \Delta y + y_0 < y < 0.01 \Delta y + y_0$, for the first time.
- The 10% settling time t_s is the time it takes from the instant in which the process variable begins to respond to the input change, until it remains within an error band described by the final steady-state value of the process variable y_∞ , and 10% of the change in the process variable Δy , i.e.: $-0.1 \Delta y + y_\infty < y < 0.1 \Delta y + y_\infty$. The resulting total stabilization time t_{sta} is the sum of the dead time and the settling time.

- 100% rise time is the time that takes from the instant at which the process variable begins to repond until it reaches y_∞ for the first time.
- The relative change RC in the process variable is calculated as in Eq. 3.19, where y_0 is the initial steady-state value of the process variable.

$$RC = 100 \frac{y_\infty - y_0}{y_0} \quad (3.19)$$

In this work the open-loop approach to transient testing was employed for generating data-sets for dynamic process model validation such as in paper II and III, and for the evaluation of the transient performance of dynamic process model of the amine plant at TCM in paper II, for transient testing at the amine plant at Technology Centre Mongstad (TCM) and for the evaluation of the transient performance of the dynamic process model of the scaled-up process with 2 absorbers and 1 desorber configuration; refer to paper IV. Settling times t_t and rise times t_r were also calculated for the response in process variables to load changes in the integrated power plant with PCC unit in paper V.

The main inputs or disturbances to the chemical absorption process applied in this work were on:

- Flue gas flow rate F_{gas} at absorber inlet.
- Solvent mass flow rate at absorber inlet F_{solv} .
- Reboiler duty Q_{reb} .

The responses of the main process variables of interest in this analysis were:

- Solvent lean CO₂ loading at absorbers inlet L_{lean} .
- Solvent rich CO₂ loading at absorbers outlet L_{rich} .
- CO₂ capture rate at absorber stack Cap .
- CO₂ product mass flow rate F_{prod} , at the outlet of the overhead condenser of the desorber. This is the CO₂ rich product flow of the PCC unit sent to conditioning, compression and transport.
- Temperature at stripper column bottom T_{str} .

3.5.3 Evaluation of control structures

The control structures presented in Section 3.5.1 were evaluated via dynamic process simulation in papers II and V and via transient testing at the amine plant at Technology Centre Mongstad in paper III.

The evaluation in paper II was for fast load changes of the upstream power plant, considering ramp rates of 10%/min in flue gas flow rate to the absorber column. The

scenarios tested consist of a plant ramp-down resulting in flue gas flow rate reduction of 100% to 70% and then a ramp-up case from 70% to 100%. The output trajectories of main process variables for the different control structures were plotted and compared. In addition, transient performance indicators were calculated for the different control structures, including accumulated reboiler energy input, accumulated CO₂ emitted and accumulated CO₂ captured; refer to paper II section 5.2 for definitions. In addition, total stabilization times for CO₂ absorbed, CO₂ desorbed and solvent lean CO₂ loading.

During the transient testing at Technology Centre Mongstad two control structures were implemented in the pilot plant, and tested for fast load changes, driven by volumetric flue gas flow rate change. Control structure D in Table 3.8 was tested during the initial 24 hours of testing for flue gas volumetric flow ramp down and ramp up (100%-to-80%-to-100% and 100%-to-60%-to-100%), while control structure A was tested for flue gas volumetric flow ramp-down and up (100%-to-80%-to-100%). Details on the tests conducted were explained in Table 6 and Table 7 of paper III. The total stabilization times of the CO₂ absorbed and CO₂ desorbed were compared for the different transient tests and control structures. The performance of the decentralized control structures were discussed based on the output trajectories of main performance process variables.

In paper V the control structures A to E in Table 3.8 were evaluated when the process is scaled-up and integrated with the NGCC power plant. The control structures were evaluated and controlled for gas turbine load changes with 5%/min GT load change, from 100% GT load to 75% GT load ramp-down and from 75% GT load to 100% GT load ramp-up. The evaluation considered comparison of the output trajectories of the main process variables of the system. In addition, the rise times and settling times were calculated for: steam turbine power output, CO₂ capture rate, steam extraction to reboiler and produced CO₂ mass flow rate. In addition, the transient performance of the combined cycle power plant with the PCC unit was demonstrated and described with control structure A (see Table 3.8) implemented in the PCC unit. The evaluation investigated interaction between the PCC unit and the power plant performance during load changes, and evaluated the effects of various GT load change ramp rates on the performance of the integrated system.

Chapter 4

Results and discussions

This chapter summarizes the main results and contributions from this Ph.D. thesis. The results presented in this chapter have been presented in papers I to V; refer to Section 1.5.1 and Appendix A. The reader is encouraged to read the papers to obtain further discussions and results. The results presented in this section do not follow chronological order of publication, they are presented following the research line within this Ph.D. Thesis.

4.1 Identifying operational requirements for flexible power plant with CCS in future energy systems

The objective of the research included in paper I was to identify operational requirements of flexible thermal power plants with CCS in different regions of Europe. The main idea was to focus on technical requirements and include a discussion on alternative power markets beyond the day-ahead power market to increase profit margins for thermal power plant owners. The results from a day-ahead market simulator illustrate the effects of wind power production on the hourly dispatch of thermal power plant units in future day-ahead power markets.

Figure 4.1 shows wind production and day-ahead market dispatch of three thermal power plants for three consecutive weeks during January 2030; a 308 MW_{el} lignite fired power plant, a 127 MW_{el} coal fired power plant and a 170 MW_{el} gas fueled power plant. It can be observed that there is correlation between hours with high wind power production and part load operation or shut-down of the thermal power generation plant. The zero marginal costs of variable renewable energies (VRE) places thermal power generation out of production with several hours when the thermal power plants are not producing electricity. These thermal power plants operate in cycling mode i.e., under part load operation and even shutting down and starting-up several times during the time span of three weeks. The transient events for load change are frequent.

In addition to day-ahead power markets, in which the majority of the energy volume is traded today, trading in intraday power markets could be an interesting opportunity for slower resources such as flexible CCS power plants to improve their profits. However, there were no technical requirements found for bidding in these markets.

In order to guarantee the balance between production and generation close to real time, the transmission system operators (TSOs) must procure and operate the so called ancillary services. Future thermal power plants with CCS should be designed for large

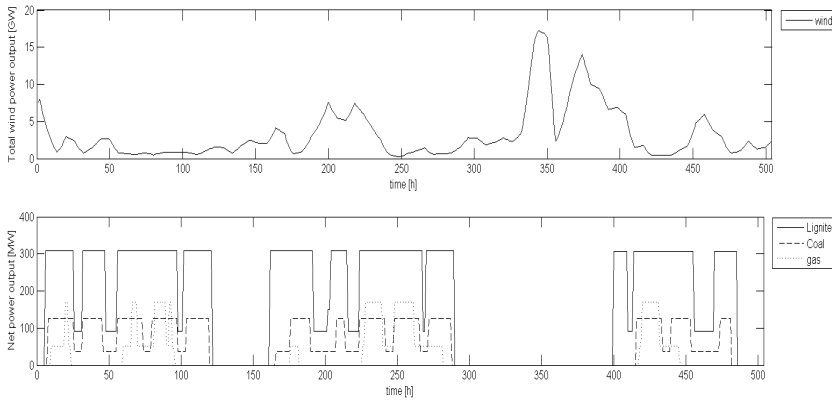


FIGURE 4.1: Total wind power production (top) and day-ahead market-based hourly dispatch of three dispatchable thermal power plants (bottom) in Northern and Continental Europe by 2030. The time span is three weeks during winter. Results from EMPS market simulation. Results presented in Figure 1 of paper I.

scale over $200 \text{ MW}_{\text{el}}$, in order to make use of economies of scale. Therefore, they should be qualified as large producers in technical codes and guidelines such as ENTSO-E codes (ENTSOE, 2012). The second-to-second balance between the generation and demand in a power system is managed by controlling the system frequency (primary, secondary and tertiary frequency response). A literature review was conducted to summarize technical requirements for generators to provide services in Spain, Germany, Great Britain and Denmark. These are presented in Table 1 of paper I. The technical requirements could be used to define market-based scenarios for dynamic process model simulations or transient testing studies, regarding ancillary services provision. In this thesis, the transient events of focus were the transient performance of the chemical absorption process and the response of the system to load changes when integrated with a power plant.

4.2 Dynamic process model validation

In order to assess the transient performance of the combined cycle power plant with post-combustion CO_2 capture, dynamic process models were developed and validated. The dynamic process model of the chemical absorption process was validated with steady-state and transient plant data from Technology Centre Mongstad in paper II. From the literature review it was concluded that dynamic process model validation of the chemical absorption process from flue gas of natural gas fired power plant is challenging due to:

- The scarcity of transient or dynamic pilot plant data.
- Most available data is found from small-scale pilot plants. That has implications on the reliability of simulation results when applying dynamic process models to scaled-up applications.
- Most of the previous validation work was done for flue gas with a typical CO₂ content from coal-based power plants.

A suitable set of steady-state cases and transient tests was selected from operations at CO₂ Technology Centre Mongstad, as presented in Section 3.4. The pilot plant was operated with around 30 wt% MEA for all cases, and the steady-state data cases represent a wide range of steady-state operating conditions, for flue gas with a CO₂ content of around 3.7 vol%. The data sets were found suitable for dynamic process model validation purposes, and were presented in Table 3 of paper II (see extended data sets in Table 3.5 and Table 3.6 in Section 3.4.2 of this thesis).

The steady-state validation results from simulations of the dynamic process model for the selected pilot plant data cases were presented in Table 4 of paper II, together with the absolute percentage errors and mean absolute percentage errors. The process variables selected for model validation were the ones considered of interest for the operation of the plant, which include lean (L_{lean}) and rich (L_{rich}) CO₂ loading, product CO₂ flow rate F_{prod} , specific reboiler duty (SRD) and stripper bottom temperature (T_{str}). Figure 4.2 shows the parity plots of dynamic process model validation results with steady-state data of CO₂ lean loading at absorber inlet and CO₂ product flow rate F_{prod} . In addition, Figure 4.3 shows dynamic process model validation results of temperature profiles of absorber column and stripper column for two steady-state operation cases.

The results showed that despite the deviations found in the absolute values predicted by the dynamic process model with respect to the reference pilot plant data, the dynamic process model can predict the variability of the main process variables for a wide range of steady-state operating conditions. The results in Figure 4.3 showed that the process model can properly predict the variation of temperature profiles for various steady-state operating conditions. However, care must be taken when applying the dynamic process models to scaled-up applications since model calibration for data fitting is required.

The dynamic process model was validated with transient data from the pilot plant with the three transient tests. The transient tests consisted of set-point changes in main process inputs to the plant consisting of flue gas flow rate, solvent flow rate and reboiler duty: i) Flue gas flow rate ramp-down; b) Flue gas flow rate ramp-up and step changes in reboiler duty; and iii) Solvent flow rate ramp-down.

Figure 4.4 shows the transient response of the pilot plant and the dynamic process model to the inputs or disturbances of test i) of flue gas flow rate ramp-down. The trajectories shown are CO₂ desorbed and CO₂ absorbed. The difference observed between the output trajectories of CO₂ absorbed and CO₂ desorbed is characteristic of the coupled operation of the absorber and desorber column due to dynamic interactions via the recycle loop. The results from the three transient tests included show that the dynamic process model can properly predict the output trajectories of main process variables for different

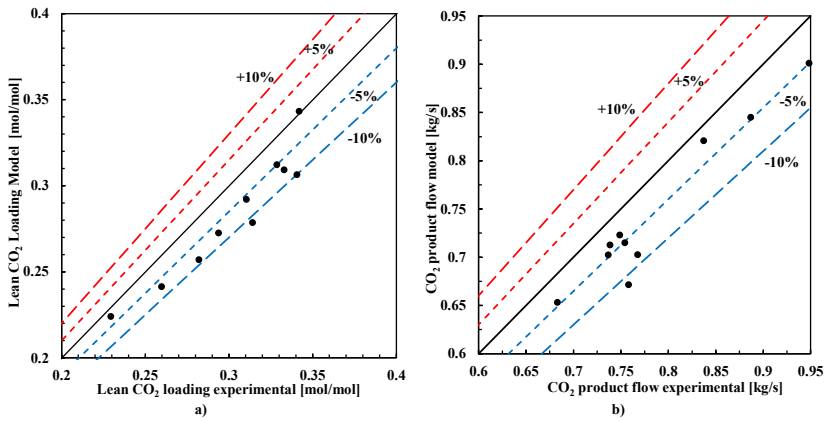


FIGURE 4.2: a) Parity plot of lean CO₂ loading; b) Parity plot of CO₂ product flow rate. Lines for +10%, +5%, -5% and -10% percentage errors are shown. The mean average error for CO₂ lean loading is 6.6% and 5.4% for CO₂ product flow rate. Presented in paper II.

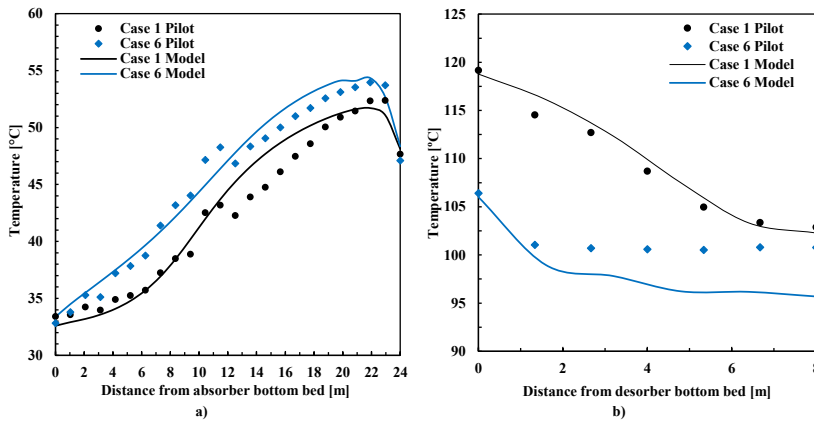


FIGURE 4.3: Temperature profiles for a) absorber column and b) stripper column for steady-state cases 1 and 6. Pilot plant and model simulation results. Presented in paper II.

inputs/disturbances applied to the plant. The dynamic process model can predict the dead times of the output trajectories and provide similar stabilization times as found in the pilot plant reference data, despite of the deviations in steady-state values between model and pilot plant data.

The dynamic process model of the combined cycle power plant was validated with reference steady-state design and off-design simulation data from GT PRO (refer to Section 3.3 for the methodology). The validation results of the steam cycle simulations were presented in paper V, which include absolute percentage errors and mean absolute percentage errors for steam turbine gross power, high-pressure admission pressure and re-heat admission pressure in the steam cycle. These results were obtained for seven steady-state operating conditions driven by different GT loads from 100% to 70% at ISO ambient conditions. The mean absolute percentage errors found are below 1.1% for all process variables. These validation results showed the suitable implementation of the regulatory control layer in the dynamic process model of the steam cycle when operated under sliding pressure mode, and that the dynamic process model can properly predict the variability of the process conditions of the steam cycle at different GT loads. In addition, the gas side HRSG's temperature profile under design conditions was validated, with a mean absolute percentage error of 0.16%. This showed the capability of the dynamic process model to predict the heat transfer distribution within the different sections of the HRSG.

The settling time of the response of steam turbine gross power for load change driven by GT load change at 5% per minute showed reasonable behavior. It resulted in similar values as the ones obtained from GT PRO simulations. Similar results were found in literature for settling times (6-9 min) based on dynamic process model simulation of a 3PRH combined cycle in (Benato, Stoppato, and Mirandola, 2015). These results show that the dynamic process model of the thermal power plant can properly predict the process dynamics with high fidelity for the purpose of application in this work. In addition, parallel work within this thesis was conducted and presented in paper XI, in which a dynamic process model of a steam cycle with OTSG technology was successfully validated with reference transient data for load changes.

4.3 Transient response of the chemical absorption process

The methodology presented in Section 3.5.2 was followed to assess the transient performance of the chemical absorption process at pilot plant scale (80 tons CO₂/day) and commercial scale (4770 tons CO₂/day); refer to papers II and IV respectively. Note that the results in paper II and paper IV are based on dynamic process model simulations. In paper III, experimental results on open-loop transient testing at the amine plant at Technology Centre Mongstad were presented. Despite of the validity of dynamic process model simulation results, it is of importance to carry out experimental transient testing and developing the learning curve of process operation by pilot plant testing at large-scale experimental facilities.

Open-loop transient response assessed with dynamic process model simulations

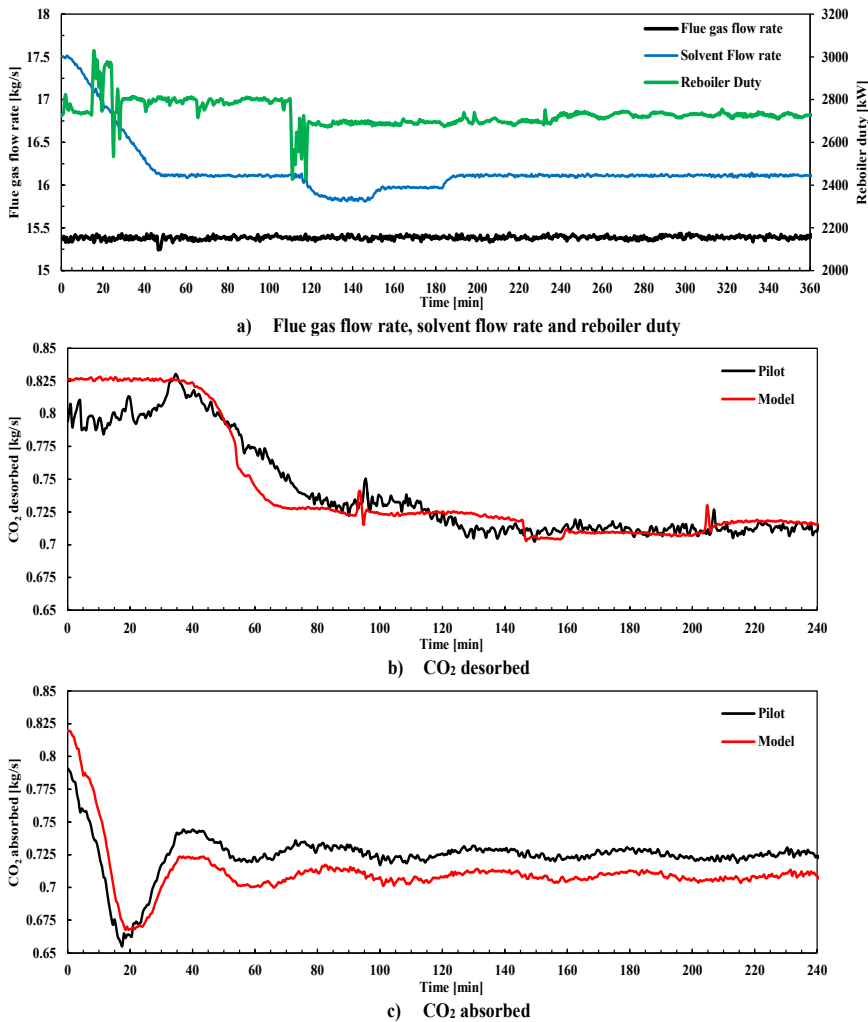


FIGURE 4.4: Transient test in paper II for flue gas flow rate ramp-down. a) Main inputs to the plant: flue gas flow rate, solvent flow rate and reboiler duty; b) Transient responses of CO₂ desorbed (pilot and model); and c) Pilot plant transient response and model output trajectory for CO₂ absorbed in absorber column.

Dynamic process models of the chemical absorption process with MEA were employed for dynamic process simulation of the open-loop response of the system to disturbances in flue gas flow rate, solvent flow rate and reboiler duty. The analysis was conducted with the dynamic process model of the amine plant at TCM in paper II. In addition, a similar analysis was conducted for the dynamic process model of the scaled-up PCC unit of the NGCC power plant, in paper IV. The open-loop transient response of the process was studied for three steady-state operating conditions of the PCC unit. Generally, a combined cycle power plant is brought to part-load operating conditions by reducing the GT load and consequently the steam turbine's power output is reduced, due to automation of the steam cycle and the reduced amount of steam being generated in the HRSG. A significant GT load reduction results in reduced GT exhaust mass flow rate sent to the HRSG of the combined cycle and to the absorbers of the PCC unit. The exhaust mass flow rate of the GT at different loads depends on the GT technology employed. For the pilot plant model in paper II, the steady-state corresponds with flue gas volumetric flow rate capacity of 100% (60000 Sm³/hr), 80% and 60%. For the PCC unit model of the combined cycle power plant in paper IV, the steady-state operating conditions correspond with 100%, 80% and 60% GT load exhaust mass flow rate. The different steady-state operating conditions were obtained by simulating the process models with control structure A (refer to Section 3.5.1) in which the capture rate Cap was controlled by manipulating solvent flow rate, and stripper bottom temperature T_{str} was controlled by manipulating reboiler duty Q_{reb} .

Figure 4.5 shows the total stabilization times t_s of the response of main process variables of the PCC unit to open-loop 10% step changes in flue gas flow rate, solvent flow rate and reboiler duty to the PCC unit of the NGCC plant. Figure 4.6 shows the trajectories of the responses in process variables to the step changes in inputs of the PCC unit of the NGCC.

Process variables respond differently to different disturbances. For the same process variable, the response observed was different when increasing or decreasing the input. This showed the non-linear behaviour of the process. In addition, the solvent recycle loop in the process from the desorber outlet to absorber inlet connects the operation of the absorber and stripper units, and the resulting dynamic interaction between the absorption and desorption unit resulted in long stabilization time of main process variables, up to 11 h. The results show the general trend that the plant responds slower when operated at lower loads, i.e. it required longer total stabilization times for the most relevant variables of the process. In general, the desorption rates stabilized faster than the absorption rates for step changes in solvent flow rate and reboiler duty. A key aspect to process dynamics is the solvent inventory distribution and solvent mass flow rate. At lower operating loads of the process, the solvent flow rate in the plant is smaller, and solvent accumulates in the buffer tank. Smaller solvent mass flow rate results in increased residence times through the components of the system hold-ups, piping and recycle loop, resulting in slower response of the process variables to changes in process inputs.

Step changes in flue gas flow rate around a given steady-state operating point do not cause a large relative change in absorption and desorption rates of the process due to the diluted nature of the CO₂ within the flue gas. In general, the capture rate response was

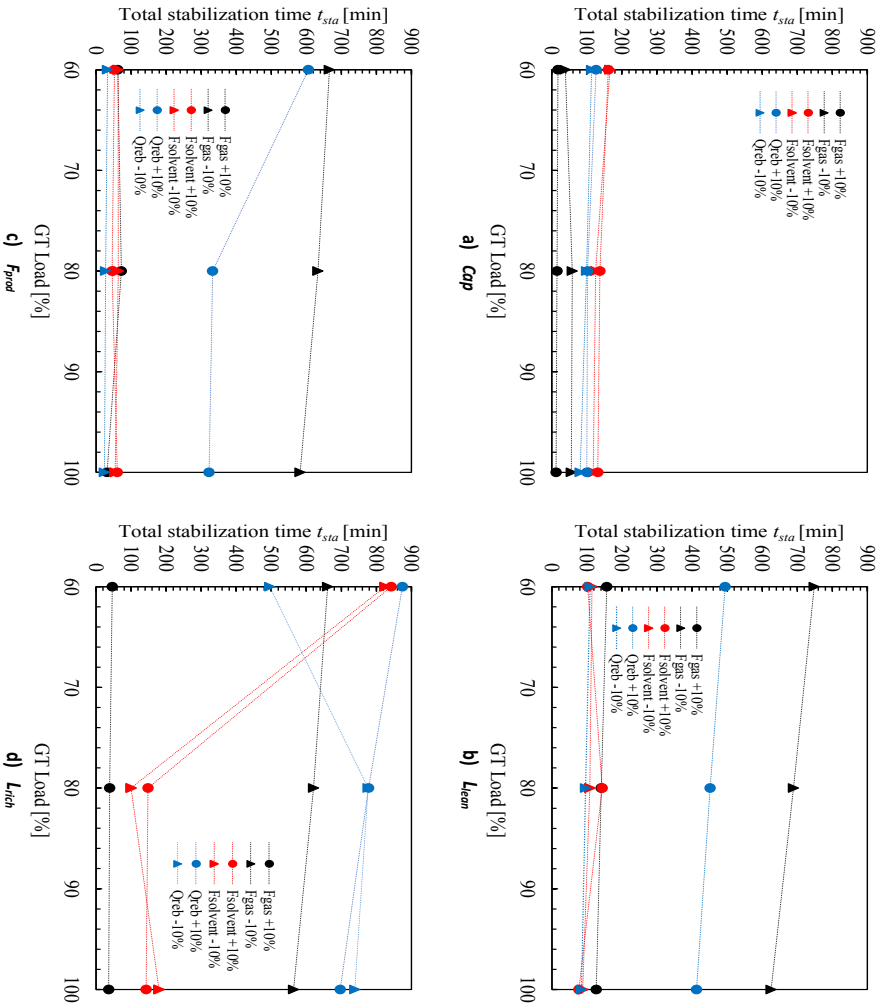


FIGURE 4.5: Trends in total stabilization times of main process variables of the PCC unit of the NGCC power plant, when disturbed by the different plant input step changes, at different GT loads. a) CO₂ capture rate; b) Solvent CO₂ loadings at absorber inlet; c) Product CO₂ mass flow rate; and d) Solvent CO₂ loading at stripper inlet. Results from paper IV.

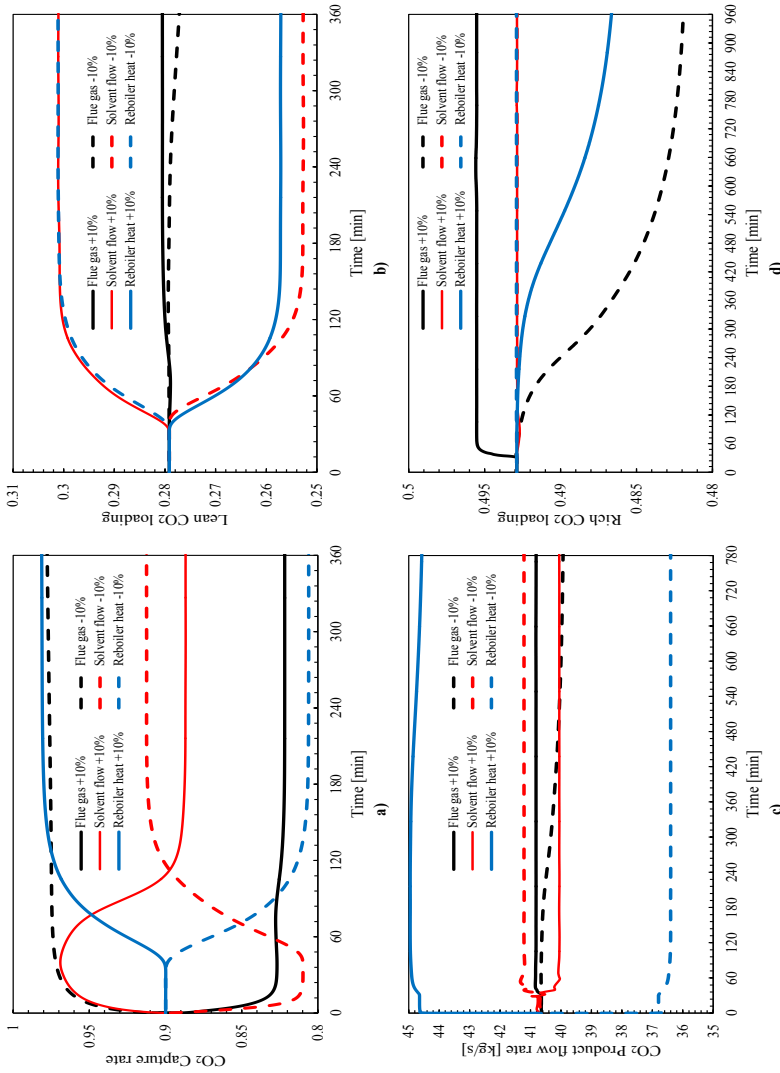


FIGURE 4.6: Transient responses to different step changes in process inputs. The simulations correspond to initial steady-state operation of the PCC unit for 60% GT load. Step changes applied at time $t = 0$. a) CO₂ capture rate; b) Solvent CO₂ loading at absorber inlet; c) Product CO₂ mass flow rate; and d) Solvent CO₂ loading at stripper inlet. Results in paper IV.

faster when increasing flue gas flow rate (<1 h) than when decreasing flue gas flow rate (<11 h) and that behaviour was consistent at different operating point of the plant. Step changes in solvent flow rate resulted in inverse responses of capture rate, as observed in Figure 4.6. Larger stabilization times were found when the plant was operated at lower loads. In addition, desorption rate stabilized faster (around 1 h) than absorption rate (around 2-3 h) for the PCC unit of the combined cycle power plant. Increasing the reboiler duty will result in higher capture rate due to the lower resulting lean loading at the inlet of the absorber. However, a relative large dead time was observed in the response of the lean CO₂ loading at the inlet of the absorber and in the response of the absorption rate due to solvent circulation through the recycle loop. That dead time consisted of 28-37 min for the PCC unit of the NGCC power plant and 13-23 min in the TCM amine pilot plant. The response of product flow rate to changes in reboiler duty (desorption rate) had a significant relative change with no dead time and very fast stabilization time. This might be explained because reboiler duty acts fastly on the generated stripping vapors of the process.

The results here presented, help process engineers to understand the process dynamics of the plant. Understanding the trends in the response of the system at various loads is of importance if the chemical absorption process has to be operated under part load operating conditions during a significant amount of the project lifetime. In addition, for pilot plant operations it is of importance to understand the open-loop response of the system since it can save time (and costs) when performing parametric testing and developing the U-curves, as described in Section 3.4.2. According to conversations with staff from TCM DA, the procedure to obtain the parametric curves (U-curves) during MEA campaigns at TCM was changed based on the process insight from the simulations in this work. In the former approach, the stripper bottom temperature was specified (changed for creating different points) and the rich solvent flow rate was modified (tuned) to achieve the desired target capture rate. In the new approach to find U-curves, the solvent flow rate is specified (changed for creating different points) and the stripper bottom temperature is modified (tuned) to achieve the desired target capture rate. With the new approach, less operating hours are required to generate the U-curves during parametric testing. In addition, these results provide process insight that can be useful when designing control strategies for flexible operation of the PCC unit.

Open-loop transient response assessed with transient testing at Technology Centre Mongstad

Transient testing on open-loop responses at the amine plant at Technology Centre Mongstad was conducted, as explained in Section 3.4.3. The analysis focused on assessing the transient response of the pilot plant to multiple and non-simultaneous step-changes in key inputs/disturbances to the plant, namely (i) flue gas flow rate, (ii) solvent flow rate. This was done for different flue gas capacities of the PCC plant, corresponding to different loads of the upstream power plant. In addition, unintended variations in steam flow rate (reboiler duty) helped to discuss transient response to disturbances in reboiler duty. The results were presented and analyzed in detail in paper III. Figure 4.7 shows capture rates

during the transient testing period.

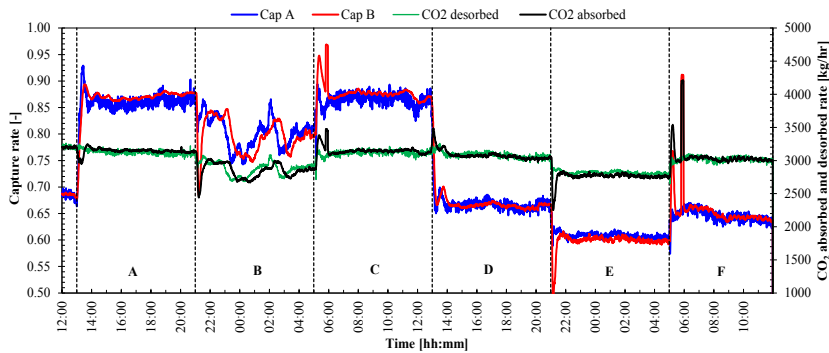


FIGURE 4.7: Transient response of capture rate Cap_A (based on desorption rate) and Cap_B (based on absorption rate). The open loop tests are shown for 48 hours of testing for the tests presented in Table 5 of paper III. The vertical lines correspond to the time at which the set-point changes are applied for tests A to F as presented in Table 5 of paper III.

Results showed that after changes in flue gas flow rate, the process required a maximum of 55 min to stabilize. In addition, changes in steam flow rate to reboiler showed that desorption rates are very sensitive to changes in reboiler duty, and CO_2 desorption rate follows tightly the changes in steam flow rate, while the CO_2 absorption rate response follows with a delay due to circulation times in the recycle loop. This means that the stripper process conditions change relatively fast in response to inputs of steam flow rate, while the response of the performance of the absorber column is slower. Furthermore, when the capture rate is defined with the absorption rate Cap_B , the output trajectory describes a slow inverse response due to solvent circulation times through the recycle loop. The testing results provided empirical evidence for the results obtained with dynamic simulations.

4.4 Evaluation of transient performance of decentralized control structures

Decentralized control structures assessed with dynamic process simulations of the amine plant at Technology Centre Mongstad

The evaluation of decentralized control structures for fast load changes applied to the dynamic process model of the amine plant at Technology Centre Mongstad were presented in paper II. Results showed that by adding closed-loop controllers on the main two degrees of freedom (reboiler duty and solvent flow rate) to control two other process

variables (including stripper bottom temperature and CO₂ capture ratio), the process could be stabilized faster and more efficiently under varying process loads.

The control structure that showed the best performance for fast load changes was control structure B, in which solvent flow rate is employed to control stripper bottom temperature and reboiler duty is employed to control capture rate; refer to Table 3.8 in Section 3.5.1.

It was found that when control structure B was employed, the process stabilized faster (approximately after 1 h) than when employing other control structures. This means that shorter total stabilization times using control structure B were found when the plant load is ramped up and down, with ramp rates typically found in NGCC power plants with fast load change capabilities. When reducing the process load, control structure B was the least energy-intensive of those evaluated. When increasing the plant load, control structure B was the one with the lowest accumulated CO₂ emissions imposed by the process inertia during load change transient operation.

Decentralized control structures assessed via transient testing at Technology Centre Mongstad

The results of transient testing of decentralized control structures were presented in paper III. The results showed the experience of implementing decentralized control structures in a demonstration scale plant for the chemical absorption process and gave insights into the challenges found for implementing these control structures in an actual process.

The results from transient testing showed that the process can reject fast disturbances in flue gas flow rate (load changes) and could bring the process towards desired off-design steady-state conditions within 60 min by employing decentralized control structures. However, care must be taken when tuning the feedback control loops of the process and especially of the regulatory control layer, since slow control loops in the regulatory control layer affects the performance of the advanced control layer to reject disturbances. Therefore, further work at TCM DA is required to tune the controllers of the regulatory control layer of the amine plant so that faster closed-loop responses are achieved, allowing for tighter control of process variables in the advanced control layer. In addition, it was observed that fast and large changes in solvent flow rate as a control measure can cause instabilities due to the interaction between the stripper temperature and the capture rate control loops.

Decentralized control structures assessed via dynamic process simulations of the scaled-up process integrated with the NGCC power plant

The transient performance of the integrated combined cycle with PCC unit was evaluated in paper V, for the five control structures implemented in the PCC unit. The analysis was separated in two main cases: one in which CO₂ capture rate was controlled to the target value of 90% at different operating conditions of the plant (control structures A and B) and one case in which CO₂ capture rate was not controlled (control structures C, D and E). The tests were conducted for load changes in the GT (up and down) from 100%

GT load to 75% GT load with a ramp-rate of 5%/min. Figure 4.8 shows the transient response of the system for the different control structures. The output trajectories shown are ST power output as a percentage of nominal value and the capture rate in the absorber columns Cap for load change scenarios.

The steam turbine power output showed similar responses in terms of transient output trajectory in the time scales of thermal power plant load change (10^0 to 10^1 min), with similar rise times (7-10 min). However, the steam turbine power output stabilized faster when the capture rate of the process is not a control objective. This means that when control structures A and B were applied to the PCC process, dynamic interactions between the power plant and the PCC unit were observed due to the steam extraction from the steam turbine being manipulated to control the capture rate or the stripper bottom temperature.

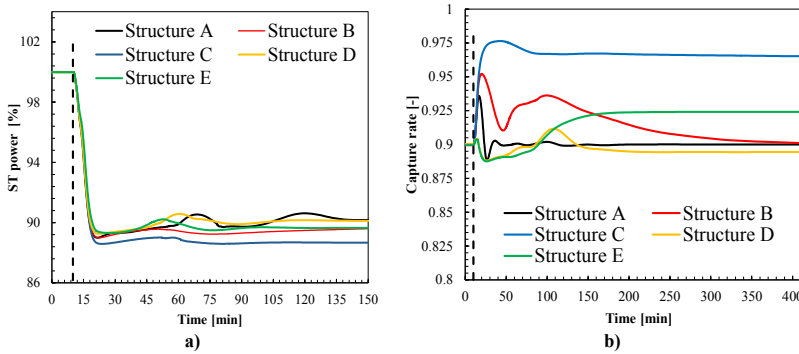


FIGURE 4.8: Transient response of a) steam turbine power output [%] and b) capture rate [-] (based on absorption rate). Response to GT load change with 5%/min ramp rate. The trajectories correspond to simulations with the full dynamic process model of the power plant with PCC unit. Each trajectory corresponds to one of the control structures in Table 3.8.

When controlling the CO_2 capture rate is not an objective (control structures C, D, and E), control structure with L/G ratio being controlled via ratio control in the absorber column and T_{str} is controlled at the stripper bottom showed faster stabilization of steam extraction and stripper bottom temperature (control structure D), the process stabilized faster in terms of steam turbine power output and stripper bottom temperature. In addition, this control structure leads to similar steady-state off-design performance than control structures A and B. However, capture rate required more time to stabilize than when capture rate is controlled in control structure A and B. If fast stabilization of CO_2 product flow rate and steam power output are required simultaneously while keeping the process close to optimal conditions, it is recommended to employ control structure D for load changes of the power plant.

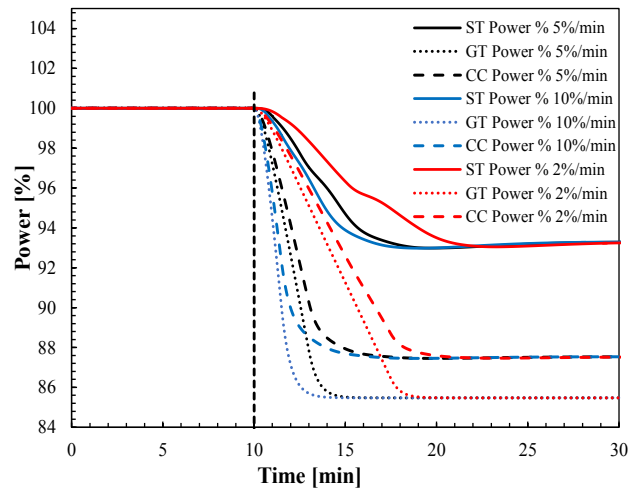
4.5 Transient performance of commercial scale natural gas combined cycle power plant with post-combustion CO₂ capture

The power plant integrated with the scaled-up PCC unit performance was studied for variable ramp rate load changes driven by GT load change in paper V. The ramp rates were chosen to represent slow load change of 2%/min, typical ramp rates from a combined cycle power plant of 5%/min and a fast load change of 10%/min. For these scenarios the PCC unit was operated with control structure A. Results are shown in Figure 4.9.

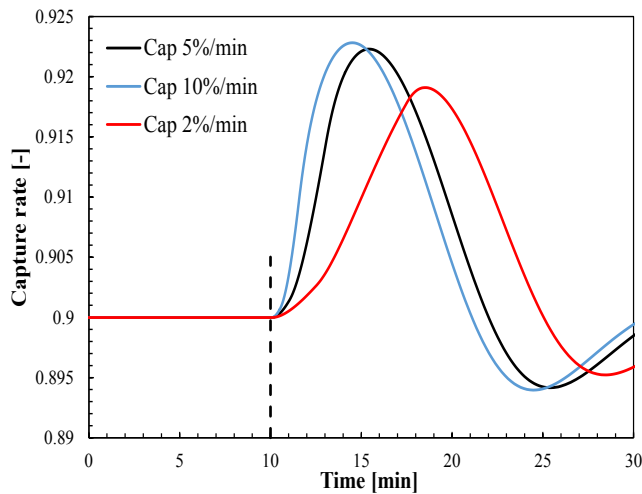
When the steam extraction is regulated by a throttle valve to control a controlled variable of the PCC process (capture rate in this case), dynamic interactions were found between the power plant and the PCC unit, in the slower time scales typical of PCC unit transient operations (10^1 to 10^2 min). Slow oscillations were found in the steam extraction from the steam turbine, that resulted in oscillation in steam turbine power output. However, the oscillations have a small amplitude (<1%) of the gross steam turbine power output.

In addition, the GT load change with a typical ramp rate of an NGCC power plant imposes a fast disturbance in terms of mass flow rate to the PCC unit that has to be stabilized with a suitable control structure. For different GT ramp rates, the output trajectories of the PCC unit show different output, with larger deviations of Cap for faster disturbances, for the faster time scales typical of power plant operation (10^0 to 10^1 min). However, in the slower time scales (10^1 to 10^2 min), the output trajectories of the chemical absorption process show similar trajectories of the studied process variables regardless of the ramp rate employed.

The results showed that the addition of the PCC unit should not impose any constraint on stable operation of the process after load change transient events. The power plant can provide fast response during load change in terms of power output, within day-ahead power markets where power is traded by the hour. Nevertheless, inefficient transient operation of the PCC unit can be expected in the long time scales and it can take up to 1-3 hours to stabilize depending on the control structure employed in the chemical absorption unit.



a)



b)

FIGURE 4.9: Transient response of a) total combined cycle, GT and steam turbine power outputs [%] and b) capture rate [-] (based on absorption rate). Response to GT load change with 2%/min, 5%/min and 10%/min ramp rates. The trajectories correspond to simulations with the full dynamic process model of the power plant with PCC unit.

Chapter 5

Conclusions and future work

5.1 Conclusions

The last years have seen an increased interest in the role of CCS power plants in the future energy systems with high penetration of variable renewable energies. Such power plants might be operated as load following plants forced by market conditions and power system operation requirements. According to the results from a day-ahead market simulation in Northern and Continental Europe by 2030, thermal power plants tend to operate in cycling mode i.e., under part load operation and even shutting down and starting-up several times under three winter weeks. It means that thermal power plants are being displaced in the merit order in scenarios with high penetration of variable renewable energies. Hence, plant operators should look at further opportunities beyond selling energy in day-ahead markets in order to increase their profits. Intraday markets have been identified as especially interesting markets for power plants with CCS since slower flexible resources can have a chance in these growing markets. Nonetheless, no specific operating requirements from the power grid are required to bid in intraday markets.

Technical grid requirements and frameworks for power units to provide ancillary services and bidding in balancing markets in four different power areas in EU have been identified. The areas comprise Spain, Germany, Great Britain, and Western Denmark. These requirements can be utilized to define market-based scenarios for dynamic process simulation studies, considering activation start, full availability and deployment end times. These scenarios will reflect today's requirements for providing the mentioned flexibility services.

In this work, high fidelity dynamic process models of a commercial scale 613 MW three-pressure reheat combined cycle power plant with amine based post-combustion CO₂ capture were successfully developed by means of the Modelica language. The models allow co-simulation of the thermal power plant and the chemical absorption process for assessing the dynamics of the integrated process for different scenarios and transient events. The physical models represent process dynamics of the thermal power plant and the chemical absorption process of CO₂ with similar level of detail. The main focus of model development was the assessment of load change transient performance. The models have been extensively simulated to provide insight on dynamics of the chemical absorption process at different operating conditions and for different disturbances, and the evaluation of control structures for the integrated power plant. In addition, the transient performance during load change transient events of the integrated plant has

been assessed for variable ramp rates and with different control structures applied in the PCC unit.

Validation of dynamic process models is a challenging task due to the scarcity of suitable validation data sets available in the literature, and that most of the data is limited to small-scale pilot plants with flue gas with concentration of CO₂ of around 11-14 vol% as typically found in coal fired plants. Therefore, this work included the design of validation cases from a state-of-the-art amine large-scale pilot plant at Technology Centre Mongstad (80 ton CO₂ captured/day when using CHP gas). The selected data from amine plant operations at TCM treats flue gas from a natural gas combined cycle combined heat and power plant, with flue gas CO₂ concentration of around 3.5 vol%. The selected and post-processed data sets for dynamic process validation include ten steady-state data sets representing a wide range of steady-state operating conditions with 30 wt% MEA as chemical solvent. The main variability is in terms of volumetric flow rate capacity in the absorber column, L/G ratio in absorber column and target CO₂ with various reboiler duty. In addition, three transient tests were obtained with variations in solvent flow rate, reboiler duty and flue gas flow rate representing the main disturbances to the chemical absorption process. The data sets were considered suitable for dynamic process model validation.

The validation results showed capabilities of dynamic process modeling of the chemical absorption process applied to large scale pilot plant data. The results also showed that the dynamic process model is suitable for simulation studies at the plant scale. These include dynamic process model simulations to analyze the plant transient performances, control tuning and advanced control layer design. However, the dynamic process model should not be used for designing equipment (sizing). In addition, these results provided confidence for employing the dynamic process model for scaled-up applications for control and transient analysis studies under power plant load changes.

The validation of the thermal power plant model was conducted with steady-state design and off-design data from a reference software. The software-to-software validation showed the proper implementation and development of the dynamic process model of the thermal power plant. The model can capture the process variability for load changes with sufficient accuracy for the purpose of application. In addition, the validation results show the suitable implementation of the regulatory control layer in the combined cycle power plant model.

The case study carried out in this work via dynamic process simulations of the amine plant model at TCM, with the validated model shows that, generally, the plant responded more slowly at lower operating loads (the load being defined by the flow rate fed to the absorber). A general trend was observed, in which it took a longer time to stabilize the main process variables of the pilot plant under open-loop step changes in the main inputs of the process, namely solvent flow rate, flue gas flow rate and reboiler duty. From the process simulations, it was found that, in general, the desorption rate stabilizes faster than the absorption rate for set-point step changes in solvent flow rate and reboiler duty. In addition, 10% step changes in flue gas flow rate around a given operating point did not cause a large relative change in the main process variables of the process.

The case study carried out in this work via dynamic process simulations of the scaled-up process unit for the NGCC showed a similar trend: in general, it was found that the

plant was slower when operating at lower loads, i.e., it required longer total stabilization times for the main variables of the process. In general, CO₂ capture rate stabilized relatively faster (1–3 h) than other process variables (1–11 h). In addition, it was found that the PCC unit responded significantly faster to an increase in flue gas mass flow rate than to reductions in flue gas mass flow rate. This could have significant implications on efficient operation of the PCC unit when ramping down the power plant's load, due to long stabilization times required of the process and the resulting inefficient operation during transient conditions, if a suitable control structure is not implemented.

For the case study on evaluation of control structures for fast load changes via dynamic simulations of the amine plant model at TCM, the evaluation of the decentralized control structures showed that by adding closed-loop controllers on the two main degrees of freedom of the plant—solvent flow rate and reboiler duty—to control two other process variables, including CO₂ capture ratio and stripper bottom solvent temperature, the plant can be stabilized faster and more efficiently under varying loads. The control structure that showed the best performance was control structure B, in which the reboiler duty is manipulated to control CO₂ capture ratio at the inlet of the absorber and the rich solvent flow rate to control the stripper bottom solvent temperature. It was observed that control structure B provides the fastest stabilization times for the main process variables under scenarios when the plant load is ramped down and up, with ramp rates typically found in NGCC power plants with fast-cycling capabilities. When reducing the PCC process load, this control structure is the least energy-intensive of those evaluated in this work. When increasing the plant load, this control structure is the one with the lowest accumulated CO₂ emissions imposed by the process inertia during load-change transient operation.

Tests for fast load change scenarios applied to the pilot plant via transient testing revealed that the process can reject fast disturbances in flue gas flow rate and could bring the process towards desired off-design steady-state conditions within 60 min by employing decentralized control structures. These tests provide empirical evidence at demonstration scale that combined cycle power plants with post-combustion CO₂ capture can keep similar operational procedures as equivalent unabated power plants, considering fast cycling load changes driven by fast GT load change. However, in response to flue gas flow rate disturbance, fast and large changes in solvent flow rate as a control measure can cause instabilities due to the interaction between the stripper temperature and the capture rate control loops.

The performance of the integrated NGCC power plant with PCC for different GT load change ramp rates was demonstrated and assessed via dynamic process model simulations. For different GT ramp rates, different trajectories of the main process variables of the PCC unit were found within the timescales of power plant transient operation. Nevertheless, within the slower timescales of 10¹- 10², the transient performance of the PCC unit was similar for different GT ramp rates. Based on these simulations, it can be concluded that the addition of the PCC unit to the NGCC plant should not impose any constraint on, or problem for, stable power plant operation under scheduled load changes, even for aggressive ramp rates. Nevertheless inefficient transient operation of the PCC unit can be expected in the long time scales. The control structure where L/G is kept constant and

reboiler temperature is controlled by the steam throttle valve, showed similar part-load off-design performance as that found in control structures with constant capture rate as CVs. In addition, this control structure resulted in relatively fast total stabilization time of the steam turbine power output and CO₂ product flow rate. It is recommended to apply control structure D, with *L/G* control, if controlling CO₂ capture rate is not an operational constraint.

5.2 Future work

Future work should include the study of the operability and controllability of the NGCC power plant with CCS with higher levels of process integration, such as the eco-reboiler concept with steam drum in the HRSG, configurations with EGR or the integration of the reboiler duty towards the cold end of the HRSG.

The dynamic process model of the thermal power plant with PCC resulted in a large DAE system which requires significant CPU time to solve. That makes the dynamic process model not suitable for optimization studies. Efforts should be done to reduce the complexity of the high fidelity dynamic process models via reduced order modeling based on physical insight or by the development of surrogate models based on simulations from the model developed in this work.

Advanced control structures, such as, model predictive control on the PCC unit and compare with the performance of decentralized control structures via the linked dynamic process models or at pilot plant testing at various scales should be investigated.

Optimal operational strategies to provide ancillary services and frequency response in the NGCC configuration with PCC unit would be important to study.

Including lifetime reduction estimation of critical components in the economic evaluation of flexible operation studies, can help to understand if the revenue provided by operating the process with a given strategy outweighs the related costs of replacing components that fail before their expected lifetime due to cycling. An example could be to study possible reboiler component life time reduction due to the application of strategies of variable solvent regeneration.

Most of the efforts regarding chemical absorption process does not emphasize the optimization of the start-up sequence. Reducing start-up times and associated costs, for example the use of fuel and CO₂ emissions during start-up, could make the power plant more competitive in power markets. Detail investigation and optimization of the start-up sequence should be object of future work, and trying to coordinate the start-up sequence of the NGCC and the PCC unit.

Future work should include the analysis of the transient performance of the chemical absorption process with other solvents.

Bibliography

- Adams, Thomas and Niall Mac Dowell (2016). "Off-design point modelling of a 420MW CCGT power plant integrated with an amine-based post-combustion CO₂ capture and compression process". In: *Applied Energy* 178, pp. 681–702.
- Akesson, Johan et al. (2012). "Nonlinear Model Predictive Control of a CO₂ Post-Combustion Absorption Unit". In: *Chemical Engineering and Technology* 35, pp. 445–454.
- Alcaráz-Calderon, Agustín Moisés et al. (2017). "Natural gas combined cycle with exhaust gas recirculation and CO₂ capture at part-load operation". In: *Journal of the Energy Institute. In Press*.
- Alobaid, Falah et al. (2017). "Progress in dynamic simulation of thermal power plants". In: *Progress in Energy and Combustion Science* 59, pp. 79–162.
- Amrollahi, Zeinab, Ivar S. Ertesvåg, and Olav Bolland (2011). "Optimized process configurations of post-combustion CO₂ capture for natural-gas-fired power plant - Exergy analysis". In: *International Journal of Greenhouse Gas Control* 5, pp. 1393–1405.
- Amrollahi, Zeinab et al. (2012). "Optimized process configurations of post-combustion CO₂ capture for natural-gas-fired power plant – Power plant efficiency analysis". In: *International Journal of Greenhouse Gas Control* 8, pp. 1–11.
- Andersson, Vibeke et al. (2013). "Operational Experience and Initial Results from the First Test Period at CO₂ Technology Centre Mongstad". In: *Energy Procedia* 37. GHGT-11 Proceedings of the 11th International Conference on Greenhouse Gas Control Technologies, 18-22 November 2012, Kyoto, Japan, pp. 6348–6356.
- Apros, *Process Simulation Software*, Fortum Power Solutions, Fortum, Finland. <http://www.apros.fi/en/>. Accessed: 2018-01-21.
- Aske, Elvira Marie B. and Sigurd Skogestad (2009). "Consistent Inventory Control". In: *Industrial & Engineering Chemistry Research* 48, pp. 10892–10902.
- Aspen HYSYS, 2018. <http://home.aspentech.com/products/engineering/aspen-hysys>. Accessed: 2018-01-21.
- Aspen Plus V8.6. 2014. <http://home.aspentech.com/>. Accessed: 2017-12-01.
- Benato, Alberto, Anna Stoppato, and Alberto Mirandola (2015). "Dynamic behavior analysis of a three pressure level heat recovery steam generator during transient operation". In: *Energy* 90, pp. 1595–1605.
- Birnbaum, Juergen et al. (2009). "Simulation of the dynamic behaviour of steam turbines with Modelica". In: 7th International Modelica Conference Proceedings. September 2012, Como, Italy.
- Biyouki, Zeinab Amrollahi (2014). *Thermodynamic analysis of CO₂ capture processes for power plants*. Ph.D. Thesis. Department of Energy and Process Engineering, Norwegian University of Science and Technology.

- Bolland, Olav (2014). *Thermal Power Plant. Compendium 2014*. NTNU - Norwegian University of Science and Technology.
- Boot-Handford, Matthew E. et al. (2014). "Carbon capture and storage update". In: *Energy and Environmental Science* 7 (1), pp. 130–189.
- Brigman, Natasha et al. (2014). "Results of Amine Plant Operations from 30 wt% and 40 wt% Aqueous MEA Testing at the CO₂ Technology Centre Mongstad". In: *Energy Procedia* 63. 12th International Conference on Greenhouse Gas Control Technologies, GHGT-12, pp. 6012–6022.
- Brouwer, Anne Sjoerd et al. (2013). "The Flexibility Requirements for Power Plants with CCS in a Future Energy System with a Large Share of Intermittent Renewable Energy Sources". In: *Energy Procedia* 37. GHGT-11 Proceedings of the 11th International Conference on Greenhouse Gas Control Technologies, 18-22 November 2012, Kyoto, Japan, pp. 2657–2664.
- Bui, Mai et al. (2014). "Dynamic modelling and optimisation of flexible operation in post-combustion CO₂ capture plants—A review". In: *Computers & Chemical Engineering* 61, pp. 245–265.
- Bui, Mai et al. (2016). "Flexible operation of CSIRO's post-combustion CO₂ capture pilot plant at the AGL Loy Yang power station". In: *International Journal of Greenhouse Gas Control* 48, pp. 188–203.
- Cammi, Antonio et al. (2011). "An object-oriented approach to simulation of IRIS dynamic response". In: *Progress in Nuclear Energy* 53, pp. 48–58.
- Can Gülen, S. and Kihyung Kim (2013). "Gas Turbine Combined Cycle Dynamic Simulation: A Physics Based Simple Approach". In: *ASME Turbo Expo 2013: Turbine Technical Conference and Exposition* 4, p. 13.
- Casella, Francesco and Piero Colonna (2012). "Dynamic modeling of IGCC power plants". In: *Applied Thermal Engineering* 35, pp. 91–111.
- Casella, Francesco and Alberto Leva (2003). "Modelica open library for power plant simulation: design and experimental validation". In: 3rd International Modelica Conference. Linköping, Sweden, pp. 41–50.
- Ceccarelli, Nicola et al. (2014). "Flexibility of Low-CO₂ Gas Power Plants: Integration of the CO₂ Capture Unit with CCGT Operation". In: *Energy Procedia* 63. 12th International Conference on Greenhouse Gas Control Technologies, GHGT-12, pp. 1703–1726.
- Cellier, F.E. (1991). *Continuous system modelling*. Springer, New York, NY.
- Chalmers (2014). *European Energy Pathways: Towards a sustainable European Energy System*. PR-Offset Mölndal, Sweden.
- Chen, Chen, Zhiqian Zhou, and George M. Bollas (2017). "Dynamic modeling, simulation and optimization of a subcritical steam power plant. Part I: Plant model and regulatory control". In: *Energy Conversion and Management* 145, pp. 324–334.
- Chinn, Daniel et al. (2005). "Cost efficient amine plant design for post-combustion CO₂ capture from power plant flue gas". In: *Proceedings of the 7th International Conference on Greenhouse Gas Control Technologies*, pp. 1133–1138.
- CSIRO PCC. <https://www.globalccsinstitute.com/projects/post-combustion-capture-pccsiro>. Accessed: 2017-11-01.

- Díaz, Abigail González et al. (2016). "Sequential supplementary firing in natural gas combined cycle with carbon capture: A technology option for Mexico for low-carbon electricity generation and CO₂ enhanced oil recovery". In: *International Journal of Greenhouse Gas Control* 51, pp. 330–345.
- Dechamps, P. J. (1994). "Modelling the transient behavior of combined cycle plants". In: International Gas Turbine and Aeroengine Congress and Exposition. The Hague, Netherlands, 94–GT–2008.
- Dowell, Niall Mac and Nilay Shah (2015). "The multi-period optimisation of an amine-based CO₂ capture process integrated with a super-critical coal-fired power station for flexible operation". In: *Computers & Chemical Engineering* 74, pp. 169–183.
- Dymola systems engineering*. <https://www.3ds.com/products-services/catia/products/dymola/>. Accessed: 2017-12-01.
- Eborn, Jonas (2001). "On Model Libraries for Thermo-hydraulic Applications". Department of Automatic Control, Lund Institute of Technology (LTH). PhD thesis. Lund University.
- ENTSOE (2012). *ENTSO-E network code requirements for grid connection applicable to all generators*. Technical Report.
- EPRI (2001). *Damage to Power Plants due to Cycling*. Technical Report 2001.1001507. Version 2001. Palo Alto: EPRI.
- European Commission (2012). *Energy roadmap 2050*. Brussels, Belgium.
- Faramarzi, Leila et al. (2017). "Results from MEA Testing at the CO₂ Technology Centre Mongstad: Verification of Baseline Results in 2015". In: *Energy Procedia* 114. 13th International Conference on Greenhouse Gas Control Technologies, GHGT-13, 14-18 November 2016, Lausanne, Switzerland, pp. 1128–1145.
- Finkenrath, Matthias et al. (2007). "Performance and Cost Analysis of a Novel Gas Turbine Cycle With CO₂ Capture". In: *ASME Turbo Expo 2007: Power for Land, Sea and Air* 3, p. 7.
- Fritzson, Peter (2003). *Object-oriented modeling and simulation with Modelica 2.1*. Wiley-IEEE Press.
- Garðarsdóttir, Stefanía Ó. et al. (2017). "Effects of CO₂-Absorption Control Strategies on the Dynamic Performance of a Supercritical Pulverized-Coal-Fired Power Plant". In: *Industrial & Engineering Chemistry Research* 56, pp. 4415–4430.
- Garðarsdóttir, Stefanía Ósk et al. (2015). "Post-combustion CO₂ capture applied to a state-of-the-art coal-fired power plant—The influence of dynamic process conditions". In: *International Journal of Greenhouse Gas Control* 33, pp. 51–62.
- Gibbins, Jon and R. I. Crane (2004). "Scope for reductions in the cost of CO₂ capture using flue gas scrubbing with amine solvents". In: *Proceedings of the Institution of Mechanical Engineers, Part A: Journal of Power and Energy* 218, pp. 231–239.
- Gjernes, Erik et al. (2017). "Results from 30 wt% MEA Performance Testing at the CO₂ Technology Centre Mongstad". In: *Energy Procedia* 114. 13th International Conference on Greenhouse Gas Control Technologies, GHGT-13, 14-18 November 2016, Lausanne, Switzerland, pp. 1146–1157.
- Global CCS Institute*. <https://www.globalccsinstitute.com/projects/test-centers-and-other-initiatives>. Accessed: 2017-11-02.

- Glover, Duncan, Mulukutla S. Sarma, and Thomas J. Overbye (2012). *Power System. Analysis and design. 5th Edition*. CENGAGE Learning.
- Gonzalez-Salazar, Miguel Angel, Trevor Kirsten, and Lubos Prchlik (2018). "Review of the operational flexibility and emissions of gas- and coal-fired power plants in a future with growing renewables". In: *Renewable and Sustainable Energy Reviews* 82, pp. 1497–1513.
- gPROMS, *Process Systems Enterprise*. <https://www.psenderprise.com/products/gproms>. Accessed: 2018-01-21.
- Groot, Mats de, Wina Crijns-Graus, and Robert Harmsen (2017). "The effects of variable renewable electricity on energy efficiency and full load hours of fossil-fired power plants in the European Union". In: *Energy* 138, pp. 575–589.
- Gule, Magnus (2016). *Dynamic process simulation of heat recovery steam generator designed for offshore oil and gas installations*. Master Thesis. Department of Energy and Process Engineering, Norwegian University of Science and Technology.
- Haar, Adam van de et al. (2017). "Dynamics of Post-combustion CO₂ Capture Plants: Modeling, Validation, and Case Study". In: *Industrial & Engineering Chemistry Research* 56, pp. 1810–1822.
- Hamborg, Espen S. et al. (2014). "Results from MEA testing at the CO₂ Technology Centre Mongstad. Part II: Verification of baseline results". In: *Energy Procedia* 63. 12th International Conference on Greenhouse Gas Control Technologies, GHGT-12, pp. 5994–6011.
- Hübel, Moritz et al. (2017). "Modelling and simulation of a coal-fired power plant for start-up optimisation". In: *Applied Energy* 208, pp. 319–331.
- He, Zhenrong and Luis A. Ricardez-Sandoval (2016). "Dynamic modelling of a commercial scale CO₂ capture plant integrated with a natural gas combined cycle (NGCC) power plant". In: *International Journal of Greenhouse Gas Control* 55, pp. 23–35.
- Hefni, Baligh El (2014). "Dynamic Modeling of Concentrated Solar Power Plants with the ThermoSysPro Library (Parabolic Trough Collectors, Fresnel Reflector and Solar-Hybrid)". In: *Energy Procedia* 49. Proceedings of the SolarPACES 2013 International Conference, pp. 1127–1137.
- Hoppe, Timm, Friedrich Gottelt, and Stefan Wischhusen (2017). "Extended Modelica model for heat transfer of two-phase flows in pipes considering various flow patterns". In: *Proceedings of the 12th International Modelica Conference, Prague, Czech Republic*, pp. 467–476.
- Huber, Matthias, Desislava Dimkova, and Thomas Hamacher (2014). "Integration of wind and solar power in Europe: Assessment of flexibility requirements". In: *Energy* 69, pp. 236–246.
- Huebel, Moritz et al. (2014). "Modelling a lignite power plant in modelica to evaluate the effects of dynamic operation and offering grid services". In: *Proceedings of the 10th International Modelica Conference, March 10-12, 2014, Lund, Sweden*, pp. 1037–1046.
- IEA (2012). *Harnessing variable renewables: A guide to the balancing challenge*. Paris, France: International Energy Agency.
- (2015a). *Energy Technology Perspectives 2015*. Paris, France: International Energy Agency.
- (2015b). *World Energy Outlook 2015*. International Energy Agency.

- (2016a). *20 years of Carbon Capture and Storage. Accelerating the future deployment*. Paris, France: International Energy Agency.
- (2016b). *Carbon Capture and Storage: The solution for deep emissions reductions*. International Energy Agency.
- (2017). *World Energy Investment 2016*. International Energy Agency.
- IEAGHG (2012). *Operating Flexibility of Power Plants with CCS*. IEA Greenhouse Gas R&D Programme.
- (2016). *Evaluation of process control strategies for normal, flexible, and upset operation conditions of CO₂ post combustion capture processes*. IEA Greenhouse Gas R&D Programme.
- IPCC (2013). *Climate Change 2013: The physical science basis. Contribution of Working Group I to the Fifth Assessment Report of the Intergovernmental Panel on Climate Change*. Cambridge, UK and New York, NY, USA: Intergovernmental Panel on Climate Change.
- (2014). *Working Group III Contribution to the Fifth Assessment Report of the Intergovernmental Panel on Climate: Climate change 2014. Mitigation of Climate change*. 10013-2473. Version 2014. New York, USA: Intergovernmental Panel on Climate Change.
- Jonshagen, Klas, Majed Sammak, and Magnus Genrup (2011). "Post combustion CO₂ Capture for Combined Cycles Utilizing Hot-Water Absorbent Regeneration". In: *J. Eng. Gas Turbines Power* 134, p. 7.
- Jordal, Kristin et al. (2012). "Design-point and part-load considerations for natural gas combined cycle plants with post combustion capture". In: *International Journal of Greenhouse Gas Control* 11, pp. 271–282.
- Kehlhofer, Rolf et al. (2009). *Combined gas and steam turbine power plants. 3rd Edition*. PennWell.
- Kim, J.H. et al. (2000). "Model Development and Simulation of Transient Behavior of Heavy Duty Gas Turbines". In: *Journal of Engineering for Gas Turbines and Power* 123, pp. 589–594.
- Koeijer, Gelein de et al. (2009). "European CO₂ test centre Mongstad–Testing, verification and demonstration of post-combustion technologies". In: *Energy Procedia* 1. Proceedings of the 9th International Conference on Greenhouse Gas Control Technologies (GHGT-9), 16–20 November 2008, Washington DC, USA, pp. 1321–1326.
- Luo, Xiaobo, Meihong Wang, and Jian Chen (2015). "Heat integration of natural gas combined cycle power plant integrated with post-combustion CO₂ capture and compression". In: *Fuel* 151. The 10th European Conference on Coal Research and its Applications, pp. 110–117.
- Matlab Simulink, Mathworks, Natick, MA*. <https://es.mathworks.com/products/simulink.html>. Accessed: 2018-01-21.
- Mechleri, Evgenia, Paul S. Fennell, and Niall Mac Dowell (2017). "Optimisation and evaluation of flexible operation strategies for coal- and gas-CCS power stations with a multi-period design approach". In: *International Journal of Greenhouse Gas Control* 59, pp. 24–39.
- Modelica and the Modelica Association*. <https://www.modelica.org/>. Accessed: 2017-12-01.
- Modelon Gas Liquid Contactors Library*. http://www.modelon.com/fileadmin/user_upload/Industries/Energy_Process/CCS/PostCombustionCapture_flyer.pdf. Accessed: 2017-12-01.

- Modelon Thermal Power Library*. http://www.modelon.com/fileadmin/user_upload/Products/Modelon/-flyers/TPL_web.pdf. Accessed: 2017-12-01.
- Montañés, Rubén M., Nina E. Flø, and Lars O. Nord (2017). "Dynamic process model validation and control of the amine plant at Technology Centre Mongstad". In: *Energies* 10, p. 1527.
- (2018). "Experimental results of transient testing at the amine plant at Technology Centre Mongstad: Open-loop responses and performance of decentralized control structures for load changes". In: *International Journal of Greenhouse Gas Control* 73, pp. 42–59.
- Montañés, Rubén M. and Lars O. Nord (2017). "Dynamic Simulations of the Post-combustion CO₂ Capture System of a Combined Cycle Power Plant". In: Proceedings of the 12th International Modelica Conference. May 15-17, 2017. Prague, Czech Republic, pp. 111–119.
- Montañés, Rubén M. et al. (2016). "Identifying Operational Requirements for Flexible CCS Power Plant in Future Energy Systems". In: *Energy Procedia* 86. The 8th Trondheim Conference on CO₂ Capture, Transport and Storage, pp. 22–31.
- Montañés, Rubén M. et al. (2017a). "Demonstrating load-change transient performance of a commercial-scale natural gas combined cycle power plant with post-combustion CO₂ capture". In: *International Journal of Greenhouse Gas Control* 63, pp. 158–174.
- Montañés, Rubén M. et al. (2017b). "Dynamic Process Model Development and Validation with Transient Plant Data Collected from an MEA Test Campaign at the CO₂ Technology Center Mongstad". In: *Energy Procedia* 114. 13th International Conference on Greenhouse Gas Control Technologies, GHGT-13, 14-18 November 2016, Lausanne, Switzerland, pp. 1538–1550.
- Montañés, Rubén M. et al. (2018). "Dynamic Modeling of a Parabolic Trough Solar Thermal Power Plant with Thermal Storage Using Modelica". In: *Heat Transfer Engineering* 39, pp. 277–292.
- Moran et al. (2012). *Principles of engineering thermodynamics. Seventh edition*. WILEY.
- National Carbon Capture Centre NCCC. <https://www.nationalcarboncapturecenter.com/>. Accessed: 2017-11-01.
- Nittaya, Thanita et al. (2014). "Dynamic modelling and control of MEA absorption processes for CO₂ capture from power plants". In: *Fuel* 116, pp. 672–691.
- NREL (2012). *Power Plant Cycling Costs*. Technical Report. Version 2012. NERL.
- Panahi, Mehdi and Sigurd Skogestad (2011). "Economically efficient operation of CO₂ capturing process part I: Self-optimizing procedure for selecting the best controlled variables". In: *Chemical Engineering and Processing: Process Intensification* 50, pp. 247–253.
- (2012). "Economically efficient operation of CO₂ capturing process. Part II. Design of control layer". In: *Chemical Engineering and Processing: Process Intensification* 52, pp. 112–124.
- Pierobon, Leonardo et al. (2014). "Design methodology for flexible energy conversion systems accounting for dynamic performance". In: *Energy* 68, pp. 667–679.

- Pröll, Katrin et al. (2011). "Dynamic model of a post-combustion absorption unit for use in a non-linear model predictive control scheme". In: *Energy Procedia* 4. 10th International Conference on Greenhouse Gas Control Technologies, pp. 2620–2627.
- ProTRAX, Trax LLC, Energy Solutions, Lynchburg, VA. <https://energy.traxintl.com/training/protrax-cloud/>. Accessed: 2018-01-21.
- Rebours, Yann et al. (2007). "A Survey of Frequency and Voltage Control Ancillary Services mdash. Part I: Technical Features". In: *IEEE Transactions on Power Systems* 22, pp. 350–357.
- Rezazadeh, Fatemeh et al. (2015). "Performance viability of a natural gas fired combined cycle power plant integrated with post-combustion CO₂ capture at part-load and temporary non-capture operations". In: *International Journal of Greenhouse Gas Control* 39, pp. 397–406.
- Rochelle, Gary (2009). "Amine Scrubbing for CO₂ Capture". In: *Science* 325, pp. 1652–1654.
- Rochelle, Gary et al. (2011). "Aqueous piperazine as the new standard for CO₂ capture technology". In: *Chemical Engineering Journal* 171. Special Section: Symposium on Post-Combustion Carbon Dioxide Capture, pp. 725–733.
- Rowen, W.I. (1983). "Simplified Mathematical Representations of Heavy-Duty Gas Turbines". In: *Journal of Engineering for Power* 105, pp. 865–869.
- Saravanamutto, H.I.H. et al. (2009). *Gas Turbine Theory. 6th Edition*. Pearson Education Limited.
- Saskpower Shand Carbon Capture Test Facility. <http://www.saskpower.com/our-power-future/carbon-capture-and-storage/shand-carbon-capture-test-facility/>. Accessed: 2017-11-01.
- Schiavo, Francesco and Francesco Casella (2007). "Object-oriented modelling and simulation of heat exchangers with finite element methods". In: *Mathematical and Computer Modelling of Dynamical Systems* 13, pp. 211–235.
- Shah, Ramesh K. and Dušan P. Sekulić (2003). *Fundamentals of heat exchanger design*. John Wiley and Sons.
- Shin, Jeeyoung Y. et al. (2002). "Analysis of the dynamic characteristics of a combined-cycle power plant". In: *Energy* 27, pp. 1085–1098.
- SIEMENS AG (2011). *The future role of thermal power generation*. Erlagen, Germany.
- Singh, Ajay and Karl Stéphane (2014). "Shell Cansolv CO₂ capture technology: Achievement from First Commercial Plant". In: *Energy Procedia* 63. 12th International Conference on Greenhouse Gas Control Technologies, GHGT-12, pp. 1678–1685.
- Sipöcz, Nikolett and Finn Andrew Tobiesen (2012). "Natural gas combined cycle power plants with CO₂ capture – Opportunities to reduce cost". In: *International Journal of Greenhouse Gas Control* 7, pp. 98–106.
- Skogestad, Sigurd and Ian Postlethwaite (2006). *Multivariable feedback control. Analysis and design*. WILEY.
- Stoppato, Alberto et al. (2012). "On the operation strategy of steam power plants working at variable load: Technical and economic issues". In: *Energy* 37. 7th Biennial International Workshop "Advances in Energy Studies", pp. 228–236.

- The Third MEA Campaign at the CO₂ Technology Centre Mongstad*. <https://az659834.vo.msecnd.net/eventsairwesteuprod/production-ieaghg-public>. Accessed: 2017-11-02.
- Thermoflow Inc*. <https://www.thermoflow.com/>. Accessed: 2017-11-23.
- Thimsen, David et al. (2014). "Results from MEA testing at the CO₂ Technology Centre Mongstad. Part I: Post-Combustion CO₂ capture testing methodology". In: *Energy Procedia* 63. 12th International Conference on Greenhouse Gas Control Technologies, GHGT-12, pp. 5938–5958.
- Tummescheit, Hubertus (2002). *Design and Implementation of Object-Oriented Model Libraries using Modelica*. Department of Automatic Control, Lund Institute of Technology (LTH). PhD Thesis. Lund University.
- UKCCSRC *Pilot-scale Advanced Capture Technology (PACT)*. <http://www.pact.ac.uk/facilities/PACT-Core-Facilities/Solvent-based-Carbon-Capture-Plant/>. Accessed: 2017-11-01.
- Unisim, Honeywell*. <https://www.honeywellprocess.com/en-US/training/programs/advanced-applications/Pages/process-simulation.aspx>. Accessed: 2018-01-21.
- Vaccarelli, Maura et al. (2016). "Combined cycle power plants with post-combustion CO₂ capture: Energy analysis at part load conditions for different HRSG configurations". In: *Energy* 112, pp. 917–925.
- VDI-Wärmeatlas, 9th edition, section Gg* (1997). Springer.
- Versteeg, Peter et al. (2013). "Cycling Coal and Natural Gas-fired Power Plants with CCS". In: *Energy Procedia* 37. GHGT-11 Proceedings of the 11th International Conference on Greenhouse Gas Control Technologies, 18-22 November 2012, Kyoto, Japan, pp. 2676–2683.
- W.A. Parish *Post-Combustion CO₂ Capture and Sequestration Project*. <https://www.netl.doe.gov/research/coal/project-information/fe0003311>. Accessed: 2017-11-01.
- Wang, Yuan et al. (2017). "A Review of Post-combustion CO₂ Capture Technologies from Coal-fired Power Plants". In: *Energy Procedia* 114. 13th International Conference on Greenhouse Gas Control Technologies, GHGT-13, 14-18 November 2016, Lausanne, Switzerland, pp. 650–665.
- Welfonder, E. (1999). "Dynamic interactions between power plants and power systems". In: *Control Engineering Practice* 7, pp. 27–40.
- Wellner, Kai, Thomas Marx-Schubach, and Gerhard Schmitz (2016). "Dynamic Behavior of Coal-Fired Power Plants with Postcombustion CO₂ Capture". In: *Industrial & Engineering Chemistry Research* 55, pp. 12038–12045.
- Zero Emissions Platform (2013). *CO₂ Capture and Storage (CCS). Recommendations for transitional measures to drive deployment in Europe*. Version 2013. Zero Emissions Platform.

Appendix A

Papers

Paper I

Rubén M. Montañés, Magnus Korpås, Lars O. Nord, Stefan Jaehnert, Identifying operational requirements for flexible CCS power plant in future energy systems, *Energy Procedia*, January 2016; 86; pp. 22-31.

Paper II

Rubén M. Montañés, Nina E. Flø, Lars O. Nord, Dynamic process model validation and control of the amine plant at CO₂ Technology Centre Mongstad, *Energies*, October 2017; 10, 1527

Paper III

Rubén M. Montañés, Nina E. Flø, Lars O. Nord, Experimental results of transient testing at the amine plant at Technology Centre Mongstad: open-loop responses and performance of decentralized control structures for load changes, *International Journal of Greenhouse Gas Control Technologies*, June 2018; 73, pp. 42-59.

Paper IV

Rubén M. Montañés and Lars O. Nord, Dynamic Simulations of the Post-combustion CO₂ Capture System of a Combined Cycle Power Plant, *Proceedings of the 12th International Modelica Conference, Prague, Czech Republic, May 15-17, 2017*, Issue 132, pp. 111-119.

Paper V

Rubén M. Montañés, Stefania Ósk Gardarsdóttir, Fredrik Normann, Filip Johnsson, Lars O. Nord, Demonstrating load change transient performance of a commercial scale natural gas combined cycle power plant with post-combustion CO₂ capture, *International Journal of Greenhouse Gas Control Technologies*, August 2017; 63, pp. 158-174.

Paper I



The 8th Trondheim Conference on CO₂ Capture, Transport and Storage

Identifying operational requirements for flexible CCS power plant in future energy systems

Rubén M. Montañés^{a*}, Magnus Korpås^b, Lars O. Nord^a, Stefan Jaehnert^b

^aDept. of Energy and Process Engineering, Norwegian University of Science and Technology, Kolbjørn Hejes v. 1B, 7491 Trondheim, Norway

^bDept. of Electric Power Engineering, Norwegian University of Science and Technology, O.S. Bragstads plass 2E, 7034 Trondheim, Norway

Abstract

This paper aims at a discussion of operational requirements for thermal power plants with carbon capture and storage in terms of their interaction with the power system, in regions with high penetration of variable renewable energy sources. Market opportunities for flexible power plants equipped with carbon capture processes have been discussed. These opportunities comprise day-ahead markets, intraday markets, balancing markets and providing ancillary services for stable operation of the power grid. In addition, technical requirements for power units to provide ancillary services and bidding in different balancing markets in four different power areas in EU have been identified. The identified technical requirements can be used to define scenarios for operational flexibility studies based on dynamic process simulation of thermal power plants with CO₂ capture.

© 2016 The Authors. Published by Elsevier Ltd. This is an open access article under the CC BY-NC-ND license

(<http://creativecommons.org/licenses/by-nc-nd/4.0/>).

Peer-review under responsibility of the Programme Chair of the 8th Trondheim Conference on CO₂ Capture, Transport and Storage

Keywords: Operational flexibility, ancillary services, balancing, power system, operating reserves, power markets, CO₂ capture;

1. Introduction and scope

The European Union is committed towards a future energy system with reduced greenhouse gas emissions to 80-95% below 1990 levels by 2050. According to the European Commission, a secure, competitive and decarbonized energy system in 2050 is possible [1]. In decarbonized scenarios, electricity will play an increased role, together with renewable energy sources. Nevertheless, the mentioned target will exert intensive pressure on energy systems.

* Corresponding author. Tel.: +47735093722.
E-mail address: ruben.m.montanes@ntnu.no

Investment models to identify the most cost-effective route towards a decarbonized European power system have been developed by the Zero Emissions Platform. Their results show the requirement of an energy mix combining hydro, wind and solar power, together with a progressive introduction, between 2030 and 2050, of lignite, coal, gas, and biomass power plants with CO₂ Capture and Storage (CCS) [2]. Thermal power plants with CCS at commercial scale will require high capital investments and therefore will need to have high capacity factors along their lifetime in order to be profitable, or receive capacity payments, in addition to other support measures for early deployment [3].

Within a power system with high penetration of variable renewable energies (VRE), thermal power plants tend to operate in cycling mode to follow demand and generation variability. Besides selling energy in day-ahead markets, flexible fossil-fueled power plants acting as mid-merit plants might increase their profit margins by participating in other markets. These markets include intraday power markets, bidding in balancing markets, and providing ancillary services for grid stability. Another interesting option is capacity markets [4], which are out of the scope of this paper.

In recent years, there has been an increased concern of the role that CCS might have in future power systems with high penetration of VRE. Increasing interest has grown in the field of operational flexibility of thermal power plants with carbon sequestration technologies. A report from IEA summarizes several aspects of operational flexibility of different power plant technologies with and without CCS [5].

The scope of this paper is to identify market opportunities for flexible thermal power plants with CCS in different areas of the pan-European power system beyond selling energy in day-ahead markets. In addition, technical requirements for power units to bid in different balancing markets and provide ancillary services have been identified.

Nomenclature

| | |
|---------|---|
| VRE | Variable renewable energy sources |
| CCS | CO ₂ capture and storage |
| TSO | Transmission system operator |
| ENTSO-E | European Network of Transmission System Operators |
| CHP | Combined heat and power |
| GB | Great Britain |
| GT | Gas Turbine |
| ASU | Air Separation Unit |

2. Methodology

Results from a day-ahead multi-area power market simulator (EMPS) used for the TWENTIES EU project has been utilized in this paper [6]. The models were previously developed by SINTEF Energy Research. These results are used to plot wind power production and the market-based electric generation dispatch of three different thermal power plants in the Nordic and Continental Europe region. The objective is to illustrate some correlations between wind power production and cycling operation requirements of dispatchable power plants by 2030.

The European Commission has stated the goal of integrating European power markets for making efficient use of energy across national borders. The Network Codes, developed by the European Network of Transmission System Operators for Electricity (ENTSO-E) [7], are meant to overcome the challenge of integrating VRE into the future pan-European power system by 2030. These network codes are currently under development, and after becoming law, power system participants will have to adhere to these codes. These include power system operation, market related codes, and grid connection codes. The technical requirements that can be found in these codes are described as general guidelines. Since each power system has its own flexibility requirements [8], there is room for decision to be made at national level and local TSOs can define specific requirements within the frameworks defined by ENTSO-E.

With the purpose of identifying the technical requirements for grid connection of thermal power plants in current and future power systems, the grid codes of four selected European countries are studied. In addition, requirements for power plants to be able to bid in balancing markets are exposed in Table 1. The selected countries are Spain, Germany, Great Britain (GB), and Denmark.

3. Power system related requirements

Flexibility of a power system is the extent to which the system can modify electricity production or consumption in response to variability. In order to have a stable working system, the balance between supply and demand of electricity must be ensured at different time scales, comprising from milliseconds to seasons [9]. Expected and promoted higher penetration of VRE such as wind and solar will accentuate the challenge of power system balancing.

When considering power system balancing in regions with high penetration of VRE, it is the net load what matters, i.e., the demand curve after subtracting the power generation by VRE. Fluctuations in net load are more frequent and have stronger uncertainty impacts. The main needs for flexibility in the power system are net load fluctuation and uncertainty in contingencies. Main sources that can provide flexibility to ensure balancing at different time scales are dispatchable power plants, demand side management and response techniques, energy storage facilities and interconnection with adjacent markets [8].

Operational flexibility is one of the main challenges for modern thermal power plants. The main technical aspects of operational flexibility of mid-merit thermal power plants are the following:

- Start-up and shutdown sequence (hot, warm and cold).
- Part-load efficiency.
- Minimum stable load turndown with acceptable emission levels.
- Load ramps and reserve capacity for providing grid services.

Adding carbon capture equipment adds complexity to the power plant, with increased process integration and increased number of processes. This requires additional construction material, auxiliary equipment, and more fluid masses providing thermal and pressure inertia. As a result, the performance of the power plant is changed compared to similar plants without CCS. Slower changes in load, transient temperatures and pressure evolutions in the system are expected [10], in addition to a reduction in net plant efficiency. The main impacts of adding the carbon capture system regarding flexible performance of the power plant depend on the technology used [5].

3.1. Day-ahead market

In day-ahead power markets, buyers and sellers bid the volume they are willing to buy or sell for each hour (or possibly other time steps) of the next day (MWh/h) with their respective bidding price (EUR/MWh). The clearing price is stipulated in a so-called marginal price setting, where generation and supply curves intersect. The displacement in the merit order can be explained by the fact that thermal power plants have higher marginal costs of production than wind and solar, which have virtual null marginal costs. Thermal power marginal costs of generation mainly consist of fuel costs and CO₂ emission costs.

Whenever the wind or solar radiation conditions are adequate for power generation, VREs will bid with reduced marginal costs and therefore displace other generation units that otherwise would have been part of the generation schedule for the given hour of the day. Studies using coupled investment and dispatch models of Europe from McCoy et al. [11] show that increased penetration of VRE tend to increase the slope of the net load curve. Consequently, base load and mid-merit capacity power plants reduce their capacity factors in future scenarios with high penetration of VRE. Studies from high wind penetration scenarios in Netherlands by Brouwer et al. [12] explain that extensive integration of VRE may have several impacts in daily operation of power systems: increased demand for reserves, efficiency reduction of thermal power generation, wind curtailment and displacement of thermal power generation in the merit order. In addition, reduced load factors of thermal power plants are expected.

Day-ahead market results of thermal power dispatch from a day-ahead multi-area power market simulator (EMPS) have been utilized in this paper. The main purpose is to illustrate effects of wind power generation in thermal power plants dispatch in future day-ahead markets.

The model includes a detailed system description for Norway, Sweden, Finland, Denmark, Belgium, the Netherlands, Germany and Great Britain, including main transmission bottlenecks in the power system. Some of the model data were developed in TWENTIES EU by SINTEF Energy Research, and a detailed explanation of the

modeling assumptions and purpose of the project can be found in Twenties report task 16.3 [6]. Scenarios are considered for Northern Europe by 2030 with detailed assumptions for generation, transmission and consumption, and their respective development. Thermal power production is modeled by 350 thermal power plants being divided into base load (mainly nuclear and CHP), mid-merit, peaking, and non-dispatchable power plants.

Thermal power plants are modelled by their available generation capacity per week (corrected by an availability factor) and their marginal costs of operation. Main marginal costs of operation are fuel costs and CO₂ emission costs, according to Eq. (1). In the model, fuel costs are considered constant from 2020 to 2030 while CO₂ emission costs were considered to increase from 13 EUR/t by 2010 up to 44 EUR/t by 2030 [6], according to the assumptions made in the IEE-EU Offshore Grid project [13].

$$\text{marginal cost} = \frac{\text{fuel cost}}{\text{fuel efficiency}} + \text{CO}_2 \text{ cost} \quad (1)$$

Figure 1 shows wind production and day-ahead market dispatch of three thermal power plants for three consecutive weeks during January 2030; a 308 MW_{el} lignite fired power plant, a 127 MW_{el} coal fired thermal power plant and a 170 MW_{el} gas fueled thermal power plant. It can be observed that there is certain correlation between hours with high wind power production and part load operation or shut down of the thermal power generation plant. The zero marginal costs of VRE places thermal power generation out of production with several hours when the thermal power plants are not producing electricity. These thermal power plants operate in cycling mode i.e., under part load operation and even shutting down and starting-up several times during the time span of three weeks. The results show similar trends to those illustrated by Bruce et al. [14]. The illustrated results depend on the above stated assumptions for fuel and CO₂ emission costs.

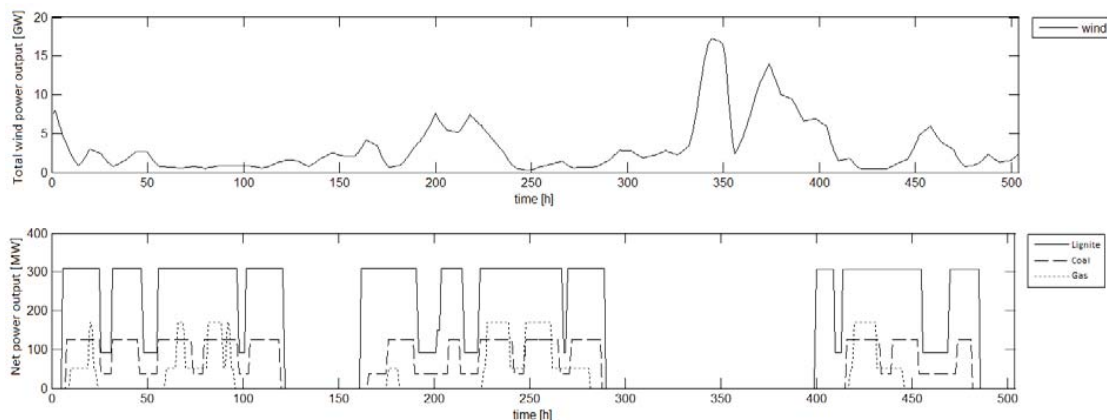


Figure 1. Total wind power production (top) and day-ahead market-based hourly dispatch of three dispatchable thermal power plants (bottom) in Northern and Continental Europe by 2030. The time span is three weeks during winter. Results from EMPS market simulation.

Changing in generation schedule of thermal power plants influences their profit margins. The profit margin is defined as the income due to electricity sold minus the production costs. To make a thermal power plant profitable, the margins should be higher than fixed maintenance and investment costs [6]. This might be a critical aspect for power plants with CCS, since such plants require additional process equipment resulting in increased fixed maintenance and investment costs [15]. Therefore, plant owners should look at other market opportunities beyond selling energy in day-ahead markets to increase their incomes.

3.2. Intraday market

Nowadays, the majority of the volume traded in liberalized wholesale power markets is through the day-ahead market, and balance between demand and supply can be mainly established there. However, incidents may occur between the closing of the day-ahead market and real-time, which comprise between 12 and 36 hours. For example, updated wind forecasts can show higher production than expected, while a nuclear or another thermal power plant may stop generating due to a contingency. In intraday markets, buyers and sellers can update their traded volumes closer to real-time. In Nordel, an intraday market known as Elbas is operated by Nord Pool Spot AB. Elbas is a continuous market, where trading takes place anytime around the clock until one hour before real-time. The price is set by matching the highest buying price with the lowest selling price.

As higher penetration of VRE enters into the grid, intraday balancing markets are expected to become more and more important. Trading in intraday markets could be an opportunity for slower flexible resources to improve their profits. It makes sense that thermal power plants with flexible carbon capture technologies operated as dispatchable thermal power plants could bid in these markets. Nevertheless, no specific operating requirements from the power grid are required to bid in such markets.

3.3. Balancing markets

In liberalized power markets, the day-ahead clearing market results in a balance between the expected consumption and the expected power generation. In intraday markets buyers and sellers can update their traded volumes closer to real-time, until around one hour before actual production and consumption. Even closer to real-time, system imbalance between the actual power generation and actual consumption occurs. System balancing is one of the main responsibilities of a transmission system operator (TSO). Power consumers or producers can provide these services. In order to guarantee system stability and security, TSOs must procure and operate the so-called ancillary services. These include frequency response, fast reserve (to provide fast energy to counteract sudden and sometimes unpredictable unbalance between generation and load), black start capability and the provision of reactive power, among others.

Power plants with CCS at commercial scale will likely be designed for capacities above 200 MW_{el}. This means that power plants with CCS would be classified as large generators in most grid connection codes, as it is the case with ENTSO-E codes [7]. Therefore, CCS power plants are likely to participate in providing services for power grid stability.

Power system frequency is a continuously changing variable that is controlled by the second-to-second balance between demand and generation. If generation is greater than demand, the frequency of the system raises, if demand is greater than generation, the system frequency drops. The TSO is in charge of keeping the frequency close to the nominal value within a narrow band. To achieve that, the responsible TSO must ensure that sufficient flexible reserves are available to provide balance between demand and supply close to real-time [16].

Primary reserve or primary frequency response is an automatic change in active power output in response to a frequency change (increase when dropping system frequency or decrease when increasing system frequency) [17]. Synchronized generators make use of automatic speed governors defined by a characteristic droop, as expressed in Eq. 2.

The droop is defined as the “ratio of the steady-state change of frequency (referred to nominal frequency) to the steady-state change in power output (referred to maximum capacity)” [7]. Note that from a control theory point of view the primary frequency control is a proportional regulator. This is meant to limit and stop main system frequency excursions from its set value, however a new steady-state point will be reached [18].

$$s = - \frac{\Delta f / f_{nom}}{\Delta P / P_{nom}} \quad (2)$$

Secondary frequency control is a centralized automatic control that has the function of restoring the system frequency. While primary frequency control limits and stops frequency excursions, secondary control restores the frequency to its set value. The units in the area where the imbalance occurs will participate. Secondary frequency control is not indispensable and thus not all power systems implement it, as it is the case of Great Britain [19].

Tertiary frequency control is utilized for restoring primary and secondary reserves, and to balance large and remaining system imbalance due to forecast errors, failures or other contingencies. It refers to manual changes in the dispatching and commitment of generating units, and it can be used as a mechanism for market participants to balance their financial positions [19]. It means that slower flexible resources than those providing primary and secondary response can also participate in tertiary frequency response [18].

This opens up an opportunity for flexible CCS units to bid in these markets. Main technical requirements for frequency related ancillary services are specified by deployment times [19]:

- Deployment start: maximum amount of time between requests from TSO to start of the response.
- Full availability: maximum time that can elapse between start of the response until the full response is established.
- Deployment end: maximum amount of time during which the service must be provided.

Table 1 contains main technical requirements for participating in balancing markets and provide ancillary services by power generation units according to regulations in Spain, Germany, Great Britain and Denmark. Primary frequency response is a mandatory and non-paid service in Spain [20], while being mandatory and paid via a holding payment and an energy payment in GB [17]. In Germany, providers of primary frequency must bid in weekly tenders to provide primary frequency response, and providers of this service will receive a capacity payment [18].

Providing secondary frequency control in Spain requires a deployment start of 30 seconds and full action should be provided within 15 minutes. Providers of this service bid the power band to be increased or decreased together with the energy price when providing that service. The allocation is based on merit order clearing [20]. In Germany, this service is procured with weekly tenders with a minimum bid amount of 5 MW and 1 MW increments, established with a pay-as-bid mechanism, being paid capacity and energy produced while providing this service [18]. In GB secondary control as defined above is not implemented [19]. In Denmark, providing secondary frequency control requires an activation time of 30 seconds followed by a full activation within 15 minutes. A capacity payment is established via a pay-as-bid method in a monthly basis and energy produced while providing the service is remunerated [21].

Tertiary frequency response in Spain consists of the maximum variation of power that can be sustained for at least 2 hours. The service remuneration price is the marginal price of the allocated bids each hour. Bids are sent the day before and can be updated until 25 minutes of the beginning of the hour [20]. In Germany, the tertiary control reserve is known as minute's reserve, and the provider has to provide the bid MW within 15 minutes [18]. In Great Britain, there are various reserve services differentiated as fast reserve and short term operating reserve [17].

Challenges for providing primary frequency control on CCS power plant should not be more demanding than for conventional thermal power plants. An important question is whether the capture processes can influence the capability of the plant to provide fast enough ramping response to bid a substantial amount of power and provide secondary and tertiary control, and how providing such fast requirements is going to affect operability and controllability of the plant. In addition, parameters such as CO₂ capture ratio can be affected during the transient performance.

Note that primary, secondary and tertiary procured reserves are limited within a given power area. Hence, the CCS flexibility resource must be able to compete with other flexible resources in order to provide ancillary services and bidding in balancing markets.

Operation of a power plant with CCS under different market conditions is of importance. These market conditions comprise fuel prices, CO₂ emission costs, possible CO₂ capture premium payments and electricity prices. Different studies are found in literature, most of them focusing in post-combustion technology [10,14,22,23,24]. These studies can give insight on which market conditions would provide value to plant owners to operate the plant in flexible mode, with different plant operation strategies.

Table 1. Technical requirements framework for generating units to provide ancillary services and bid in balancing markets in Spain, Germany, GB, and Denmark.

| Area | TSO | Primary reserve | Secondary reserve | Tertiary reserve |
|----------------------------------|---|--|---|--|
| Spain [20] | Red Eléctrica de España (50 Hz) | <i>Primary regulation</i> Mandatory for all generation units. Load change of 1.5% of nominal (0<t<15 sec) for frequency changes ≤100 mHz. Lineal from 15<t<30 sec. Non-paid service. | <i>Secondary regulation</i> Automatic and hierarchical control. Start ≤ 30 sec from notice and full action in 15 min. Licensed generation units bid power band to be increased and reduced (MW) and power band price (€/MWh). Reserve allocation based on economic merit order. Uniform price. | <i>Tertiary regulation</i> Maximum variation of power within 15 min. that deployment end of at least 2 h. Bids sent the day before and updated until 25 min. before the beginning of the hour. <i>Slow reserve</i> Running reserves of connected thermal units providing power output in 30 min. and can be sustained up to 4-5 hours. |
| Germany [18] | Amprion 50 Hertz TenneT TSO EnBW Transportnetze (50 Hz) | Primary reserve TSO responsible for provision of primary regulation required for its area. 30 sec to be activated. Weekly tender period (competitive bidding). Minimum bid amount 1 MW (1 MW increment). Call for tender as capacity price merit-order. Remunerated as pay-as-bid. | Secondary reserve Should be activated after 30 sec. from call and achieve full response within 5 minutes. Sustained 15 min. Weekly tender period. Minimum bid amount 5 MW (1 MW increment). Positive and negative differentiation. Energy price merit-order. Pay-as-bid (Capacity price and energy price). | <i>Minutes reserve</i> Activated in quarterly hour intervals if needed. Complete activation within 15 min. Sustained for t>15 min up to several hours. Daily tender period. Minimum bid amount (blocks of maximum 25 MW with 1 MW increment). Energy price merit-order. Pay-as-bid (Capacity price and energy price). |
| GB [17] | National Grid (50 Hz) | <i>Primary</i> Mandatory for large units ≥ 100MW. Droop 3-5%. Active power provided within 10 sec. and sustained for further 20 sec. Holding Payment (£/h). Monthly basis price. Response energy payment (£/MWh). <i>Secondary</i> Mandatory for large units ≥ 100 MW. Droop 3-5%. Active power provided within 30 sec. and sustained for further 30 min. Capacity Payment (£/h). Response energy payment (£/MWh). | | <i>Fast reserve</i> Dispatch instruction from TSO. Must start after 2 min. of dispatch instruction. Delivery rate in excess of 25 MW/min. Full response sustained for a minimum of 15 min (min. 50 MW). Monthly procurement. Availability fee (£/h) and utilization fee for energy delivered ((£/MWh). |
| Denmark (Western) [21] | Energinet.dk (50 Hz) | <i>Primary reserve</i> Droop normal operation 4-6% at 50±0.1 Hz. Daily auction in six equally divided blocks. Marginal price principle for capacity payments. | <i>Secondary reserve</i> Activation time of 30 sec. Full activation 15 min. Monthly pay-as-bid method for capacity payment. Energy payment. | <i>Manual reserve</i> Daily auctions The reserve must be able to be provided within 15 minutes. |

4. Discussion

An assessment of potential flexibility of power plants with CCS by IEA Greenhouse Gas R&D Program summarizes main flexibility issues and reviews suggested strategies to provide flexibility [5]. The main impacts of adding the carbon capture system regarding flexible performance of the power plant depend on the technology used.

Conventional NGCC and ultra-super critical pulverized coal power plant (USC PC) have good cycling properties, with relatively short hot start-up and fast load changes together with good part-load efficiency and low minimum turndown. However, adding a post-combustion capture unit to these power plants can impose bottlenecks for turndown (due to the minimum CO₂ compressor load of 70%, and the capture unit minimum load [5]). In addition, longer start-up time due to the need for regenerator preheating can extend the start-up process. To the extent of the authors' knowledge, effects on transient performance during load changes are still unclear, due to the lack of transient data from actual large-scale plants.

Several options have been proposed to operate flexible thermal power plants equipped with post-combustion capture in order to provide peak electricity when electricity prices are high, and to participate in providing ancillary services. Three main options are [5]:

- Varying the CO₂ capture rate, depending on electricity prices and CO₂ costs.
- Turning on and off the CO₂ capture unit and providing solvent storage to decouple plant operation (boiler or GT) from the CO₂ capture.
- Allowing the power plant to increase or decrease load, following its own ramp up or down rates.

The first option is also known as flue gas bypass, which consists of stopping the CO₂ capture plant and venting the CO₂, therefore increasing plant net power output by reducing the energy penalty. E. Delarue et al. [15] discusses that profit maximization by using this option depends on the ratio of electricity selling price and CO₂ emission allowances price. At relatively high CO₂ emission prices, the cost of emitting CO₂ can offset the benefit from flexible operation, and therefore capturing CO₂ becomes more interesting. It also discusses the option for providing ancillary services, assuming that the plant is fast enough to provide substantial amount of power within the typical 15 minutes framework for full activation. Their sensitivity studies conclude that only at relatively low CO₂ emission prices this operation mode could be profitable and competitive against open cycle gas turbines to provide ramp-up reserve, in the case of power shortage. Therefore, this option might be interesting for implementation under policies that support CO₂ carbon capture implementation without extensive CO₂ emission price increase [22].

Another suggested option to provide net power flexibility in post-combustion capture power plants is the use of solvent storage to decouple the absorption and desorption processes storing rich solvent during peak electricity demand to delay the energy penalty to times with low electricity price. This option would be profitable if relatively high profits are obtained, since further capital investment is to be expected due to the need for storage vessels, more solvent inventory and larger compression and stripper equipment [10] [23].

Several technical challenges remain in order to make this technology attractive. Among them, and as stated by K. Jordal et al. [24], there is need for research for understanding part load operation and behavior of a power plant with integrated post-combustion capture of CO₂, as well as understanding the dynamic interaction between the capture process unit and the power plant during start-up, load change and shut-down.

Regarding oxy-combustion power plants there are different options due to different process schemes proposed in literature, but most flexibility studies discuss the possibility of bypassing flue gas before the purification and compression processes, or making use of intermediate storage of liquid O₂ between the cryogenic air separation unit (ASU) and the combustion process.

Bypassing the flue gas just before the CO₂ compression process, therefore the energy for compression can be used to provide electricity, with the penalty of higher CO₂ emissions. With liquid oxygen storage, the oxygen production is switched towards hours with low electricity prices, to switch off the ASU during peak electricity prices and gain the extra power for running the ASU (mainly the air compression process). Similar to post-combustion, bypassing is only profitable if the relationship between electricity selling price and CO₂ emission certificates is high. Oxygen storage can be an interesting option if sufficient profits are obtained during peak hours to pay-off the increased capital investment [10]. The air separation unit is the main component affecting the cyclic performance of oxy-combustion

power plants using ASU due to its minimum turndown of around 50% and its slow start-up and relatively slow ramp rate 3%/min [5].

Despite of the potential greater income obtained by plant owners in the short term due to a cyclic operating mode, a reduction of lifetime of the most critical components is likely to occur, due to thermo-mechanic fatigue loadings together with creep loads, corrosion and erosion mechanisms [25]. This causes accelerated ageing, and therefore additional costs related to unplanned maintenance and unavailability of the plant due to outages [26].

Due to the necessity to evaluate the plant performance under transient operation and the scarce availability of transient performance data from commercial scale plants with CCS, an increasing interest has grown during recent years in the field of dynamic modeling, simulation and optimization of thermal power plants with CCS [27].

Simulations from properly validated models can give insight on which are the bottlenecks for different transient operations of power plants, developing proper plant control strategies and assesses the feasibility of different strategies for flexible operation of the power plant, during the design phase. The requirements collated in Table 1 can be utilized to define market-based scenarios for dynamic process simulation studies, regarding ancillary services provision.

It might be done by considering activation start, full availability and deployment end times. Valuing the flexible operation of a power plant with CCS under different market conditions is of importance. These market conditions comprise fuel prices, CO₂ emission costs, possible CO₂ capture premium payments and electricity prices. Different studies are found in literature, most of them focusing in post-combustion technology [10,14,22,23,24]. These studies can give insight on which market conditions would provide value to plant owners to operate the plant in flexible mode, with different plant operation strategies.

5. Conclusions

An increased interest has arisen within the last years concerning the role that CCS power plants might have in future energy systems with high penetration of variable renewable energies. Such power plants might be operated as load following plants forced by market conditions and power system operation requirements. According to the results from an EMRS day-ahead market simulation in Northern and Continental Europe by 2030, thermal power plants tend to operate in cycling mode i.e., under part load operation and even shutting down and starting-up several times along three winter weeks. It means that thermal power plants are being displaced in the merit order in scenarios with high penetration of variable renewable energies. Hence, plant operators should look at further opportunities beyond selling energy in day-ahead markets in order to increase their profits. Intraday markets have been identified as especially interesting markets for power plants with CCS since slower flexible resources can have a chance in these growing markets. Nonetheless, no specific operating requirements from the power grid are required to bid in intraday markets.

Technical grid requirements and frameworks for power units to provide ancillary services and bidding in balancing markets in four different power areas in EU have been identified. The areas comprise Spain, Germany, GB, and Western Denmark. These requirements can be utilized to define market-based scenarios for dynamic process simulation studies, considering activation start, full availability and deployment end times. These scenarios will reflect today's requirements for providing the mentioned flexibility services.

Future work should consist of the development of dynamic process simulation models of power plants with carbon capture technologies. These models must be validated against plant data to the greatest extent possible. Simulation from plant models will be utilized to study the flexible operation of the plant and implications of adding capture technology on the plant controllability and capture plant transient performance. In addition, the models might help to identify possible bottlenecks for transient performance under different transient scenarios, and the possible implications on the power plant design. The transient scenarios should include transient performance on load changes and strategies for providing ancillary services, defining the scenarios by using the requirements identified in this paper. Current work comprises the ongoing development of dynamic process models for a Natural Gas Combined Cycle power plant with post-combustion CO₂ capture.

Acknowledgements

The authors would like to acknowledge the Department of Energy and Process Engineering at the Norwegian University of Science and Technology for funding this project.



References

- [1] European Commission, “Energy roadmap 2050,” Brussels, 2012.
- [2] ZEP, “CO₂ Capture and Storage (CCS). Recommendations for transitional measures to drive deployment in Europe. Zero Emissions Platform,” 2013.
- [3] Zero Emissions Platform, “ZEP report on CCS and the Electricity Market. Modeling the lowest-cost route to decarbonising European power,” 2014.
- [4] Chalmers University of Technology, European Energy Pathways: Towards a sustainable European Energy System, Gothenburg, 2014.
- [5] IEA-GHG, “Operating Flexibility of Power Plants with CCS,” June 2012.
- [6] H. Farahmand, S. Jaehnert, T. Aigner and D. Huertas-Hernando, “Twenties Task 16.3 "Grid restriction study: Nordic Hydropower and Northern European Wind Power",” European Commission. Seventh framework Programme, Trondheim Norway, 2013.
- [7] ENTSO-E, “ENTSO-E Network Code for Requirements for Grid Connection Applicable to all Generators,” 2012.
- [8] IEA, “Harnessing Variable Renewables. A guide to the balancing challenge.,” 2011.
- [9] M. Huber, D. Dimkova and T. Hamacher, “Integration of wind and solar power in Europe: Assessment of flexibility requirements,” *Energy*, vol. 69, pp. 236-246, 2014.
- [10] M. Nitz and K. Hans-Joachim, “Flexible Operation of CCS Power Plants to Match Variable Renewable Energies,” *Energy Procedia*, pp. 294-303, 2013.
- [11] S. McCoy, J. Bertsch, C. Growitsch, S. Lorenczik, S. Nagl, D. Volk, M. Finkenrath and J. Davison, “The role of CCS with high levels of renewables penetration,” *Energy Procedia*, vol. 37, no. GHGT-11, pp. 2665-2675, 2013.
- [12] A. S. Brouwer, M. van den Broek, A. Seebregts and A. P. C. Faaij, “The Flexibility Requirements for Power Plants with CCS in a Future Energy System with a Large Share of Intermittent Renewable Energy Sources,” *Energy Procedia*, pp. 2657-2664, 2013.
- [13] 3E, dena, EWEA, ForWind, IEO, NTUA, Senergy and SINTEF, “Offshore Electricity Grid Infrastructure in Europe. A Techno-Economic Assessment,” OffShore Grid, October 2011.
- [14] A. R. Bruce, G. P. Harrison, J. Gibbins and H. Chalmers, “Assessing Operating Regimes of CCS Power Plants in High Wind and Energy Storage Scenarios,” *Energy Procedia*, pp. 7529-7540, 2014.
- [15] E. Delanue, P. Martens and W. D'haeseleer, “Market opportunities for power plants with post-combustion carbon capture,” *International Journal of Greenhouse Gas Control*, vol. 6, pp. 12-20, 2012.
- [16] J. Duncan and M. S. Sarma, *Power System Analysis & Design 5th Edition*, Stamford USA: Cengage Learning, 2012.
- [17] National Grid Electricity Transmission Plc, “The grid code. Issue 5 Revision 13,” January 2015.
- [18] Consentec GmbH, “Description of load-frequency control concept and market for control reserves,” Aachen, Germany, February 2014.
- [19] Y. G. Rebours, D. S. Kirschen and M. Trotignon, “A Survey of Frequency and Voltage Control Ancillary services - Part I: Technical Features,” *IEEE Transactions on power systems*, vol. 22, no. 1, pp. 350-357, February 2007.
- [20] I. de la Fuente, “Ancillary Services in Spain: Dealing with High Penetration of RES,” Red Eléctrica, Madrid, 210.
- [21] Energinet.dk, “Energinet.dk's Ancillary services strategy,” 2011.
- [22] D. L. Oates, P. Versteeg, E. Hittinger and P. Jaramillo, “Profitability of CCS with flue gas bypass and solvent storage,” *International Journal of Greenhouse Gas Control*, vol. 27, pp. 279-288, 2014.
- [23] S. M. Cohen, G. T. Rochelle and M. E. Webber, “Optimal CO₂ Capture Operation in an Advanced Electric Grid,” *Energy Procedia*, pp. 2585-2594, 2013.
- [24] K. Jordal, P. Ystad, R. Anantharaman, A. Chikukwa and O. Bolland, “Design-point and part load considerations for natural gas combined cycle plants with post combustion capture,” *International Journals of Greenhouse Gas Control*, vol. 11, pp. 271-282, 2012.
- [25] A. Stoppato, A. Mirandola, G. Meneghetti and E. L. Casto, “On the operation strategy of steam power plants working at variable load: Technical and economic issues,” *Energy*, vol. 37, pp. 228-236, 2011.
- [26] P. Keatley, A. Shibli and N. Hewitt, “Estimating power plant start costs in cyclic operation,” *Applied Energy*, vol. 111, pp. 550-557, 2013.
- [27] M. Bui, I. Gunawan, V. Verheyen, P. Feron, E. Meuleman and S. Adeloju, “Dynamic modelling and optimisation of flexible operation in post-combustion CO₂ capture plants - A review,” *Computers and Chemical Engineering*, vol. 61, pp. 245-265, 2014.

Paper II

Article

Dynamic Process Model Validation and Control of the Amine Plant at CO₂ Technology Centre Mongstad

Rubén M. Montañés ^{1,*} , Nina E. Flø ² and Lars O. Nord ¹ 

¹ Department of Energy and Process Engineering, NTNU—Norwegian University of Science and Technology, NO-7491 Trondheim, Norway; lars.nord@ntnu.no

² CO₂ Technology Center Mongstad, NO-5954 Mongstad, Norway; nflo@tcmda.no

* Correspondence: ruben.m.montanes@ntnu.no; Tel.: +47-73-5073722

Received: 24 August 2017; Accepted: 26 September 2017; Published: 1 October 2017

Abstract: This paper presents a set of steady-state and transient data for dynamic process model validation of the chemical absorption process with monoethanolamine (MEA) for post-combustion CO₂ capture of exhaust gas from a natural gas-fired power plant. The data selection includes a wide range of steady-state operating conditions and transient tests. A dynamic process model developed in the open physical modeling language Modelica is validated. The model is utilized to evaluate the open-loop transient performance at different loads of the plant, showing that pilot plant main process variables respond more slowly at lower operating loads of the plant, to step changes in main process inputs and disturbances. The performance of four decentralized control structures is evaluated, for fast load change transient events. Manipulation of reboiler duty to control CO₂ capture ratio at the absorber's inlet and rich solvent flow rate to control the stripper bottom solvent temperature showed the best performance.

Keywords: pilot plant; transient data; dynamic simulation; flexibility; post-combustion; decentralized control; process dynamics; chemical absorption; CO₂ capture

1. Introduction

Carbon capture and storage (CCS) is a group of technologies that can significantly contribute to the reduction of anthropogenic CO₂ emissions from thermal power generation and other carbon-intensive industries [1]. There are two commercial-scale coal-fired power plants with post-combustion CO₂ capture (PCC) using amines being operated today, at Boundary Dam in Canada [2] and at Petra Nova project at the Parish Power Station in the US [3]. These projects prove the technical feasibility of the technology at commercial scale. Among the different options and technologies for CO₂ capture in thermal power generation, post-combustion CO₂ capture with chemical absorption is considered the more mature technology that can contribute to significantly reducing the carbon intensity (kgCO₂/kWh_{el}) of fossil-fueled thermal power plants. In future energy systems with a high penetration of renewable energy sources, the variability in demand and generation will introduce a change in the operating patterns of thermal power generation plants, which will have to change operating conditions [4–6]; there will also be a higher frequency of significant transient events including load changes, and start-up and shut-down events [7,8]. In this regard, Boot-Handford et al.'s carbon capture and storage update 2014 concludes that the financial case for CCS requires that it operates in a flexible manner and that load-following ability is extremely important to the long-term economics [9].

Among the different features of flexible operation of power plants with CCS, an important aspect is the transient behavior of the system when varying operating conditions. This means that efficient operation and emissions and the related operational costs during transient operation will gain importance. However, the operational experience from commercial-scale power plants with post

combustion CO₂ capture is scarce and the published transient pilot plant data from test campaigns is limited. Therefore, there is a need for the development of dynamic process models. Dynamic process models can contribute to developing the learning curve for flexible operation of PCC plants. These tools can assist in evaluating the feasibility of flexible operation strategies as well as design process configurations and operational strategies that can lead to the reduction of operational costs and increased revenue during power plant operation. The study of the transient performance with dynamic process models can contribute to identifying process bottlenecks and ease the process scale-up.

Dynamic process models allow the study of the open-loop transient performance of the plant [10], the evaluation of different process configurations and designs [11], the development and implementation of optimal control strategies [12–20], as well as the study of the plant behavior under different operational flexibility scenarios [21,22]. In addition, the power plant and the PCC unit can be treated as an integrated system and dynamic process models can be utilized to analyze the response of the capture unit to changes that occur upstream in the power plant [12,15,19,23–25]. Furthermore, the operational flexibility of the PCC plant can be improved with plant design or using control strategies [26–29]. The core purpose of dynamic process models is to capture the time-dependent behavior of the process under transient conditions. However, the validation of dynamic process models with experiments and pilot plant data is necessary in order to assess the reliability of simulation results.

Kvamsdal et al. [30] developed a dynamic process model of a CO₂ absorber column and used steady-state data from a pilot plant to validate liquid temperature profiles, capture ratio % and rich loading. That work highlighted the necessity of building up a dynamic process model of the integrated system (including stripper, lean/rich heat exchanger, mixing tank and main process equipment), to understand the complexities of dynamic operation of the plant. Gaspar and Cormos [31] developed a dynamic process model of the absorber/desorber process and validated with steady-state plant data. Several publications are available, in which the models were validated only with steady-state pilot plant data [11,32–35]. Bilyok et al. [36] presented a dynamic model validation study where transient data was driven by decrease in solvent flow rate to the absorber, fluctuating concentration of CO₂ at absorber inlet and a varying absorber's feed flue gas stream temperature to the absorber. A dynamic process model developed in Modelica language was validated with transient data from the Esbjerg pilot plant by Åkesson et al. [37]. That data consisted of the transient performance after one step-change in flue gas mass flow rate. An extensive review work by Bui et al. [38] concluded that research efforts are required on producing transient pilot plant data.

More recent works have included validation of dynamic process models with transient plant data from pilot plants. A K-Spice model by Flø et al. was validated with pilot plant data from the Brindisi pilot plant [39]. Flø et al. [40] validated a dynamic process model of CO₂ absorption process, developed in Matlab, with steady-state and transient pilot plant data from the Gløshaugen (Norwegian University of Science and Technology (NTNU)/SINTEF) pilot plant. Van de Haar et al. [41] conducted dynamic process model validation of a dynamic process model in Modelica with transient data from a pilot plant located at the site of the coal-fired Maasvlakte power plant in the Netherlands. Gaspar et al. [42] conducted model validation with transient data from two step changes in flue gas volumetric flow rate from the Esbjerg pilot plant. Other works include the validation of equilibrium-based models such as that of Dutta et al. [43]; or the work by Chinen et al. [44] which conducted dynamic process model validation of a process model in Aspen Plus[®] with transient plant data from the National Carbon Capture Center (NCCC) in the US. Manaf et al. [45] developed a data-driven black box mathematical model, based on transient pilot plant data, by means of system identification. In addition, dynamic process models have been developed to study the transient behavior of the chemical absorption CO₂ capture process using piperazine (PZ) as chemical solvent [19,20]. It should be noted that the majority of work has been conducted for typical flue gas compositions from coal-based power plants with CO₂ concentration around 12 vol % [38].

From the literature review it can be concluded that dynamic process model validation is a challenging process due to:

- The scarce availability of transient or dynamic pilot plant data.
- Most available data is found from small-scale pilot plants. That has implications for the reliability of simulation results when applying dynamic process models to scaled-up applications.
- The works involving transient data generally include the response of the plant to disturbances in a few process variables.
- Most of the validation work was done for flue gas with a typical CO₂ content from coal-based power plants.

Flexible operation of PCC plants has been studied with pilot plant test facilities in test campaigns. Faber et al. [46] conducted open-loop step change responses at the Esbjerg pilot plant; this type of analysis helps in understanding the transient performance of the process. They concluded that the overall system acts as a buffer to perturbations at the plant inlet and that the coupled operation of the absorber/desorber unit led to fluctuations in the system when all parameters—flue gas and solvent mass flow rates and reboiler duty—are changed simultaneously. Bui et al. [47] presented a flexible operation campaign conducted at the Commonwealth Scientific and Industrial Research Organization (CSIRO)'s PCC pilot plant in Australian Gas Light Company (AGL) Loy Yang, a brown-coal-fired power station in Australia. The generated transient data included step changes in flue gas flow rate, solvent flow rate and steam pressure. The purpose of the study was to generate a set of data for validation of dynamic process models, and to gain insight into process behavior under varying operating conditions. A different approach was taken by Tait et al. [48] who conducted experiments that simulated flexible operation scenarios on a pilot plant to treat synthetic flue gas with a CO₂ concentration of 4.3 vol%, typical of a natural gas combined cycle (NGCC) plant. Tests for transient operation have been conducted at the amine plant at CO₂ Technology Center Mongstad (TCM DA). De Koeijer et al. presented two cases: a first case with controlled stop-restart of the plant, driven by a controlled stop of flue gas and steam sent to the PCC plant; and a second case with sudden stop of the blower upstream of the absorber [49]. Nevertheless, a limited amount of transient testing can be conducted during test campaigns. A thoroughly validated dynamic process model can help to study the transient performance, controllability, and flexible operation of the plant and process dynamics via dynamic process simulation.

In this work, a suitable set of steady-state and transient plant data, collected from a MEA campaign at CO₂ Technology Center Mongstad, is selected for dynamic process model validation purposes. The plant was operated with flue gas from a natural gas fueled combined heat and power plant. The selected data is utilized to validate a dynamic process model of the amine-based CO₂ absorption-desorption process at TCM DA. Then, the validated model is employed to carry out two case studies on the process dynamics of the TCM DA amine plant. In the first case study, the open-loop transient response of the pilot plant at different operating loads of the plant is analyzed. In the second case study, the performance of four decentralized control structures of TCM DA amine pilot plant is evaluated for fast disturbances in flue gas volumetric flow rate.

2. Materials and Methods

2.1. Plant Description

CO₂ Technology Center Mongstad test site has a pilot-scale amine-based chemical absorption process plant. The amine plant can be configured to treat flue gas from a catalytic cracker from the Mongstad refinery, with CO₂ content of around 13–14 vol%, typically found in flue gas from coal-fired power plants, and also to treat exhaust gas coming from a combined cycle gas turbine combined heat and power plant (CHP), with CO₂ content of around 3.5 vol%. A fraction of the product CO₂ mass flow rate can be re-circulated back upstream of the direct contact cooler (DCC) to increase the CO₂ content, so CO₂ concentrations of between 3.5 and 13–14 vol% could be fed to the plant to simulate the effects of exhaust gas recirculation [50]. Table 1 presents data of the main process equipment of TCM DA amine plant when configured to treat CHP flue gas, which has a total flue gas capacity of

60,000 Sm³/h and can capture around 80 ton CO₂/day. Figure 1 shows a simplified process flow sheet of the amine plant at TCM DA when configured for CHP gas. A slipstream of exhaust gas is extracted from the CHP plant placed next to the TCM DA facility, and it consists of about 3% of the total exhaust gas. An induced draft blower is utilized to blow the flue gas flow. It has variable speed drives that allow the flue gas volumetric flow rate fed to the absorber column to be manipulated. Upstream the absorber column, a direct contact cooler cools down and saturates the flue gas with water, by means of a counter-current flow stream of water.

Table 1. Size and materials of main process equipment at the amine plant at TCM DA with CHP stripper configuration.

| Absorber | |
|---|-----------------------------|
| Column cross sectional area (m ²) | 3.55 × 2 |
| Column height (m) | 62 |
| Packing height (12 + 6 + 6) (m) | 24 |
| Water wash section height (3 + 3) (m) | 6 |
| Absorber packing type | Koch Glitsch Flexipac 2X |
| Absorber washer packing type | Koch Glitsch Flexipac 2Y HC |
| CHP Stripper | |
| Column cross sectional area (m ²) | 1.33 |
| Diameter (m) | 1.3 |
| Packing height (m) | 8 |
| Water wash section height (m) | 1.6 |
| Absorber packing type | Koch Glitsch Flexipac 2X |
| Absorber washer packing type | Koch Glitsch Flexipac 2Y HC |
| Heat Exchanger L/Rich | |
| Duty (kW) | 10358 |
| Heat transfer area (m ²) | 308 |
| Material | SS 316L |
| Reboiler | |
| Duty (kW) | 3365 |
| Heat transfer area (m ²) | 142 |
| Material | SS 316L |
| Lean Amine Cooler | |
| Duty (kW) | 5182 |
| Heat transfer area (m ²) | 78.8 |
| Material | TITANIUM |

A chemical absorption process occurs in the absorber column, where the chemical solvent, flowing from top to bottom, meets the flue gas flowing in counter-current. The absorber column consists of a rectangular polypropylene-lined concrete column with a height of 62 m and a cross-section of 2 × 3.55 m. The absorber-packed sections consisting of Flexipac 2X (Koch-Glitsch Italia, Vimercate, Italy) structured stainless-steel packing are distributed from bottom to top in three sections of 12 m, 6 m and 6 m. Two water-wash systems are installed in the top of the absorption column, consisting of two sections of Flexipac 2Y HC (Koch-Glitsch Italia, Vimercate, Italy) structured stainless-steel packing. The water-wash sections limit emissions and are used to keep the water balance of the plant. The upper water-wash sections can be operated as acid wash [51]. In addition, the plant can be configured to use different packing heights in the absorber column resulting in 12, 18 or 24 m. This can be implemented at TCM plant by introducing all the lean solvent flow at 12 m of absorber packing, 18 m of absorber packing (12 + 6) m or 24 m of absorber packing (12 + 6 + 6) m.

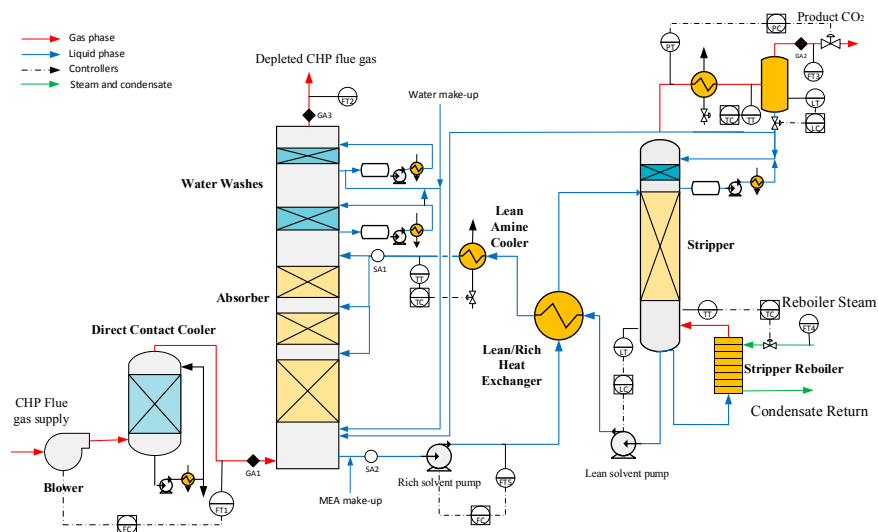


Figure 1. Simplified process flow sheet of the amine plant at CO₂ Technology Center Mongstad, when configured to treat flue gas from a natural gas-fired power plant. The figure shows the location of some gas analyzers (GA), solvent analyzers (SA), flow transmitters (FT), pressure transmitters (PT), temperature transmitters (TT) and level transmitters (LT). The main process controllers of the regulatory control layer are shown, including flow controllers (FC), temperature controllers (TC), pressure controllers (PC) and level controllers (LC).

A 10.4 MW plate and frame heat exchanger is present at the plant where the cold rich amine solution coming from the absorber sump cools down the hot lean amine solution coming from the stripper. In addition, a 5.2 MW lean amine cooler is utilized to set the temperature of the lean solvent conducted to the top of the absorber packing sections, by using a stream of cooling water. The rich solvent is pumped to the top of the stripper column, where it meets the stripping vapors generated in the reboiler. The CHP stripper with overhead condenser system consists of an 8 m column of Koch Glitsch Flexipac 2X structured stainless-steel packing of 1.3-m-diameter, and a water-wash system with Koch Glitsch Flexipac 2Y HC structured stainless-steel packing of 1.6 m of height. The stripper reboiler consists of a 3.4 MW thermosiphon steam-driven system that supplies the heat required for the desorption process. The steam supplied to the reboiler comes from the refinery situated next to the TCM DA facility. Details on the steam supply system can be found in Faramarzi et al. [51].

2.2. Pilot Plant Configuration and Instrumentation

The TCM DA amine plant can be utilized to test various chemical solvents. In this work, the tests were conducted with 30 wt. % aqueous monoethanolamine (MEA). During the tests conducted in the test campaign, the responses and performance of the pilot plant were logged and extracted every 30 s. Gas composition was logged with gas analyzers at the inlet of the absorber, outlet of the absorber, and the product CO₂. A gas chromatograph (GC) installed at TCM DA plant can measure concentrations of CO₂, N₂, H₂O and O₂ at the three locations in a nearly simultaneous manner, which is a desired feature for transient tests; refer to GA1, GA2 and GA3 in Figure 1. Details on gas analyzers and instrumentation at TCM DA plant can be found in [51].

Gas phase flow rates were measured at the plant during the tests. The flue gas volumetric flow rate fed to the absorber is measured with an ultra-sonic flow meter (FT1). As discussed by Faramarzi et al. in [51], the depleted flue gas flow meter (FT2) had a higher degree of variability than FT1, and some transients were observed on the FT2 measurement that were not explained by changes

in process parameters at the plant. Therefore the depleted flue gas flow rate was calculated in the test campaign by considering that all O₂ and N₂ fed to the absorber goes out of the plant with the depleted flue gas. The cooled product CO₂ discharge flow (FT3) was measured with a vortex flow meter. Other flow rates measured at the plant include the steam fed to the reboiler, the lean amine flow rate at the absorber inlet and the rich amine flow rate at the absorber outlet. For flue gas flow meters, the standard conditions are 15 °C and 101.3 kPa [51].

Pressures and pressure drops at different components of the plant were logged. In addition, main process temperatures were logged. For process model validation, it is common to assess the model prediction of the absorber and stripper temperature profiles. Within the absorber and stripper columns of TCM DA's amine plant there are four temperature sensors distributed in the radial plane per meter of packing in the axial direction. Thus, there are 96 temperature sensors within packed segments of absorber column and 28 temperature sensors within the packed segment in the stripper column. These measurements allow the creation of clear temperature profiles of the absorber and stripper columns in the axial direction (at each column height, the resulting temperature value is the average of the four measurements distributed in the radial plane).

Online solvent analysis measurements (SA) were taken at the inlet (SA1) and outlet of the absorber (SA2); refer to Figure 1. The measurements include pH, density and conductivity. In addition, solvent samples were regularly taken manually and analyzed onsite. These analyses allow MEA concentration and CO₂ loadings to be calculated at the sampling points on a periodic basis. The actual reboiler duty was estimated as suggested in Thimsen et al. [52]. Equation (1) shows the calculation of the actual reboiler duty, where F_{steam} is the logged measurement data of steam mass flow rate (refer to FT4 in Figure 1), T_c is the condensate temperature, T_g is the superheated steam inlet temperature, p_g is the steam pressure at inlet, and p_c is the condensate pressure. Enthalpy was calculated with the use of accurate steam tables, with the condensate at the reboiler outlet assumed to be saturated liquid at T_c or p_c . The specific reboiler duty (SRD) in kJ/kgCO₂ is calculated as in Equation (2), where F_{prod} is the CO₂ rich product mass flow rate; refer to FT3 in Figure 1.

$$\dot{Q}_{reb} = F_{steam}(h_g(T_g, p_g) - h_c(T_c, p_c)) \quad (1)$$

$$SRD = \frac{\dot{Q}_{reb}}{F_{Prod}} \quad (2)$$

During the tests presented in this work, the averaged total inventory of aqueous MEA was around 38.2 m³. Averaged values of liquid hold-ups and its distribution at different components of the plant during the steady-state tests included in this work are presented in Table 2. Detailed data on solvent inventory distribution throughout the plant is of importance in order to obtain suitable dynamic process simulation results. The regulatory control layer of the plant was active during the tests conducted in the MEA campaign. The main control loops of the regulatory control layer are presented in Figure 1. Note that the actual regulatory control layer of the amine plant at TCM DA is more complex and includes more control loops for auxiliary equipment, stable and safe operation of the plant, and start-up and shut-down sequences. The control loops included here are those the authors found relevant for the purposes of dynamic process modeling and simulation of this plant during online operation, and considering the time scales of interest for process operation.

Table 2. Averaged values of total solvent inventory and its distribution within the main components of the TCM plant.

| PCC Plant Main Components | Solvent Inventory (m ³) |
|---|-------------------------------------|
| Absorber sump | 8.1 |
| Absorber packing | 8.4 |
| CHP stripper packing | 1.0 |
| CHP stripper sump | 2.3 |
| CHP reboiler | 0.4 |
| Cold rich solvent pipe | 2.2 |
| Cold lean solvent pipes | 5.2 |
| Hot rich solvent pipe | 1.1 |
| Hot lean solvent pipes (including reboiler pipes) | 8.2 |
| Lean/rich hx—lean side | 0.5 |
| Lean/rich hx—rich side | 0.5 |
| Lean cooler | 0.3 |
| TOTAL | 38.2 |

2.3. Dynamic Process Model

Dynamic process modeling was carried out by means of the physical modeling language Modelica [53]. Modelica allows development of systems of differential and algebraic equations that represent the physical phenomena occurring in the different components of the system. The process models of the equipment typically found in a chemical absorption plant were obtained from a Modelica library called Gas Liquid Contactors (Modelon AB, Lund, Sweden) [54], and the commercial tool Dymola (Dassault Systèmes, Vélizy-Villacoublay, France) [55] was utilized to develop the models and carry out the simulations. The component models include absorber and stripper columns, sumps, lean and rich heat exchanger, stripper reboiler, overhead condenser, condensers, pipe models, pumps, valves, measurements and controllers. The dynamic process model of the amine plant at TCM DA presented in Figure 1 was developed by parameterizing, modifying and connecting the different models. For this purpose, the main process equipment, size, geometry and materials were considered; refer to Table 1. A key aspect for obtaining suitable dynamic simulation results is the consideration of the distribution of solvent inventory at the different equipment of the plant. Therefore, solvent inventory distribution was implemented in the dynamic process model; refer to Table 2. Finally, the equivalent regulatory control layer of the plant was applied in the dynamic process model; discussed later in Section 5.2. The models contained in the library have been presented elsewhere [56,57]; therefore only an overview of the models is presented in the following. Numerical integration of the resulting system of differential and algebraic equations was carried out in Dymola with the differential algebraic system solver (DASSL) implemented in Dymola [55]. The main assumptions applied are [56]:

- All chemical reactions occur in the liquid phase and are assumed to be in equilibrium.
- The flue gas into the absorber contains only CO₂, O₂, H₂O and N₂.
- MEA is non-volatile and not present in the gas phase.
- The total amount of liquid in the column is defined as the packing hold-up and the sump liquid hold-up.
- The reboiler is modeled as an equilibrium flash stage.
- The liquid in the column sumps and other large volumes are assumed to be ideally mixed.
- Mass and heat transfer between liquid and gas phase is restricted to packed section.
- Negligible temperature difference between the liquid bulk and interface to gas phase.
- No storage of mass and energy in the gas phase.
- All liquid from the packing bottom in the stripper is fed to the reboiler with a constant liquid level.
- Constant target packing hold-up.

The models of the absorber and stripper columns are developed based on the two-film theory; therefore, at the gas and liquid interface thermodynamic equilibrium is assumed. Interface mass transfer phenomena is modeled in packed sections with a rate-based approach with enhancement factor E [30], which takes into account the enhanced mass transfer due to chemical reactions; refer to Equations (3) and (4), where $c_{i,if}$ and $c_{i,b}$ are molar concentrations at liquid bulk and interface, A_{if} is the contact area, k_i are the mass transfer coefficients by Onda [58], T is the bulk phase temperature, and p_i are the partial pressures of the species in the gas phase. The pseudo-first order enhancement factor E is calculated as in Equation (5), where k_{CO_2} is the overall reaction constant for CO_2 and C_{MEA} the molar free MEA-concentration taken from [59], the diffusivity D_{CO_2} of CO_2 in aqueous MEA is calculated by the Stokes-Einstein relation and the diffusivity of CO_2 in water from [60]. C_{ef} is a pre-multiplying coefficient for calibration of enhancement factor. The packing characteristics of Koch Glitsch Flexipac 2X were considered for parameterizing the packing segments of the dynamic process model for absorber and stripper columns, with a surface area of $225 \text{ m}^2/\text{m}^3$ and a void fraction of 0.97.

$$\dot{n}_{i,l} = A_{if}k_{i,l}E(c_{i,b} - c_{i,if}) \quad i = CO_2 \quad (3)$$

$$\dot{n}_{i,v} = \frac{A_{if}K_{i,v}(p_{i,b} - p_{i,if})}{RT} \quad i = CO_2, H_2O \quad (4)$$

$$E = C_{ef} \frac{\sqrt{C_{MEA}k_{CO_2}D_{CO_2}}}{k_{i,l}} \quad i = CO_2 \quad (5)$$

Phase equilibrium at the gas-liquid interface is calculated as in Equations (6) and (7), where the solubility of CO_2 in water is considered by Henry's law, with He_i from [61]; activity coefficients γ_i are implemented from [61]; chemical equilibrium is assumed at the interface and liquid bulk, and the chemical equilibrium constants K_i implemented in the process model are obtained from Böttinger [61]. The Van't Hoff equation is utilized in order to infer the heats of reaction ΔH_r from the equilibrium constant; refer to Equation (8). The Chilton-Colburn analogy was employed to correlate sensible heat transfer between phases with the gas phase mass transfer coefficient. Latent heat connected to the transferred mass flow from one phase to the other is considered in the specific enthalpies of the individual species. The heat of evaporation and heat of solution are a function of temperature but are considered constant with solvent CO_2 loading. The gas phase model assumes ideal gas law, and the pressure of the column p is determined by the gas phase pressure drop.

$$y_i p = \gamma_i x_i He_i \quad i = CO_2 \quad (6)$$

$$y_i p = \gamma_i x_i p_{i,sat}(T) \quad i = H_2O \quad (7)$$

$$\frac{d \ln K}{dT} = \frac{\Delta H_r}{RT^2} \quad (8)$$

The lean-rich heat exchanger is modeled as a static heat exchanger model with the ϵ -NTU (effectiveness—number of thermal units), and pure transport delay models are used to account for dead times included by the solvent hold-up within piping' volumes.

At the top of the absorber column a washer model is implemented, consisting of a volume model with phase separation that saturates the gas with water at the targeted temperature. A make-up stream of water is injected in the absorber sump to keep the H_2O mass balance of the system. MEA is assumed non-volatile in the model and therefore it is only present in the liquid phase. However, in the actual plant make-up MEA is required for operation and it is injected upstream the rich amine pump; refer to Figure 1.

3. Steady-State Validation of Dynamic Process Model

3.1. Steady-State Operating Cases

A test campaign was conducted at the amine plant at TCM DA using MEA, operated from 6 July until 17 October 2015. Table 3 shows the steady-state cases generated during the test campaign that were used in this work for dynamic process model validation purposes. The plant was operated with 30 wt. % MEA for all cases. The objective was to select a set of steady-state cases from the MEA campaign that could represent a wide range of steady-state operating conditions, including data from full capacity of volumetric flow rate fed to the absorber column. The steady-state cases were generated by varying the set points of the main pilot plant inputs, namely solvent circulation flow rate F_{solv} (refer to FT5 in Figure 1), reboiler duty (\dot{Q}_{reb}), and flue gas volumetric flow rate (F_{gas}). The steady-state cases represent a variation in operating conditions of the plant, especially on the flue gas volumetric flow rate load of the absorber, CO₂ capture rate, L/G ratio in the absorber and absorber packing height. Cases 1 to 5 are operated at absorber full flue gas capacity of around 60,000 Sm³/h. A similar mass-based L/G ratio, of around 0.89, is kept in the absorber column during the steady-state operating cases with full capacity, with the exception of Case 4, where it is changed to 0.8, by varying the rich solvent mass flow rate. The main process variability in these cases is the change in reboiler duty, with CO₂ capture rate ranging from 85 to 68%. CO₂ capture rate was calculated with the method 1 described by Thimsen et al. [52]; refer to Equation (9), where F_{prod} refers to the product CO₂ flow rate (FT3 in Figure 1), and X_{CO_2} is the mass fraction of CO₂ in the absorber inlet (measured at GA1 in Figure 1). Note that here CO₂ capture rate has been named Des as it defines the desorption ratio utilized in Section 5.2. In addition, Cases 2 to 5 were operated with 18 m absorber packing, i.e., the uppermost absorber-packing segment is kept dry. Cases 6 to 10 are operated with 24 m absorber packing and the absorber column at 80% volumetric flue gas flow rate capacity. The mass-based L/G ratios on the absorber range from 1.34 to 0.75 for Cases 6 to 10, by varying solvent circulation mass flow rate. The capture rate is kept constant at around 85% by varying the reboiler duty.

Table 3. A selection of steady-state data cases obtained from the test campaign conducted at TCM plant during autumn 2015. The plant was operated with 30 wt. % aqueous MEA.

| Case | 1 | 2 | 3 | 4 | 5 | 6 | 7 | 8 | 9 | 10 |
|--|--------|--------|--------|--------|--------|--------|--------|--------|--------|--------|
| Gas flow rate (Sm ³ /h) | 59,461 | 59,468 | 59,442 | 59,499 | 59,544 | 46,973 | 46,973 | 46,973 | 46,973 | 46,973 |
| Rich solvent flow rate (kg/s) | 17.33 | 17.31 | 17.22 | 15.50 | 17.24 | 20.56 | 17.50 | 16.11 | 12.74 | 11.46 |
| L/G ratio (kg/kg) | 0.89 | 0.89 | 0.89 | 0.80 | 0.89 | 1.34 | 1.14 | 1.05 | 0.83 | 0.75 |
| Reboiler duty (kW) | 3417 | 3159 | 2664 | 2397 | 3056 | 2745 | 2669 | 2667 | 2659 | 2682 |
| Absorber inlet gas CO ₂ (vol%) | 3.64 | 3.61 | 3.59 | 3.58 | 3.59 | 3.60 | 3.62 | 3.62 | 3.62 | 3.62 |
| Absorber inlet gas O ₂ (vol%) | 15.52 | 15.54 | 15.55 | 15.46 | 15.35 | 15.30 | 15.48 | 15.49 | 15.51 | 15.52 |
| Absorber inlet gas H ₂ O (vol%) | 3.98 | 3.92 | 3.93 | 4.01 | 4.22 | 3.80 | 3.36 | 3.46 | 3.52 | 3.43 |
| Absorber inlet gas N ₂ (vol%) | 79.09 | 79.02 | 78.85 | 78.57 | 78.20 | 78.18 | 78.88 | 78.94 | 79.06 | 78.96 |
| Loading rich (mol/mol) | 0.490 | 0.485 | 0.498 | 0.500 | 0.495 | 0.475 | 0.488 | 0.486 | 0.493 | 0.491 |
| Loading lean (mol/mol) | 0.280 | 0.294 | 0.333 | 0.341 | 0.314 | 0.342 | 0.329 | 0.310 | 0.260 | 0.229 |
| Stripper bottom temperature (°C) | 120.9 | 121.1 | 119.1 | 118.9 | 120.1 | 116.6 | 118.3 | 119.1 | 121.4 | 121.8 |
| CO ₂ product flow (kg/s) | 0.95 | 0.89 | 0.75 | 0.68 | 0.84 | 0.74 | 0.74 | 0.75 | 0.77 | 0.76 |
| CO ₂ capture rate (%) | 85 | 80 | 68 | - | 75 | 85 | 85 | 85 | 85 | 85 |
| Absorber packing height (m) | 24 | 18 | 18 | 18 | 18 | 24 | 24 | 24 | 24 | 24 |

The first series of tests during the MEA campaign were dedicated to verification of mass balances of the plant [50]. CO₂ mass balance gives results close to 100%, and Gjernes et al. [50] conclude that CO₂ mass balance based on gas phase can be maintained at a level better than 100 ± 5%. In this work, the suggested method in [50] was used during data selection in order to ensure that the steady-state data cases presented in Table 3 have acceptable CO₂ mass balance.

In order to develop the overall dynamic process model of the plant, the steady-state data for Case 1, refer to Table 3, was used as a reference to calibrate the dynamic process model, and the main outputs from the model simulations were compared with the plant data. This data set was chosen since

it represents the baseline operating conditions of the amine plant at TCM DA when using aqueous MEA as chemical solvent, as presented in Faramarzi et al. [51]. The models of the different subsystems of the plant consisting of (i) absorber column; (ii) lean/rich heat exchanger; and (iii) stripper column with overhead condenser and reboiler were calibrated separately, and then linked to form the overall dynamic process model. The model was calibrated by tuning a pre-multiplying coefficient C_{ef} for the enhancement factor E . It was set to 0.28 in absorber packed segments and 0.01 in stripper packed segments. The validation section included in this work extends on work conducted previously [62].

$$Des = \frac{F_{prod}}{F_{gas} \cdot X_{CO_2}} \quad (9)$$

3.2. Validation Results of Dynamic Process Model with Steady-State Plant Data

The results from the simulated dynamic process model for the steady-state operating cases, described in Section 3.1, are displayed in Table 4. The results shown are for main process variables during pilot plant operation, namely CO₂ lean (L_l) and rich (L_r) loadings, product CO₂ flow rate (F_{prod}), specific reboiler duty (SRD) and stripper bottom temperature T_{str} . Possible deviations in dynamic process model prediction arise from errors related to measurement uncertainty and to modeling uncertainty, the latter being related to the fact that a physical model is always a simplification of reality. This means that it is natural to observe some deviation in the prediction of the dynamic process model simulation. Therefore, it is of importance to quantify these errors so that they are kept within reasonable bounds. The absolute percentage errors (AP) and the mean absolute percentage errors (MAP) are calculated as in Equations (10) and (11), where x_m is the value of the process variable predicted by the process model simulation, x_p is the value of the process variable measured at the pilot plant at the given steady-state operation case, and n is the number of steady-state cases studied.

$$AP = 100 \cdot \left| \frac{(x_m - x_p)}{x_p} \right| \quad (10)$$

$$MAP = 100 \cdot \sum_i^n \frac{\left| \frac{(x_{m,i} - x_{p,i})}{x_{p,i}} \right|}{n} \quad (11)$$

The results for lean CO₂ loading are presented in Figure 2 with a parity plot, where $\pm 5\%$ and $\pm 10\%$ error lines are also shown. It is clear that the dynamic process model under-predicts lean loading for most of the cases, with a $MAP < 6.6\%$. In addition, Figure 2 shows the parity plot for CO₂ product flow rate; in this case, the CO₂ product flow rate is also under-predicted by the dynamic process model, with a $MAP < 5.3\%$. Figure 3 shows the parity plot for stripper bottom temperature, with the $\pm 2\%$ error lines plotted; stripper bottom temperature T_{str} presented a $MAP < 1\%$. From the parity plots, one can observe that, despite the errors found in the absolute values predicted by the dynamic process model with respect to the reference plant data, the dynamic process model can predict the variability in the main process variables for a wide range of steady-state operating conditions.

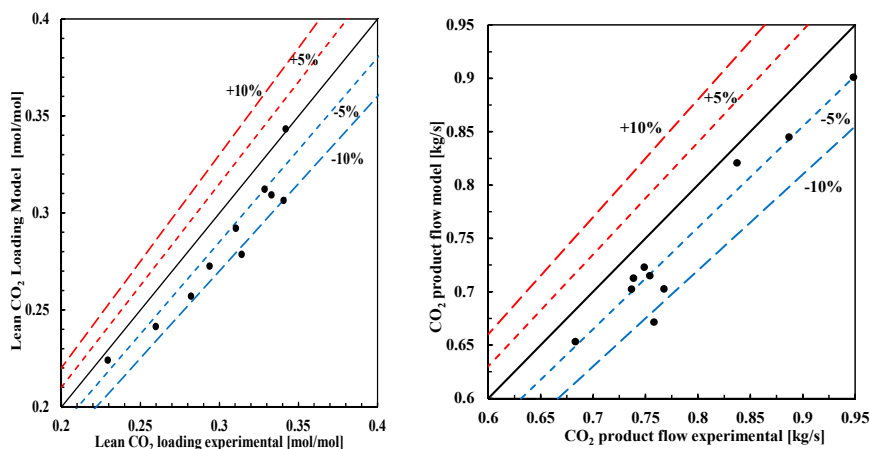


Figure 2. Parity plots of lean CO₂ loading (left) and CO₂ product flow rate (right). Lines for +10%, +5%, −5% and −10% percentage error are shown. The mean percentage error is <6.6% for CO₂ lean loading and <5.3% for product CO₂ flow rate (F_{prod}).

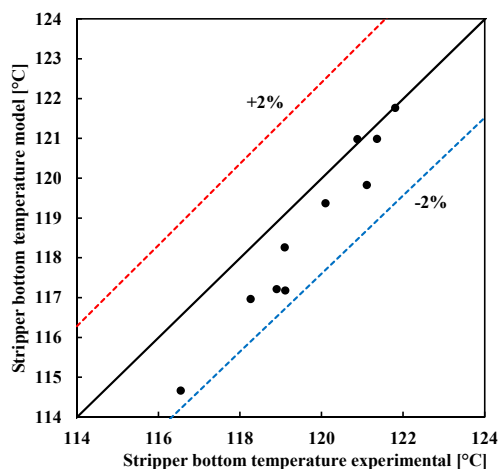


Figure 3. Parity plot for stripper bottom temperature for the 10 steady-state operation cases. Lines for +2% and −2% percentage errors are shown. The mean percentage error is 0.86 for stripper bottom temperature.

Temperature within absorber and stripper column is an important process variable since it affects phase equilibrium at liquid and gas-liquid interface. Some important model parameters and thermophysical properties depend on temperature, including heat capacity, water heat of condensation, heats of reaction, equilibrium constants and CO₂ solubility. Therefore, it is desirable that the dynamic process model can predict with good accuracy absorber and stripper columns' temperature profiles. Figure 4 shows the comparison between the pilot plant temperature profiles of the absorber and desorber columns with the predictions from the simulation of the dynamic process models. Two steady-state operating cases are presented: Case 1 (Table 3) with absorber flue gas volumetric capacity of 100%, mass-based L/G ratio of 0.89 and capture target of 85%; and Case 6 (refer to Table 3) with 80% flue gas volumetric capacity, mass-based L/G ratio of 1.34 and capture target of 85%.

Both cases were operated with 24 m of wet absorber packing, and represent two operating cases with different flue gas capacities and L/G ratios.

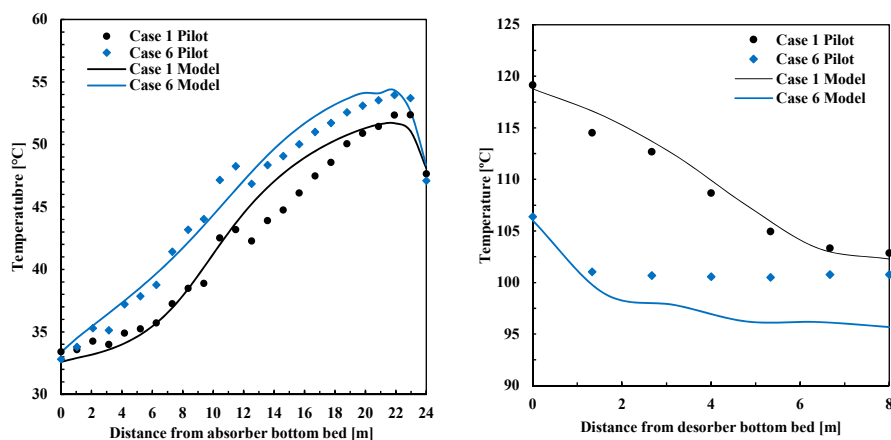


Figure 4. Temperature profiles for absorber column (left) and stripper column (right) for steady-state cases 1 and 6. In both steady-state operation cases, 24 m of absorber packing were utilized.

Validation of absorber and stripper temperature profiles is normally considered a challenging task for several reasons. At TCM DA the temperature profiles are the resulting averaged values of the 4 measurements distributed radially in a given axial position within the column; refer to Section 3. A given pilot plant temperature value presented in Figure 4 is the resulting average over time during one hour of steady-state operating conditions, of the averaged 4 temperature measurements radially distributed within the absorber or stripper column, at the given axial position of the column. The individual temperature measurements are considered reliable and the resulting temperature profiles are reasonable. However, some sensors are located closer to the center of the packing while others closer to the wall. This results in a maximum variation ($<6\text{ }^{\circ}\text{C}$) which is observed between the measurements in the same radial plane, which depends on operating conditions and is different at different radial planes. Based on the results presented in Figure 4, the dynamic process model can properly predict absorber and stripper column temperature profiles with sufficient accuracy considering the purpose of application. Absorber temperature profiles predicted by the model show a good agreement with the experimental pilot plant data, and the model is capable of properly predicting the trends in temperature along the column. The absorber temperature profiles have a mean absolute percentage error ($<2.5\%$) for Case 1 and ($<2.1\%$) for Case 6, which is within the observed maximum variability of the temperature measurements in a given radial plane. In addition, desorber temperature profiles have a mean average error ($<0.6\%$) for Case 1 and ($<3.6\%$) for Case 6. It is the desorber temperature profile for Case 6 that presents the less accurate prediction. In addition, it can be concluded that the process model is capable of properly predicting the variation of temperature profiles for various steady-state operating conditions.

4. Validation of Dynamic Process Model with Transient Plant Data

For dynamic process model validation purposes transient tests are conducted by means of open-loop step changes in the main process inputs to the plant. The transient behavior occurs between the initial steady-state operating conditions until the new steady-state operating conditions are reached. In this work, the experiments consist of set-point changes in rich solvent flow rate, flue gas volumetric flow rate fed to the absorber and reboiler duty. The output trajectories of main process variables are observed and compared with the model output trajectories. In order to obtain good sets of data

for validation, it is desired to apply the step changes in plant inputs in a non-simultaneous manner. However, this is not normally easy to implement in practice. In order to compare the pilot plant experimental output trajectories with the output trajectories predicted by the dynamic process models, input trajectories were utilized in the dynamic simulations. This means that the measured time series of the inputs applied to the pilot plant during the tests were applied as disturbances or inputs to the dynamic process model; refer to Figures 5a, 6a and 7a. During the three tests, the regulatory control layer of the plant was active. In Figures 5 and 6, the time $t = 0$ corresponds to the point from which the set point of flue gas volumetric flow rate was changed. In Figure 7 the time $t = 0$ is the point from when the set point of rich solvent flow rate was changed.

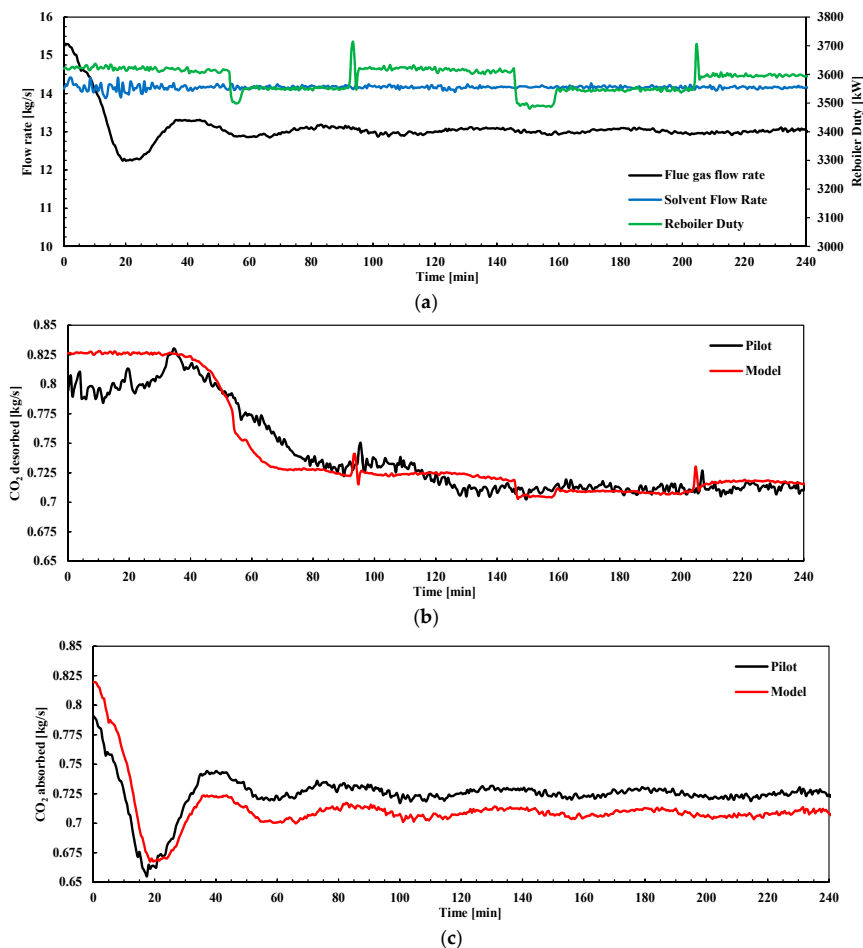


Figure 5. (a) Main inputs to the plant for test with flue gas flow rate set-point reduction (kg/s). Rich solvent flow rate from absorber (kg/s) and reboiler duty (kW); (b) Pilot plant transient response and model output trajectory for CO₂ product flow rate F_{prod} or CO₂ desorbed (refer to FT3 in Figure 1); (c) Pilot plant transient response and model output trajectory for CO₂ absorbed in absorber column, refer to Equation (11). The time $t = 0$ corresponds to the point from which the set point of flue gas volumetric flow rate was changed.

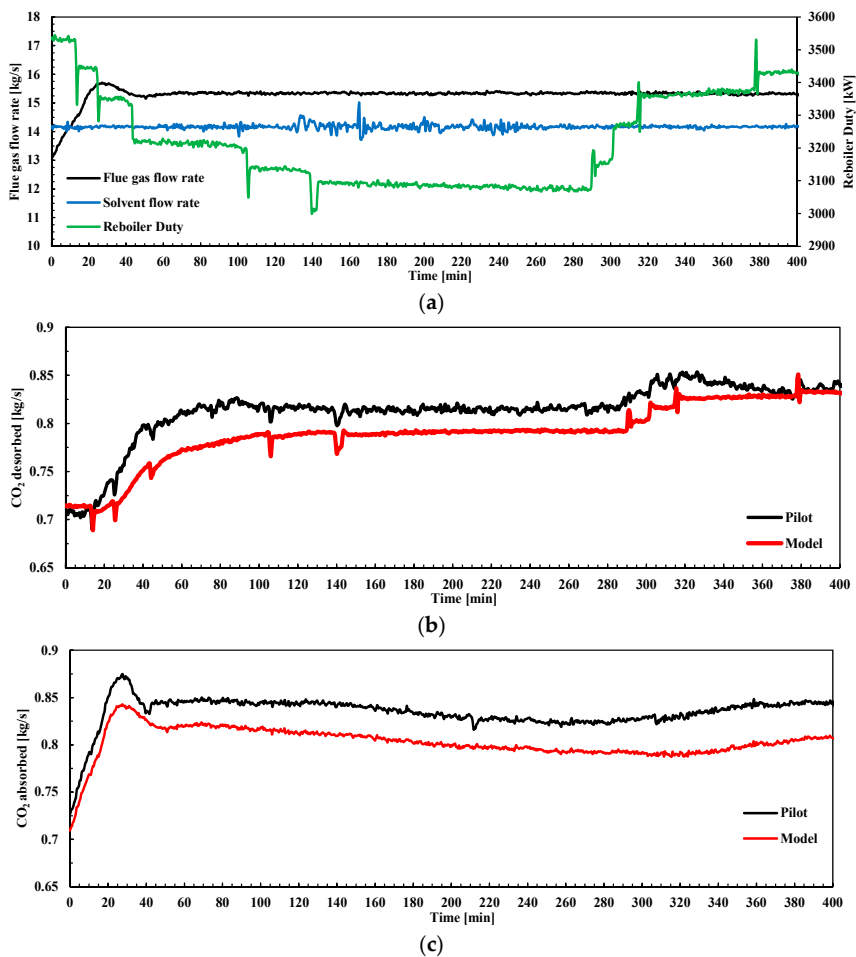


Figure 6. (a) Main inputs to the plant for test with flue gas flow rate set-point increase (kg/s). Rich solvent flow rate from absorber (kg/s) and reboiler duty (kW); (b) Pilot plant transient response and model output trajectory for CO₂ product flow rate F_{prod} or CO₂ desorbed (refer to FT3 in Figure 1); (c) Pilot plant transient response and model output trajectory for CO₂ absorbed in absorber column, refer to Equation (11). The time $t = 0$ corresponds to the point from which the set point of flue gas volumetric flow rate was changed.

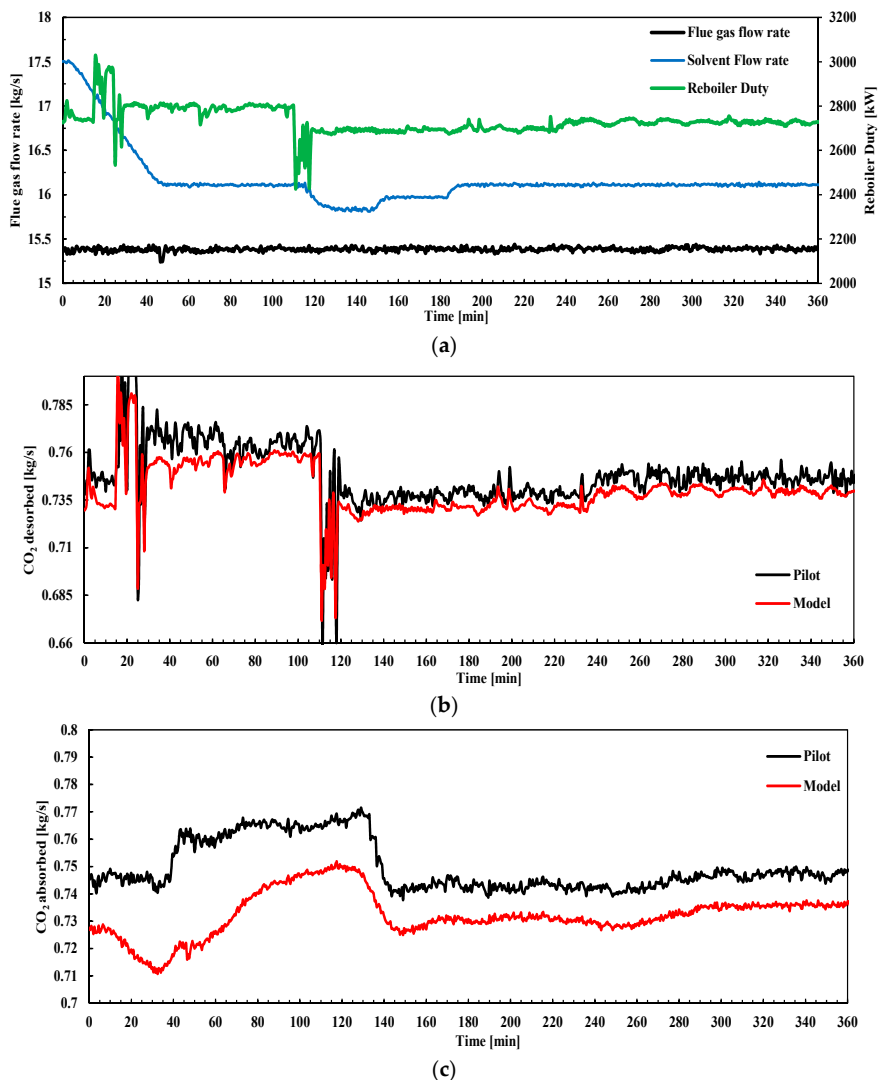


Figure 7. (a) Main inputs to the plant. Flue gas volumetric flow rate set-point change increase (kg/s). Rich solvent flow rate from absorber (kg/s) and steam flow to reboiler (kg/s); (b) Pilot plant transient response and model output trajectory for CO₂ product flow rate F_{prod} or CO₂ desorbed (refer to FT3 in Figure 1); (c) Pilot plant response in CO₂ absorbed mass flow rate (kg/s). The time $t = 0$ corresponds to the point from which the set point of rich solvent flow rate was changed.

4.1. Flue Gas Flow Rate Ramp-Down

The main disturbance applied in this transient test consisted of a reduction in flue gas volumetric flow rate at the inlet of the absorber. It was implemented at TCM DA pilot plant by changing the set point of the blower cascade controller from 47,000 Sm³ to 40,000 Sm³; refer to FT1 in Figure 1. This corresponds with flue gas volumetric flow capacities in the absorber column of 80% and 67% respectively. Figure 5a shows the three main inputs of the plant for this test. During the test, reboiler duty was changed in steps around the value of 3550 kW; this might be due to the effects of the

regulatory control layer on steam mass flow rate. The solvent mass flow rate had small amplitude oscillations around the set point.

$$CO_{2,abs} = F_{gas} \cdot X_{CO_2} - F_{depleted} \cdot X_{CO_{2,out}} \quad (12)$$

Figure 5b,c show the output trajectories of CO₂ product flow rate (or CO₂ desorbed) and CO₂ absorbed to the disturbance applied in this test. CO₂ absorbed is calculated as the difference between CO₂ mass flow rate at the absorber inlet and the CO₂ mass flow rate leaving the absorber with the depleted flue gas at the top of the absorber; refer to Equation (12). In Figure 5b, a dead time of around 40 min was observed, i.e., no significant changes are found in the CO₂ desorbed until around 40 min after the disturbance was applied to the pilot plant. In addition, the plant did not reach steady-state operating conditions until around 4 h later. As shown in Figure 5c, there is not significant dead time in the response of CO₂ absorbed. The difference observed between the output trajectories is characteristic of the coupled transient performance of the absorber and stripper columns. Figure 5b,c shows that the process model is capable of predicting the main process dynamics for CO₂ product mass flow rate (CO₂ desorbed), including an adequate prediction of dead times and stabilization time. In addition, the CO₂ absorbed transient performance trends are predicted in a satisfactory manner.

4.2. Flue Gas Flow Rate Ramp-Up and Step Changes in Reboiler Duty

These tests consist of combined input changes to the plant in terms of flue gas volumetric flow rate and reboiler duty. A set-point increase of the flue gas volumetric flow rate fed to the absorber from 40,000 to 47,000 Sm³/h was applied. This corresponds with 67% and 80% of the absorber column capacity, respectively. In addition, step-changes in reboiler duty were applied during the transient test. Figure 6a shows the three main inputs of the plant during the test. Figure 6b,c show the CO₂ product flow and CO₂ absorbed for the model and the pilot plant data. In this test a dead time of around 20 min in the response of CO₂ desorbed was observed. This confirms the buffering effect by the chemical process in terms of the response of CO₂ desorbed when the flue gas volumetric flow rate is changed. There is evidence to support this observation in previous pilot plant studies [46–48]. The delay in the response is partly attributed to solvent circulation time and the redistribution of liquid. Despite the steady-state offset shown on CO₂ absorbed in Figure 6b, a good prediction of the main transient response is seen. It is possible that the reduction in reboiler duty at around 10 min flattens out the response in CO₂ product flow rate.

4.3. Solvent Flow Rate Ramp-Down

In this test, the plant is operated in steady-state until the rich solvent mass flow rate set point is ramped down from around 17.5 kg/s to around 16.1 kg/s; refer to FT5 in Figure 1. The reboiler duty and flue gas volumetric flow rate were intended to be kept constant. Figure 7a shows the three main inputs of the plant during this transient test. In addition, the pilot plant performance in terms of product CO₂ mass flow F_{prod} (or CO₂ desorbed) and absorbed CO₂ flow rate are presented, together with the dynamic process model simulations for this test. Again, a satisfactory agreement is found between the plant trajectories and the output trajectories predicted by the dynamic process model.

From the three transient tests presented above, it can be concluded that the dynamic process model predicts the transient trends of the main output trajectories of the process for different inputs to the plant. In addition, the dead times and stabilization times of the process are properly predicted by the dynamic process models, despite the steady-state deviations observed and already quantified in Section 3.2. This means that the dynamic process model is suitable for simulation studies at the plant scale, including dynamic process simulations to analyze the plant transient performance, and for control tuning and advanced control layer design, including control structure studies.

5. Case Study: Open-Loop Performance and Decentralized Control Structures

5.1. Open-Loop Step Responses at Different Plant Flue Gas Capacities

A power plant operated in a power market with a high penetration of renewables will most likely be operated in load-following mode [7,63]. This means that the power plant with PCC will be operated during a significant amount of its lifetime at part loads. In the case of a natural gas combined cycle power plant with post-combustion CO₂ capture it means that, at part-load operation, the gas turbine (GT) load will be reduced, generating a reduced mass flow rate of flue gas that would be conducted to the PCC unit. The purpose of this case study is to investigate the transient performance of the PCC pilot plant via dynamic process simulation by implementing open-loop step changes to the dynamic process model, and to compare the response of the plant at different part-load operating points, defined by different mass flow rates of flue gas to be treated. The analysis will assess the transient response of the plant to multiple and non-simultaneous step changes in three key inputs to the plant, namely (i) flue gas flow rate F_{gas} (ii) solvent flow rate F_{solv} ; and (iii) reboiler duty \dot{Q}_{reb} , at different flue gas mass flow rate capacities of the plant. In order to define the part-load operating points, a decentralized control structure was utilized, in which reboiler duty was the manipulated variable to control stripper bottom temperature T_{str} to 120.9 °C, and the solvent flow rate was the manipulated variable to control CO₂ capture ratio Cap to 0.85, as defined in Equation (13). When operating the plant at different flue gas mass flow rates, corresponding to 100%, 80% and 60% of nominal mass flow rate, this results in the three steady-state operating points presented in Tables 5 and 6. The control structure is defined as control structure A in Table 7.

$$Cap = \frac{F_{gas} \cdot X_{CO_2} - F_{depleted} \cdot X_{CO_2, out}}{F_{gas} \cdot X_{CO_2}} \quad (13)$$

Table 5. Simulated pilot plant inputs' set points for the three operating points to be studied, corresponding to 100%, 80% and 60% of flue gas mass flow rate capacity of the pilot plant. With $Cap = 0.85$ and $T_{str} = 120.9$ °C for all cases.

| Pilot Load (%) | F_{gas} (kg/h) | F_{solv} (kg/s) | \dot{Q}_{reb} (MW) |
|----------------|------------------|-------------------|----------------------|
| 100 | 19.3 | 17.6 | 3.5 |
| 80 | 15.3 | 13.2 | 2.7 |
| 60 | 11.6 | 9.5 | 2.1 |

Table 6. Simulated pilot plant values for the process variables, lean CO₂ loading L_l , rich CO₂ loading L_r , CO₂ capture ratio Cap and CO₂ product flow rate, at three different operating points of the plant, corresponding to 100%, 80% and 60% of flue gas mass flow rate capacity of the pilot plant. With $Cap = 0.85$ and $T_{str} = 120.9$ °C for all cases.

| Pilot Load (%) | L_l (mol/mol) | L_r (mol/mol) | Cap | F_{prod} (kg/s) |
|----------------|-----------------|-----------------|-------|-------------------|
| 100 | 0.280 | 0.501 | 0.85 | 0.91 |
| 80 | 0.246 | 0.514 | 0.85 | 0.72 |
| 60 | 0.228 | 0.514 | 0.85 | 0.55 |

Table 7. Control structures for the supervisory control layer of the TCM amine plant. Key manipulated variables (MVs) are solvent flow rate F_{solv} and reboiler duty Q_{reb} . Controlled variables are CO₂ capture ratio Cap to 85%, defined in Equation (12), and stripper bottom temperature T_{str} to 120.9 °C. Control structure D controls Cap via a feed forward FF controller.

| Control Structure | Pairing 1 | | Pairing 2 | |
|-------------------|----------------------|---------------------|----------------------|---------------------|
| | Manipulated Variable | Controlled Variable | Manipulated Variable | Controlled Variable |
| A | F_{solv} | Cap | Q_{reb} | T_{str} |
| B | Q_{reb} | Cap | F_{solv} | T_{str} |
| C | F_{solv} | L/G | Q_{reb} | T_{str} |
| D | F_{solv} | $Cap, with FF$ | Q_{reb} | T_{str} |

The open-loop response was studied for the process variables (i) CO₂ absorbed $CO_{2,abs}$, in Equation (11); (ii) CO₂ desorbed $CO_{2,abs}$ (or F_{prod}); (iii) lean CO₂ loading L_l at the inlet of the absorber; and (iv) rich CO₂ loading L_r at the outlet of the absorber. To characterize the transient response, dead time θ , settling time t_s , total stabilization time t_t , and relative change (RC) were calculated:

- Dead time θ : it is the time that takes before a process variable starts to change from the initial steady-state conditions as a response to the disturbance or input.
- Settling time: The 10% settling time t_s is the time taken from when the process variable begins to respond to the input change (dead time) until it remains within an error band described by 10% of the change in the process variable Δy and the final steady-state value of the process variable y_∞ , i.e.: $-0.1 \Delta y + y_\infty < y < 0.1 \Delta y + y_\infty$.
- Total stabilization time: the sum of the dead time θ and the settling time t_s is the resulting total stabilization time t_t .
- Relative change RC: Change in the observed process variable from initial steady-state conditions y_0 to the final steady-state conditions; refer to Equation (14).

$$RC(\%) = 100 \cdot \frac{y_\infty - y_0}{y_0} \quad (14)$$

The detailed results of the process simulations are presented in Tables A1–A3 in Appendix A. Figure 8 shows the total stabilization times for the selected process variables at the three operating points, for step changes in solvent flow rate and reboiler duty. The responses for step changes in flue gas flow rate are not presented, since it is shown in Table A1 that the relative change RC in the output process variables is very small or negligible (RC ranges from -0.81% to 0.21%). This can be explained by the highly diluted nature of the CO₂ in the flue gas (ca. 3.5 vol%). The results show the non-linear behavior of the plant, with different transient responses to step change set-point increase and decrease in key plant inputs, and at different loads of the plant.

Figure 8a shows the total stabilization time for lean CO₂ loading L_l at the inlet of the absorber, which ranges from 25 to 45 min in all cases. The results show that the required time for total stabilization increases when the plant is operated at lower loads. As shown in Appendix A (Tables A1 and A2), a general trend was that the dead time θ in the response of L_l to step changes in reboiler duty and rich solvent mass flow rate increases at part-load points. This could be explained by the fact that at lower loads the solvent mass flow rate is smaller (refer to F_{solv} in Table 6), resulting in longer residence times of the solvent through each equipment hold-up, piping, and recycle loop, this is, larger circulation time. This can also explain why dead times are generally larger when decreasing solvent flow rate than when increasing it; refer to Table A2 in Appendix A.

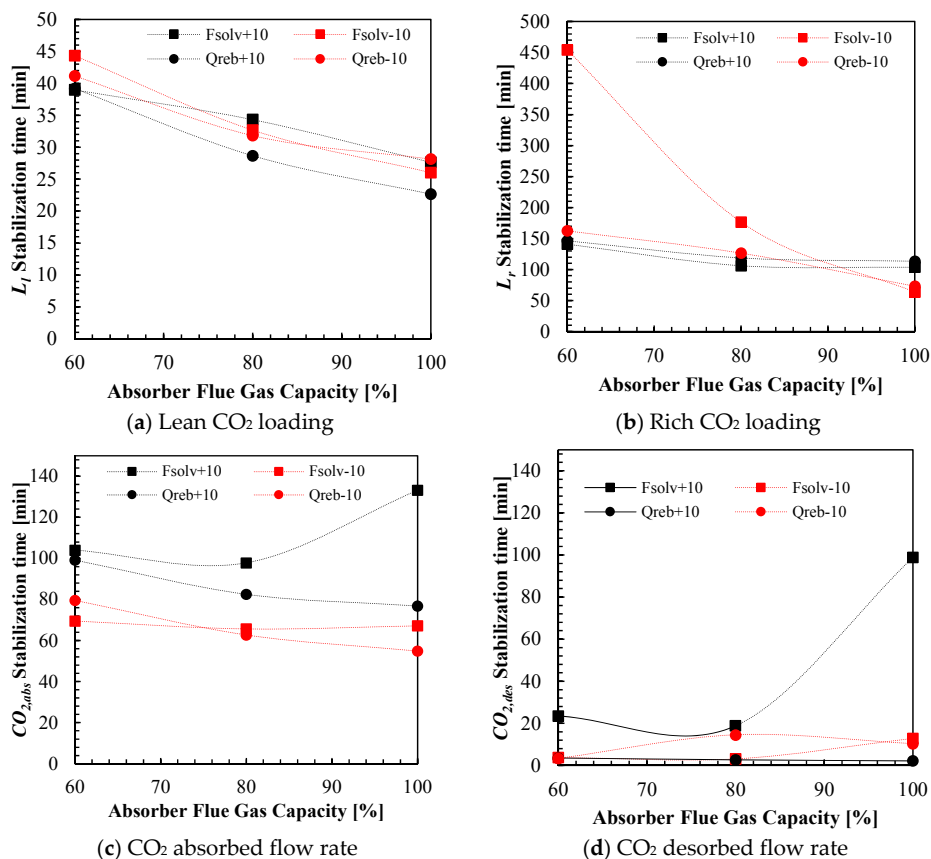


Figure 8. Simulation results. Total stabilization times t_s for open-loop $\pm 10\%$ step changes in solvent flow rate and reboiler duty for the process variables (a) Lean CO₂ loading L_r ; (b) rich CO₂ loading L_r ; (c) CO₂ absorbed $CO_{2,abs}$ and (d) CO₂ desorbed $CO_{2,des}$. Stabilization times are calculated for the response when the plant is operated at three different operating points in terms of flue gas mass flow rate, 100%, 80% and 60% of nominal capacity; refer to Tables 5 and 6.

Figure 8b shows the total stabilization times for rich CO₂ loading L_r at the outlet of the absorber sump. In this case, the stabilization times range from 60 to 450 min. It should be mentioned that the relative change RC in rich CO₂ loading is also small or negligible for the disturbances studied (see Appendix A), due to the fact that the solvent is operated close to its maximum loading capacity of 0.51 mol/mol CO₂ loading. The total stabilization times of the responses of rich CO₂ loading L_r to disturbances in solvent flow rate and reboiler duty are larger at lower plant loads. At 60% flue gas capacity, a very slow response is found in L_r when the solvent flow rate is decreased by a -10% step change; however, the relative change RC of L_r in this process variable is negligible for this plant disturbance; refer to Table A2 in Appendix A.

The total stabilization times for CO₂ absorbed $CO_{2,abs}$ response to disturbances in rich solvent mass flow rate F_{solv} and reboiler duty \dot{Q}_{reb} are shown in Figure 8c. Total stabilization times range from 55 to 135 min. When the rich solvent mass flow rate is increased by 10%, this results in an increase in CO₂ absorbed with a relative change RC of 0.35% to 4.18% (refer to Table A2), due to the increased L/G ratio in the absorber column. However, since the reboiler duty is kept constant, the lean loading will increase (see RC values of L_l in Table A2). Due to the residence time in the hot solvent piping,

lean/rich heat exchanger and lean amine cooler of the recycle loop, it takes time for the solvent to be distributed towards the inlet of the absorber. A dead time in CO_2 lean loading L_l at the inlet of the absorber of 11 to 22 min is observed (see Table A2). This results in it taking a long time for the $\text{CO}_{2,abs}$ to stabilize. When the rich solvent mass flow rate is decreased by 10%, it is observed that the CO_2 absorbed $\text{CO}_{2,abs}$ decreases (relative change RC between -3.14% and -5.59% in Table A2). This is a result of the combination of the reduction in L/G ratio and the decrease in lean loading L_l . $\text{CO}_{2,abs}$ requiring time for stabilization (stabilization time of 65 to 69 min). When reboiler duty \dot{Q}_{reb} is increased by 10%, the lean loading L_l is decreased significantly (RC ranging from 6.75 to 8.59%), which results in increase of $\text{CO}_{2,abs}$ (relative change RC of 4.0% to 6.07%). The change in lean loading L_l is observed at the absorber inlet with a dead time of 13 to 23 min (due to circulation time of the solvent in the recycle loop), and the total stabilization time for $\text{CO}_{2,abs}$ for increase in reboiler duty ranges from 76 to 99 min. When reboiler duty \dot{Q}_{reb} is decreased by 10%, the solvent lean loading increases (RC of 6.63% to 8.46%), resulting in less CO_2 being absorbed. Relatively slower response in $\text{CO}_{2,abs}$ to disturbances in solvent flow rate and reboiler duty were found when the PCC was operated at lower loads (55 to 99 min). An exception is found for the case when the solvent flow rate is increased at 100% mass flow rate operating conditions of the plant.

Figure 8d shows the stabilization times for CO_2 desorbed $\text{CO}_{2,des}$. For disturbances in rich solvent flow rate and reboiler duty, the desorbed CO_2 stabilizes slightly faster at lower loads (ranging from 2 to 100 min). In general, it was found that the desorption rate stabilized faster than the absorption rate $\text{CO}_{2,abs}$ for the disturbances in solvent flow rate and reboiler duty applied to the process. When solvent flow rate is decreased, this results in smaller L/G ratio in the absorber column and less CO_2 being desorbed in the stripper column. Since the rich CO_2 loading does not change significantly (RC in L_r from 0 to 0.08%), the CO_2 desorbed $\text{CO}_{2,des}$ stabilizes faster than the CO_2 absorbed (circulation time through the recycle loop is not affecting the stabilization of $\text{CO}_{2,abs}$). When the reboiler duty \dot{Q}_{reb} is increased by 10%, the relative change in CO_2 desorbed is large (4 to 6.07% in Table A3), and with fast total stabilization time (2 to 3 min in Table A3). A change in reboiler duty results in a fast response in the produced stripping vapors, which also results in a fast response in CO_2 product flow rate (CO_2 desorbed). The longest stabilization time for CO_2 desorbed is found when the solvent flow rate is increased at 100% operating conditions. It is notable that there is a big difference in total stabilization times for solvent flow rate increase at different loads of the plant.

5.2. Decentralized Control Structures

In this section, four control structures for the TCM DA amine plant were tested via dynamic process model simulations. The scenario considers realistic load changes on the power plant, by changing flue gas flow rate feed to the absorber column. From a control analysis perspective, flue gas flow rate change can be considered as a disturbance applied to the PCC process. A load change event would result in a significant change in flue gas flow rate, at a ramp rate given by GT operation and controls. Fast ramp rates are the goal of power plant operators, since a fast power plant can respond to the variability in costs in a day-ahead power market [7,64]. For a NGCC power plant, a fast ramp rate is considered to be around 10%/min GT load [4,65]. Two tests were considered and simulated:

- Test 1: Ramping down flue gas flow rate from 100 to 70% in 3 min. The transient event starts at $t_0 = 0$ min, and sufficient simulation time is allowed for the plant to reach the new steady-state.
- Test 2: Flue gas flow rate is ramped up from 70 to 100% in 3 min. The transient event starts at $t_0 = 0$ min, and sufficient simulation time is allowed for the plant to reach the new steady-state.

The supervisory or advanced control layer of the TCM DA amine plant has three main degrees of freedom, consisting of set point of flue gas volumetric flow rate F_{gas} , set point of rich pump solvent flow rate F_{solvr} , and steam flow rate to feed the reboiler duty \dot{Q}_{reb} ; refer to FT1, FT5 and FT4, respectively in Figure 1. Under normal and stable operation of the pilot plant at TCM DA, such degrees of freedom

are changed manually by the operators to bring the plant to different operating conditions. If flue gas flow rate is considered to be a disturbance, there are two degrees of freedom left for operation. Note that here we do not consider the degrees of freedom available to the operators in the stabilizing or regulatory control layer, or for other auxiliary operations of the plant, or start-up procedures. Several studies in the literature suggest that keeping the capture ratio Cap and a temperature in the stripper column constant can lead to efficient operation of the process for varying loads of the PCC absorber-desorber process [13]. In this analysis, four control structures were tested, as presented in Table 7. All the feedback control loops are PI controllers, and were tuned with the simple internal model control (SIMC) tuning rules [66].

- **Control structure A** uses F_{solv} to control capture ratio at the top of the absorber Cap defined by Equation (13) to the set point of 0.85, and reboiler duty \dot{Q}_{reb} to control the solvent temperature at the stripper bottom T_{str} to the set point of 120.9 °C. This control structure has been previously proposed in the literature in different studies including [14,16], where it shows a fast response and the capability to reject disturbances.
- **Control structure B** uses F_{solv} to control the solvent temperature at the stripper bottom T_{str} to the set point of 120.9 °C, and reboiler duty \dot{Q}_{reb} to control capture ratio at the top of the absorber Cap to the set point of 0.85. Note that changes in reboiler duty result in a big change in solvent lean CO₂ loading (large relative change RC ; see Appendix A). A similar version was suggested by Panahi and Skogestad [14], where it was found that this control structure showed similar dynamic behavior, in response to disturbances in flue gas flow rate, compared with a model predictive control scheme (MPC).
- **Control structure C** utilizes solvent flow rate F_{solv} to control the mass-based L/G ratio in the absorber column at the same value as that in the close-to-design-point operating conditions. This control structure has been studied previously in [12,15]. This control loop is implemented via ratio control. In addition, reboiler duty is manipulated to control T_{str} to 120.9 °C. The control structure leads to different final steady-state operating conditions when ramping down the plant load than the other three alternatives.
- **Control structure D** is a modification of control structure A. In this control structure, the solvent flow rate set point is changed via a feed forward (FF) action to control the capture ratio Cap at 0.85; in addition, the stripper bottom temperature is controlled by manipulating the reboiler duty. The feed forward controller is implemented by a set-point ramp change in the solvent flow rate with the same total duration as the flue gas flow rate ramp change, to the final value that gives a Cap of 0.85 under final steady-state conditions.

Figure 9 shows the simulated time input trajectories during the test with flue gas flow rate reduction. The manipulated variables F_{solv} and \dot{Q}_{reb} are shown for the different control structures evaluated. Figure 10 shows the output trajectories of CO₂ capture ratio Cap , desorption ratio Des , CO₂ absorbed and CO₂ desorbed for the transient tests of flue gas flow rate reduction. Figure 11 shows the trajectories of lean loading L_l and stripper bottom solvent temperature T_{str} for flue gas flow rate reduction. In addition, Figure 12 shows the simulated time input trajectories during the test with flue gas flow rate increase. Figure 13 shows the output trajectories of CO₂ capture ratio Cap , desorption ratio Des , CO₂ absorbed and CO₂ desorbed for the transient tests of flue gas flow rate increase, and Figure 14 shows the trajectories of lean loading L_l and stripper bottom solvent temperature T_{str} for flue gas flow rate increase. In order to compare the different control structure performances during transient load change, the total stabilization times of the selected process variables are shown in Table 8. These will indicate how fast the plant achieves stabilization of the different floating (not controlled) process variables when moving from one operating condition to the next one. In addition, three transient performance indicators have been considered and presented in Table 9. Note that, for this analysis auxiliary consumptions of the plant are not considered.

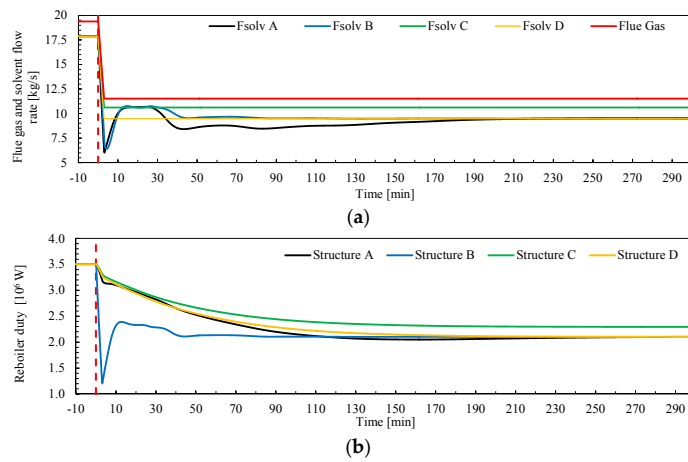


Figure 9. Inputs to the pilot plant during simulations for load change ramp-down (Test 1) from 100 to 70% with a ramp rate of 10%/min reduction in flue gas flow rate, for control structures A, B, C and D. (a) Flue gas flow rate (kg/s), as a disturbance, and solvent flow rates (kg/s) of the rich pump as manipulated variables (MVs); (b) Reboiler duty (W) as MV. The red vertical dotted line shows when the transient event starts at t_0 .

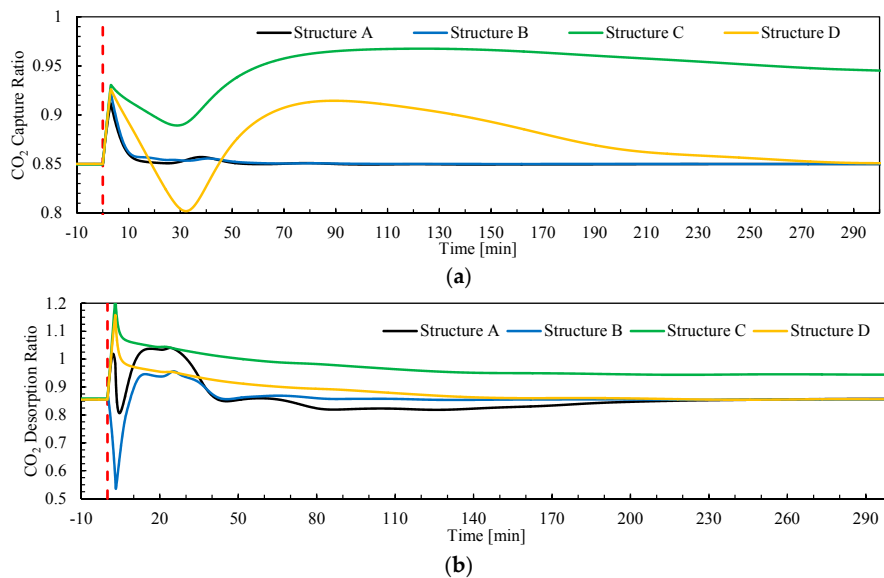


Figure 10. Cont.

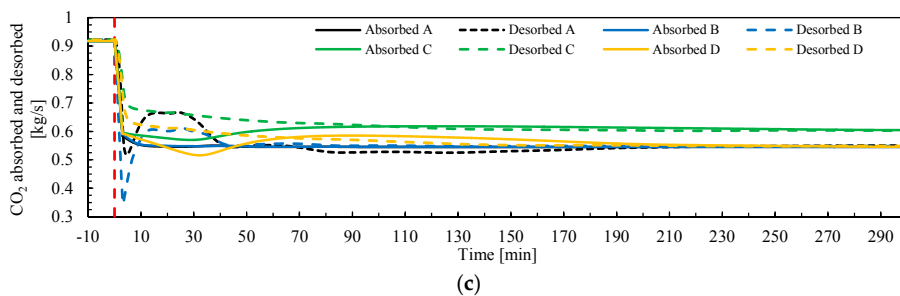


Figure 10. Outputs from pilot plant model during simulations for load change ramp-down (Test 1) from 100 to 70% with a ramp rate of 10%/min reduction in flue gas flow rate, for control structures A, B, C and D. (a) CO₂ capture ratio C_{ap} , as controlled variable (CV); (b) CO₂ desorption ratio Des ; (c) CO₂ absorption and desorption rates (kg/s). The red vertical dotted line shows when the transient event starts at t_0 .

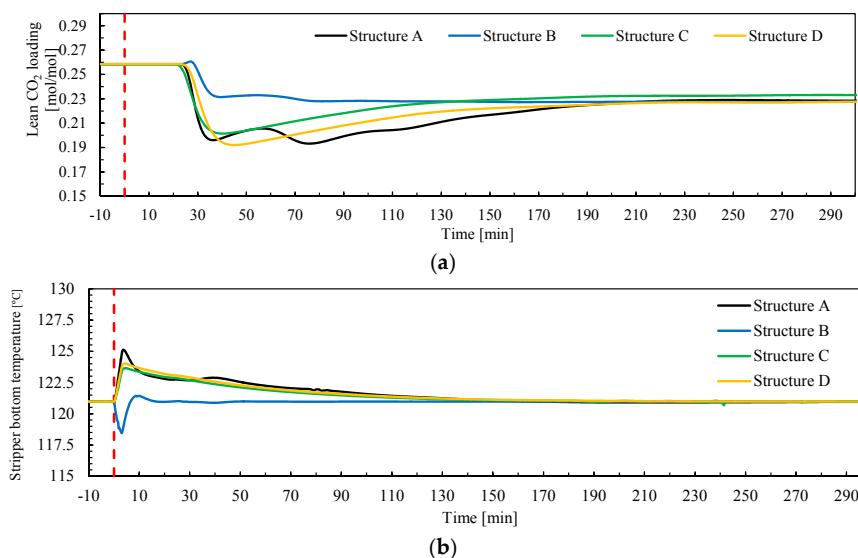


Figure 11. Outputs from pilot plant model during simulations for load change ramp-down (Test 1) from 100 to 70% with a ramp rate of 10%/min reduction in flue gas flow rate, for control structures A, B, C and D. (a) Lean CO₂ loading at the inlet of the absorber; (b) Stripper bottom temperature as controlled variable (°C). The red vertical dotted line shows when the transient event starts at t_0 .

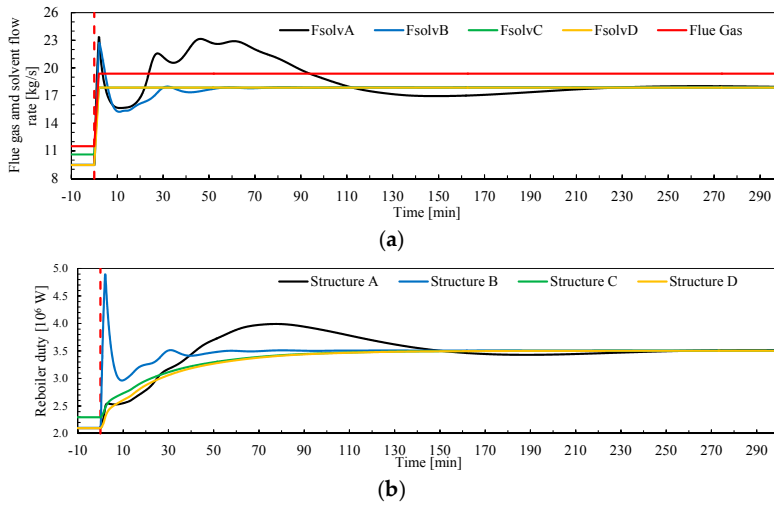


Figure 12. Inputs to the pilot plant during simulations for load change ramp-up (Test 2) from 70 to 100% with a ramp rate of 10%/min increase in flue gas flow rate, for control structures A, B, C and D. (a) Flue gas flow rate (kg/s), as a disturbance, and solvent flow rates (kg/s) of the rich pump as manipulated variables (MVs); (b) Reboiler duty (W) as MV. The red vertical dotted line shows when the transient event starts at t_0 .

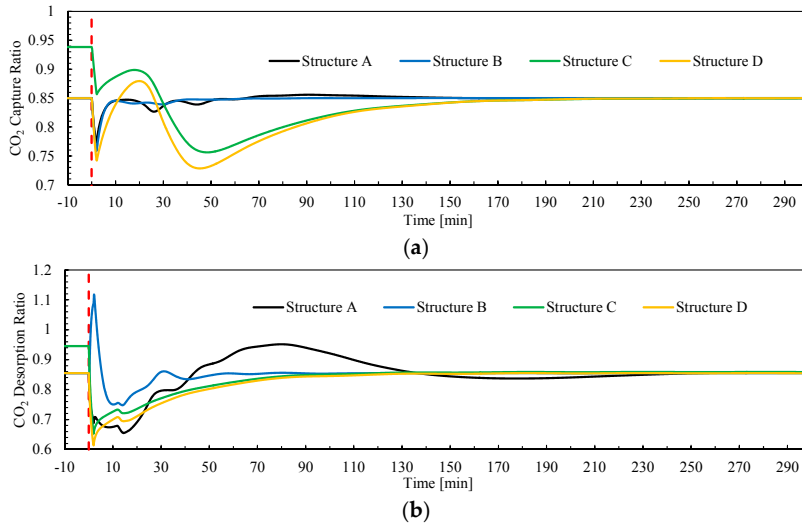


Figure 13. Cont.

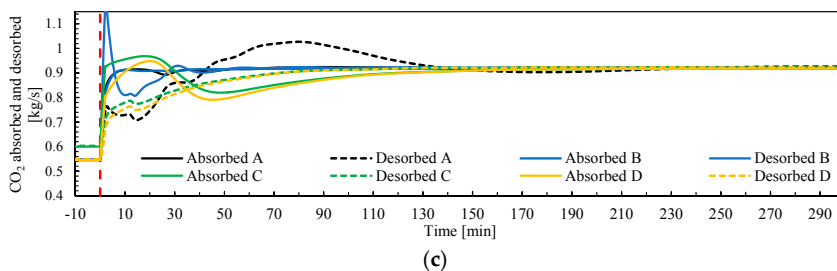


Figure 13. Outputs from pilot plant model during simulations for load change ramp-up (Test 2) from 70 to 100% with a ramp rate of 10%/min increase in flue gas flow rate, for control structures A, B, C and D. (a) CO₂ capture ratio *Cap*, as controlled variable (CV); (b) CO₂ desorption ratio *Des*; (c) CO₂ absorption and desorption rates (kg/s). The red vertical dotted line shows when the transient event starts at t_0 .

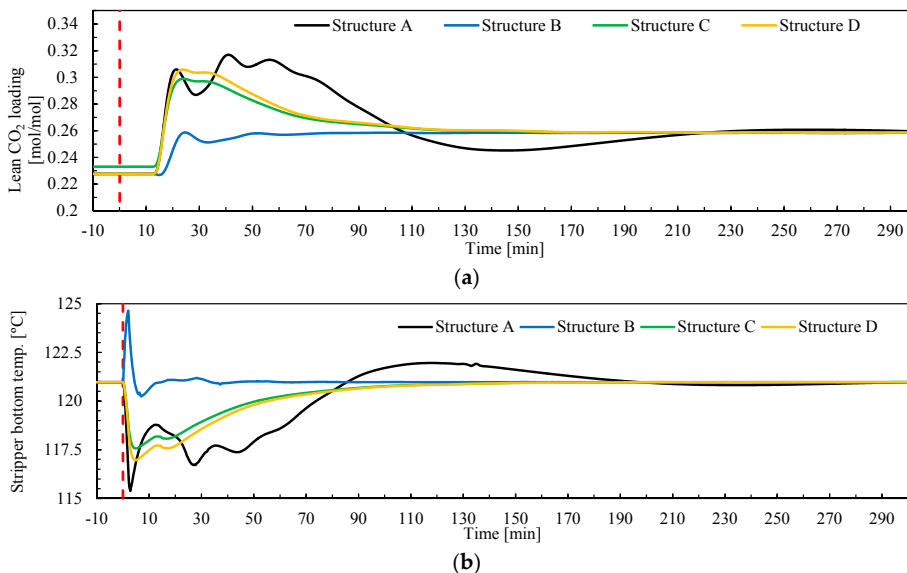


Figure 14. Outputs from pilot plant model during simulations for load change ramp-up (Test 2) from 70 to 100% with a ramp rate of 10%/min increase in flue gas flow rate, for control structures A, B, C and D. (a) Lean CO₂ loading at the inlet of the absorber; (b) Stripper bottom temperature as controlled variable (°C). The red vertical dotted line shows when the transient event starts at t_0 .

Table 8. Total stabilization times of the floating process variables for the different control structures, when ramping down the plant $t_{t,down}$ from 100% flue gas mass flow rate to 70%; and when ramping up the plant $t_{t,up}$ from 70% flue gas mass flow rate to 100%.

| Control Structure | Process Variable | $t_{t,down}$ (min) | $t_{t,up}$ (min) |
|-------------------|--------------------------|--------------------|------------------|
| A | CO ₂ Absorbed | 3.3 | 71.0 |
| | CO ₂ Desorbed | 36.3 | 112.7 |
| | L_I | 187.7 | 201.0 |
| B | CO ₂ Absorbed | 4.0 | 5.2 |
| | CO ₂ Desorbed | 35.3 | 27.5 |
| | L_I | 68.2 | 46.7 |
| C | CO ₂ Absorbed | 3.6 | 97.7 |
| | CO ₂ Desorbed | 56.5 | 63.7 |
| | L_I | 172.2 | 115.5 |
| D | CO ₂ Absorbed | 6.2 | 96.8 |
| | CO ₂ Desorbed | 50.3 | 59.2 |
| | L_I | 185.0 | 113.8 |

Table 9. Simulation results for accumulated reboiler energy consumption Q_{reb} (MJ), accumulated CO₂ emitted CO_{2,em} and accumulated CO₂ captured CO_{2,cap} during the transient event (8 h) for the different control structures A,B, C and D (refer to Table 7), when ramping up and down the plant (between 100% and 70% of flue gas mass flow rate). Static plant refers to an ideal static plant that changes from the initial operating conditions to the final operating conditions instantaneously at time $t = 0$. An integration time of $t_f = 480$ min was utilized to calculate the values for the ideal static plant.

| Transient Event | Indicator | Static Plant | A | B | C | D |
|-----------------|----------------------------|--------------|---------|---------|--------|--------|
| Ramp down | Q_{reb} (MJ) | 60,441 | 63,353 | 60,926 | 69,045 | 64,046 |
| | CO _{2,em} (tons) | 2.66 | 2.64 | 2.65 | 0.96 | 2.39 |
| | CO _{2,cap} (tons) | 15.70 | 15.76 | 15.75 | 17.44 | 16.01 |
| Ramp up | Q_{reb} (MJ) | 100,924 | 100,898 | 100,655 | 98,973 | 98,667 |
| | CO _{2,em} (tons) | 4.49 | 4.51 | 4.53 | 4.77 | 4.94 |
| | CO _{2,cap} (tons) | 26.41 | 26.39 | 26.37 | 26.13 | 25.96 |

- **Accumulated reboiler energy input Q_{reb} (MJ):** see Equation (15). This is calculated by integration of the \dot{Q}_{reb} trajectory under the transient event, from the initial time $t_0 = 0$ min to the final time $t_f = 480$ min (8 h). The final time was defined to ensure that the plant was already under steady-state conditions at the final operating point. This value Q_{reb} represents the main energy consumption of the process during the transient event of load change. In addition, the consumption of an ideal static plant is included for comparison (see Table 9). The ideal static plant is assumed to change from initial to the final steady-state operating conditions instantaneously at time t_0 , and would operate until t_f . The static plant value represents the minimum value when ramping down and a maximum value when ramping up.

$$Q_{reb} = \int_{t_0}^{t_f} \dot{Q}_{reb}(t) dt \quad (15)$$

- **Accumulated CO₂ emitted CO_{2,em} (tons):** see Equation (16). This is calculated by integration of the \dot{m}_{CO_2} trajectory under the transient event, from the initial time $t_0 = 0$ min to the final time $t_f = 480$ min; this represents the CO₂ emitted at the absorber stack. The final time was defined to ensure that the plant was already under steady-state conditions at the final operating point. This measure represents the CO₂ emitted during the transient event of load change.

For comparison, the CO₂ emitted by an ideal static plant is calculated (considered as the maximum value when ramping down and a minimum value when ramping up), shown in Table 9.

$$CO_{2,em} = \int_{t_0}^{t_f} \dot{m}_{CO_2}(t)dt = \int_{t_0}^{t_f} \dot{m}_{depleted}(t) \cdot X_{CO_2}(t)dt \quad (16)$$

- **Accumulated CO₂ captured $CO_{2,cap}$ (tons):** see Equation (17). This is calculated by integration of the CO₂ absorbed $CO_{2,abs}$ trajectory (Equation (12)) under the transient event, from the initial time $t_0 = 0$ min to the final time $t_f = 480$ min. The final time was defined to ensure that the plant was already under steady-state conditions at the final operating point. This measure represents the CO₂ captured during the transient event of load change. For comparison, the CO₂ captured by an ideal static plant is calculated (considered as the minimum value when ramping down and a maximum value when ramping up), shown in Table 9.

$$CO_{2,cap} = \int_{t_0}^{t_f} (F_{gas}(t) \cdot X_{CO_2}(t) - F_{depleted}(t) \cdot X_{CO_{2,out}}(t))dt \quad (17)$$

Figure 10 shows that the CO₂ capture ratio Cap had similar trajectories for control structures A and B during Test 1 (flue gas ramp-down), and that Cap reached stabilization conditions faster (20–50 min) than control structures C and D (around 270 min). Cap had also larger excursions from the set point than when control structures A and B are utilized. The same trends are found for Test 2 with flue gas flow rate ramp-up (Figure 13). When ramping up, control structures C and D stabilize faster (around 160 min) than when ramping down. This showed that the utilization of close-loop feedback control (structures A and B) allows shorter stabilization times to be reached for the controlled variable CO₂ capture ratio Cap . The desorption ratio Des trajectories in Figure 10 show that the plant requires the shortest stabilization time for this process variable when employing control structure B (around 60 min), followed by control structure A and C (around 200 min). This can be explained by the fact that for a change in reboiler duty the response of CO₂ desorbed has a fast total stabilization time and a large static relative change RC (where RC ranges from 4 to 6.29% and total stabilization time range from 2.2 to 3.5 min for a +10% step in reboiler duty); refer to Table A3. When it comes to the stabilization time required for Des for Test 1, structures C and D presented a poorer performance as the trajectories for Cap and Des deviate from the set point significantly. For control structure A, Des showed slow performance for Test 2 (around 210 min total stabilization time) with significant oscillations around set point; refer to Figure 13.

When ramping down the plant, CO₂ absorbed and CO₂ desorbed require similar stabilization times for control structures A and B (around 3 min for $CO_{2,abs}$ and 36 min for $CO_{2,des}$), while the control structures C and D require longer stabilization times for CO₂ desorbed (around 50 to 57 min); refer to Table 8. The trajectory of CO₂ lean loading again shows shorter stabilization time for control structure B. This can be explained by the large static relative change RC of the response of CO₂ lean loading to changes in reboiler duty (where RC ranges from −6.29% to −4.97% and total stabilization time range from 22.7 to 39.2 min for a +10% step in reboiler duty); refer to Table A3. This contributes to the tight control of CO₂ capture ratio Cap achieved by control structure B, since the CO₂ lean loading L_l is a key process variable that connects the operation of the stripper and the absorber columns via the recycle loop. In addition, control structure B shows the shortest stabilization times and smaller excursions of the stripper bottom temperature T_{str} (around 15 to 30 min), in Figures 11 and 14.

When the plant load is ramped up from 70 to 100% (Test 2), the control structure B in general showed a faster dynamic performance with significantly shorter stabilization times required for the floating process variables considered (5.2 min for $CO_{2,abs}$, 27.5 min for $CO_{2,des}$ and 46.7 min for L_l), see Table 9; followed by C, D and A. Note that control structure B presented a faster dynamic performance towards stabilization while ramping up (L_l stabilizes in 46.7 min) than when ramping down the process (L_l stabilizes in 68.2 min). Control structures A, C and D required shorter stabilization

times for CO₂ absorption and CO₂ desorption when ramping down the process load, while CO₂ lean loading stabilized faster when ramping up the plant load; refer to the stabilization time values in Table 9. When the plant is operated under control structure C, the optimum solvent flow rate F_{solv} and lean loading L_l are not reached at the 70% absorber capacity steady-state operating conditions; refer to time >250 min in Figures 9a and 11a, and time <0 min in Figures 12a and 14a. This leads to a higher Cap than specified (refer time $t > 290$ min in Figure 10a and time $t < 0$ min in Figure 13a), and therefore higher reboiler duty (time $t > 290$ min in Figure 9b and time $t < 0$ min in Figure 12b), even though the stripper bottom temperature T_{str} criterion is satisfied.

During the ramp-down transient event of the plant (i.e., period of 8 h from the time change was implemented), the least energy-intensive performance measured by Q_{reb} in Table 9 was observed for control structure B. In addition, this structure shows the largest CO₂ emissions during the transient event, albeit still lower than the ideal static plant. The fast stabilization time of the plant process variables achieved by control structure B provides a transient performance that is the closest to the ideal static plant. Control structures C and D showed the largest CO₂ captured during the transient event. However, when ramping down the plant load, this means that the plant is emitting less CO₂ during the transient event with control structures A, B, C and D than that established by the operational objective and represented by the ideal static plant case. Consequently, when ramping down the plant load, CO₂ emissions will always be lower than those of the equivalent ideal static plant. In addition, the plant is capturing more CO₂ than the ideal static plant. Figure 10a shows how there are periods of time in which the capture ratio Cap is above the target of 0.85, leading to more CO₂ being captured than the ideal static plant during the transient event. Control structures A and B showed the largest CO₂ emitted when compared with the ideal static case. Despite control structure A presenting a similar amount of CO₂ emitted during the transient event, it requires a larger amount of energy input during this period than control structure B. Therefore, control structure B shows the best performance in terms of energy consumption and CO₂ emissions during the transient load change event of ramping down the PCC plant load. When ramping up the plant load the most energy-intensive control structure is control structure B. However CO₂ emissions are the lowest, being closer to the minimum established by the static plant. This means that, when ramping up the plant load, CO₂ emissions will always be higher than those of the equivalent ideal static plant. While control structure D is the least energy-intensive process during the transient event of load change increase, it is the control structure with the largest CO₂ emissions during this transient event.

6. Conclusions

The pilot plant data obtained in this work from an MEA campaign at TCM DA amine plant includes ten steady-state operating data sets. The data sets consist of a wide range of steady-state operating conditions of the chemical absorption process in terms of L/G ratio in the absorber column, different absorber packing heights, CO₂ capture ratios, reboiler duty and flue gas flow rate fed to the absorber. The data is considered reliable and valid and can be used for process model validation purposes. In addition, the three transient data sets presented in this work represent transient operation of the pilot plant driven by set-point changes in flue gas flow rate, solvent circulation flow rate and reboiler duty. The transient data sets are considered reliable and suitable for dynamic process model validation purposes, provided that input trajectories can be applied to the dynamic process model.

The validation of the dynamic process model with the steady-state and transient data shows that the process model has a good capability of predicting the steady-state and transient behavior of the plant for a wide range of operating conditions. The validation included in this work proves the capacities of dynamic process modeling applied to large-scale experimental data. The model is considered suitable for studies including transient performance analysis and control structure evaluation studies at the plant scale. In addition, it provides confidence towards using the dynamic process model for analysis of larger-scale PCC plants.

The case study carried out in this work via dynamic process simulations with the validated model shows that, generally, the plant responds more slowly at lower operating loads (the load being defined by the flow rate fed to the absorber). A general trend is observed, in which it takes a longer time to stabilize the main process variables of the pilot plant under open-loop step changes in the main inputs of the process, namely solvent flow rate, flue gas flow rate and reboiler duty. From the process simulations, it is found that, in general, the desorption rate stabilizes faster than the absorption rate for set-point step changes in solvent flow rate and reboiler duty. In addition, $\pm 10\%$ step changes in flue gas flow rate around a given operating point do not cause a large relative change in the main process variables of the process (RC ranges from -0.81% to 0.21%).

The evaluation of the decentralized control structures shows that by adding closed-loop controllers on the two main degrees of freedom of the plant—solvent flow rate and reboiler duty—to control two other process variables, including CO_2 capture ratio and stripper bottom solvent temperature, the plant can be stabilized faster and more efficiently under varying loads. The control structure that showed the best performance was control structure B, in which the reboiler duty is manipulated to control CO_2 capture ratio at the inlet of the absorber and the rich solvent flow rate to control the stripper bottom solvent temperature. It was observed that control structure B provides the fastest stabilization times for the main process variables under scenarios when the plant load is ramped down and up, with ramp rates typically found in NGCC power plants with fast-cycling capabilities. When reducing the PCC process load, this control structure is the least energy-intensive of those evaluated in this work. When increasing the plant load, this control structure is the one with the lowest accumulated CO_2 emissions imposed by the process inertia during load-change transient operation.

Acknowledgments: The authors acknowledge the Department of Energy and Process Engineering at NTNU-Norwegian University of Science and Technology and TCM DA owners Gassnova, Shell, Statoil and Sasol, for funding this project. The funds for covering the costs to publish in open access were provided by the Norwegian University of Science and Technology—NTNU.

Author Contributions: Rubén M. Montañés contributed to the selection of experimental data; processed the experimental data; developed the models; carried out the calibration, validation and simulation of the dynamic process models; defined and carried out the case studies; analyzed the results; and wrote the manuscript. Nina E. Flø contributed to the experimental data selection; contributed to the critical analysis of the results; and reviewed the manuscript. Lars O. Nord contributed to the critical analysis of the results; reviewed the manuscript; and supervised the work.

Conflicts of Interest: The authors declare no conflict of interest.

Abbreviations and Symbols

| | |
|--------------------|--|
| A_{if} | Contact area |
| AP | Absolute percentage error |
| Cap | CO_2 capture ratio |
| CHP | Combined heat and power |
| CCS | Carbon capture and storage |
| CO_2 | Carbon dioxide |
| $\text{CO}_{2,em}$ | CO_2 emitted (kg/s) |
| c_i | Molar concentration |
| C_{ef} | Pre-multiplying coefficient |
| DCC | Direct contact cooler |
| Des | Desorption ratio |
| D_{CO_2} | Diffusivity of CO_2 in aqueous monoethanolamine |
| E | Enhancement factor |
| F | Mass flow rate (kg/s) |

| | |
|--------------------|--|
| FB | Feedback |
| FC | Flow controller |
| FF | Feed-forward |
| FT | Flow transmitter |
| GA | Gas analyzer |
| GC | Gas chromatograph |
| GT | Gas turbine |
| He_i | Henry's constant |
| H ₂ O | Water |
| HX | Heat exchanger |
| k_i | Mass transfer coefficient |
| K_i | Equilibrium constant |
| LC | Level controller |
| L_l | Lean CO ₂ loading |
| L_r | Rich CO ₂ loading |
| L/G | Mass-based liquid to gas ratio (kg/kg) |
| LT | Level transmitter |
| MAP | Mean absolute percentage error |
| MEA | Monoethanolamine |
| MPC | Model predictive control |
| N ₂ | Nitrogen |
| NCCC | National carbon capture center |
| NGCC | Natural gas combined cycle |
| O ₂ | Oxygen |
| p | Pressure (Pa) |
| PC | Pressure controller |
| PCC | Post-combustion CO ₂ capture |
| PT | Pressure transmitter |
| PZ | Piperazine |
| \dot{Q}_{reb} | Reboiler duty (W) |
| Q_{reb} | Reboiler energy input (J) |
| RC | Relative change |
| SA | Solvent analyzer |
| SIMC | Simplified internal model control |
| SRD | Specific reboiler duty (kJ/kgCO ₂) |
| T | Temperature (K) |
| TC | Temperature controller |
| TCM DA | CO ₂ Technology Cener Mongstad |
| t_s | Settling time |
| t_t | Total stabilization time |
| TT | Temperature transmitter |
| X | Mass fraction |
| x_p | Value measured at pilot plant |
| x_m | Value simulated model |
| y_∞ | Steady-state final value |
| θ | Dead time |
| γ_i | Activity coefficient |
| ΔH_r | Heat of reaction |
| Δy | Change in process variable |
| ε -NTU | Effectiveness number of thermal units |

Appendix A

Tables A1–A3 show the simulation results in terms of the dead time θ , 10% settling time t_s , total stabilization time t_t and relative change RC %, for the open-loop response to step-changes in the main inputs to the plant. The step changes are applied to the plant when it is operated at three different steady-state operating conditions defined by three different mass flow rate capacities of the absorber column. The inputs are:

- Flue gas mass flow rate $\pm 10\%$ step-change.
- Solvent mass flow rate $\pm 10\%$ step-change.
- Reboiler duty $\pm 10\%$ step-change.

The output process variables studied are:

- CO_2 lean loading L_l (mol/mol).
- CO_2 rich loading L_r (mol/mol).
- CO_2 absorbed $\text{CO}_{2,abs}$ (kg/s).
- CO_2 desorbed $\text{CO}_{2,abs}$ (kg/s).

Table A1. Open-loop response to $\pm 10\%$ step-changes in flue gas mass flow rate for three different operating points of the pilot plant. Responses in CO_2 lean loading L_l , CO_2 rich loading L_r , CO_2 absorbed, and CO_2 desorbed.

| Plant Load | Input Process Variable | $F_{gas} +10\%$ | | | | $F_{gas} -10\%$ | | | |
|------------|---------------------------|-----------------|-------------|-------------|----------|-----------------|-------------|-------------|----------|
| | | θ (min) | t_s (min) | t_t (min) | RC (%) | θ (min) | t_s (min) | t_t (min) | RC (%) |
| 100% | L_l | 40.5 | 296.5 | 337.0 | 0.01 | 33.5 | 133.2 | 166.7 | -0.35 |
| | L_r | 0.0 | 41.7 | 41.7 | 0.09 | 19.0 | 116.3 | 135.3 | -0.76 |
| | $\text{CO}_{2,abs}$ | 0.0 | 95.2 | 95.2 | 0.05 | 0.0 | 168.7 | 168.7 | -0.81 |
| | $\text{CO}_{2,abs}$ | 22.2 | 244.3 | 266.5 | 0.04 | 22.7 | 128.7 | 151.3 | -0.80 |
| 80% | L_l | 50.3 | 260.8 | 311.2 | -0.03 | 42.7 | 442.0 | 484.7 | 0.04 |
| | L_r | 0.0 | 53.3 | 53.3 | 0.21 | 67.2 | 117.5 | 184.7 | -0.15 |
| | $\text{CO}_{2,abs}$ | 0.0 | 61.8 | 61.8 | -0.03 | 0.0 | 334.5 | 334.5 | -0.06 |
| | $\text{CO}_{2,abs}$ | 25.5 | 393.7 | 419.2 | -0.03 | 23.8 | 364.7 | 388.5 | -0.06 |
| 60% | L_l | 51.9 | 424.9 | 476.8 | -0.03 | 53.7 | 318.5 | 372.2 | 0.08 |
| | L_r | 0.0 | 96.1 | 96.1 | 0.00 | 0.0 | 192.8 | 192.8 | -0.05 |
| | $\text{CO}_{2,abs}$ | 0.0 | 113.7 | 113.7 | -0.05 | 0.0 | 141.2 | 141.2 | 0.09 |
| | $\text{CO}_{2,abs}$ | 27.7 | 363.4 | 391.1 | -0.05 | 25.6 | 369.9 | 395.5 | 0.09 |

Table A2. Open-loop response to $\pm 10\%$ step-changes in solvent mass flow rate for three different operating points of the pilot plant. Responses in CO_2 lean loading L_l , CO_2 rich loading L_r , CO_2 absorbed, and CO_2 desorbed.

| Plant Load | Input Process Variable | $F_{solv} +10\%$ | | | | $F_{solv} -10\%$ | | | |
|------------|---------------------------|------------------|-------------|-------------|----------|------------------|-------------|-------------|----------|
| | | θ (min) | t_s (min) | t_t (min) | RC (%) | θ (min) | t_s (min) | t_t (min) | RC (%) |
| 100% | L_l | 11.8 | 15.8 | 27.7 | 8.59 | 14.5 | 11.5 | 26 | -7.50 |
| | L_r | 14.2 | 89.7 | 103.8 | -0.10 | 0 | 63.83 | 63.83 | 0.08 |
| | $\text{CO}_{2,abs}$ | 0.0 | 133.2 | 133.2 | 0.35 | 0 | 67.16 | 67.16 | -3.14 |
| | $\text{CO}_{2,abs}$ | 0.0 | 98.8 | 98.8 | 0.35 | 0 | 12.83 | 12.83 | -3.15 |
| 80% | L_l | 15.8 | 18.5 | 34.3 | 7.85 | 19.5 | 13.16 | 32.66 | -6.87 |
| | L_r | 0.0 | 106.3 | 106.3 | -0.04 | 0 | 176.66 | 176.66 | 0.02 |
| | $\text{CO}_{2,abs}$ | 0.0 | 97.8 | 97.8 | 2.09 | 0 | 65.66 | 65.66 | -4.38 |
| | $\text{CO}_{2,abs}$ | 0.0 | 18.8 | 18.8 | 2.09 | 0 | 3.16 | 3.16 | -4.39 |
| 60% | L_l | 22.0 | 17.0 | 39.0 | 6.75 | 27 | 17.33 | 44.33 | -6.28 |
| | L_r | 0.0 | 141.0 | 141.0 | -0.02 | 0 | 454 | 454 | 0.00 |
| | $\text{CO}_{2,abs}$ | 0.0 | 104.0 | 104.0 | 4.18 | 0 | 69.5 | 69.5 | -5.59 |
| | $\text{CO}_{2,abs}$ | 0.0 | 23.5 | 23.5 | 4.18 | 0 | 3.8 | 3.8 | -5.59 |

Table A3. Open-loop response to $\pm 10\%$ step-changes in reboiler duty for three different operating points of the pilot plant. Responses in CO₂ lean loading L_l , CO₂ rich loading L_r , CO₂ absorbed, and CO₂ desorbed.

| Plant Load | Input Process Variable | $\dot{Q}_{reb} + 10\%$ | | | | $\dot{Q}_{reb} - 10\%$ | | | |
|------------|------------------------|------------------------|-------------|-------------|--------|------------------------|-------------|-------------|--------|
| | | θ (min) | t_s (min) | t_t (min) | RC (%) | θ (min) | t_s (min) | t_t (min) | RC (%) |
| 100% | L_l | 13.0 | 9.7 | 22.7 | −6.29 | 12.7 | 15.5 | 28.2 | 8.46 |
| | L_r | 31.8 | 81.5 | 113.3 | −0.22 | 29.5 | 43.3 | 72.8 | 0.00 |
| | CO _{2,abs} | 6.0 | 70.8 | 76.8 | 6.07 | 5.0 | 49.8 | 54.8 | −8.48 |
| | CO _{2,abs} | 0.0 | 2.2 | 2.2 | 6.07 | 0.0 | 10.3 | 10.3 | −8.48 |
| 80% | L_l | 17.0 | 11.7 | 28.7 | −5.60 | 17.0 | 14.8 | 31.8 | 7.78 |
| | L_r | 40.7 | 78.0 | 118.7 | −0.03 | 38.3 | 88.0 | 126.3 | 0.02 |
| | CO _{2,abs} | 7.8 | 74.7 | 82.5 | 5.19 | 5.7 | 57.0 | 62.7 | −7.16 |
| | CO _{2,abs} | 0.0 | 2.7 | 2.7 | 5.19 | 0.0 | 14.5 | 14.5 | −0.05 |
| 60% | L_l | 23.2 | 16.0 | 39.2 | −4.97 | 23.8 | 17.3 | 41.2 | 6.63 |
| | L_r | 47.0 | 99.3 | 146.3 | −0.01 | 47.8 | 114.7 | 162.5 | 0.00 |
| | CO _{2,abs} | 9.5 | 89.6 | 99.1 | 4.00 | 7.5 | 72.0 | 79.5 | −5.30 |
| | CO _{2,abs} | 0.0 | 3.5 | 3.5 | 4.00 | 0.0 | 3.3 | 3.3 | −5.30 |

References

1. The International Energy Agency (IEA). *CO₂ Capture and Storage: A Key Carbon Abatement Option*; International Energy Agency: Paris, France, 2008.
2. Singh, A.; Stéphenne, K. Shell Cansolv CO₂ capture technology: Achievement from first commercial plant. *Energy Procedia* **2014**, *63*, 1678–1685. [CrossRef]
3. Laboratory, N.E.T. Petra Nova Parish Holdings. W.A. Parish Post-Combustion CO₂ Capture and Sequestration Project. Available online: <https://www.netl.doe.gov/research/coal/project-information/fe0003311-ppp> (accessed on 28 September 2017).
4. Hentschel, J.; Babić, U.A.; Spliethoff, H. A parametric approach for the valuation of power plant flexibility options. *Energy Rep.* **2016**, *2*, 40–47. [CrossRef]
5. Mac Dowell, N.; Staffell, I. The role of flexible CCS in the UK's future energy system. *Int. J. Greenh. Gas Control* **2016**, *48*, 327–344. [CrossRef]
6. Gaspar, J.; Jorgensen, J.B.; Fosbol, P.L. Control of a post-combustion CO₂ capture plant during process start-up and load variations. *IFAC-PapersOnLine* **2015**, *48*, 580–585. [CrossRef]
7. Montañés, R.M.; Korpås, M.; Nord, L.O.; Jaehnert, S. Identifying operational requirements for flexible CCS power plant in future energy systems. *Energy Procedia* **2016**, *86*, 22–31. [CrossRef]
8. Johnsson, F.; Odenberger, M.; Göransson, L. Challenges to integrate CCS into low carbon electricity markets. *Energy Procedia* **2014**, *63*, 7485–7493. [CrossRef]
9. Boot-Handford, M.E.; Abanades, J.C.; Anthony, E.J.; Blunt, M.J.; Brandani, S.; Mac Dowell, N.; Fernandez, J.R.; Ferrari, M.-C.; Gross, R.; Hallett, J.P.; et al. Carbon capture and storage update. *Energy Environ. Sci.* **2014**, *7*, 130–189. [CrossRef]
10. Flø, N.E.; Kvamsdal, H.M.; Hillestad, M.; Mejdell, T. Dominating dynamics of the post-combustion CO₂ absorption process. *Comput. Chem. Eng.* **2016**, *86*, 171–183. [CrossRef]
11. Karimi, M.; Hillestad, M.; Svendsen, H.F. Investigation of the dynamic behavior of different stripper configurations for post-combustion CO₂ capture. *Int. J. Greenh. Gas Control* **2012**, *7*, 230–239. [CrossRef]
12. Gardarsdóttir, S.Ó.; Montañés, R.M.; Normann, F.; Nord, L.O.; Johnsson, F. Effects of CO₂-absorption control strategies on the dynamic performance of a supercritical pulverized-coal-fired power plant. *Ind. Eng. Chem. Res.* **2017**, *56*, 4415–4430. [CrossRef]
13. Panahi, M.; Skogestad, S. Economically efficient operation of CO₂ capturing process part i: Self-optimizing procedure for selecting the best controlled variables. *Chem. Eng. Process. Process Intensif.* **2011**, *50*, 247–253. [CrossRef]
14. Panahi, M.; Skogestad, S. Economically efficient operation of CO₂ capturing process. Part II. Design of control layer. *Chem. Eng. Process. Process Intensif.* **2012**, *52*, 112–124. [CrossRef]

15. Montañés, R.M.; Garðarsdóttir, S.Ó.; Normann, F.; Johnsson, F.; Nord, L.O. Demonstrating load-change transient performance of a commercial-scale natural gas combined cycle power plant with post-combustion CO₂ capture. *Int. J. Greenh. Gas Control* **2017**, *63*, 158–174. [[CrossRef](#)]
16. Nittaya, T.; Douglas, P.L.; Croiset, E.; Ricardez-Sandoval, L.A. Dynamic modelling and control of MEA absorption processes for CO₂ capture from power plants. *Fuel* **2014**, *116*, 672–691. [[CrossRef](#)]
17. Zhang, Q.; Turton, R.; Bhattacharyya, D. Development of model and model-predictive control of an MEA-based postcombustion CO₂ capture process. *Ind. Eng. Chem. Res.* **2016**, *55*, 1292–1308. [[CrossRef](#)]
18. International Energy Agency Greenhouse Gas R&D Programme (IEAGHG). *Evaluation of Process Control Strategies for Normal, Flexible, and Upset Operation Conditions of CO₂ Post Combustion Capture Processes*; July 2016; IEAGHG: Cheltenham, UK, September 2016.
19. Walters, M.S.; Edgar, T.F.; Rochelle, G.T. Regulatory control of amine scrubbing for CO₂ capture from power plants. *Ind. Eng. Chem. Res.* **2016**, *55*, 4646–4657. [[CrossRef](#)]
20. Gaspar, J.; Ricardez-Sandoval, L.; Jørgensen, J.B.; Fosbøl, P.L. Controllability and flexibility analysis of CO₂ post-combustion capture using piperazine and MEA. *Int. J. Greenh. Gas Control* **2016**, *51*, 276–289. [[CrossRef](#)]
21. Mac Dowell, N.; Shah, N. The multi-period optimisation of an amine-based CO₂ capture process integrated with a super-critical coal-fired power station for flexible operation. *Comput. Chem. Eng.* **2015**, *74*, 169–183. [[CrossRef](#)]
22. Flø, N.E.; Kvamsdal, H.M.; Hillestad, M. Dynamic simulation of post-combustion CO₂ capture for flexible operation of the brindisi pilot plant. *Int. J. Greenh. Gas Control* **2016**, *48 Pt 2*, 204–215. [[CrossRef](#)]
23. Ceccarelli, N.; van Leeuwen, M.; Wolf, T.; van Leeuwen, P.; van der Vaart, R.; Maas, W.; Ramos, A. Flexibility of low-CO₂ gas power plants: Integration of the CO₂ capture unit with CCGT operation. *Energy Procedia* **2014**, *63*, 1703–1726. [[CrossRef](#)]
24. Wellner, K.; Marx-Schubach, T.; Schmitz, G. Dynamic behavior of coal-fired power plants with postcombustion CO₂ capture. *Ind. Eng. Chem. Res.* **2016**, *55*, 12038–12045. [[CrossRef](#)]
25. Olaleye, A.K.; Oko, E.; Wang, M.; Kelsall, G. Dynamic modelling and analysis of supercritical coal-fired power plant integrated with post-combustion CO₂ capture. In *Clean Coal Technology and Sustainable Development, Proceedings of the 8th International Symposium on Coal Combustion, Beijing, China, 19-22 July 2015*; Yue, G., Li, S., Eds.; Springer: Beijing, China, 2016; pp. 359–363.
26. Mechleri, E.; Lawal, A.; Ramos, A.; Davison, J.; Dowell, N.M. Process control strategies for flexible operation of post-combustion CO₂ capture plants. *Int. J. Greenh. Gas Control* **2017**, *57*, 14–25. [[CrossRef](#)]
27. Mechleri, E.; Fennell, P.S.; Dowell, N.M. Optimisation and evaluation of flexible operation strategies for coal-and gas-CCS power stations with a multi-period design approach. *Int. J. Greenh. Gas Control* **2017**, *59*, 24–39. [[CrossRef](#)]
28. Sanchez Fernandez, E.; Sanchez del Rio, M.; Chalmers, H.; Khakharia, P.; Goetheer, E.L.V.; Gibbins, J.; Lucquiaud, M. Operational flexibility options in power plants with integrated post-combustion capture. *Int. J. Greenh. Gas Control* **2016**, *48*, 275–289. [[CrossRef](#)]
29. Dutta, R.; Nord, L.O.; Bolland, O. Selection and design of post-combustion CO₂ capture process for 600 MW natural gas fueled thermal power plant based on operability. *Energy* **2017**, *121*, 643–656. [[CrossRef](#)]
30. Kvamsdal, H.M.; Jakobsen, J.P.; Hoff, K.A. Dynamic modeling and simulation of a CO₂ absorber column for post-combustion CO₂ capture. *Chem. Eng. Process. Process Intensif.* **2009**, *48*, 135–144. [[CrossRef](#)]
31. Gaspar, J.; Cormos, A.-M. Dynamic modeling and absorption capacity assessment of CO₂ capture process. *Int. J. Greenh. Gas Control* **2012**, *8*, 45–55. [[CrossRef](#)]
32. Harun, N.; Nittaya, T.; Douglas, P.L.; Croiset, E.; Ricardez-Sandoval, L.A. Dynamic simulation of MEA absorption process for CO₂ capture from power plants. *Int. J. Greenh. Gas Control* **2012**, *10*, 295–309. [[CrossRef](#)]
33. Jayarathna, S.A.; Lie, B.; Melaaen, M.C. Amine based CO₂ capture plant: Dynamic modeling and simulations. *Int. J. Greenh. Gas Control* **2013**, *14*, 282–290. [[CrossRef](#)]
34. He, Z.; Sahraei, M.H.; Ricardez-Sandoval, L.A. Flexible operation and simultaneous scheduling and control of a CO₂ capture plant using model predictive control. *Int. J. Greenh. Gas Control* **2016**, *48*, 300–311. [[CrossRef](#)]
35. Luu, M.T.; Abdul Manaf, N.; Abbas, A. Dynamic modelling and control strategies for flexible operation of amine-based post-combustion CO₂ capture systems. *Int. J. Greenh. Gas Control* **2015**, *39*, 377–389. [[CrossRef](#)]
36. Biliyok, C.; Lawal, A.; Wang, M.; Seibert, F. Dynamic modelling, validation and analysis of post-combustion chemical absorption CO₂ capture plant. *Int. J. Greenh. Gas Control* **2012**, *9*, 428–445. [[CrossRef](#)]

37. Åkesson, J.; Laird, C.D.; Lavedan, G.; Pröhl, K.; Tummescheit, H.; Velut, S.; Zhu, Y. Nonlinear model predictive control of a CO₂ post-combustion absorption unit. *Chem. Eng. Technol.* **2012**, *35*, 445–454. [[CrossRef](#)]
38. Bui, M.; Gunawan, I.; Verheyen, V.; Feron, P.; Meuleman, E.; Adeloju, S. Dynamic modelling and optimisation of flexible operation in post-combustion CO₂ capture plants—A review. *Comput. Chem. Eng.* **2014**, *61*, 245–265. [[CrossRef](#)]
39. Enaasen, N.; Zangrilli, L.; Mangiaracina, A.; Mejdell, T.; Kvamsdal, H.M.; Hillestad, M. Validation of a dynamic model of the brindisi pilot plant. *Energy Procedia* **2014**, *63*, 1040–1054. [[CrossRef](#)]
40. Enaasen Flø, N.; Knuutila, H.; Kvamsdal, H.M.; Hillestad, M. Dynamic model validation of the post-combustion CO₂ absorption process. *Int. J. Greenh. Gas Control* **2015**, *41*, 127–141. [[CrossRef](#)]
41. Van De Haar, A.; Trapp, C.; Wellner, K.; De Kler, R.; Schmitz, G.; Colonna, P. Dynamics of postcombustion CO₂ capture plants: Modeling, validation, and case study. *Ind. Eng. Chem. Res.* **2017**, *56*, 1810–1822. [[CrossRef](#)] [[PubMed](#)]
42. Gaspar, J.; Gladis, A.; Jørgensen, J.B.; Thomsen, K.; von Solms, N.; Fosbøl, P.L. Dynamic operation and simulation of post-combustion CO₂ capture. *Energy Procedia* **2016**, *86*, 205–214. [[CrossRef](#)]
43. Dutta, R.; Nord, L.O.; Bolland, O. Prospects of using equilibrium-based column models in dynamic process simulation of post-combustion CO₂ capture for coal-fired power plant. *Fuel* **2017**, *202*, 85–97. [[CrossRef](#)]
44. Chinen, A.S.; Morgan, J.C.; Omell, B.P.; Bhattacharyya, D.; Miller, D.C. Dynamic data reconciliation and model validation of a MEA-based CO₂ capture system using pilot plant data. In Proceedings of the 11th IFAC Symposium on Dynamics and Control of Process Systems, Including Biosystems, Trondheim, Norway, 6–8 June 2016.
45. Abdul Manaf, N.; Cousins, A.; Feron, P.; Abbas, A. Dynamic modelling, identification and preliminary control analysis of an amine-based post-combustion CO₂ capture pilot plant. *J. Clean. Prod.* **2016**, *113*, 635–653. [[CrossRef](#)]
46. Faber, R.; Köpcke, M.; Biede, O.; Knudsen, J.N.; Andersen, J. Open-loop step responses for the MEA post-combustion capture process: Experimental results from the esbjerg pilot plant. *Energy Procedia* **2011**, *4*, 1427–1434. [[CrossRef](#)]
47. Bui, M.; Gunawan, I.; Verheyen, V.; Feron, P.; Meuleman, E. Flexible operation of CSIRO's post-combustion CO₂ capture pilot plant at the AGL Loy Yang power station. *Int. J. Greenh. Gas Control* **2016**, *48*, 188–203. [[CrossRef](#)]
48. Tait, P.; Buschle, B.; Ausner, I.; Valluri, P.; Wehrli, M.; Lucquiaud, M. A pilot-scale study of dynamic response scenarios for the flexible operation of post-combustion CO₂ capture. *Int. J. Greenh. Gas Control* **2016**, *48*, 216–233. [[CrossRef](#)]
49. De Koeijer, G.M.; Aasen, K.I.; Steinseth Hamborg, E. *Scale-Up and Transient Operation of CO₂ Capture Plants at CO₂ Technology Centre Mongstad*; Society of Petroleum Engineers: Abu Dhabi, UAE, 2014.
50. Gjernes, E.; Pedersen, S.; Cents, T.; Watson, G.; Fostås, B.F.; Shah, M.I.; Lombardo, G.; Desvignes, C.; Flø, N.E.; Morken, A.K.; et al. Results from 30 wt % MEA performance testing at the CO₂ Technology Centre Mongstad. *Energy Procedia* **2017**, *114*, 1146–1157. [[CrossRef](#)]
51. Faramarzi, L.; Thimsen, D.; Hume, S.; Maxon, A.; Watson, G.; Pedersen, S.; Gjernes, E.; Fostås, B.F.; Lombardo, G.; Cents, T.; et al. Results from MEA testing at the CO₂ Technology Centre Mongstad: Verification of baseline results in 2015. *Energy Procedia* **2017**, *114*, 1128–1145. [[CrossRef](#)]
52. Thimsen, D.; Maxson, A.; Smith, V.; Cents, T.; Falk-Pedersen, O.; Gorset, O.; Hamborg, E.S. Results from MEA testing at the CO₂ Technology Centre Mongstad. Part I: Post-combustion CO₂ capture testing methodology. *Energy Procedia* **2014**, *63*, 5938–5958. [[CrossRef](#)]
53. Modelica Association. Available online: <https://www.Modelica.Org/> (accessed on 28 September 2017).
54. Modelon. Post-Combustion Capture with Amine Solutions. Available online: <http://www.Modelon.Com/industries/energy-process/carbon-capture-and-sequestration/> (accessed on 28 September 2017).
55. Dassault Systems, Dymola. Available online: <http://www.3ds.Com/products-services/catia/products/dymola> (accessed on 28 September 2017).
56. Pröhl, K.; Tummescheit, H.; Velut, S.; Åkesson, J. Dynamic model of a post-combustion absorption unit for use in a non-linear model predictive control scheme. *Energy Procedia* **2011**, *4*, 2620–2627. [[CrossRef](#)]
57. Garðarsdóttir, S.Ó.; Normann, F.; Andersson, K.; Pröhl, K.; Emilsdóttir, S.; Johnsson, F. Post-combustion CO₂ capture applied to a state-of-the-art coal-fired power plant—The influence of dynamic process conditions. *Int. J. Greenh. Gas Control* **2015**, *33*, 51–62. [[CrossRef](#)]

58. Onda, K.; Takeuchi, H.; Okumoto, Y. Mass transfer coefficients between gas and liquid phases in packed columns. *J. Chem. Eng. Jpn.* **1968**, *1*, 56–62. [[CrossRef](#)]
59. Versteeg, G.F.; Van Dijck, L.A.J.; Van Swaaij, W.P.M. On the kinetics between CO₂ and alkanolamines both in aqueous and non-aqueous solutions. An overview. *Chem. Eng. Commun.* **1996**, *144*, 113–158. [[CrossRef](#)]
60. Holst, J.V.; Versteeg, G.F.; Brilman, D.W.F.; Hogendoorn, J.A. Kinetic study of CO₂ with various amino acid salts in aqueous solution. *Chem. Eng. Sci.* **2009**, *64*, 59–68. [[CrossRef](#)]
61. Böttinger, W. *Nmr-Spektroskopische Untersuchung der Reaktivabsorption von Kohlendioxid in Wässrigen Aminlösungen*; VDI-Verlag: Düsseldorf, Germany, 2006.
62. Montañés, R.M.; Flø, N.E.; Dutta, R.; Nord, L.O.; Bolland, O. Dynamic process model development and validation with transient plant data collected from an mea test campaign at the CO₂ technology center mongstad. *Energy Procedia* **2017**, *114*, 1538–1550. [[CrossRef](#)]
63. International Energy Agency Greenhouse Gas R&D Programme (IEAGHG). *Operating Flexibility of Power Plants with CCS*; IEAGHG: Cheltenham, UK, June 2012.
64. Christopher, H.J.; James, K. How to Determine a Unit Ramp Rate (MW/min) for Lowest Total Production Cost. Available online: <http://www.heatrate.com/docs/Value-of-Ramp-Rate-1987.pdf> (accessed on 28 September 2017).
65. Genrup, M.; Thern, M. *Ny Gasturbinteknik 2012–2014: Gas Turbine Developments*; Report 2012; ELFORSK: Stockholm, Sweden, 2013.
66. Skogestad, S.; Grimholt, C. The SIMC method for smooth PID controller tuning. In *Pid Control in the Third Millennium: Lessons Learned and New Approaches*; Vilanova, R., Visioli, A., Eds.; Springer: London, UK, 2012; pp. 147–175.



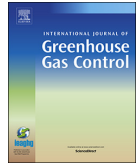
© 2017 by the authors. Licensee MDPI, Basel, Switzerland. This article is an open access article distributed under the terms and conditions of the Creative Commons Attribution (CC BY) license (<http://creativecommons.org/licenses/by/4.0/>).

Paper III



Contents lists available at ScienceDirect

International Journal of Greenhouse Gas Control

journal homepage: www.elsevier.com/locate/ijggc

Experimental results of transient testing at the amine plant at Technology Centre Mongstad: Open-loop responses and performance of decentralized control structures for load changes

Rubén M. Montañés^{a,*}, Nina E. Flø^b, Lars O. Nord^a

^a Department of Energy and Process Engineering, NTNU – Norwegian University of Science and Technology, Kolbjørn Hejes v. 1B, 7491, Trondheim, Norway

^b Technology Centre Mongstad, 5954, Mongstad, Norway

ARTICLE INFO

Keywords:

Post combustion
Chemical absorption
MEA
CO₂ capture
Dynamic behaviour
Pilot plant
Operational flexibility

ABSTRACT

Flexible operation of combined cycle thermal power plants with chemical absorption post combustion CO₂ capture is a key aspect for the development of the technology. Several studies have assessed the performance of decentralized control structures applied to the post combustion CO₂ capture process via dynamic process simulation, however there is a lack of published data from demonstration or pilot plants. In this work, experiments on transient testing were conducted at the amine plant at Technology Centre Mongstad, for flue gas from a combined cycle combined heat and power plant (3.7–4.1 CO₂ vol%). The experiments include six tests on open-loop responses and eight tests on transient performance of decentralized control structures for fast power plant load change scenarios.

The transient response of key process variables to changes in flue gas volumetric flow rate, solvent flow rate and reboiler duty were analyzed. In general the process stabilizes within 1 h for 20% step changes in process inputs, being the absorber column absorption rates the slowest process variable to stabilize to changes in reboiler duty and solvent flow rate. Tests on fast load changes (10%/min) in flue gas flow rate representing realistic load changes in an upstream power plant showed that decentralized control structures could be employed in order to bring the process to desired off-design steady-state operating conditions within (< 60 min). However, oscillations and instabilities in absorption and desorption rates driven by interactions of the capture rate and stripper temperature feedback control loops can occur when the rich solvent flow rate is changed significantly and fast as a control action to reject the flue gas volumetric flow rate disturbance and keeping liquid to gas ratio or capture rate constant.

1. Introduction

The anthropogenic greenhouse gas emissions have led to the increase in concentration of CO₂ in the atmosphere, being the main cause of global warming and climate change (IPCC, 2014). Carbon capture and storage (CCS) is a group of technologies that can significantly reduce the CO₂ emissions from the use of fossil fuels for thermal power generation and other industrial sources (IEA, 2008). According to the International Energy Agency, the global average carbon intensity of the power sector in 2015 was around 500 kgCO₂/MWh and global average of 100 kgCO₂/MWh should be achieved by 2040 to be consistent with a 2°C scenario (IEA, 2016). In this regard, natural gas combined cycle power plants could be considered today as low carbon alternatives due to their carbon intensity levels of 400–450 kgCO₂/MWh. However, in

the mid-to-long term it might be required to decarbonize natural gas combined cycle power plants by retrofitting existing units with post-combustion CO₂ capture (PCC) or by designing new CCS power plants. Post-combustion CO₂ capture with chemical absorption using amines is considered a mature technology for CCS from thermal power plants (Boot-Handford et al., 2014), and it has been demonstrated at commercial scale in CCS projects from coal-fired thermal power plants, at Boundary Dam project in Canada (Singh and Stéphenne, 2014) and the Petra Nova project in US (NETL, 2018).

In current and future energy systems with high penetration of renewable energy sources, the operational role of thermal power plants changes. Load-following operation of thermal power plants and flexible operation will become a key aspect of the technology development (NETL, 2012; Gonzalez-Salazar et al., 2017). Thermal power plants will

* Corresponding author at: Department of Energy and Process Engineering, NTNU – Norwegian University of Science and Technology, Kolbjørn Hejes vei 1b, Varmeteknisk * B347, NO – 7491, Trondheim, Norway.

E-mail address: ruben.m.montanes@ntnu.no (R.M. Montañés).

<https://doi.org/10.1016/j.ijggc.2018.04.001>

Received 16 January 2018; Received in revised form 19 March 2018; Accepted 2 April 2018
1750-5836/ © 2018 Elsevier Ltd. All rights reserved.

Nomenclature

| | |
|-------------|---|
| 3PRH | Three pressure reheat |
| CCS | Carbon capture and storage |
| CHP | Combined heat and power |
| F_{gas} | Flue gas volumetric flow rate [Sm^3/h] |
| F_{prod} | CO_2 product mass flow rate [kg/h] |
| F_{solv} | Rich solvent mass flow rate [kg/h] |
| F_{steam} | Reboiler steam mass flow rate [kg/h] |
| Cap | Capture rate |
| DDC | Direct contract cooler |

| | |
|-----------|---|
| GT | Gas turbine |
| L/G | Liquid to gas ratio [kg/Sm^3] |
| MEA | Monoethanolamine |
| PCC | Post combustion CO_2 capture |
| PI | Proportional-Integral feedback controller |
| SIMC | Simple internal model control |
| SRD | Specific reboiler duty [$\text{kJ}/\text{kg CO}_2$] |
| T_{str} | Stripper bottom temperature [$^{\circ}\text{C}$] |
| TCM DA | Technology Centre Mongstad |
| TPM | Throughput manipulator |

need to cycle on and off and to ramp up and down more frequently, rapidly and cost-effectively (Lew et al., 2012), in order to keep the balance between generation and demand and back-up renewable energies, and to be competitive in the power markets. Regarding thermal power plants with CCS, load following capabilities and operational flexibility are considered as extremely important aspects of the technology (Boot-Handford et al., 2014; IEAGHG, 2012; Montañés et al., 2016).

The transient performance of the post-combustion CO_2 capture system during start-up and shut down, load changes and flexible operation strategies is a key aspect that has been subject of extensive study via dynamic process simulation tools. Dynamic process modeling and simulation has been used to assess aspects of flexible operation and control of thermal power plants integrated with PCC (Walters et al., 2016; Gardarsdóttir et al., 2017; Montañés et al., 2017a; van de Haar et al., 2017; Wellner et al., 2016; Zhang et al., 2016; Dutta et al., 2017). Bui et al. (2014) concluded that work should focus on providing sets of transient data from PCC pilot plants for dynamic process model validation and for gathering more knowledge on pilot plant flexible operation. Nevertheless, pilot plant testing requires expensive resources and there are limited published data with transient operation available in the literature. Transient pilot plant testing is normally conducted with two methodologies, open-loop transient testing or testing flexible operation scenarios.

During open-loop testing, step changes are applied in set-points of some inputs to the plant, and the transient response of the process variables of the system are monitored. This approach helps to characterize and analyze the transient response of the process and contributes to generate suitable data sets that can be utilized for dynamic process model validation. The open-loop tests are desired since they minimize data variability and also allow to identify the effects that one input or disturbance to the plant have on important process variables of the process. In addition, the influence of the control loops of the advanced control layer of the chemical plant on the resulting transient performance is reduced. Test campaigns have been conducted for the chemical absorption process with aqueous monoethanolamine (MEA). Faber et al. (2011) conducted transient tests with the Esbjerg pilot plant at the coal-fired power plant Esbjergværket, in Denmark. They conclude that the capture process acts as a buffer for any perturbation at the inlet, and that the process required between 1 h 15 min and 1 h 45 min for stabilization after the disturbances applied. Validation of dynamic process models with data from Esbjerg transient tests was conducted by Åkesson et al. (2012) and Gaspar et al. (2016). Flø et al. conducted transient tests at the Gløshaugen pilot plant to provide sets of data and carry out dynamic process model validation by applying set-point step changes (Enaasen Flø et al., 2015). Several publications have described transient tests by applying step-changes in main inputs to the process in pilot plants with the purpose of generating data for dynamic process model validation (van de Haar et al., 2017; Montañés et al., 2017c; Enaasen et al., 2014; Chinen et al., 2016; Bui et al., 2016). In addition, research is carried out to reduce the heat required for solvent regeneration (Zhang et al., 2017; Liu et al., 2017).

Bui et al. (2016) conducted a flexible operation campaign at the AGL Loy Yang power station, with the post-combustion CO_2 capture pilot plant that treats a slipstream of flue gas from the coal fired power plant. This experimental study verifies that flexible operation is feasible, and highlights the lack of experimental tests involving control structure analysis during dynamic operation of pilot plants. Tait et al. (2016) conducted a pilot scale study of dynamic response scenarios for flexible operation of the PCC process. Five scenarios were tested: gas turbine shut down, gas turbine start-up and three scenarios for power output maximization. Their conclusions include that large solvent inventory increases total circulation times, and those have a significant effect on capture rate during dynamic operation, and that the plant requires longer time for stabilization when operated with larger amounts of solvent inventory.

A key aspect of transient operation of the process is related to the control structure implemented in the PCC plant. The transient response of the system to disturbances differs for different control strategies. Several contributions in the literature have utilized validated dynamic process models and simulations in order to assess the controllability and evaluated the capability of different control structures to reject disturbances (Gardarsdóttir et al., 2017; Montañés et al., 2017a; IEAGHG, 2016; Nittaya et al., 2014; Panahi and Skogestad, 2012). The work conducted via dynamic process simulation contributes to develop the learning curve for flexible operation of the system in the scarcity of commercial scale operational experience. However, to the authors knowledge these control strategies have not been implemented or tested at pilot or demonstration scale plants. Therefore, this work focuses on getting hands on experience on the implementation of decentralized control structures and testing them for fast load change disturbances at a pilot plant for flue gas from a natural gas fueled combined cycle power plant. In this work the tests were conducted at the amine plant at Technology Centre Mongstad (TCM DA), which is a larger scale pilot plant than the pilot plants and laboratory set-ups employed for previous transient testing dedicated papers available in the literature (Faber et al., 2011; Bui et al., 2016; Tait et al., 2016).

The objectives of this work were to evaluate the performance of a demonstration plant to open-loop step-changes in main inputs to the process, and to evaluate the performance of decentralized control structures applied to a demonstration PCC plant. The tests were conducted at the amine plant at Technology Centre Mongstad (TCM DA) in Norway during the MEA-3 test campaign (Faramarzi et al., 2017a). Validated dynamic process models developed in previous work (Montañés et al., 2017b) were employed to carry out the test planning. The tests were conducted at the plant for disturbances representing fast load changes of the upstream power plant.

2. Chemical absorption pilot plant with amines at Technology Centre Mongstad

The amine plant at the Technology Centre Mongstad is a flexible plant that can be configured to treat flue gas with a wide range of CO_2 concentrations and with different absorption solvents. That includes

flue gas coming from the residue fluid catalytic cracker (RFCC) of the Statoil refinery placed next to TCM DA facility with typical CO₂ concentration of coal-fired power plants (14 vol% CO₂), and flue gas from the natural gas combined cycle combined heat and power plant (CHP) with a CO₂ concentration of around 3.5 vol%. Fig. 1 shows a simplified process flow sheet of the plant when it is configured with the CHP stripper. Details on the amine pilot plant are presented in previous modeling, validation and simulation work by (Montañés et al., 2017b, 2017c), and other published works with the amine plant when using aqueous MEA as chemical solvent (Gjernes et al., 2017; Faramarzi et al., 2017b; Hamborg et al., 2014). The process configuration consists of the simple absorber-desorber solvent regeneration process with chemical absorption of CO₂, and the chemical solvent employed was 30% aqueous MEA. The plant can capture around 80 tonCO₂/day for operation with CHP gas conditions and the flue gas volumetric flow rate capacity is 60 000 Sm³/hr. Here standard S means 1 atm and 15 °C.

A slipstream of flue gas coming from the natural gas fired CHP plant is conducted by a blower towards the pilot plant. The blower has variable speed drives that allows manipulating the flue gas volumetric flow rate to the plant. As shown in Fig. 1, a closed-loop controller on FT1 allows to specify the set-point of the flue gas volumetric flow rate at the inlet of the absorber, by manipulating the speed of the blower at the inlet of the direct contact cooler (DCC). The blower also provides the pressure required to overcome the pressure drop induced by the DCC and absorber column.

The flue gas is conducted towards the DCC, where it is cooled down and saturated with a countercurrent flow of water. The flue gas flows through the absorber column, where it contacts the chemical solvent in the absorption packing segments of the column. Then it flows towards the two water wash sections that are operated to control the water balance of the plant and to limit the gas emissions. A water make-up stream is injected in the water wash system. The packing material in which the chemical solvent meets the flue gas, and where the heat and mass transfer phenomena related to the exothermic chemical

absorption process occurs, is divided in three sections. The three sections consist of structured stainless steel Koch Glitsch Flexipack 2X (Hamborg et al., 2014). The packing has a rectangular cross section of 3.55 × 2 m² with a total of 24 m of absorber packing (12 m at the bottom, 6 m in the middle and 6 m at the top). The water wash section consists of two sections of 3 m each, of structured stainless steel Koch Glitsch Flexipack 2Y HC (Hamborg et al., 2014). The depleted flue gas leaves the process at the top of the column.

The solvent loaded with CO₂ (rich solvent), accumulates in the absorber sump. The absorber sump at TCM DA amine plant also has the function of surge tank, in which the solvent will accumulate at different operating loads of the plant, and where the water streams of the process (from water wash and stripper reflux) are recirculated. The rich flow (FT5) is pumped by a variable speed pump, which sends the flow through the lean/rich integration heat exchanger, where the rich solvent is heated up by the lean solvent from the stripper bottom. The lean/rich heat exchanger consists of a plate and frame heat exchanger. The solvent loaded with CO₂ flows downwards through the stripper packing material, consisting of 8 m of Koch Glitsch Flexipack 2X (Hamborg et al., 2014) with diameter of 1.3 m, where it meets the stripping vapors of CO₂ and H₂O generated in the reboiler. The reboiler consists of a thermosiphon type heat exchanger, where heat is provided by steam from the refinery. Details on the steam supply system are presented in Faramarzi et al. (2017b). The stripping vapors flow through a water wash section where some more water is removed, and then through the overhead cooler and condenser where the water condensates. The CO₂ rich stream, product CO₂ (FT3), is sent to the CO₂ stack. The lean solvent accumulates in the stripper sump, and it is pumped towards the lean/rich heat exchanger and the direct contact cooler by means of the lean solvent pump. The lean amine cooler allows to control the temperature of the lean solvent at the inlet of the absorber column, by manipulating the flow of cooling water.

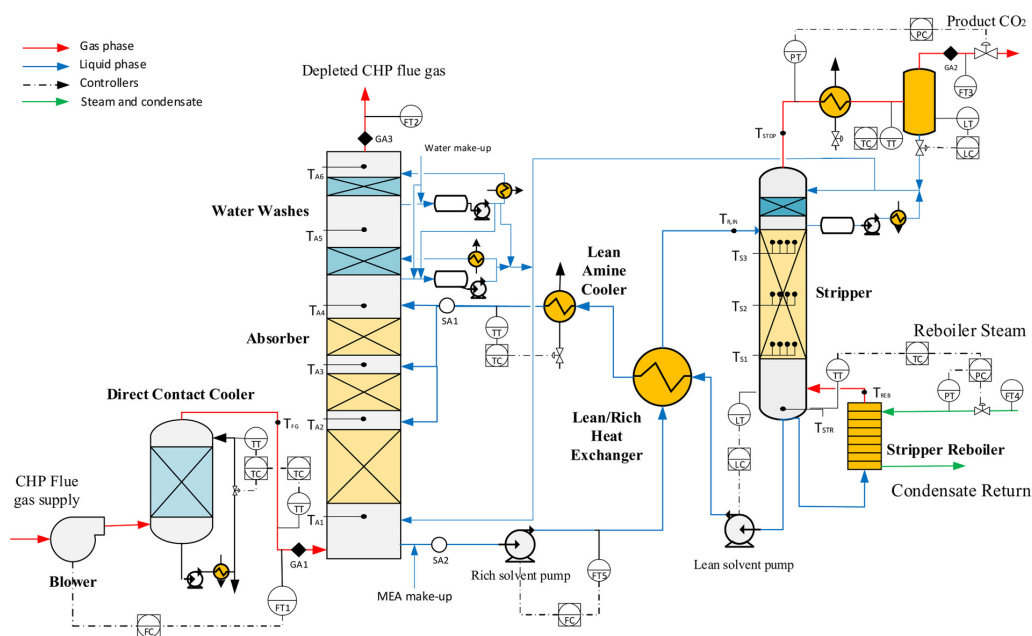


Fig. 1. Simplified process flow sheet of the amine plant at TCM DA when configured to treat flue gas from the CHP plant. Figure obtained and modified from (Montañés et al., 2017b). The figure shows transmitters (–T), Controllers (–C) and the location of gas analyzers (GA), solvent analysis sampling points (SA). Flow transmitters (FT), level transmitters (LT), temperature transmitters (TT), pressure transmitters (PT).

Table 1

Flue gas averaged process conditions at the inlet of the absorber column, refer to GA1 in Fig. 1. The process conditions are the averaged values during 25 min of operation before the first test 1 started, refer to Section 3.3.1.

| CHP flue gas process conditions | Unit | Value |
|---|--------------------|--------|
| Operating capacity | % | 100 |
| CHP flue gas supply rate F_{gas} | Sm ³ /h | 60 528 |
| CHP flue gas supply temperature | °C | 30.0 |
| CPH flue gas supply pressure | barg | 0.0485 |
| CHP flue gas supply CO ₂ (wet) | vol% | 4.12 |
| CHP flue gas supply O ₂ (wet) | vol% | 14.09 |
| CHP flue gas supply water content | vol% | 4.43 |
| Depleted flue gas temperature | °C | 31.1 |

3. Description and objectives of experiments

3.1. Process conditions during the tests

The pilot plant was operated under similar process conditions as in the baseline presented in Faramarzi et al. (2017b). This was implemented by setting similar independent parameters, i.e., the process variables that are available for control for the operators (Thimsen et al., 2014). The initial steady-state process conditions for the control structures testing period for flue gas at the inlet of the absorber column (refer to GA1 in Fig. 1) are presented in Table 1. Note that the steady-state process conditions presented in this section of the paper were obtained as averaged values during 25 min of steady-state operation before test 1 on control structures was initiated (refer to Fig. 2 and Section 3.2). This differs from the baseline data from (Faramarzi et al., 2017b), which have been obtained with a larger amount of operating hours and with third party verification of instrumentation and data.

During the whole test period of open-loop testing (refer to Section 3.1) and part of the test period for control structure testing, flue gas at the inlet of the absorber had a higher CO₂ content of around 4.1 vol% compared to typical values of CO₂ content of around 3.7 vol% when running the plant with CHP flue gas. This was because the CHP power plant located upstream the pilot plant process was fired with a different fuel during parts of the test period, the fuel consisting of a mixture of natural gas and refinery gas. From a pilot plant operation perspective, this can be considered as a boundary condition and could not be modified. That resulted in a lower capture rate (around 74% instead of around 85% (Faramarzi et al., 2017b)) and higher specific reboiler duty (SRD), 3.80 kJ/kgCO₂ instead of 3.63 kJ/kgCO₂ (Faramarzi et al., 2017b) compared to the baseline presented in (Faramarzi et al., 2017b). During the test period for tests 1–8, the CO₂ vol% changed; refer to Fig. 2. The CO₂ content in flue gas was around 4.1 vol% until around 29 h of testing in which it was reduced in a close-to-step manner towards 3.7 vol%. This corresponded to a disturbance during the test 6 (refer to Section 3.3.2). In addition, the CO₂ content was reduced to around 3.6 vol% at around 32.5 h of testing. This happened during test

Table 2

Solvent averaged process conditions at different locations of the plant, refer to Fig. 1. The process conditions are the averaged values during 25 min of operation before the first test 1 started, refer to Section 3.3.1. Lean loading L_i and lean MEA concentration c_{MEA} are taken at the SA1 sampling point, while rich loading at SA2 sampling point.

| Solvent process conditions | Unit | Value |
|----------------------------------|------------------------------|--------|
| Lean MEA concentration | wt% | 28.7 |
| Lean CO ₂ loading | mol CO ₂ /mol MEA | 0.22 |
| Lean amine supply flow rate | kg/h | 62 283 |
| Lean amine supply temperature | °C | 36.8 |
| Lean amine density | kg/m ³ | 1069 |
| Rich CO ₂ loading | mol CO ₂ /mol MEA | 0.53 |
| Rich solution supply flow rate | kg/h | 65 663 |
| Rich solution supply temperature | °C | 111.1 |
| Rich solution density | kg/m ³ | 1 120 |
| Rich solution return temperature | °C | 32.8 |
| Lean solution return temperature | °C | 120.4 |

7. The effect of these disturbances is discussed in Section 4.2.2. The flue gas supply temperature can be controlled by manipulating the cooling water temperature at the inlet of water stream to the DCC; refer to Fig. 1. For the experiments, the flue gas temperature was controlled to around 30 °C. Note that, during open-loop testing, the CO₂ vol% was close to 4.1 for all the tests A–F; refer to Section 3.1.

Process conditions of aqueous MEA solvent during the initial steady-state conditions of test 1 on control structure testing, are presented in Table 2. Solvent lab samples were collected regularly during the testing at the inlet of the absorber and at the outlet of absorber (refer to SA1 and SA2 in Fig. 1). During the tests, lean MEA concentration was slightly below 30 wt% MEA. Note that consistent inventory control and a proper configuration of the regulatory control layer of the plant is required for stable operation of the process (Aske and Skogestad, 2009). The solvent flow network is defined by changing the set-point of the rich solvent mass flow rate, which acts as a throughput manipulator (TPM) of the process. The lean solvent flow rate is manipulated with a PI controller to control the stripper's sump level, so it is automatically adjusted when changing the rich solvent flow rate, while the temperature of the lean solvent at the inlet of the absorber column is controlled at a value of around 37 °C by a varying stream of cooling water to the amine cooler. Table 3 shows the solvent inventories at different operating conditions of the plant. Fig. 3 shows the block diagram with the different main volumes of equipment at the pilot plant, and the circulation times at each of these components. The circulation times are calculated considering rich and lean volumetric flows and solvent inventories at the different components of the pilot plant for three selected operating conditions. Fig. 3 shows the influence of solvent flow rate on the circulation times. At high solvent flow rates (case 1 in Table 3), the resulting circulation times were smaller, with a total circulation time of the pilot plant of around 41 min, while for the case with lowest solvent flow rate (case 3 in Table 3) the total

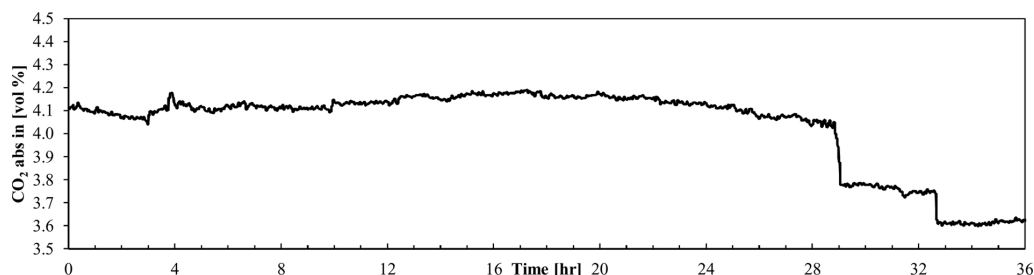


Fig. 2. CO₂ content of flue gas at the absorber inlet during the hours of testing for control structures (test 1–8). CO₂ vol% (wet) measured with the gas chromatograph (GC) installed at TCM DA at point GA1 (refer to Fig. 1).

Table 3

Solvent inventory distribution at different components of the amine pilot plant at TCM DA during the tests campaign. The three cases were selected to represent different process conditions with different rich solvent mass flow rate (F_{solv}) of 65 700 kg/h (Case 1 on 17 July 2017 at 11:30), 52 000 kg/h (Case 2 on July 23 at 04:00) and 40 000 kg/h (Case 3 on 17 July at 23:00). Total circulation times are calculated considering the addition of circulation times in Fig. 3, for each case.

| Solvent flow rates | Case 1 | Case 2 | Case 3 |
|---|--------|--------|--------|
| Rich solvent mass flow rate [kg/h] | 65 630 | 52 025 | 40 042 |
| Rich solvent volumetric flow rate [m ³ /h] | 58.7 | 46.4 | 35.7 |
| Lean solvent mass flow rate [kg/h] | 62 286 | 49 074 | 37 487 |
| Lean solvent volumetric flow rate [m ³ /h] | 58.0 | 45.8 | 33.9 |

| Pilot plant component | Solvent inventory Case 1 [m ³] | Solvent inventory Case 2 [m ³] | Solvent inventory Case 3 [m ³] |
|---|--|--|--|
| Absorber sump | 3.67 | 4.87 | 5.67 |
| Absorber packing | 9.09 | 8.15 | 7.36 |
| CHP stripper packing | 1.07 | 0.94 | 0.85 |
| CHP stripper sump | 2.35 | 2.28 | 2.29 |
| CHP reboiler | 0.42 | 0.42 | 0.42 |
| Carbon filter | 6.1 | 6.1 | 6.1 |
| Cold rich solvent pipe | 2.22 | 2.22 | 2.22 |
| Cold lean solvent pipes | 5.21 | 5.21 | 5.21 |
| Hot rich solvent pipe | 1.13 | 1.13 | 1.13 |
| Hot lean solvent pipes (including reboiler pipes) | 8.2 | 8.2 | 8.2 |
| Lean/rich hx – lean side | 0.485 | 0.485 | 0.485 |
| Lean/rich hx – rich side | 0.485 | 0.485 | 0.485 |
| Lean amine cooler | 0.29 | 0.29 | 0.29 |
| TOTAL inventory | 40.7 | 40.7 | 40.8 |
| Total circulation time [min] | 41.4 | 54.6 | 71.4 |

circulation time was around 71 min. This has implications on the transient operation of the plant, since when the process is operated with lower solvent flow rates, it requires longer times to reach steady-state operating conditions, according to dynamic process simulation analyses (Montañés et al., 2017b). When the solvent circulation flow rate is decreased, excess solvent accumulates mainly in the absorber sump, i.e. the absorber sump also has the function of a surge tank. This can explain the increase in solvent hold up in the absorber sump from Case 1 to Case 3 (see Table 3). Together with the lower solvent flow rate, it results in an increase in circulation time from around 3 min to around 10 min in the absorber sump; refer to Fig. 3. Note that during the tests presented in this work, the pilot plant was operated with a relatively low amount of solvent inventory in the absorber sump, 3.7 m³–5.7 m³, compared with other test campaigns (Montañés et al. reported a total solvent inventory in the absorber sump of 8.1 m³ (Montañés et al., 2017b)).

The process operating conditions at the desorber-reboiler section of the process during test 1 on control structures are presented in Table 4. The steam flow rate is changed at the plant by manipulating the set-point of the steam pressure, which can be as well set on stripper sump temperature control; refer to Section 3.3. The stripper overhead pressure is controlled by the product CO₂ valve to a set-point of around 1.9 bar. The actual reboiler duty is calculated considering the steam and condensate process conditions (pressures, temperatures and mass flow rate) as presented in literature (Montañés et al., 2017b; Thimsen et al., 2014).

3.2. Tests on open-loop performance

The purpose of the open-loop dynamic tests was to investigate the transient performance of the PCC pilot plant by implementing open-loop step-changes. The analysis aims to assess transient response of the plant to multiple and non-simultaneous step-changes in key inputs/

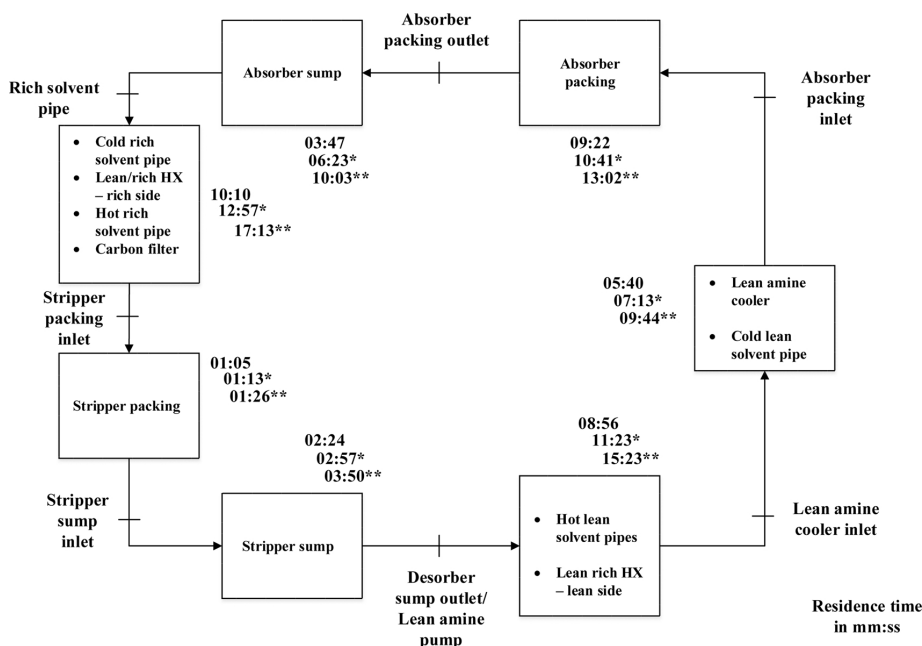


Fig. 3. Block diagram of solvent inventory distribution at the amine plant of Technology Centre Mongstad when operated with CHP flue gas configuration. Circulation times are shown for the plant operated with rich solvent flow rate (F_{solv}) of 65 700 kg/h (Case 1 on 17 July 2017 at 11:30), 52 000 kg/h (*) (Case 2 on July 23 at 04:00) and 40 000 kg/h (**) (Case 3 on 17 July at 23:00). The circulation times are calculated considering solvent inventory distribution in Table 3. The circulation time in each unit of the process is expressed in mm:ss.

Table 4

Process conditions at the desorber and reboiler sections of the TCM DA amine plant during initial steady-state operating conditions of test 1 (refer to Section 3.3.1).

| Desorber process conditions | Unit | Value |
|---|------------------------|-------|
| Reboiler steam flow rate | kg/h | 6 012 |
| Reboiler steam temperature | °C | 164.6 |
| Reboiler steam pressure | barg | 2.90 |
| Stripper overhead pressure | barg | 0.90 |
| Stripper overhead temperature | °C | 98.5 |
| Reboiler solution temperature | °C | 124.0 |
| Reboiler duty | kW | 3 737 |
| Specific reboiler duty | GJ/ton CO ₂ | 3.80 |
| Product CO ₂ flow rate | kg/h | 3 593 |
| Product CO ₂ discharge temperature | °C | 12.9 |
| Product CO ₂ water content | vol% | 0.98 |

disturbances to the plant, namely (i) flue gas flow rate, and (ii) solvent flow rate. This was done for different flue gas capacities of the PCC plant, corresponding to different loads of the power plant. In addition, the data generated can be utilized for dynamic process model validation. The objectives were to:

- Investigate the transient response of the plant when reducing flue gas flow rate (step-change) and when increasing flue gas flow rate (step-change).
- Investigate the transient performance of the plant for changes in solvent flow rate, at different plant flue gas flow rate capacities (different loads of the plant).

The tests were conducted at TCM DA during a total of 48 h of testing. Table 5 shows the main inputs to the plant during the tests, in terms of steam flow rate (F_{steam}), rich solvent flow rate (F_{solv}) and flue gas flow rate (F_{gas}). A step-change is applied and then enough time (8 h) is allowed for the process to stabilize, when the next step is applied.

3.3. Tests on decentralized control structures

The objective of the tests on decentralized control structures was to get experience with the operation and control of the process during transient events of fast load changes, and to observe the capability of the system to reject disturbances in terms of fast load changes of the upstream power plant. Two decentralized control structures were implemented, considering as main degrees of freedom for operation (manipulable variables), the rich solvent mass flow rate (F_{solv}) and the steam flow rate to the reboiler (F_{steam}).

For significant load changes in a combined gas and steam turbine cycle power plant, the load change is driven by gas turbine (GT) load reduction or increase. The gas turbine load is changed, and this normally implies a significant change of the exhaust mass flow rate sent to the heat recovery steam generator. Then, the steam cycle is automated to follow this change in load and steam production and reach the new steady-state operating conditions (Montañés et al., 2017a; Kehlhofer et al., 2009). When the power plant is integrated with CCS, the load change represents a disturbance to the PCC unit in terms of flue gas mass flow rate, composition and temperature, and the available steam from the power plant. Two key aspects are required to define a load change in a combined cycle power plant, one is the minimum operating GT load of the system, and the other is the rate of change of load, the so called ramp rate.

The flue gas flow rate at minimum operating load and at different loads of the integrated system will depend on the GT technology and specific GT burner with controls, and the resulting exhaust gas characteristics. Simulation work by Jordal et al. (2012) have reported that for a three-pressure reheat (3PRH) configuration with PCC, the flue gas flow rate at minimum load of 40% GT load with a GE 9371FB GT

Table 5

Test matrix for open-loop tests during the MEA3 test campaign. The values for the main inputs to the process are shown: flue gas volumetric flow rate (F_{gas}), rich solvent flow rate (F_{solv}), steam flow rate (F_{steam}). The cell highlighted in grey color shows the main change from the previous test. The tests begun at 13:00 on 21 July 2017 and finalized on 23 July 2017 at 13:00.

| Test | F_{gas} [Sm ³ /hr] | F_{solv} [kg/hr] | F_{steam} [kg/hr] |
|---------------------------|---------------------------------|--------------------|----------------------|
| Initial conditions | 60 000 | 65 700 | 5 400 |
| A (0 to 8 hr) | 47 000 | 65 700 | 5 400 |
| B (8 to 16 hr) | 47 000 | 52 000 | 5 100 (Oscillations) |
| C (16 to 24 hr) | 47 000 | 65 700 | 5 400 |
| D (24 to 32 hr) | 60 000 | 65 700 | 5 400 |
| E (32 to 40 hr) | 60 000 | 52 000 | 5 100 |
| F (40 to 48 hr) | 60 000 | 65 700 | 5 400 |

(47.3% combined cycle load with PCC), the flue gas flow rate is 64.5% of the total flow rate at design point of 100% GT load. Rezazadeh et al. (Rezazadeh et al., 2015) sets the limit to 60% on minimum GT load for the integrated 3PRH combined cycle with PCC. The reasons are that at lower loads, the impacts on cost of electricity of the fuel price are more pronounced and that the stable and efficient operation of the main compressors of the system require a minimum flow of 70–75% of flue gas flow rate. In their study, 60% GT load for the General Electric 7 Frame (GE 7F.05) (69.4% combined cycle load with PCC) corresponds to 75.2% flue gas flow rate with respect to the design point at 100% GT load (Rezazadeh et al., 2015). Off-design simulations with the models presented by Montañés et al. (Montañés et al., 2017a) show that at 60% GT load with the Mitsubishi 701 JAC (66.48% combined cycle with PCC load), the flue gas flow rate is 73.6% of design load. At 40% GT load, the flue gas mass flow rate is 61.9% of design load. In order to cover the full operating window presented in literature, it was decided in this work to define the minimum load of the PCC unit as 60% of flue gas volumetric flow rate (F_{gas}) in the absorber column (36 000 Sm³/hr).

The ramp rate is the rate at which a power generator can change load. In general, faster ramp rates are the objectives of thermal power plant operators. A power unit that can ramp fast will be capable of following the variability in electricity prices in liberalized power markets, and save fuel costs (Christopher and James, 1987). However, excessively aggressive ramp rates will incur in lifetime reduction of components of the plant due to related thermal stresses (Can Gülen and Kim, 2013; Genrup and Thern, 2013). Load change ramp rates for natural gas combined cycle power plants are around 2–10%/min (Genrup and Thern, 2013; Hentschel et al., 2016). In this work, it was decided to change the flue gas volumetric flow rate fed to the absorber column at TCM DA with a ramp rate of 10%/min. This can be considered a fast ramp rate for a combined cycle, since that would correspond to 13–14%/min combined cycle load change or around 15–16%/min GT load change, considering the steady-state off-design simulation results in Jordal et al. (Jordal et al., 2012).

3.3.1. Tests with control structure with L/G control

The test matrix for tests 1–4 is presented in Table 6. For the four tests, rich solvent flow rate (F_{solv}) is manipulated manually to keep the liquid to gas ratio L/G in the absorber column to a value of around 1.04 kg/Sm³. This was implemented at the pilot plant by changing the set-point of the rich pump flow rate controller (FT5 in Fig. 1). The set-point of F_{solv} was changed with the same rate as the flue gas volumetric flow rate (F_{gas}) was changed. For a given test, the new set-point was defined to obtain a similar L/G ratio under initial and final steady-state operating conditions of the PCC pilot plant. In addition, steam flow rate is manipulated via a feedback control loop to control the stripper

Table 6

Test matrix for test 1–4 on load changes to test the performance of L/G ratio controller for fast cycling capabilities. Feed forwards (FF).

| Test | Description | Active Controllers | Manual changes |
|------|------------------------------------|-----------------------|--|
| 1 | Load reduction with L/G FF control | T_{str} at 120.9 °C | F_{gas} from 100% to 80% with ramp rate of 10%/min. F_{rich} from 65 000 to 52 000 kg/h with set-point change in 120 s, and resulting rise time of 5.5 min. |
| 2 | Load increase with L/G FF control | T_{str} at 120.9 °C | F_{gas} from 80% to 100% with ramp rate of 10%/min. F_{rich} from 52 000 to 65 000 kg/h with set-point change in 120 s, and resulting rise time of 3.5 min. |
| 3 | Load reduction with L/G FF control | T_{str} at 120.9 °C | F_{gas} from 100% to 60% with ramp rate of 10%/min. F_{rich} from 65 000 to 40 000 kg/h with set-point change in 120 s, and resulting rise time of 5.5 min. |
| 4 | Load increase with L/G FF control | T_{str} at 120.9 °C | F_{gas} from 60% to 100% with ramp rate of 10%/min. F_{rich} from 40 000 to 65 000 kg/h with set-point change in 120 s, and resulting rise time of 5 min. |

bottom liquid temperature (T_{str}), measured at the desorber sump.

Tests 1 and 3 represent a load decrease of the power plant resulting in flue gas volumetric flow changes from 100% to 80% and from 100% to 60%, respectively. The same rate of change was applied for solvent flow rate (F_{sob}) set-point. The objective was to test the influence of the magnitude of the disturbance on the capability of the control structure to reject the disturbance. Tests 2 and 4 represent load increase from the power plant, implemented by increasing the flue gas volumetric flow rate from 80% to 100% (test 2) and from 60% to 100% (test 4). In the four tests presented in Table 6, the flue gas volumetric flow rate was changed with a ramp rate of 10%/min.

3.3.2. Tests with control structure with CO₂ capture rate control

Tests 5–8 were designed to test control structures with CO₂ capture rate being controlled. Controlling CO₂ capture rate has been found to be a suitable controlled variable to bring the process close to optimal operating conditions under the presence of disturbances (Panahi and Skogestad, 2011). Among the different methods to calculate capture rate at the amine plant at TCM DA presented by Faramarzi et al. (2017b), method 1 was selected. In method 1, CO₂ capture rate is calculated based on CO₂ product flow rate (F_{prod}) (refer to FT3 in Fig. 1) and the CO₂ supply at the inlet of the absorber column. The CO₂ capture (Cap_A) is defined in Eq. (1), where \dot{m}_{gas} is the mass flow rate of flue gas at the inlet of the absorber column and x_{CO_2} is the mass fraction of CO₂ in the flue gas at the inlet of absorber column. In addition, CO₂ capture rate has been defined considering gas measurements in the absorber column (Cap_B), refer to method 3 in Faramarzi et al. (2017b) for details on instrumentation and calculation. It is calculated considering the CO₂ absorbed in the absorber column, as expressed in Eq. (2), where \dot{m}_{dep} is the mass flow rate of depleted flue gas and $x_{CO_2,out}$ is the mass fraction of CO₂ in the gas leaving the absorber. Note that Cap_A was utilized as controlled variable during tests 5–8, while Cap_B was used for observation and comparison during all tests on control structures.

$$Cap_A = \frac{CO_2(Desorbed)}{CO_2(Supply)} = \frac{CO_2(Product)}{CO_2(Supply)} = \frac{F_{prod}}{\dot{m}_{gas} \cdot x_{CO_2}} \quad (1)$$

$$Cap_B = \frac{CO_2(absorbed)}{CO_2(Supply)} = \frac{CO_2(supply) - CO_2(depleted)}{CO_2(Supply)} = \frac{\dot{m}_{gas} \cdot x_{CO_2} - \dot{m}_{dep} \cdot x_{CO_2,out}}{\dot{m}_{gas} \cdot x_{CO_2}} \quad (2)$$

For tests 5–8 Cap_A was controlled by manipulating the set-point of the rich mass flow rate (F_{sob}) cascade controller (refer to FT5 in Fig. 1). During the MEA3 campaign there was no time for fine tuning this controller. Therefore, a validated dynamic process model of the process was utilized for preliminary tuning of the controller (Montañés et al., 2017b). The simple internal model control (SIMC) tuning rules (Skogestad and Grimholt, 2012) were employed to tune the master controller. For this cascade controller, the slave controller manipulates the pump speed to control the rich solvent mass flow rate, while the master controller manipulates the set point of the rich solvent flow rate controller to control Cap_A .

Firstly, open-loop testing responses to set-point change in solvent flow rate at the pilot plant were analyzed, and a closed-loop time

constant of 3–5 min in the actual response of measured solvent flow (F_{sob}) to the set-point changes was observed. This is the closed-loop time constant of the slave controller in this cascade (inner). Normally, it is desired to have a good time scale separation in terms of closed-loop time constant between slave and master, a rule of thumb is a larger value by a factor of at least 5 (Skogestad and Postlethwaite, 2005). Therefore, it was decided to start with a value of τ_c of 25 min. Simulations were conducted with the validated dynamic process models to tune the master controller with SIMC rules. The resulting values are a proportional gain K_c of 0.14 and an integral time K_I of 8 min. These are considered conservative for the controller tuning.

The test matrix for tests 5–8 is shown in Table 7. The tests consisted of volumetric flue gas flow rate (F_{gas}) decrease from 100% to 80% (tests 5 and 7) and increase from 80% to 100% (tests 6 and 8). For tests 5 and 6 the stripper bottom temperature (T_{str}) controller was also active. For tests 7 and 8, the steam sent to the reboiler was changed with a ramp set-point change. Cap_A was controlled by manipulating rich solvent mass flow rate in all tests with the closed feedback control loop.

4. Results

4.1. Open-loop step responses

The results from open-loop testing experiments described in Section 2.2 and Table 5 are shown and discussed in this section. In the figures shown the tests are separated by vertical lines, with a period of 8 h between experiments. The vertical lines indicate the time at which a step-change in a set-point is applied for a given test. Fig. 4 shows the main inputs to the process for the six open-loop tests applied to the process, from A to F in Table 5. The inputs shown are flue gas volumetric flow rate (F_{gas}), solvent mass flow rate (F_{sob}), steam mass flow rate (F_{steam}) and the calculated actual reboiler duty (\dot{Q}_{reb}). Fig. 5 shows the transient response for tests A–F of capture rates Cap_A and Cap_B , refer

Table 7Test matrix for test 5–8 on load changes to test the performance of Cap_A ratio controller for fast cycling capabilities.

| Test | Description | Active Controllers | Manual changes |
|------|-------------------------------------|---|--|
| 5 | Load reduction with Cap_A control | T_{str} at 120.9 °C Cap_A at 74% | F_{gas} from 100% to 80% with ramp rate of 10%/min. |
| 6 | Load increase with Cap_A control | T_{str} at 120.9 °C Cap_A at 74% | F_{gas} from 80% to 100% with ramp rate of 10%/min. |
| 7 | Load reduction with Cap_A control | Cap_A at 74% | F_{gas} from 100% to 80% with ramp rate of 10%/min. F_{steam} from 5330 to 3900 kg/h in 40 min. |
| 8 | Load increase with Cap_A control | Cap_A at 74% | F_{gas} from 80% to 100% with ramp rate of 10%/min. F_{steam} from 3900 to 5330 kg/h in 40 min. |

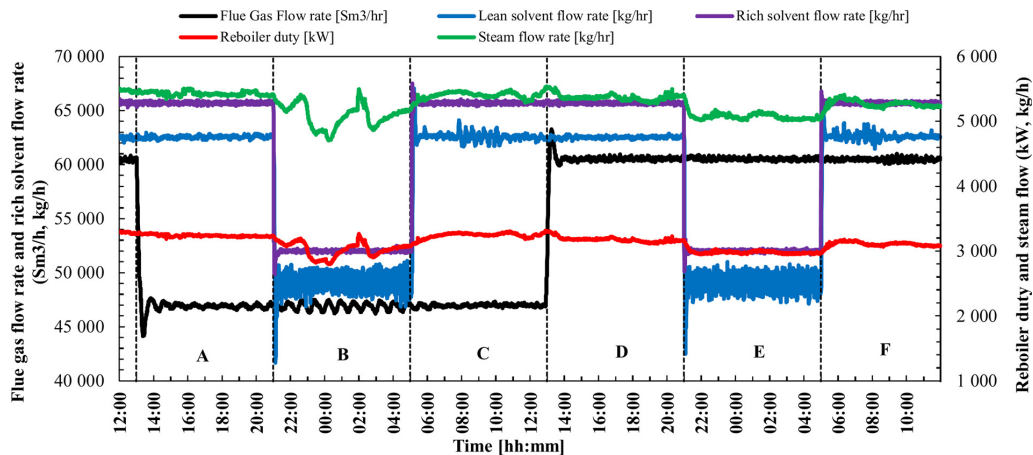


Fig. 4. Open-loop tests during the MEA3 campaign. The test duration was 48 h and was conducted between 12:00 on July 21–12:00 on July 23. The vertical lines indicate the time at which the set-point in flue gas flow rate (F_{gas}) or solvent flow rate (F_{sol}) was changed, and indicates the beginning of the tests from A to F; refer to Table 5. The steam flow rate (F_{steam}) and calculated actual reboiler duty (\dot{Q}_{reb}) are also shown.

to Eqs. (1) and (2) respectively, and CO_2 absorbed and CO_2 desorbed. Note that for tests C and F, a spike in Cap_B is observed at around 05:50, due to a failure in the measurement of CO_2 vol% in the depleted flue gas. Fig. 6 shows the transient response of various temperatures in the absorber column, while Fig. 7 shows the response of various temperatures in the desorber column and the reboiler. Fig. 8 shows the response of lean and rich amine density at measured at locations SA1 and SA2 in Fig. 1, and the lean and rich loading from lab samples taken during the open-loop tests.

In test A, flue gas flow rate set-point was reduced from around 60 000 Sm^3/hr to around 47 000 Sm^3/hr , while the rest of plant inputs were kept approximately constant; refer to Fig. 4. This corresponds with a flue gas capacity of 100% to around 78%. The rise time on flue gas flow volumetric flow rate was around 16 min. So even if the set-point is changed in a step manner, it results in a second order response of measured flue gas volumetric flow rate, due to the integral action of the PI cascade controller; refer to FT1 in Fig. 1. When reducing flue gas flow rate, the L/G ratio in the absorber column increased (from 1.04 kg/Sm^3 to 1.33 kg/Sm^3). This increased the capture rate of the process from around 68% to 86%; refer to test A in Fig. 5. However, the CO_2 input into the plant was also reduced from around 4670 kg/h to around

3600 kg/h (not shown) as a result of decreasing flue gas flow rate. The combination of reduced CO_2 mass flow rate fed into the process with increased L/G ratio in the absorber column lead to similar absorption rate in the absorber column and desorption rate in stripper columns during initial and final steady-state conditions. In addition, the capture rate defined with the product flow rate Cap_A was more sensitive to changes in flue gas flow rate than the capture rate defined with the absorbed CO_2 or Cap_B . Cap_A peaked at around 13:25 with a value of 0.93 while Cap_B peaked at a value of around 0.88 at 13:32. This was because the stripper conditions were not significantly affected by the change in flue gas flow rate. The reduction in flue gas flow rate resulted in a shift in temperature profile in the absorber column, which resulted in higher temperature values; refer to temperatures T_{a1} , T_{a2} and T_{a3} in Fig. 6 during test A. This is because a similar amount of CO_2 being absorbed leads to a similar amount of exothermal absorption heat being released, which is transferred to a lower volumetric flow of gas within the absorber column. The rise time of the transient response of T_{a3} was around 33 min, which was 17 min larger than the rise time on flue gas volumetric flow change of 16 min. This shows the effects of thermal and chemical inertia of the process to reach the new steady-state conditions of the temperature profiles in the absorber column when the flue gas

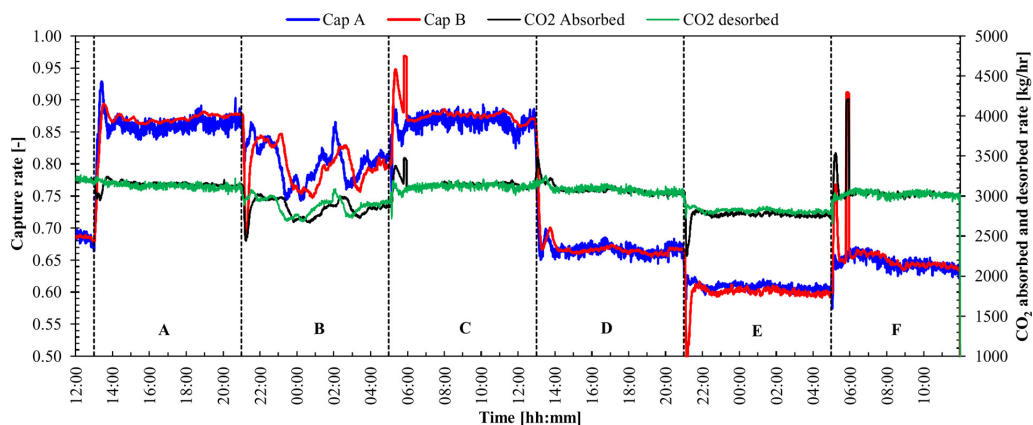


Fig. 5. Transient response of capture rate Cap_A and Cap_B calculated as presented in Eqs. (1) and (2), respectively. The open loop tests are shown for 48 h of testing from July 21 to July 23. The vertical lines correspond to the time at which the set-point changes are applied for tests A–F as presented in Table 5.

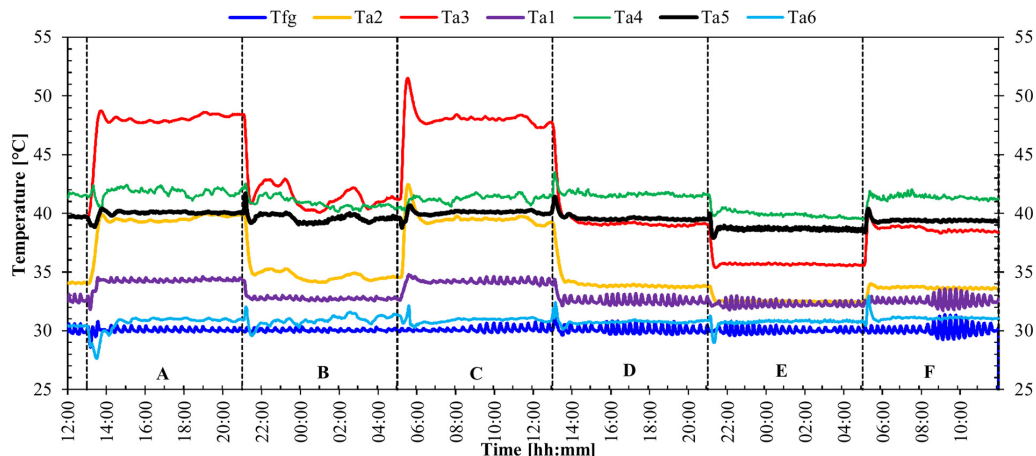


Fig. 6. Transient response of absorber temperatures: T_{a1} , T_{a2} , T_{a3} , T_{a4} and T_{a5} and T_{a6} are temperatures at the inlet of the column, in between the different packing segments from bottom to top; refer to Fig. 1. T_{fg} is the flue gas temperature at the inlet of the absorber column. The open-loop tests are shown for 48 h of testing from July 21 to July 23. The vertical lines correspond to the time at which the set-point changes are applied for tests A–F as presented in Table 5.

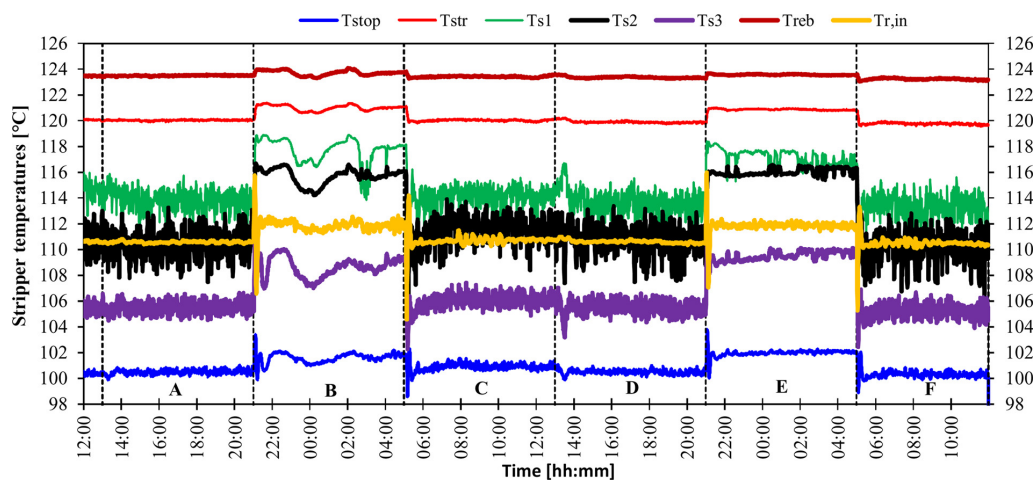


Fig. 7. Transient response of stripper temperatures: T_{s1} , T_{s2} and T_{s3} are averaged stripper packed temperatures at the packing bottom, middle and top, respectively. T_{str} is the liquid temperature at stripper sump, T_{reb} is the reboiler solution temperature and T_{stop} is the stripper temperature at the top of the packing and $T_{r,in}$ is the rich solvent temperature at the inlet of the stripper column. The open-loop tests are shown for 48 h of testing from July 21 to July 23. The vertical lines correspond to the time at which the set-point changes are applied for tests A–F as presented in Table 5.

flow rate is changed. The stripper temperature remained with similar values at initial and final steady-state conditions; refer to Fig. 7. This suggests that a significant change in flue gas flow rate does affect the absorber temperature profiles while the stripper temperature profiles are not so sensitive to changes in flue gas flow rate, when the rest of process inputs are kept constant. The lean and rich amine density is kept fairly constant as well during test A (refer to Fig. 8) which is an indicator that there were not significant variations in CO_2 loadings for the change in flue gas flow rate. Considering the transient trajectories of Cap_A and Cap_B and 10% settling time, the process stabilized after approximately 45 min.

Test B was designed to obtain the response of the process to a reduction of rich solvent flow rate set-point. For tests B and E in which rich solvent flow rate was reduced, there were oscillations of the measured lean solvent flow rate around the final steady-state point; refer to Fig. 4. This is related to flashing in the lean/rich heat exchanger

that leads to oscillations in solvent flow at the inlet of the stripper. In Section 4.2, it is explained how this effect was solved for the closed-loop tests. In test B, the rich solvent mass flow rate (F_{solv}) set-point was changed from 65 700 kg/h to 52 000 kg/h at the beginning of test B, which corresponds with a 20% reduction of solvent flow rate. The fall time on measured F_{solv} is around 4 min, while for the lean solvent flow rate is around 6 min (despite of the oscillation found due to flashing). This shows that the solvent flow rate network responds generally faster than the rest of the process variables, and that changes in rich solvent flow rate are followed tightly by the lean solvent flow rate. However, from a control perspective, it would be desired to have an even faster response of measured rich solvent flow rate to changes in rich solvent flow rate set-point, for tighter control of process variables under load changes of the process. In addition, during test B some changes in steam flow rate were implemented (refer to Fig. 4), which resulted in changes in reboiler duty during the test period. However, these unintended

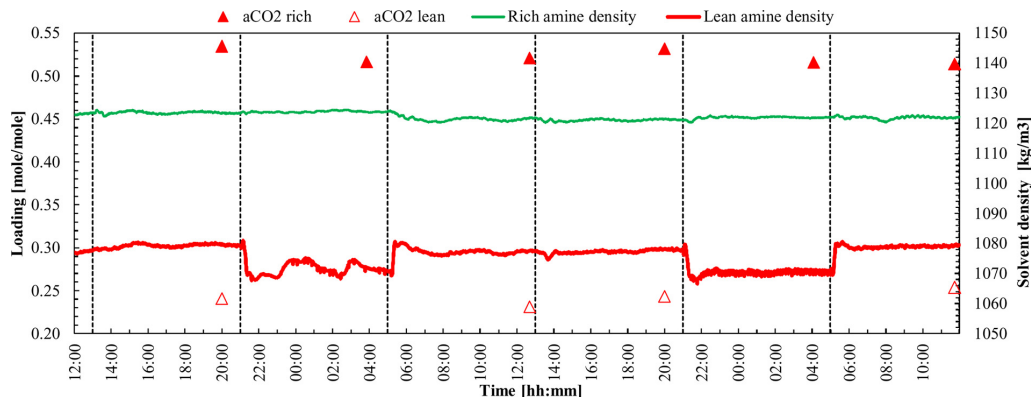


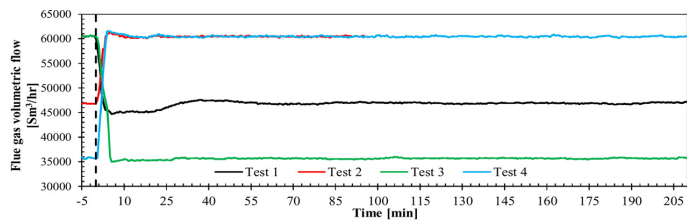
Fig. 8. Transient response of lean and rich solvent densities; and values of lean and rich loading samples taken before the beginning of each test. The open-loop tests are for 48 h of testing from July 21 to July 23. The vertical lines correspond to the time at which the set-point changes are applied for tests A–F as presented in Table 5.

disturbances in reboiler duty applied to the process allowed us to add a discussion on the effects of changes in reboiler duty on the response of the system process variables. Fig. 5 shows the response of CO₂ capture rates to the input changes in test B. It can be observed that CO₂ capture rates and CO₂ absorption and desorption rates were very sensitive to changes in reboiler duty. CO₂ desorption rate trajectory (and Cap_A) followed tightly the input trajectory in steam flow rate during test B, and CO₂ absorption (and Cap_B) followed with a larger delay. For example, steam flow rate (F_{steam}) peaked at time 02:01 during test B, while CO₂ desorption peaked 5 min later at 02:06 and CO₂ absorption peaked after 22 min at 02:23. This shows two effects. One is that the performance of process variables in the stripper column respond fast to changes in reboiler duty, as it is also shown by the peak in T_{s3} at 2:04, i.e. 3 min later than steam flow rate; refer to Fig. 7. The other is the effect of the circulation times through the recycle loop of chemical solvent on the response of the absorber column to changes in reboiler duty. The response of CO₂ absorbed (and Cap_B) shows a peak with a delay of around 22 min, with respect to the steam flow rate (F_{steam}) in the reboiler. As was shown in Fig. 3 and Table 3 case 2, the solvent circulation time from stripper sump to absorber inlet is around 18.5 min, similar to the delay in CO₂ absorbed with respect to F_{steam} . When increasing steam flow rate the lean loading of the chemical solvent will be reduced. This increases the capacity of the solvent to absorb CO₂, and the driving force for CO₂ absorption at the top of the absorption column. However, the solvent has to circulate through the recycle loop, and the resulting circulation time from stripper sump outlet to absorber column inlet results in a delay in the CO₂ absorbed and Cap_B , and also on the absorber column temperature profiles; refer to Fig. 6. In addition, it can be seen that Cap_A is more sensitive to changes in reboiler duty (peak at a value of 0.866) than Cap_B (peak at a value of 0.827). The changes in lean amine density observed in Fig. 8 are good indicators of the fluctuations in lean loading above described, following the fluctuations in steam mass flow rate and resulting reboiler duty during test B.

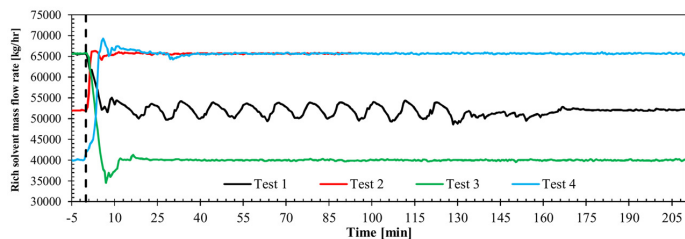
Test C shows the response of the process to changes in rich solvent flow rate (F_{sol}) from 52 000 kg/h to 65 700 kg/h. In this case the rest of process inputs (flue gas flow rate and steam flow rate) were kept reasonably constant during the test. In this case the rise time for F_{sol} was 2 min while for lean solvent flow rate was around 6 min. An inverse response was observed in CO₂ absorbed Cap_B trajectory to change in F_{sol} . When lean solvent flow rate was increased, this resulted in an increase of the L/G ratio in the absorber column, in this case from 1.043 kg/Sm³ to 1.325 kg/Sm³. Initially, this resulted in an increase of the absorption rate of CO₂ in the absorber column, as can be seen in the

trajectory of Cap_B and CO₂ absorbed in Fig. 5. However, after a while the CO₂ absorbed decreased. The peak of CO₂ absorbed was reached at around 05:22 in test C, around 22 min after the set-point change in solvent flow rate was implemented. The change in the trend can be explained by that when solvent flow rate is increased (while keeping constant reboiler duty), the lean loading tends to increase. This was also observed by the decrease in reboiler solvent temperature which is considered a good indicator of solvent lean loading; refer to Fig. 7. However, this change in lean loading does not reach the inlet of the absorber column until a delayed time due to the circulation times from stripper sump outlet to absorber inlet (in this case around 14 min with the solvent flow rate of Case 1 in Fig. 3 and Table 3). In addition, the rise time required for the response in lean flow rate of around 6 min adds to a total delay of around 20 min in the recycle loop. Once the increase in solvent lean loading reaches the absorber column the Cap_B and CO₂ absorbed tends to decrease. In general, it can be said that the Cap_A (and CO₂ desorbed) reaches stabilization with a smoother trajectory (without significant inverse response). Note that Cap_B peaked at a value of 0.941 and Cap_A peaked at a value of 0.890. The inverse response is also shown in the transient response of the absorber temperature profile, refer to T_{a2} and T_{a3} in test C of Fig. 6. However, the peak in temperature T_{a3} in the absorber column happened after around 33 min, which is a longer delay than capture rate. This could be due to the effects of thermal inertia in the absorber column. For solvent flow rate increase it can be observed that the stripper temperature profile was displaced towards relatively lower temperature values; refer to Fig. 7 test C. This can explain the higher resulting desorption ratio in the stripper column. In addition, the response of stripper temperature profiles is faster (rise time of T_{s1} of around 4 min) than for absorber temperature profiles. The inverse response observed in test C was also observed in tests B (initial part of the test until around 22.30), test E and test F. Analog explanations to test C could be written for the output trajectories observed in tests B, E and F for absorber temperature profiles, CO₂ absorbed and Cap_B . For all the tests with solvent flow rate change (B, C, E and F), the observed response of CO₂ desorbed and Cap_A was smoother (without significant inverse response and with relatively larger peaking values) and faster (took less time to stabilize) than CO₂ absorbed and Cap_B , respectively. In addition, the stripper temperature profiles seem to stabilize faster than absorber temperature profiles for set-point step changes in solvent flow rate. The process stabilized after around 45 min for test C.

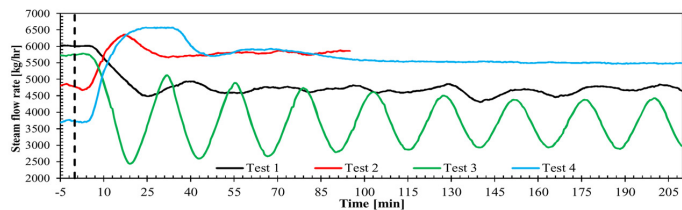
In test D, flue gas volumetric flow rate was increased from 47 000 Sm³/hr to 60 000 Sm³/hr, which corresponds with 78%–100% flue gas volumetric flow rate capacity in the absorber column, respectively.



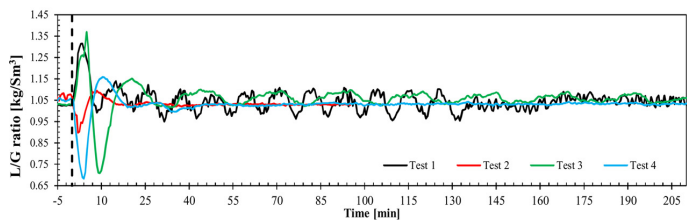
a) Flue gas volumetric flow rate [Sm³/hr]



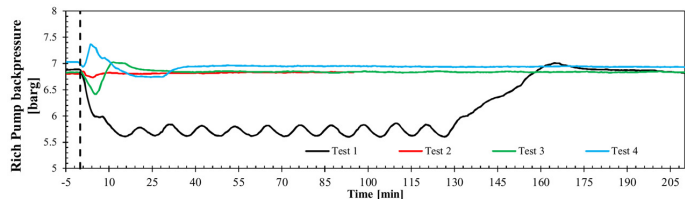
b) Rich solvent mass flow rate [kg/hr]



c) Steam flow rate [kg/hr]



d) L/G ratio [kg/Sm³]



e) Backpressure of rich amine pump [barg]

Fig. 9. Experimental results for tests on load change driven by flue gas flow rate reduction and increase for tests 1–4 in Table 6. The process variables measured are the main inputs to the amine plant during the tests.

The rise time for measured flue gas flow rate was 8 min; refer to Fig. 4. During test D the rich and lean solvent flow rates remain constant, while small fluctuations were observed in steam flow rate to the reboiler and calculated reboiler duty. The capture rate changed significantly from around 86% to around 68%. In this case the trajectory of capture rate followed quite well the variation of flue gas volumetric flow rate, since the CO₂ mass flow rate fed to the absorber column is included in the calculation of capture rates (refer to Eqs. (1) and (2)). In addition, the change in flue gas flow rate does not significantly change the amount of CO₂ being absorbed at initial and final steady-state conditions, as observed in test A. As in test A, a significant change in volumetric flow rate had an impact on absorber temperature profiles, with a change in T_{a3} from around 47 °C to around 39 °C. In this case the response of T_{a3} to the change in flue gas flow rate had a time constant of 17 min and a rise time of around 34 min. This shows again the effects of thermal inertia of the process of heat and mass transfer in the absorber column to changes in flue gas volumetric flow rate. The stripper temperature profile remained constant during the tests A and D of step-change in flue gas flow rate, as shown in Fig. 7. The transient trajectories of Cap_A and Cap_B stabilized after approximately 55 min.

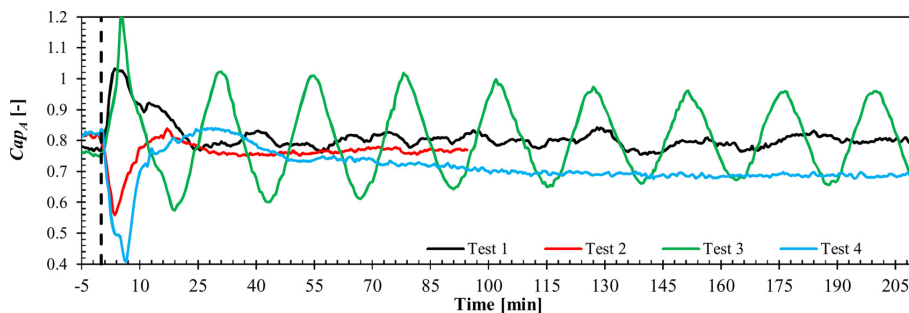
4.2. Decentralized control structures

4.2.1. Control of liquid to gas ratio (L/G) and stripper bottom temperature (T_{sb})

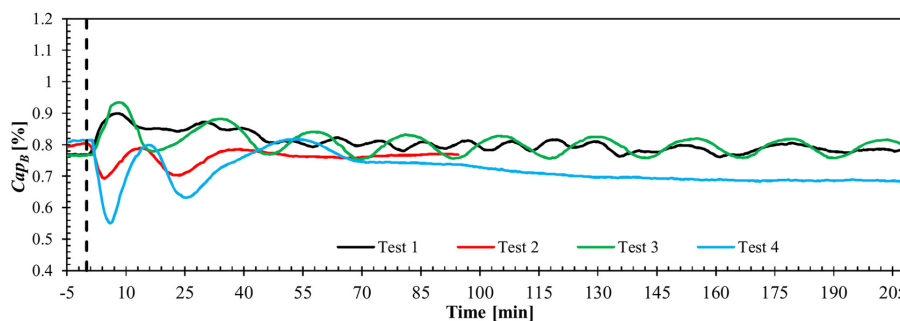
In this section, the results from the tests on fast load change with L/G ratio control are presented, refer to Table 6 in Section 2.3.1. In the figures included in this section, the vertical dotted line indicates the time at which the tests begin with the change in flue gas flow rate. Note

that test 2 was stopped after 95 min, since it was considered that stabilization of process variables was achieved. Fig. 9 shows the trajectories of volumetric flue gas flow rate (F_{gas}), rich solvent mass flow rate (F_{solv}), steam mass flow rate (F_{steam}) to the reboiler, the resulting L/G ratio in the absorber column, and the backpressure of the rich amine solvent pump. Fig. 10 shows the trajectories for capture rates Cap_A and Cap_B , while Fig. 11 shows the trajectories of stripper bottom temperature (T_{sb}), CO₂ desorbed and CO₂ absorbed. In addition, Table 8 shows the resulting total stabilization times for CO₂ absorbed and CO₂ desorbed trajectories for tests 1–4. Here total stabilization times are calculated considering 10% settling times.

Fig. 9a shows the trajectories of flue gas flow rate disturbances applied to the pilot plant for tests 1–4. In this case the operators changed directly the fan speed in order to achieve the desired ramp trajectory, instead of changing the flue gas flow rate controller F_{gas} set-point. This avoided the oscillatory behavior of the flue gas volumetric flow rate trajectory presented in test A, Section 3.1. Fig. 9b shows the trajectory of rich solvent flow rate. The set-point was changed with a ramp rate of 10%/min, and the resulting rise times vary from 3.5 to 5.5 min, refer to Table 6. In test A, marginally stable oscillations around the final set-point of 52 000 kg/h were observed in the trajectory of rich solvent flow rate, from time 5 min to time 130 min. This was due to flashing of rich solvent. In Fig. 9e oscillations of rich pump backpressure during test 1 are shown. To solve this problem, the operator increased the backpressure of the rich pump by throttling a valve located in the hot side of the rich piping between lean/rich heat exchanger and stripper column; refer to rich pump backpressure in test 1 from 130 min to 170 min in Fig. 9e. In following tests 2, 3 and 4 the operator manipulated this valve opening in order to avoid flashing and

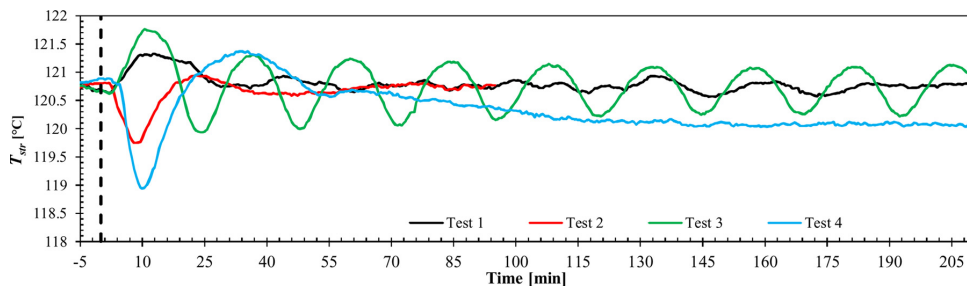


a) Capture rate Cap_A

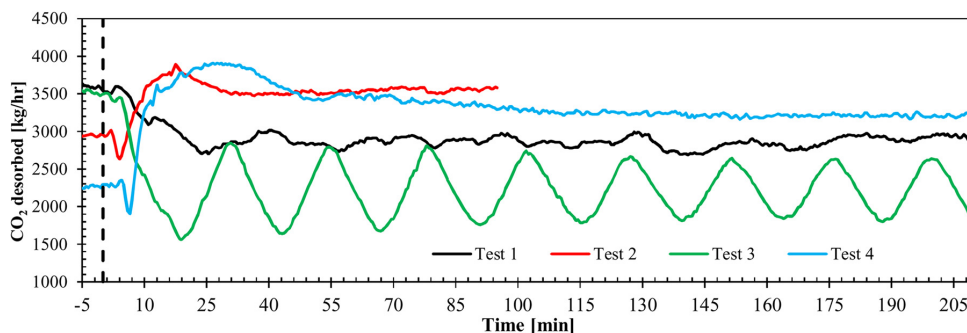


b) Capture rate Cap_B

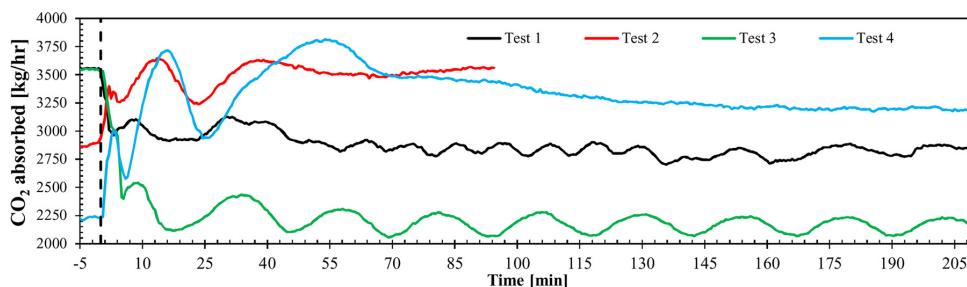
Fig. 10. Experimental results for tests 1–4 in Table 6. Capture rates Cap_A and Cap_B calculated as in Eqs. (1) and (2), respectively. Capture rates are shown for the four transient events in which L/G ratio is kept constant by manipulating the solvent flow rate in order to keep constant the L/G ratio.



a) Stripper bottom temperature [°C]



b) CO₂ desorbed [kg/hr]



c) CO₂ absorbed [kg/hr]

Fig. 11. Experimental results for tests 1–4 in Table 6. Stripper bottom temperature, CO₂ desorbed and CO₂ absorbed during transient load changes of the amine plant.

Table 8

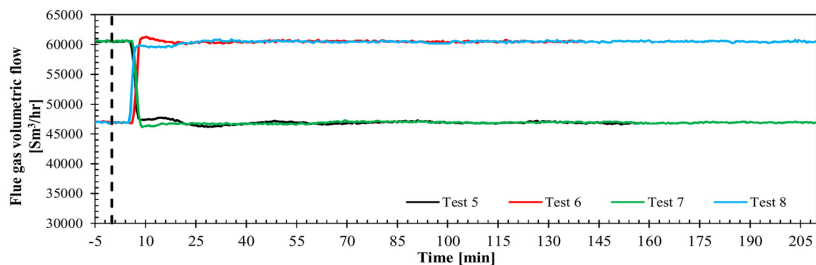
Total stabilization times [min] for CO₂ desorbed and CO₂ absorbed trajectories for tests 1–8. The trajectories were calculated considering the 10% settling time, and for disturbances in flue gas volumetric flow rate.

| Stabilization times [min] | Test 1 | Test 2 | Test 3 | Test 4 | Test 5 | Test 6 | Test 7 | Test 8 |
|---------------------------|--------|--------|--------|--------|--------|--------|--------|--------|
| CO ₂ Desorbed | 45 | 26 | – | 41 | – | 41 | 48 | 48 |
| CO ₂ Absorbed | 53 | 37 | – | 63 | – | 49 | 68 | 107 |

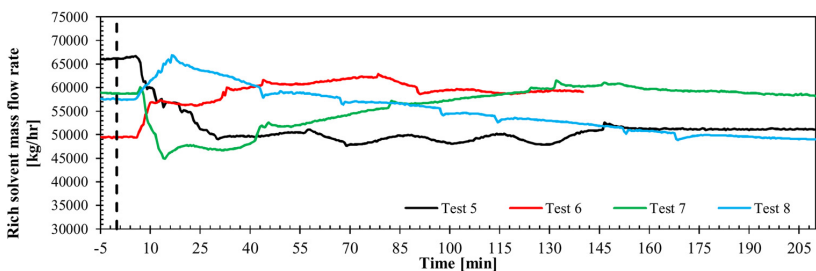
the consequent oscillation in the rich flow rate (and lean solvent flow rate); refer to Fig. 9.

Test 1 consisted of a reduction of flue gas flow rate from 60 000 Sm³/hr to 47 000 Sm³/hr, and the solvent flow rate was reduced to keep L/G ratio to a value of around 1.04 kg/Sm³. Due to the solvent flashing phenomena, the L/G ratio in the absorber column oscillated

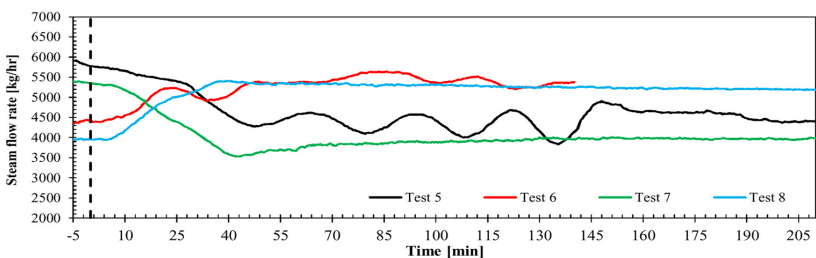
around the final steady-state value; refer to Fig. 9d. This lead to small amplitude oscillations around the final steady-state for all the process variables shown in Figs. 10 and 11, and it can be considered that the process achieved conditions of marginal stability. Considering the averaged value of CO₂ absorbed and CO₂ desorbed once the marginal stability was achieved, the total stabilization time was longer for CO₂ absorbed (53 min) than for CO₂ desorbed (45 min); refer to Table 8. In addition, it seems that Cap_A reaches stabilization faster than Cap_B. However, the trajectory of Cap_A was more sensitive to the disturbance and peaked at a value of 1.05 at time 5 min (see Fig. 10a), while Cap_B peaked at a value of 0.90 at 8.5 min; refer to Fig. 10b. A capture rate value of Cap_A higher than 1 means that there is more CO₂ being desorbed than what is being fed to the process, during the transient conditions. This high peak can be explained by the dead time observed on steam flow rate in Fig. 9c (around 5 min), due to the fact that there is a dead time of around 3 min for a significant change to be observed in the



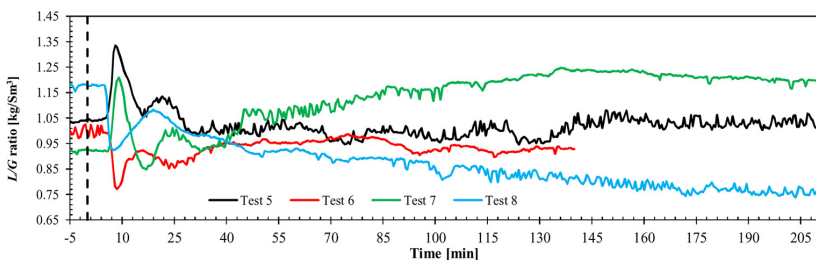
a) Flue gas volumetric flow rate [Sm³/hr]



b) Rich solvent mass flow rate [kg/hr]



c) Steam flow rate [kg/hr]



d) L/G ratio [kg/Sm³]

Fig. 12. Experimental results for tests on load change driven by flue gas flow rate reduction and increase. The process variables measured are the main inputs to the amine plant during the tests. The control structure tries to keep constant the capture rate in absorber column by manipulating rich solvent flow rate, refer to Table 7.

stripper bottom temperature (T_{str}). Once the stripper bottom temperature began to increase due to the lower amount of solvent being sent to the stripper, the T_{str} controllers reduced the solvent flow rate sent to the reboiler. The temperature controller kept the T_{str} close to the desired set point of 120.9 °C without excessive variations (< 1 °C). Despite of the marginal stable behavior due to solvent flashing, the process can reject the disturbance and it reached stabilization within 55 min.

Test 2 was a test for fast load change with a flue gas flow rate increase from 47 000 Sm³/hr to 60 000 Sm³/hr; refer to Table 6. In addition, L/G ratio was kept constant to a value of around 1.04 kg/Sm³ by a ramp up of rich solvent flow rate; refer to Fig. 9b. As for the case on load reduction (test 1), it took longer for the trajectory of CO₂ absorbed to stabilize (37 min) than CO₂ desorbed (26 min); refer to Table 8. Cap_A was again more sensitive to the disturbance with a peak down at value of 0.56 at time 2.5 min (refer to Fig. 10a), while Cap_B peaked down at 0.65 at time 3 min. In addition, the temperature of the stripper is controlled to 120.9 °C without excessive excursions (< 1.2 °C). The process can reject the disturbance of flue gas flow rate change and can bring the process towards stable desired steady-state conditions within 37 min. This was significantly faster than for load reduction in test 1, that took 55 min (refer to Table 8). This suggests that it can be faster to reach stabilization and to reject disturbances when ramping up the volumetric flow rate than when ramping it down.

Test 3 consisted of a reduction of flue gas volumetric flow rate from 60 000 Sm³/hr to 36 000 Sm³/hr (corresponding to 100%–60% flue gas volumetric capacity in absorber column). The solvent flow rate was reduced in order to keep L/G ratio at a value of around 1.05 kg/Sm³ in the absorber column; refer to Fig. 9d. The inputs to the process F_{gas} and F_{solv} reached stabilization, with a rise time of 6 min. However, significant instabilities were found in the steam mass flow rate sent to the reboiler (F_{steam}) which oscillated around the value of 3600 kg/h and had initial peaks of 2540 kg/h at time 20 min and 5130 kg/h at time 32 min; refer to Fig. 9c. The large reduction in solvent flow rate (F_{solv}) resulted in a significant disturbance to the flow network. Fluctuations in the steam flow rate resulted in significant fluctuations of Cap_A and Cap_B (see Fig. 10), CO₂ absorbed, CO₂ desorbed and stripper bottom temperature (T_{str}) (see Fig. 11). This was due to the stripper temperature controller, which was very sensitive to changes in stripper bottom temperature (T_{str}). This suggests that the value of the controller gain was too large. Actually, oscillation disappeared when the operator set the temperature controller on manual and setting a given value of steam flow rate (not shown). Again, Cap_A and desorbed CO₂ were more sensitive to the fluctuations of steam flow rate than Cap_B and CO₂ absorbed, as can be observed in Figs. 10a and 11a. Comparing with test 1, for larger disturbances in flue gas volumetric flow rate it can be more complicated to reject the disturbance and reach stabilization of the process variables with feedback control. This suggests that further work should be done at the TCM amine pilot plant to fine tune the controllers of the regulatory control layer of the process, if large and fast disturbances in flue gas flow rate are to be rejected.

Test 4 shows a flue gas volumetric flow increase from 36 000 Sm³/h to 60 000 Sm³/h with a rise time of 5 min, which represents 60% to 100% of absorber flue gas volumetric flow rate capacity. Rich solvent flow rate (F_{solv}) was increased from 45 000 kg/h to 65 000 kg/h with a rise time of 5 min, in order to keep the L/G ratio at a value of around 1.03 kg/Sm³ at the initial and final steady-state operating conditions. It can be observed how steam flow rate saturated (reached a maximum value of 6 560 kg/h) from around $t = 25$ min to around $t = 35$ min; refer to Fig. 9c. Input saturation is not desired in control for smooth operation of the process. This suggests that the controller gain for the T_{str} controller is too large, and that the stripper temperature set-point was too large for the given process conditions. However, at time $t = 35$ min the steam mass flow rate was reduced by the action of the steam temperature controller. The operators considered that the process achieved stabilization at around time $t = 70$ min, and injected liquid water in the steam supply line to avoid excessive temperature of the

supply superheated steam (limited to 150 °C) according to TCM pilot plant operation guidelines. This reduced the available heat and the resulting stripper bottom temperature (T_{str}). However, it can be considered that the process stabilized at around 70 min. CO₂ desorbed stabilized faster (41 min) than CO₂ absorbed (63 min); refer to Table 8.

4.2.2. Control of capture rate Cap_A

In this section the results from the tests on fast load change with CO₂ capture rate control are presented, refer to Table 7 in Section 2.3.2. In the figures included in this section, the vertical dotted lines indicate the time at which the tests begin. Note that test 6 was stopped after 140 min because it was considered that the plant was operated under steady-state conditions. Fig. 12 shows the trajectories of flue gas volumetric flow rate (F_{gas}), rich solvent mass flow rate (F_{solv}), steam mass flow rate (F_{steam}) to the reboiler and the resulting L/G ratio in the absorber column. Fig. 13 shows the trajectories for capture rates Cap_A and Cap_B , while Fig. 14 shows the trajectories of stripper bottom temperature (T_{str}), CO₂ desorbed and CO₂ absorbed. In addition, Table 8 shows the resulting total stabilization times for CO₂ absorbed and CO₂ desorbed trajectories for tests 5–8.

Test 5 consisted of a reduction of flue gas flow rate from 60 000 Sm³/hr to 47 000 Sm³/hr; refer to Fig. 12a. Solvent flow rate was set to control capture rate Cap_A to a set point of 0.74, and steam flow rate was set to control stripper bottom temperature (T_{str}) to a value of 120.5 °C. The manipulated variables of the controller layer F_{solv} and F_{steam} are shown in Fig. 12b and d. It can be seen that the solvent flow rate was reduced by the controller after the disturbance was introduced. At time $t = 32$ min, the solvent flow rate began to increase and started to have small amplitude oscillations. As observed in the trajectory of Cap_A (in Fig. 13a), at the initial part of the transient (from time $t = 0$ min to time $t = 45$ min) the controller brought the process Cap_A towards the target set point, however from time $t = 50$ min the trajectory of Cap_A showed an oscillatory trajectory with increasing amplitude. As in test 3, solvent flow rate (F_{solv}) variations induced variations in the stripper bottom temperature, hence the steam sent to reboiler was modified by the T_{str} controller, resulting in an oscillatory trajectory with growing amplitude of F_{steam} . Since Cap_A is sensitive to changes in F_{steam} , the capture rate trajectory Cap_A will follow the variations in F_{steam} . Then, the controller of Cap_A modifies further solvent flow rate, resulting in the unstable behavior of the process. At the time around $t = 150$ min, the operator disconnected the T_{str} controller and set a given value of steam pressure, and the oscillatory behavior stopped, bringing the process towards steady-state conditions. This test illustrates the interaction between the feedback control loops, that results in unstable performance of the process in response to the disturbance in flue gas flow rate reduction. In addition, this test shows the challenge of tuning the feedback controllers of the process if decentralized control structures are to be applied to control the chemical absorption process for fast load change disturbances, especially when ramping down the flue gas volumetric flow rate capacity.

Test 6 shows a transient test on load change increase by implementing an increase in flue gas volumetric flow rate from 47 000 Sm³/hr to 60 000 Sm³/hr. The same control structure as the one utilized in test 5 was implemented; refer to Table 7. In this case the control structure managed to bring the process towards the desired steady-state operating conditions after the disturbance in flue gas volumetric flow rate was applied to the process; refer to Fig. 12a. CO₂ desorption rate required a total stabilization time of 41 min, and stabilized faster than CO₂ absorption rate CO₂ (49 min). This test contributed to emphasize that ramping up flue gas flow rate towards full capacity (or close to design conditions) is less challenging than ramping down flue gas flow rate (towards steady-state off-design conditions within the operating window of the process). In addition, the disturbance in CO₂ vol% from a value of 4.1–3.7 happened at time $t = 72$ min with a rise time of 6 min; refer to Fig. 2. This disturbance affects significantly the Cap_A output trajectory, which increases

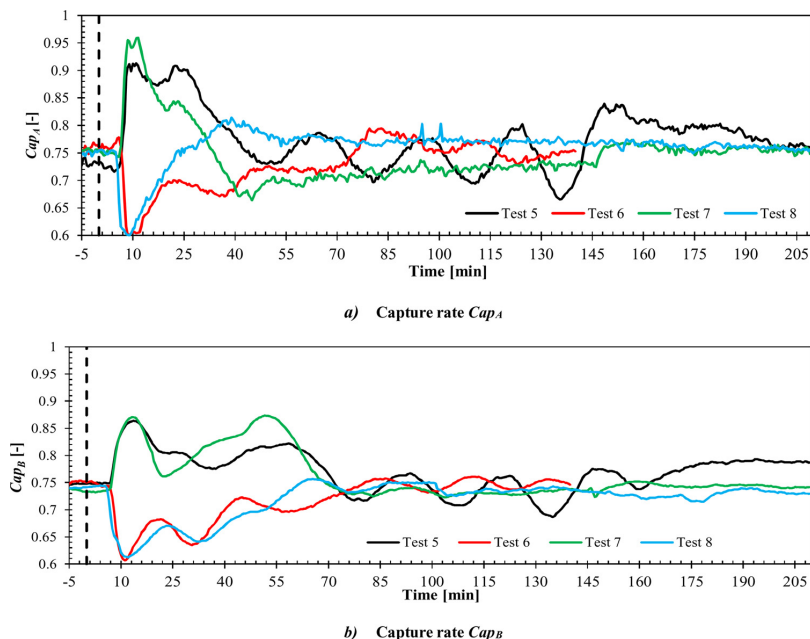


Fig. 13. Experimental results for tests 5–8 in Table 7. Absorption and desorption rates are shown for the four transient events in which L/G ratio is kept constant by manipulating the solvent flow rate in order to keep constant the L/G ratio.

instantaneously, since the amount of CO₂ fed to the process is reduced due to this disturbance; refer to Fig. 13a at time $t = 72$ min. However, it seems that the buffering effect of the process to disturbances at the inlet to the plant avoids a significant change in the trajectories of the rest of process variables presented in this section, and hence the disturbance in terms of CO₂ vol% is properly rejected with this control structure.

Test 7 shows the response of the process when operated with control structure in which Cap_A is controlled by manipulating solvent flow rate F_{solv} , and in this case steam flow rate is reduced by applying a ramp from around 5300 kg/h to 4000 kg/h in 40 min. This ramp was specified based on the steam flow rate trajectory during the first 50 min of transient test 5, in order to test the response of the process when steam flow rate was operated with a feedforward action by modifying the steam pressure (disconnecting the T_{str} feedback control loop). Note that during test 7 the initial conditions were significantly different than those for test 5. Even if both had 100% volumetric flow rate in the absorber column (refer to Fig. 12a time $t = -5$ min to $t = 0$ min), the initial process conditions in terms of F_{solv} and F_{steam} were different in order to reach a similar Cap_B value of 0.74; refer to Fig. 13b. In addition, this could be explained by the lower CO₂ content during test 7 (3.7 vol%) than for test 1 (4.1 vol%), since lower amount of CO₂ needs to be absorbed and desorbed in the absorber and stripper column; refer to time $t = -5$ to time $t = 0$ min in Fig. 14. It can be seen that for test 7 oscillations and instabilities are not found as for the similar test 5 when ramping down flue gas flow rate. This confirmed that the control loop triggering the instabilities was the stripper bottom temperature (T_{str}) controller during test 5. The CO₂ desorbed stabilizes after around 48 min, while CO₂ absorbed took 68 min; refer to Table 8. The final steady-state conditions result in a larger L/G ratio of around 1.15 kg/Sm³ (refer to test 7 in Fig. 12d), and lower stripper bottom temperature (T_{str}), refer to Fig. 14a.

Test 8 shows the response of the process when operated with control structure in which Cap_A is controlled by manipulating solvent flow rate (F_{solv}), and steam flow rate was increased by applying a ramp from around 4000 kg/h to 5300 kg/h in 40 min. This ramp was specified

based on the steam flow rate trajectory during the first 50 min of transient test 6, in order to test the response of the process when steam flow rate was operated with a feedforward action by modifying the steam pressure (disconnecting the T_{str} feedback control loop). The controller managed to control the capture rate Cap_A and stabilized the plant without significant oscillations after around 107 min (refer to CO₂ absorbed in Table 8 and Fig. 14). Therefore, the process stabilized faster when using feedback control for T_{str} (in test 6). The resulting final steady-state process conditions presented a relatively low L/G ratio (Fig. 12d) and larger stripper bottom temperature (T_{str}).

5. Conclusions

Tests on open-loop responses of the plant revealed that for step changes in flue gas volumetric flow rate the absorption and desorption rate did not change significantly from initial to final steady-state conditions. While the absorber temperature profiles are affected by changes in volumetric flow rate, the stripper temperature profile remains approximately constant with same values for the step changes in flue gas flow rate applied in test A and D. For changes in flue gas flow rate the process will take a maximum of around 55 min to stabilize. Changes in steam flow rate to reboiler showed that desorption rates are sensitive to changes in reboiler duty, and CO₂ desorption rate follows tightly the changes in steam flow rate, while the CO₂ absorption rate response follows with a delay due to circulation times in the recycle loop. The stripper process conditions change relatively fast in response to inputs of steam flow rate, while the response of the performance of the absorber column is slower. In addition, for step changes in rich solvent flow rate the solvent flow network stabilizes within 6 min, which is faster compared to rest of process variables. When the capture rate is defined with the absorption rate Cap_B , the output trajectory describes a slow inverse response due to solvent circulation times through the recycle loop, while the capture rate Cap_A defined with CO₂ desorbed reaches stabilization without a significant inverse response. For all tests with solvent flow rate it took less time to stabilize CO₂ desorbed than

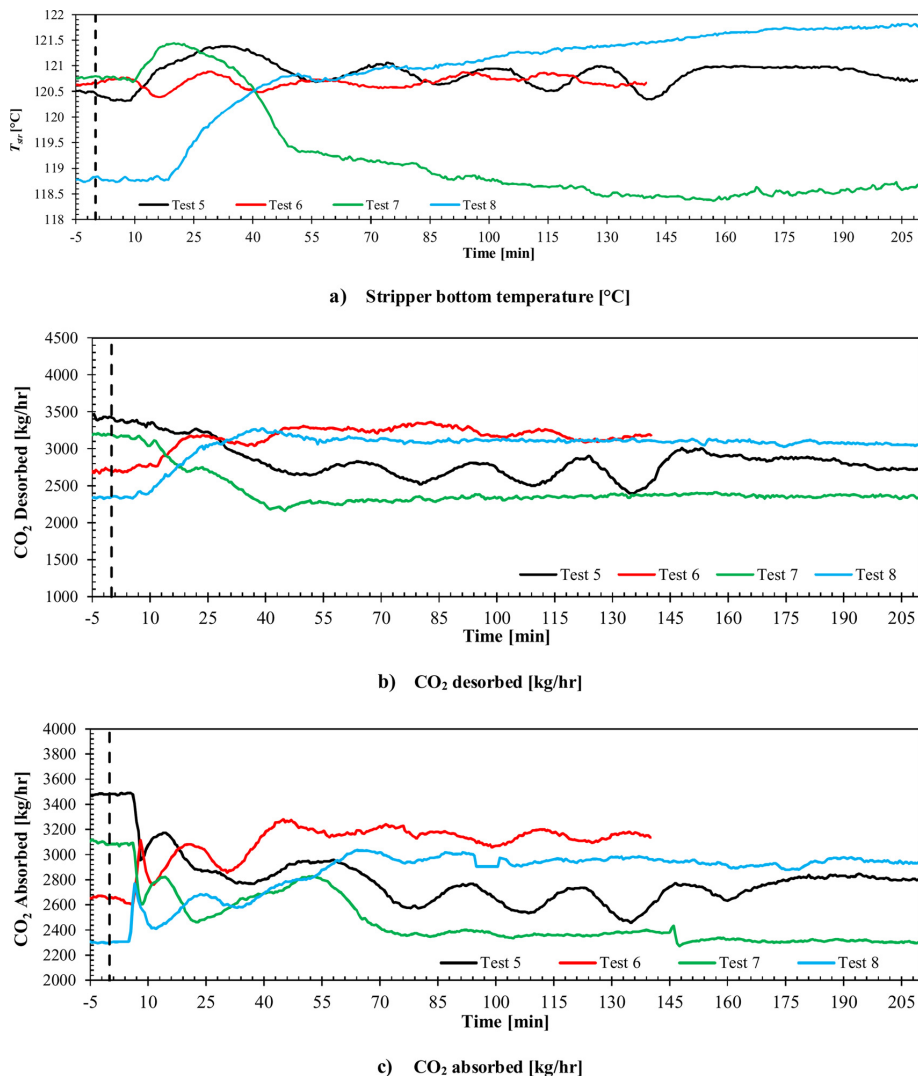


Fig. 14. Experimental results for tests 5–8 in Table 7. Stripper bottom temperature T_{str} , CO₂ desorbed and CO₂ absorbed during transient load changes of the amine plant.

CO₂ absorbed (around 45 min in test C).

Tests for fast load change scenarios applied to the pilot plant revealed that the process can reject fast disturbances in flue gas flow rate and could bring the process towards desired off-design steady-state conditions within 60 min by employing decentralized control structures. These tests provide empirical evidence at demonstration scale that combined cycle power plants with post combustion CO₂ capture can keep similar operational procedures as equivalent unabated power plants, considering fast cycling load changes driven by fast GT load change. However, care must be taken when tuning the feedback control loops of the process and especially of the regulatory control layer. Further work at TCM DA is required to tune the controllers of the regulatory control layer of the amine plant so that faster closed-loop responses are achieved, allowing for tighter control of process variables in the advanced control layer.

Large load changes from maximum to minimum online operation

flue gas volumetric flow rate (100%–60% volumetric flow rate) in the pilot plant can cause instabilities due to the low rich solvent flow. At low solvent flow rates (desired at low loads for efficient off-design steady-state operation of the plant) the circulation times within process equipment increases, slowing the plant response to change in solvent flow rate and hence making more difficult to achieve tight control of capture rate Cap_A and stripper bottom temperature (T_{str}). In response to flue gas flow rate disturbance, fast and large changes in solvent flow rate as a control measure can cause instabilities due to the interaction between the stripper temperature and the capture rate control loops. Unintended disturbances in CO₂ vol% showed the importance of feedback control in order to keep the plant within desired steady-state operating conditions. A combination of feedforward and feedback algorithms could be a solution to achieve fast and stable disturbance rejection.

Acknowledgements

The authors acknowledge the Department of Energy and Process Engineering at NTNU-Norwegian University of Science and Technology and TCM DA owners Gassnova, Shell, Statoil, Sasol and Total, for funding this project.

References

Åkesson, J., Laird, C.D., Lavedan, G., Pröhl, K., Tummescheit, H., Velut, S., Zhu, Y., 2012. Nonlinear model predictive control of a CO₂ post-combustion absorption unit. *Chem. Eng. Technol.* 35, 445–454.

Aske, E.M.B., Skogestad, S., 2009. Consistent inventory control. *Ind. Eng. Chem. Res.* 48, 10892–10902.

Boot-Handford, M.E., Abanades, J.C., Anthony, E.J., Blunt, M.J., Brandani, S., Mac Dowell, N., Fernandez, J.R., Ferrari, M.-C., Gross, R., Hallett, J.P., Haszeldine, R.S., Heptonstall, P., Lyngfelt, A., Makuch, Z., Mangano, E., Porter, R.T.J., Pourkashanian, M., Rochelle, G.T., Shah, N., Yao, J.G., Fennell, P.S., 2014. Carbon capture and storage update. *Energy Environ. Sci.* 7, 130–189.

Bui, M., Gunawan, I., Verheyen, V., Feron, P., Meuleman, E., Adeloju, S., 2014. Dynamic modelling and optimisation of flexible operation in post-combustion CO₂ capture plants—a review. *Comput. Chem. Eng.* 61, 245–265.

Bui, M., Gunawan, I., Verheyen, V., Feron, P., Meuleman, E., 2016. Flexible operation of CSIRO's post-combustion CO₂ capture pilot plant at the AGL Loy Yang power station. *Int. J. Greenh. Gas Control* 48, 188–203.

Can Gülen, S., Kim, K., 2013. Gas turbine combined cycle dynamic simulation: a physics based simple approach. *J. Eng. Gas Turbines Power* 136 011601-011601.

Chinen, A.S., Morgan, J.C., Omell, B.P., Bhattacharyya, D., Miller, D.C., 2016. Dynamic data reconciliation and model validation of a MEA-based CO₂ capture system using pilot plant data. 11th IFAC Symposium on Dynamics and Control of Process Systems, Including Biosystems.

Christopher, H.J., James, K., 1987. How to Determine A Unit Ramp Rate (MW/min) for Lowest Total Production Cost. www.heatrate.com.

Dutta, R., Nord, L.O., Bolland, O., 2017. Selection and design of post-combustion CO₂ capture process for 600 MW natural gas fueled thermal power plant based on operability. *Energy* 121, 643–656.

Enaasen Flo, N., Knuutila, H., Kvamsdal, H.M., Hillestad, M., 2015. Dynamic model validation of the post-combustion CO₂ absorption process. *Int. J. Greenh. Gas Control* 41, 127–141.

Enaasen, N., Zangrilli, L., Mangiaracina, A., Mejdell, T., Kvamsdal, H.M., Hillestad, M., 2014. Validation of a dynamic model of the Brindisi pilot plant. *Energy Procedia* 63, 1040–1054.

Faber, R., Köpcke, M., Biede, O., Knudsen, J.N., Andersen, J., 2011. Open-loop step responses for the MEA post-combustion capture process: experimental results from the Esbjerg pilot plant. *Energy Procedia* 4, 1427–1434.

Faramarzi, E.S., Pedersen, S., Fostås, B.F., Flo, N.E., Morken, A.K., Gjernes, E., Cazenove, T.D., 2017a. The third MEA campaign at CO₂ Technology Centre Mongstad. 4th Post Combustion CO₂ Capture Conference PCC4.

Faramarzi, L., Thimsen, D., Hume, S., Maxon, A., Watson, G., Pedersen, S., Gjernes, E., Fostås, B.F., Lombardo, G., Cents, T., Morken, A.K., Shah, M.I., de Cazenove, T., Hamborg, E.S., 2017b. Results from MEA testing at the CO₂ Technology Centre Mongstad: verification of baseline results in 2015. *Energy Procedia* 114, 1128–1145.

Gardarsdóttir, S.Ó., Montañés, R.M., Normann, F., Nord, L.O., Johnsson, F., 2017. Effects of CO₂-absorption control strategies on the dynamic performance of a supercritical pulverized-coal-fired power plant. *Ind. Eng. Chem. Res.* 56, 4415–4430.

Gaspar, J., Gladis, A., Jørgensen, J.B., Thomsen, K., von Solms, N., Fosbøl, P.L., 2016. Dynamic operation and simulation of post-combustion CO₂ capture. *Energy Procedia* 86, 205–214.

Genrup, M., Thern, M., 2013. Ny gasturbinteknik 2012–2014: Gas Turbine Developments. Report 2012. ELFORSK March.

Gjernes, E., Pedersen, S., Cents, T., Watson, G., Fostås, B.F., Shah, M.I., Lombardo, G., Desvignes, C., Flo, N.E., Morken, A.K., de Cazenove, T., Faramarzi, L., Hamborg, E.S., 2017. Results from 30 wt% MEA performance testing at the CO₂ Technology Centre Mongstad. *Energy Procedia* 114, 1146–1157.

Gonzalez-Salazar, M.A., Kirsten, T., Prchlik, L., 2017. Review of the operational flexibility and emissions of gas- and coal-fired power plants in a future with growing renewables. *Renew. Sustain. Energy Rev.* 82, 1497–1513.

Hamborg, E.S., Smith, V., Cents, T., Brigman, N., Pedersen, O.F., De Cazenove, T., Chhaganlal, M., Feste, J.K., Ullestad, Ø., Ulvatn, H., Gorset, O., Askestad, I., Gram, L.K., Fostås, B.F., Shah, M.I., Maxson, A., Thimsen, D., 2014. Results from MEA testing at the CO₂ Technology Centre Mongstad. Part II: verification of baseline results. *Energy Procedia* 63, 5994–6011.

Hentschel, J., Babić, U.A., Splithoff, H., 2016. A parametric approach for the valuation of power plant flexibility options. *Energy Reports* 2, 40–47.

IEA, 2008. CO₂ Capture and Storage: A Key Carbon Abatement Option. Energy Technology Analysis International Energy Agency.

IEA, 2016. World Energy Investment 2016.

IEAGHG, 2012. Operating Flexibility of Power Plants with CCS. IEAGHG.

IEAGHG, 2016. Evaluation of Process Control Strategies for Normal, Flexible, and Upset Operation Conditions of CO₂ Post Combustion Capture Processes. 2016/07. IEAGHG September.

IPCC, 2014. Climate change 2014: synthesis report. In: Contribution of Working Groups I, II and III to the Fifth Assessment Report of the Intergovernmental Panel on Climate Change. IPCC, Geneva, Switzerland. pp. 151.

Jordal, K., Ystad, P.A.M., Anantharaman, R., Chikukwa, A., Bolland, O., 2012. Design-point and part-load considerations for natural gas combined cycle plants with post combustion capture. *Int. J. Greenh. Gas Control* 11, 271–282.

Kehlhofer, R., Rukes, B., Hannemann, F., Stirnimann, F., 2009. Combined-Cycle Gas and Steam Turbine Power Plants, 3rd edition. PennWell.

Lew, D., Brinkman, G., Kumar, N., Besuner, P., Agan, D.L.S., 2012. Impacts of wind and solar on fossil-fueled generators. In: IEEE Power and Energy Society General Meeting, San Diego, California.

Liu, H., Gao, H., Idem, R., Tontiwachwuthikul, P., Liang, Z., 2017. Analysis of CO₂ solubility and absorption heat into 1-dimethylamino-2-propanol solution. *Chem. Eng. Sci.* 170, 3–15.

Montañés, R.M., Korpås, M., Nord, L.O., Jaehnert, S., 2016. Identifying operational requirements for flexible CCS power plant in future energy systems. *Energy Procedia* 86, 22–31.

Montañés, R.M., Garðarsdóttir, S.Ó., Normann, F., Johnsson, F., Nord, L.O., 2017a. Demonstrating load-change transient performance of a commercial-scale natural gas combined cycle power plant with post-combustion CO₂ capture. *Int. J. Greenh. Gas Control* 63, 158–174.

Montañés, R.M., Flo, N.E., Nord, L.O., 2017b. Dynamic process model validation and control of the amine plant at CO₂ Technology Centre Mongstad. *Energies* 10.

Montañés, R.M., Flo, N.E., Dutta, R., Nord, L.O., Bolland, O., 2017c. Dynamic process model development and validation with transient plant data collected from an MEA test campaign at the CO₂ Technology Centre Mongstad. *Energy Procedia* 114, 1538–1550.

NETL, 2012. Impact of Load Following on Power Plant Cost and Performance.

NETL, 2018. Petra Nova Parish Holdings. W.A. Parish Post-Combustion CO₂ Capture and Sequestration Project.

Nittaya, T., Douglas, P.L., Croiset, E., Ricardez-Sandoval, L.A., 2014. Dynamic modelling and control of MEA absorption processes for CO₂ capture from power plants. *Fuel* 116, 672–691.

Panahi, M., Skogestad, S., 2011. Economically efficient operation of CO₂ capturing process part I: self-optimizing procedure for selecting the best controlled variables. *Chem. Eng. Process. Process Intensif.* 50, 247–253.

Panahi, M., Skogestad, S., 2012. Economically efficient operation of CO₂ capturing process. Part II. Design of control layer. *Chem. Eng. Process. Process Intensif.* 52, 112–124.

Reza zadeh, F., Gale, W.F., Hughes, K.J., Pourkashanian, M., 2015. Performance viability of a natural gas fired combined cycle power plant integrated with post-combustion CO₂ capture at part-load and temporary non-capture operations. *Int. J. Greenh. Gas Control* 39, 397–406.

Singh, A., Stéphenne, K., 2014. Shell cansolv CO₂ capture technology: achievement from first commercial plant. *Energy Procedia* 63, 1678–1685.

Skogestad, S., Grimholt, C., 2012. The SIMC method for smooth PID controller tuning. In: Vilanova, R., Visioli, A. (Eds.), *PID Control in the Third Millennium: Lessons Learned and New Approaches*. Springer London, London, pp. 147–175.

Skogestad, S., Postlethwaite, I., 2005. *Multivariable Feedback Control: Analysis and Design*. John Wiley & Sons.

Tait, P., Buschle, B., Ausner, I., Valluri, P., Wehrli, M., Lucquiaud, M., 2016. A pilot-scale study of dynamic response scenarios for the flexible operation of post-combustion CO₂ capture. *Int. J. Greenh. Gas Control* 48, 216–233.

Thimsen, D., Maxson, A., Smith, V., Cents, T., Falk-Pedersen, O., Gorset, O., Hamborg, E.S., 2014. Results from MEA testing at the CO₂ Technology Centre Mongstad. Part I: post-combustion CO₂ capture testing methodology. *Energy Procedia* 63, 5938–5958.

van de Haar, A., Trapp, C., Wellner, K., de Kler, R., Schmitz, G., Colonna, P., 2017. Dynamics of postcombustion CO₂ capture plants: modeling, validation, and case study. *Ind. Eng. Chem. Res.* 56, 1810–1822.

Walters, M.S., Edgar, T.F., Rochelle, G.T., 2016. Regulatory control of amine scrubbing for CO₂ capture from power plants. *Ind. Eng. Chem. Res.* 55, 4646–4657.

Wellner, K., Marx-Schubach, T., Schmitz, G., 2016. Dynamic behavior of coal-fired power plants with postcombustion CO₂ capture. *Ind. Eng. Chem. Res.* 55, 12038–12045.

Zhang, Q., Turton, R., Bhattacharyya, D., 2016. Development of model and model-predictive control of an MEA-based postcombustion CO₂ capture process. *Ind. Eng. Chem. Res.* 55, 1292–1308.

Zhang, X., Zhang, X., Liu, H., Li, W., Xiao, M., Gao, H., Liang, Z., 2017. Reduction of energy requirement of CO₂ desorption from a rich CO₂-loaded MEA solution by using solid acid catalysts. *Appl. Energy* 202, 673–684.

Paper IV

Dynamic Simulations of the Post-combustion CO₂ Capture System of a Combined Cycle Power Plant

Rubén M. Montañés Lars O. Nord

Department of Energy and Process Engineering, NTNU – Norwegian University of Science and Technology, Trondheim, Norway

Abstract

Dynamic process models of the capture unit of a 600 MW combined cycle power plant with post-combustion CO₂ capture were developed in the Modelica language. The process models were utilized to understand the transient response of the capture unit when the plant was initially operated at steady-state conditions at different power plant's loads. Simulations to characterize the open-loop response of main process variables of the process to step-change disturbances in flue gas mass flow rate, solvent circulation mass flow rate and reboiler duty were performed. It was found that the plant was slower when operated at lower loads, i.e., it required longer total stabilization times for the most relevant variables of the process. Simulations revealed that the PCC unit responded significantly faster to an increase in exhaust gas mass flow rate than to a reduction in exhaust gas mass flow rate.

Keywords: transient, carbon capture, gas liquid contactors, operational flexibility, chemical absorption.

1 Introduction

CO₂ capture and storage (CCS) comprises a group of technologies that can significantly reduce the CO₂ emissions from thermal power plants and other industrial sources (IEA, 2016). Post-combustion CO₂ capture based on the chemical absorption-desorption process using amines is a technology that has been technically proven at commercial scale from coal fired power plants in projects such as Boundary Dam in Saskatchewan, Canada, and the Petra Nova project in Texas, USA.

The introduction of large shares of variable renewable energy sources such as wind and solar in power systems is changing the operating patterns of thermal power generation units, including coal power plants and natural gas combined cycle plants (IEA, 2011). Power plants traditionally operated as base load units are operated as load-following units (Montañés, et al., 2016). Therefore, during the last years, interest has grown in the field of operating flexibility of thermal power plants with CO₂ capture technologies (IEA-GHG, 2012).

The low amount of existing commercial-scale post-combustion capture plants (PCC) and the scarcity of published transient performance data of such systems claims for an interest for the development of dynamic process models (Bui, et al., 2014). These models allow studying plant dynamic performance, analyzing various plant transient events as well as developing and implementing optimal control strategies for PCC plants integrated with thermal power plants. Dynamic process simulation provides process insight and contributes to the development of the learning curve for flexible operation of future thermal power plants with CO₂ capture.

The purpose of the study is to provide understanding of the open-loop transient performance of the main process variables of the PCC unit at different load operation points of the power plant. A thermal power plant operated as load-following unit will be operated at part-load conditions during a significant amount of hours during its lifetime (Montañés, et al., 2016). Therefore it is of importance to find out differences in the transient behavior of the process at part-load operating conditions with respect to those of nameplate capacity. In this work, a dynamic process model of the PCC unit of a 600 MW combined cycle power plant with post-combustion CO₂ capture using aqueous monoethanolamine (MEA) as chemical solvent is utilized for providing understanding of the open-loop response of key performance variables to different disturbances applied to the PCC plant. The process insight and understanding developed in this work will be valuable to develop control strategies of the process when integrated with the thermal power plant.

2 Post-combustion CO₂ capture with chemical absorption

2.1 Chemical absorption process

The process of CO₂ capture by chemical absorption is a two-steps regenerative process; one involves the absorption of CO₂ into a solvent, while the other involves the desorption or stripping of CO₂ from the solvent and the regeneration of the solvent. The process conditions change in the absorption and desorption

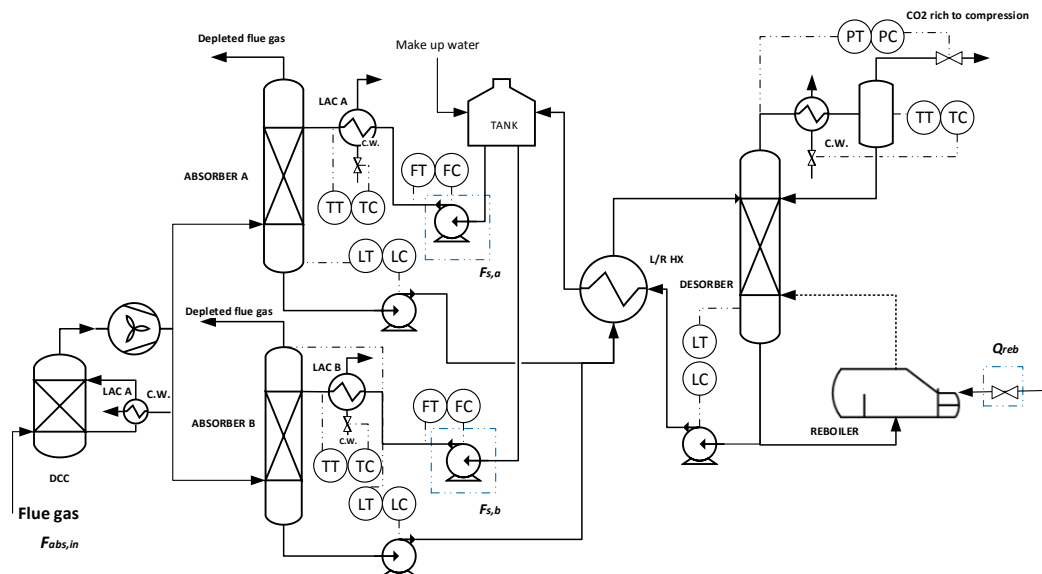


Figure 1. Process configuration of the post combustion CO₂ capture unit (PCC) of the natural gas combined cycle power plant studied in this work. Includes temperature (T), level (L), flow (F) and pressure (P); transmitters (T) and controllers (C).

process, being main changes temperature and pressure, and also solvent concentrations and pH. For absorption, low temperature and high partial pressure of CO₂ is desired, while for desorption, high temperature and low partial pressure of CO₂ is desired.

When the process is utilized for flue gas treatment from a power plant, the exhaust gases are normally cooled down by means of a direct contact cooler (DCC), that reduces the flue gas temperature and the water content. A fan allows overcome the gas pressure drop in the absorber, which is operated slightly above atmospheric conditions, and at around 40 °C, refer to Figure 1. In the absorber column, the exhaust gas flowing upwards meets the chemical solvent flowing downwards. Packing material allows having a thin film of liquid with high surface contact area for heat and mass transfer between the gas and liquid phases, and the exothermal chemical absorption process. Depleted flue gas leaves the absorber at the top through a stack, normally after flowing through a water wash section that allows keeping the water mass balance of the process and reduces chemical solvent emissions due to solvent droplets or solvent vapor carry over. The rich solvent, i.e., solvent with a lot of bounded CO₂, accumulates in the absorber sump and is then pumped towards the top of the stripper. An intermediate heat exchanger allows for heat integration between the absorber and stripper columns. The rich solvent is heated up by the lean solvent coming from the stripper bottom towards around 110 °C and then enters the stripper at the top of the column. This heat integration allows reducing reboiler and cooling duties. A mixing tank allows for

accumulation of the solvent at different operating conditions of the plant.

The desorption process normally occurs at around 100 to 130 °C. Steam supplied from the power plant provides the reboiler duty required to regenerate the solvent (endothermal desorption process), and to generate the stripping vapors flowing upwards in the stripper column, consisting mainly of H₂O and CO₂. The regenerated lean solvent is sent to the absorber inlet via the heat integration exchanger and a lean amine cooler that controls the temperature of the solvent at the inlet of the absorber to around 40 °C. At the top of the stripper there is a condenser and a cooler where the solvent and steam condenses. The condensate is conducted back to the column via a reflux. The product CO₂ rich flow the top of the stripper is conducted to the compression section where it will be conditioned for transport and storage purposes.

2.2 Process configuration

The PCC unit was designed to treat flue gas from a 611 MW combined cycle power plant. The gas turbine (GT) of the power plant was the heavy duty Mitsubishi JAC 701, and the steam cycle consisted of a three-pressure reheat (3PRH) configuration. The design of the PCC unit included the process integration with the power plant through the flue gas line from the HRSG outlet and a steam extraction from the steam turbine's IP/LP crossover. The steam extraction was utilized to feed the reboiler duty required to produce the stripping vapors needed for chemical desorption in the stripper column. The design point chosen for the post-

combustion unit was 100% GT load under ISO conditions, which, for the gas turbine, corresponded to flue gas with a mass flow rate of 887.1 kg/s with 4.33 vol % CO₂ (wet). The chemical solvent utilized was 30%wt aqueous MEA and the target capture rate was 90%. Further details on design aspects of PCC units for combined cycle power plants can be found in (Dutta, et al., 2017).

The resulting process configuration of the PCC unit consisted of a two absorbers and one stripper layout, as shown in Figure 1. Each absorber column had dimensions of 16.3 m in diameter and 23.2 m height, while the desorber had a 9.7 m diameter with 10 m height. The process equipment included absorber columns, desorber column and reboiler, overhead condenser, internal lean/rich heat exchanger, mixing tank for water and MEA makeups, direct contact coolers and circulation pumps. A fan was included in the process to overcome the pressure drop imposed by the absorber column.

3 Dynamic process model development and validation

The Modelica library Gas Liquid Contactors (GLC) (Modelon AB, 2016), from Modelon AB, was utilized as a basis to develop the dynamic process model of the PCC unit. The library contains dynamic process models of the main equipment for systems' level modeling of the absorber-desorber process with monoethanolamine (MEA) as chemical solvent. That equipment includes absorber and desorber columns, sumps, reboiler, condensers, water wash sections, pumps, valves, mixing tank, and property media packages.

The chemical absorption-desorption process within packed segments was modelled considering the two-film theory approach for heat and mass transfer. Chemical equilibrium for reactions was assumed, and mass transfer was modeled considering rate-based models with enhancement factor (Kvamsdal, et al., 2009). Detailed description of the dynamic process models included in the GLC library has been presented previously in literature (Prölb, et al., 2011).

The dynamic process models included in the GLC library have been previously validated with large-scale experimental data by (Montañés, et al., 2017). The validation consisted of modeling the whole absorber-desorber system of the demonstration scale chemical absorption plant at CO₂ Technology Centre Mongstad (TCM DA), in Norway. The amine plant at TCM DA was configured to treat exhaust gases coming directly from the exhaust of a natural gas fueled combined heat and power (CHP) plant placed at Mongstad's refinery. The exhaust gas from two GE 9001E gas turbines contains about 3.5 %vol CO₂, and around 3% of the total exhaust gas mass flow rate is conducted to the amine plant for CO₂ absorption. The PCC plant at TCM can

treat up to 60 000 Sm³/hr of exhaust gas and can capture around 80 ton CO₂/day at nameplate capacity when configured to treat CHP gas. The experimental data utilized for validation includes steady-state data for a wide range of operating conditions and multiple transient events. The plant was operated with 30 wt % aqueous MEA. The conclusion of the work in (Montañés, et al., 2017) is that the process models can capture, with sufficient accuracy, the steady-state and transient phenomena of the process at the demonstration plant scale. In addition, it gives confidence towards using the models for simulation and analysis of the transient performance of the scaled-up process to commercial scale of 4770 ton/day CO₂ captured.

Rules for consistent inventory control (Aske & Skogestad, 2009) were applied to design the regulatory control layer of the PCC unit in Figure 1. It included level controllers for absorbers and stripper sumps, overhead condenser pressure control, lean solvent temperature at absorbers inlet, and exhaust gas temperature at absorber inlet. The controllers were tuned by means of the SIMC tuning rules.

The supervisory control layer for this process has three degrees of freedom, consisting of the two solvent mass flow rates at absorber inlet $\dot{F}_{s,a}$ and $\dot{F}_{s,b}$, and the reboiler duty \dot{Q}_{reb} .

4 Process simulations description

Generally, a combined cycle power plant is brought to part-load operating conditions by reducing the GT load and consequently the steam turbine's power output will be reduced. A GT load reduction results in reduced GT exhaust gas mass flow rate sent to the HRSG of the combined cycle and to the absorbers of the PCC unit. The open-loop transient performance of the plant is studied for three steady-state operating conditions of the power plant, corresponding to 100%, 80% and 60% GT load.

4.1 Steady-state operating conditions at 100%, 80% and 60% GT load

In order to obtain the steady-state operating conditions of the PCC unit at the three operating points, simulations were run with different flue gas mass flow rates as input boundary conditions to the dynamic process model, corresponding to different GT loads, refer to Table 1. The exhaust gas temperature and composition of the absorber was considered constant as boundary condition (input). Note that the exhaust temperature at the inlet of the absorber is normally controlled by the DCC, and that it was observed that exhaust gas composition did not change considerably for the purpose of this study, considering the part load range analyzed of 100% to 60% GT load, and for the specific GT utilized in this work. In addition, a decentralized control structure for the supervisory control layer was included. Several

studies, including the one based on self-optimizing control theory by (Panahi, 2011), suggest that keeping the capture ratio Cap and a temperature in the stripper column constant can lead to efficient operation of the process for varying loads of the absorption-desorption process. Therefore, the available degrees of freedom for operation were utilized to control these process variables. Solvent mass flow rates $\dot{F}_{s,a}$ and $\dot{F}_{s,b}$ were utilized to control the respective CO₂ capture rates Cap_a and Cap_b at the top of the absorbers to the design value of 0.9, while reboiler duty was used as manipulated variable to control reboiler temperature T_{reb} to the value 119 °C. CO₂ capture rates are calculated for each absorber column at the top, by using Equation (1), where $\dot{F}_{abs,in}$ is the exhaust flue gas at the inlet of the absorber column, $X_{abs,in}$ is the CO₂ mass fraction in the exhaust gas at the absorber inlet, $\dot{F}_{abs,out}$ is the depleted flue gas mass flow rate at the absorber stack and $X_{abs,out}$ is the CO₂ mass fraction in the flue gas at the absorber stack. The resulting operating conditions of the PCC at different GT loads are shown in Table 1 and Table 2.

Table 1. Values of PCC unit input variables at different power plant's load operating conditions. Note that both absorber columns were operated in parallel, so $\dot{F}_{s,a}$ was equal to $\dot{F}_{s,b}$.

| GT load [%] | $\dot{F}_{abs,in}$ [kg/s] | $\dot{F}_{s,a}$ [kg/s] | \dot{Q}_{reb} [MW] |
|-------------|---------------------------|------------------------|----------------------|
| 100 | 887.1 | 613.3 | 205.9 |
| 80 | 765.1 | 535.2 | 176.2 |
| 60 | 653.5 | 464.1 | 149.6 |

$$Cap_a = \frac{\dot{F}_{abs,in} \cdot X_{abs,in} - \dot{F}_{abs,out} \cdot X_{abs,out}}{\dot{F}_{abs,in} \cdot X_{abs,in}} \quad (1)$$

Table 2. Values of most relevant process variables of the PCC unit at different operating conditions of the power plant. Note that both absorber columns were operated in parallel, so Cap_a was equal to Cap_b (in the table shown as Cap). It also resulted in same value of solvent loading at absorbers inlets ($L_{i,abs}$).

| GT load [%] | $L_{i,abs}$ | $L_{i,str}$ | Cap | $Prod$ [kg/s] |
|-------------|-------------|-------------|-------|---------------|
| 100 | 0.280 | 0.501 | 0.9 | 55.2 |
| 80 | 0.280 | 0.497 | 0.9 | 47.6 |
| 60 | 0.279 | 0.493 | 0.9 | 40.7 |

4.2 Open-loop step response simulations

The simulations consisted of step-changes of $\pm 10\%$ of main PCC inputs, or disturbances, when the plant was at steady-state operating conditions at the three GT operating points. Step-changes were applied to each process input at a time, keeping the remaining process inputs constant. The output in main process variables was recorded and dead times and 10% settling times were calculated.

- Dead time θ describes how long it takes before a process variable begins to respond to a change in the process input. With begins to respond it is meant that the trajectory of the process variable moves out of the band defined by the initial steady-state value of the process variable y_0 , and a $\pm 1\%$ change in the process variable Δy , i.e.: $-0.01 \Delta y + y_0 < y_0 < 0.01 \Delta y + y_0$, for the first time.
- The 10% settling time t_s is the time it takes from the instant in which the process variable begins to respond to the input change, until it remains within an error band described by the final steady-state value of the process variable y_∞ , and 10% of the change in the process variable Δy , i.e.: $-0.1 \Delta y + y_\infty < y_\infty < 0.1 \Delta y + y_\infty$.
- The resulting total stabilization time t_{sta} is the sum of the dead time and the settling time. In addition, the relative change RC in the process variable is calculated as in Equation (2), where y_0 is the initial steady-state value of the process variable.

$$RC (\%) = 100 \cdot \frac{y_\infty - y_0}{y_0} \quad (2)$$

The main inputs/disturbances applied to the process in this analysis were:

- Flue gas mass flow rate $\dot{F}_{abs,in}$. Note that the flow was split and the absorber columns were operated in parallel. This means that each absorber column treated an exhaust gas mass flow rate of $\dot{F}_{abs,in}/2$.
- Solvent mass flow rates at absorbers inlets $\dot{F}_{s,a}$ and $\dot{F}_{s,b}$.
- Reboiler duty \dot{Q}_{reb} .

The responses of the main process variables of interest in this analysis were:

- Solvent lean CO₂ loading at absorbers inlet $L_{i,abs}$.
- Solvent rich CO₂ loading at stripper inlet $L_{i,str}$.
- CO₂ capture rate at absorbers stacks Cap_a and Cap_b .
- CO₂ product mass flow rate $Prod$, at the outlet of the overhead condenser of the desorber. This is the CO₂ rich product flow of the PCC unit sent to conditioning, compression and transport.
- Temperature at stripper column bottom T_{reb} .

The difference in solvent loading at inlet and outlet of the absorber determines the capability of the solvent to carry CO₂. This in turn depends on the absorber size, operating conditions, regeneration of the solvent and CO₂ partial pressure. Solvent CO₂ loading L is defined as the ratio between moles of CO₂ and moles of solvent (mol/mol) in Equation (3).

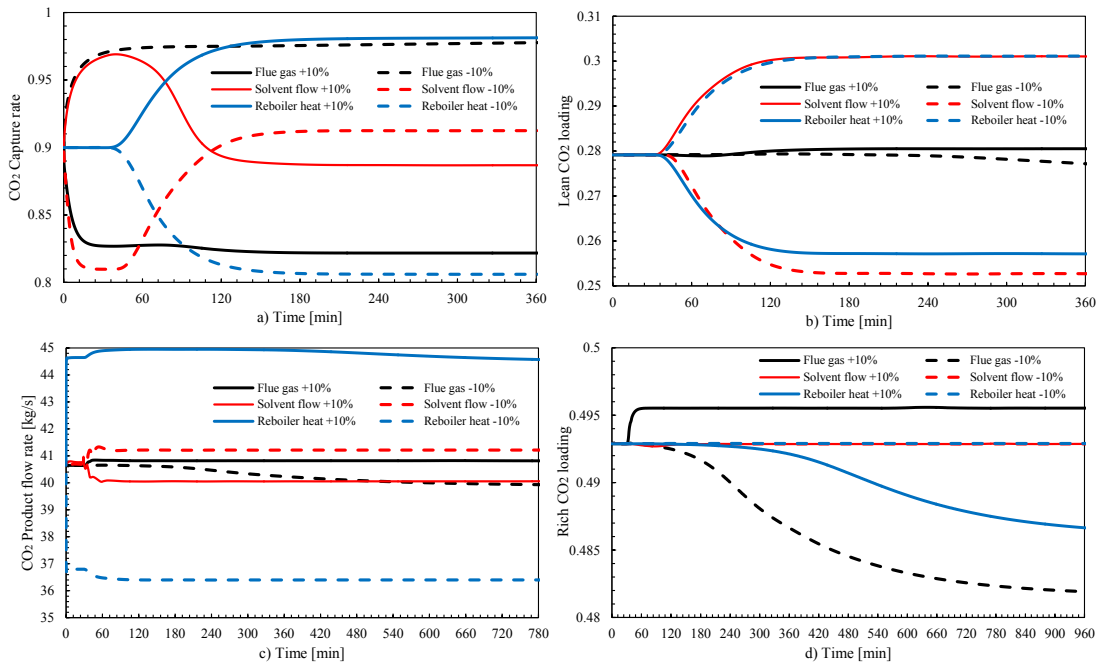


Figure 2. Transient responses of the relevant process variables to different step-changes in process inputs. These simulations correspond to the initial steady-state operation of the PCC unit for 60% GT load. Step-changes were applied at $t = 0$ min.

$$L = \frac{\text{mols of } CO_2}{\text{mols of solvent}} \quad (3)$$

5 Results and discussion

5.1 Response to step changes in flue gas mass flow rate $F_{abs,in}$

The resulting response times of the PCC unit's main process variables to step-changes in flue gas mass flow rate are shown in Table 3 and Table 4. Figure 2 shows the transient response of the main process variables for the different step changes studied in this work. In addition, Figure 3 shows trends of total stabilization times t_{sta} for the main variables of the process when operating the plant at different loads.

It can be observed that CO_2 capture rate Cap stabilized relatively fast, within 1 h, after a disturbance in flue gas mass flow rate. The CO_2 capture rate decreased for increased flue gas mass flow rate (+10%). A faster response in Cap was observed when the flue gas flow rate was increased (+10%) than when it was decreased (-10%), showing the non-linear performance of the PCC system. This behavior was consistent at the different operating points of the PCC plant. The dead time of this response was negligible, since the flue gas mass flow rate was included in the calculation and naturally changes when a step change is applied.

The CO_2 product flow rate $Prod$ required larger stabilization times than Cap . This shows the differences in performance of the absorbers and desorber columns during transient conditions when a disturbance is applied to the PCC unit. The dead times observed in the CO_2 product mass flow rate can be explained by the residence time imposed by the solvent hold-ups in the cold side of the internal heat exchanger's piping and rich solvent piping. These residence times resulted in dead times in convectively transported variables of the liquid solvent from absorber outlet to stripper inlet, including rich solvent loading at the stripper inlet $L_{i,str}$. Note that the dead times of $L_{i,str}$ and $Prod$ responses are similar in Table 3 and Table 4. Stabilization of the $Prod$ was significantly faster when increasing flue gas mass flow rate (around 1 h) than when flue gas mass flow rate was decreased (9 to 11 h). It can also be observed that the $Prod$ response was slower at lower power plant loads, refer to Figure 3.

For flue gas flow rate increase (+10%), the relative change in solvent loadings was small. This is because the solvent capacity was close to the limit under these operating conditions. In general, it was found that lean solvent loading at the inlet of the absorber $L_{i,abs}$ required larger stabilization times t_{sta} than rich loading at stripper inlet $L_{i,str}$. This can be explained by the buffering effect introduced by the mixing tank placed in the recycle loop (from stripper sump to absorber liquid inlet). In addition, larger dead times to this specific disturbance were found for $L_{i,abs}$ than for $L_{i,str}$, due to the additional

Table 3. Response to +10% step increase in flue gas mass flow rate $\dot{F}_{abs,in}$ at various GT loads. Dead times Θ , settling times t_s and total stabilization times t_{sta} are shown.

| GT load [%] | | 10 % | | | |
|-------------|-------------|----------------|-------------|-----------------|--------|
| | | Θ [min] | t_s [min] | t_{sta} [min] | RC [%] |
| 100 | $L_{i,abs}$ | 74 | 53 | 127 | 0.45 |
| | $L_{i,str}$ | 26 | 11 | 36 | 0.45 |
| | Cap | 0 | 12 | 12 | -8.79 |
| | Prod | 26 | 5 | 31 | 0.29 |
| | T_{reb} | 0 | 127 | 127 | -0.05 |
| 80 | $L_{i,abs}$ | 36 | 105 | 141 | 0.47 |
| | $L_{i,str}$ | 27 | 12 | 39 | 0.50 |
| | Cap | 0 | 15 | 15 | -8.74 |
| | Prod | 28 | 45 | 72 | 0.35 |
| | T_{reb} | 0 | 54 | 54 | -0.05 |
| 60 | $L_{i,abs}$ | 68 | 88 | 156 | 0.48 |
| | $L_{i,str}$ | 34 | 13 | 46 | 0.54 |
| | Cap | 0 | 17 | 17 | -8.70 |
| | Prod | 34 | 28 | 62 | 0.42 |
| | T_{reb} | 0 | 60 | 60 | -0.06 |

Table 4. Response to -10% step decrease in flue gas mass flow rate $\dot{F}_{abs,in}$ at various GT loads. Dead times Θ , settling times t_s and total stabilization times t_{sta} are shown.

| GT load [%] | | -10 % | | | |
|-------------|-------------|----------------|-------------|-----------------|--------|
| | | Θ [min] | t_s [min] | t_{sta} [min] | RC [%] |
| 100 | $L_{i,abs}$ | 47 | 578 | 626 | -2.50 |
| | $L_{i,str}$ | 26 | 538 | 564 | -2.62 |
| | Cap | 0 | 55 | 55 | 8.55 |
| | Prod | 27 | 556 | 583 | -0.98 |
| | T_{reb} | 3 | 572 | 575 | 0.30 |
| 80 | $L_{i,abs}$ | 50 | 639 | 689 | -2.31 |
| | $L_{i,str}$ | 29 | 592 | 621 | -2.53 |
| | Cap | 0 | 58 | 58 | 8.84 |
| | Prod | 30 | 603 | 633 | -1.90 |
| | T_{reb} | 0 | 625 | 625 | 0.27 |
| 60 | $L_{i,abs}$ | 129 | 619 | 748 | -1.99 |
| | $L_{i,str}$ | 131 | 529 | 661 | -2.26 |
| | Cap | 0 | 39 | 39 | 8.88 |
| | Prod | 163 | 503 | 666 | -1.85 |
| | T_{reb} | 5 | 667 | 672 | -2.83 |

residence time introduced by liquid hold-ups in desorber packed segments and sump, lean amine piping and hot side piping of the integral heat exchanger, mixing tank and lean amine cooler. Again, the plant response in

solvent CO₂ loadings was faster when flue gas mass flow rate was increased for all power plant loads studied, refer to Figure 3. It must be mentioned that the relative change in process variables to step-changes is more significant the step-down than step-up of the flue gas flow rate. This can be explained by the fact that the solvent rich loading at the steady-state operating conditions is close to the solvent limit CO₂ loading capacity, which is limited by stoichiometry.

5.2 Response to step-changes in solvent mass flow rate $\dot{F}_{s,a}$ and $\dot{F}_{s,b}$

The resulting response times of the PCC unit's main process variables to step-changes in solvent circulation mass flow rates are shown in Table 5 and Table 6.

Table 5. Response of the main process variables to 10% step increase in solvent circulation mass flow rate $\dot{F}_{s,a}$ and $\dot{F}_{s,b}$ at the inlet of the absorbers, for different GT loads. Dead times Θ , settling times t_s and total stabilization times t_{sta} are shown.

| GT load [%] | | 10 % | | | |
|-------------|-------------|----------------|-------------|-----------------|--------|
| | | Θ [min] | t_s [min] | t_{sta} [min] | RC [%] |
| 100 | $L_{i,abs}$ | 27 | 50 | 77 | 8.04 |
| | $L_{i,str}$ | 25 | 118 | 143 | -0.02 |
| | Cap | 0 | 131 | 131 | -1.46 |
| | Prod | 21 | 40 | 60 | -1.48 |
| | T_{reb} | 0 | 25 | 25 | -1.04 |
| 80 | $L_{i,abs}$ | 31 | 113 | 144 | 8.19 |
| | $L_{i,str}$ | 37 | 112 | 149 | -0.01 |
| | Cap | 0 | 137 | 137 | -1.77 |
| | Prod | 25 | 21 | 46 | -1.78 |
| | T_{reb} | 0 | 35 | 35 | -1.05 |
| 60 | $L_{i,abs}$ | 35 | 67 | 102 | 7.85 |
| | $L_{i,str}$ | 29 | 813 | 842 | 0.00 |
| | Cap | 0 | 161 | 161 | -1.47 |
| | Prod | 31 | 22 | 52 | -1.46 |
| | T_{reb} | 0 | 39 | 39 | -0.99 |

Solvent circulation mass flow rate step changes resulted in inverse responses in CO₂ capture rates, refer to Figure 2. This can be explained by the coupled operation of the absorbers and desorber columns via the recycle loop. When increasing the solvent circulation flow rate (10%), the Cap increases during the first part of the transient. However, since the reboiler duty is kept constant, the lean loading at the inlet of the absorber $L_{i,abs}$ will increase (more solvent being circulated for the same regeneration energy introduced in the process \dot{Q}_{reb}), resulting in a reduction of Cap, with a delay imposed by solvent hold-ups (residence time) through piping and mixing components in the recycle loop.

Observe the large dead time in $L_{i,abs}$ in Figure 2. An analog explanation could be used for the inverse response observed when solvent circulation mass flow rate was reduced. Larger stabilization times were required when the plant was operated at lower loads, see Figure 3.

For these disturbances, CO_2 product mass flow rate $Prod$ stabilizes relatively faster (around 1 h) than CO_2 capture rate Cap (2–3 h). Similar stabilization times t_{sta} were noted when increasing (10%) and when decreasing (-10%) the solvent circulation mass flow rates \dot{F}_s .

The relative change in stripper inlet rich solvent loading $L_{i,str}$ was very small, so it can be considered constant when changing the solvent circulation rate by 10%. It shows that the solvent's capacity was working at the limit. However, lean loading $L_{i,abs}$ relative change was large. A large dead time was observed in $L_{i,abs}$ (27–47 minutes), due to the large amount of solvent inventory within the plant (residence time), and in the recycle loop. In addition, a settling time of 1 to 2 hours was observed, this is likely due to the buffering effect introduced by the absorber tank and other mixing components, such as, desorber and absorber sumps.

Table 6. Response of the main process variables to -10% step decrease in solvent circulation mass flow rate $\dot{F}_{s,a}$ and $\dot{F}_{s,b}$ at the inlet of the absorbers, for different GT loads. Dead times Θ , settling times t_s and total stabilization times t_{sta} are shown.

| GT load [%] | | -10 % | | | |
|-------------|-------------|----------------|-------------|-----------------|--------|
| | | Θ [min] | t_s [min] | t_{sta} [min] | RC [%] |
| 100 | $L_{i,abs}$ | 35 | 53 | 88 | -10.26 |
| | $L_{i,str}$ | 29 | 150 | 180 | 0.00 |
| | Cap | 0 | 118 | 118 | 2.05 |
| | $Prod$ | 26 | 29 | 55 | 2.03 |
| | T_{reb} | 0 | 8 | 8 | 1.09 |
| 80 | $L_{i,abs}$ | 35 | 74 | 108 | -10.60 |
| | $L_{i,str}$ | | | | 0.00 |
| | Cap | 0 | 125 | 125 | 2.11 |
| | $Prod$ | 30 | 33 | 64 | 2.85 |
| | T_{reb} | 0 | 37 | 37 | 1.13 |
| 60 | $L_{i,abs}$ | 43 | 71 | 115 | -9.47 |
| | $L_{i,str}$ | 37 | 788 | 825 | 0.00 |
| | Cap | 0 | 166 | 166 | 1.38 |
| | $Prod$ | 35 | 28 | 63 | 1.40 |
| | T_{reb} | 0 | 9 | 9 | 0.99 |

5.3 Response to step-changes in reboiler duty \dot{Q}_{reb}

Simulations in which reboiler duty \dot{Q}_{reb} was changed with step-changes by $\pm 10\%$ were performed. Flue gas conditions and solvent circulation flow rates were kept

constant at each operating point of the plant. The resulting response times of the PCC unit's main process variables are shown in Table 7 and Table 8.

Table 7. Response of the main process variables to 10% step increase in reboiler duty \dot{Q}_{reb} , for different GT loads. Dead times Θ , settling times t_s and total stabilization times t_{sta} are shown.

| GT load [%] | | 10 % | | | |
|-------------|-------------|----------------|-------------|-----------------|--------|
| | | Θ [min] | t_s [min] | t_{sta} [min] | RC [%] |
| 100 | $L_{i,abs}$ | 28 | 384 | 412 | -10.00 |
| | $L_{i,str}$ | 172 | 526 | 697 | -1.80 |
| | Cap | 31 | 69 | 100 | 9.54 |
| | $Prod$ | 0 | 322 | 322 | 9.70 |
| | T_{prod} | 0 | 335 | 335 | 1.09 |
| 80 | $L_{i,abs}$ | 33 | 419 | 451 | -9.42 |
| | $L_{i,str}$ | 247 | 531 | 778 | -1.52 |
| | Cap | 35 | 67 | 102 | 9.06 |
| | $Prod$ | 0 | 332 | 332 | 9.67 |
| | T_{reb} | 0 | 353 | 353 | 1.02 |
| 60 | $L_{i,abs}$ | 37 | 457 | 494 | -8.91 |
| | $L_{i,str}$ | 335 | 539 | 874 | -1.34 |
| | Cap | 40 | 87 | 126 | 9.24 |
| | $Prod$ | 0 | 606 | 606 | 9.44 |
| | T_{reb} | 0 | 368 | 368 | 0.96 |

Table 8. Response of the main process variables to -10% step decrease in reboiler duty \dot{Q}_{reb} , for different GT loads. Dead times Θ , settling times t_s and total stabilization times t_{sta} are shown.

| GT load [%] | | -10 % | | | |
|-------------|-------------|----------------|-------------|-----------------|--------|
| | | Θ [min] | t_s [min] | t_{sta} [min] | RC [%] |
| 100 | $L_{i,abs}$ | 28 | 56 | 85 | 8.448 |
| | $L_{i,str}$ | 44 | 694 | 739 | 0.008 |
| | Cap | 29 | 52 | 81 | -10.81 |
| | $Prod$ | 0 | 24 | 24 | -10.84 |
| | T_{reb} | 0 | 11 | 11 | -1.10 |
| 80 | $L_{i,abs}$ | 29 | 66 | 96 | 8.1519 |
| | $L_{i,str}$ | 92 | 685 | 777 | 0.0058 |
| | Cap | 34 | 65 | 99 | -10.62 |
| | $Prod$ | 0 | 27 | 27 | -10.63 |
| | T_{reb} | 0 | 13 | 13 | -1.05 |
| 60 | $L_{i,abs}$ | 37 | 72 | 109 | 7.88 |
| | $L_{i,str}$ | 93 | 403 | 496 | -0.006 |
| | Cap | 39 | 75 | 113 | -10.44 |
| | $Prod$ | 0 | 33 | 33 | -10.44 |
| | T_{reb} | 0 | 12 | 12 | -1.01 |

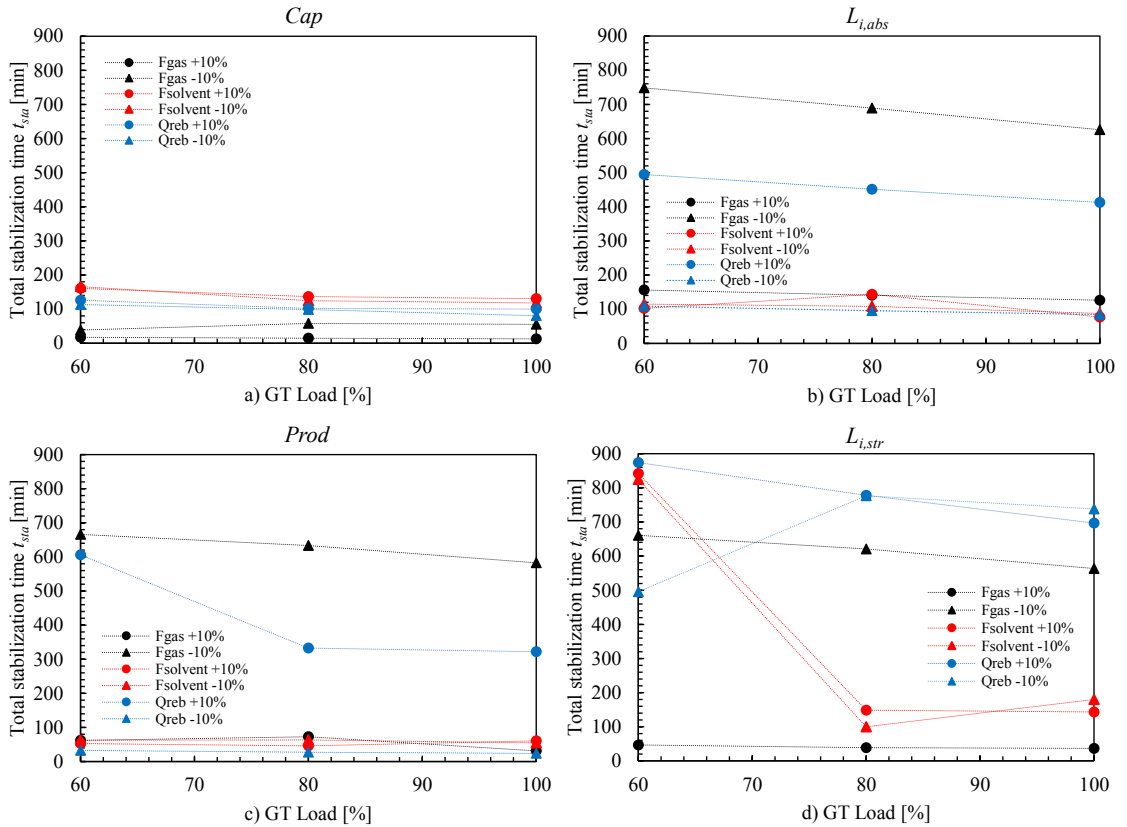


Figure 3. Trends in total stabilization times of main process variables of the PCC unit, when disturbed by the different plant input step changes, at different GT loads. a) CO₂ capture rate Cap ; b) Solvent CO₂ loadings at absorbers inlets $L_{i,abs}$; c) Product CO₂ mass flow rate $Prod$; and d) solvent CO₂ loading at stripper inlet $L_{i,str}$.

Increasing the reboiler duty will result in increased CO₂ capture rate Cap due to the lower resulting lean loading at the inlet of the absorber $L_{i,abs}$. Reducing reboiler duty will result in reduced Cap due to the increase in $L_{i,abs}$. A relatively large dead time in the Cap response of 28–37 min was found. This dead time was larger when the plant was operated at lower power plant loads. This is because at lower power plant loads solvent circulation rates are smaller (refer to Table 1), resulting in larger residence time through piping and mixing tank in the recycle loop.

The relative change in CO₂ product mass flow rate $Prod$ was also large, but with practically no dead time. This is because the reboiler duty introduced in the reboiler is physically closer to the overhead of the stripper. However, the recycle loop and coupled operation of the absorber and desorber makes the total stabilization time t_{sta} of the $Prod$ longer than for Cap . Observe the slow response in $L_{i,str}$ in Figure 3. In general, longer total stabilization times were found for

both Cap and $Prod$ when the plant was operated at lower loads, refer to Figure 3.

The relative change was also significant for lean loading at absorber inlet $L_{i,abs}$ with a large dead time, as previously mentioned. The dead times were even larger for rich loading at the inlet of the stripper $L_{i,str}$, and longer total stabilization times than for $L_{i,abs}$ were observed.

6 Conclusions

The open-loop transient performance of the main process variables of the plant were studied when the plant was operated at different power plant's load conditions, and for different disturbances to the PCC unit. In general, it is found that the plant was slower when the plant was operated at lower loads, i.e., it required longer total stabilization times for the main variables of the process. In general, CO₂ capture rate stabilized relatively faster (1–3 h) than other process variables (1–11 h).

In addition, it was found that the PCC unit responded significantly faster to the increase in flue gas mass flow rate than to reductions in flue gas mass flow rate. This could have significant implications on efficient operation of the PCC unit when ramping down the power plant's load, due to long stabilization times require of the process and the resulting inefficient operation during transient conditions, if a suitable control structure cannot be implemented.

Process variables respond differently to different disturbances. For the same process disturbance and process variable, the response was different when increasing or decreasing the input. This shows the non-linear behavior of the process. The recycle loop in the process from desorber outlet to absorber inlet connects the operation of the absorbers units and the stripper, and the resulting dynamic interaction between the absorption and desorption unit resulted in long stabilization time of main process variables, up to 11 h.

Current and future work includes the integration of the PCC unit with a dynamic process model of the power plant. That will allow the study of dynamic interactions between the power plant and the PCC unit under transient events of the power plant, and to analyze optimal control structures and operation of the integrated process for efficient flexible operation.

References

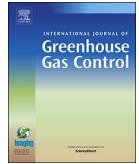
- Aske, E. M. B. & Skogestad, S., 2009. Consistent inventory control. *Industrial engineering chemistry research*, Volume 48, pp. 10892-10902.
doi: <http://pubs.acs.org/doi/abs/10.1021/ie801603j>
- Bui, M., Gunawan, I., Verheyen, V., Feron, P., Meuleman, E., Adeloju, S., 2014. Dynamic modeling and optimisation of flexible operation in post-combustion CO₂ capture plants - A review. *Computers and Chemical Engineering*, Volume 61, pp. 245 - 265.
doi: <http://dx.doi.org/10.1016/j.compchemeng.2013.11.015>
- Dutta, R., Nord, L. O. & Bolland, O., 2017. Selection and design of post-combustion CO₂ capture process for 600 MW natural gas fueled thermal power plant based on operability. *Energy*, Volume 121, pp. 643-656.
doi: <http://dx.doi.org/10.1016/j.energy.2017.01.053>
- Flø, N. E., 2015. *Doctoral Thesis: Post-combustion absorption-based CO₂ capture: modeling, validation and analysis of process dynamics*. Trondheim (Norway): Doctoral Theses at NTNU, 2015:244.
doi: <http://hdl.handle.net/11250/301562>
- IEA, 2011. *Harnessing Renewable Energies: A guide to the balancing challenge*, 9, rue de la Fédération, 75739 Paris Cedex 15, France: International Energy Agency.
- IEA, 2016. *20 years of carbon capture and storage - Accelerating future deployment*, Paris, France: IEA.
- IEA-GHG, 2012. *Operating Flexibility of Power Plants with CCS*.
- Kvamsdal, H. M., Jakobsen, J. P. & Hoff, K., 2009. Dynamic modeling and simulation of a CO₂ absorber column for post-combustion CO₂ capture. *Chemical Engineering Process*, Volume 48, pp. 135-144.
doi: <http://dx.doi.org/10.1016/j.cep.2008.03.002>
- Modelon AB, *Post-combustion capture with amine solutions*. Montañés, R. M., Flø N. E., Dutta, R., Nord, L. O., Bolland, O., 2017. Dynamic process model development and validation with transient plant data collected from an MEA test campaign at the CO₂ Technology Center Mongstad. *Energy Procedia*. (accepted for publication).
doi: 10.1016/j.egypro.2017.03.1284
- Montañés, R. M., Korpås, M., Nord, L. O. & Jaehnert, S., 2016. Identifying operational requirements for flexible CCS power plant in future energy systems. *Energy Procedia*, 86(TCCS-8), pp. 22-31.
doi: <https://doi.org/10.1016/j.egypro.2016.01.003>
- Panahi, M., 2011. *Ph.D. Thesis: Plantwide control for economically optimal operation of chemical plants - Applications to GTL plants and CO₂ capturing processes*. Trondheim: Norwegian University of Science and Technology. doi: <http://hdl.handle.net/11250/248272>
- Prölb, K., Tummerscheit, H., Velut, S. & Åkesson, J., 2011. Dynamic model of a post-combustion absorption unit for use in a non-linear model predictive control scheme.. *Energy Procedia*, 4(GHGT-11), pp. 2620-2627.
doi: <https://doi.org/10.1016/j.egypro.2011.02.161>

Paper V



Contents lists available at ScienceDirect

International Journal of Greenhouse Gas Control

journal homepage: www.elsevier.com/locate/ijggc

Demonstrating load-change transient performance of a commercial-scale natural gas combined cycle power plant with post-combustion CO₂ capture

Rubén M. Montañés^{a,*}, Stefanía Ó. Garðarsdóttir^b, Fredrik Normann^b, Filip Johnsson^b, Lars O. Nord^a

^a Department of Energy and Process Engineering, NTNU – Norwegian University of Science and Technology, Trondheim, Norway

^b Department of Energy and Environment, Chalmers University of Technology, Göteborg, Sweden

ARTICLE INFO

Keywords:

Natural gas
Post-combustion
Control
Dynamic simulation
Operational flexibility

ABSTRACT

The present work aims to study the transient performance of a commercial-scale natural gas combined cycle (NGCC) power plant with post-combustion CO₂ capture (PCC) system via linked dynamic process simulation models. The simulations represent real-like operation of the integrated plant during load change transient events with closed-loop controllers. The focus of the study was the dynamic interaction between the power plant and the PCC unit, and the performance evaluation of decentralized control structures. A 613 MW three-pressure reheat NGCC with PCC using aqueous MEA was designed, including PCC process scale-up. Detailed dynamic process models of the power plant and the post-combustion unit were developed, and their validity was deemed sufficient for the purpose of application.

Dynamic simulations of three gas turbine load-change ramp rates (2%/min, 5%/min and 10%/min) showed that the total stabilization times of the power plant's main process variables are shorter (10–30 min) than for the PCC unit (1–4 h). A dynamic interaction between the NGCC and the PCC unit is found in the steam extraction to feed the reboiler duty of the PCC unit. The transient performance of five decentralized PCC plant control structures under load change was analyzed. When controlling the CO₂ capture rate, the power plant performs in a more efficient manner at steady-state part load; however, the PCC unit experiences longer stabilization times of the main process variables during load changes, compared with control structures without CO₂ capture rate being controlled. Control of L/G ratio of the absorber columns leads to similar part load steady-state performance and significantly faster stabilization times of the power plant and PCC unit's main process variables. It is concluded that adding the PCC unit to the NGCC does not significantly affect the practical load-following capability of the integrated plant in a day-ahead power market, but selection of a suitable control structure is required for efficient operation of the process under steady-state and transient conditions.

1. Introduction

Atmospheric concentrations of CO₂ have increased by 40% relative to pre-industrial levels, primarily from fossil fuel emissions, and there is unequivocal base evidence that it is one of the major drivers of climate change (IPCC, Climate Change, 2013, 2014). Limiting climate change would require maintained and substantial reductions of anthropogenic greenhouse gas (GHG) emissions during the next decades and near zero GHG emissions by the end of the 21st century (IPCC, Climate Change, 2014). Nevertheless, it is expected that coal and natural gas will remain as important energy sources for electricity generation in long-term global prospects to 2040 (IEA, 2015). Implementation of carbon capture and storage technologies (CCS) can significantly reduce the life

cycle CO₂ emissions of fossil fuel power plants (Dixon et al., 2014).

Natural gas combined cycle power plants have moderate capital costs, short construction times and high efficiency and flexibility (Möller et al., 2007; IEAGHG, 2012). State-of-the art large-scale natural gas combined cycle (NGCC) power plants with three-pressure reheat configurations (3PRH) have recently reached lower heating value (LHV) fuel efficiencies of above 60% by different vendors (World, 2016). This LHV fuel efficiency is higher than most efficient coal-based power plants with up to 47% LHV fuel efficiency. In addition, at 350–450 kgCO₂/MWh, combined cycle power plants are less carbon intense than their coal-based counterparts at 750–1000 kgCO₂/MWh (IEA, 2016). These facts might drive the implementation of combined cycle natural gas-fueled power plants in the transition towards future

* Corresponding author at: Department of Energy and Process Engineering NTNU – Norwegian University of Science and Technology, Kolbjørn Hejes Vei 1b, Varmeteknisk * B347, NO – 7491, Trondheim, Norway.

E-mail address: ruben.m.montanes@ntnu.no (R. M. Montañés).

<http://dx.doi.org/10.1016/j.ijggc.2017.05.011>

Received 13 January 2017; Received in revised form 28 April 2017; Accepted 14 May 2017

Available online 03 June 2017

1750-5836/© 2017 Elsevier Ltd. All rights reserved.

| Nomenclature | |
|----------------------|---|
| AP | Absolute percentage error |
| Ar | Argon |
| Cap | Capture rate [%] |
| CCS | Carbon capture and storage |
| CH ₄ | Methane |
| CO ₂ | Carbon dioxide |
| CV | Control variable |
| CW | Cooling water |
| DA | Deaerator |
| DCC | Direct contact cooler |
| EGR | Exhaust gas recycle |
| F | Mass flow rate [kg/s] |
| F _a | Arrangement factor |
| FWC | Feedwater cooler |
| GHG | Greenhouse gas |
| GT | Gas turbine |
| h | Enthalpy [J/kg] |
| HP | High pressure |
| HPB | High pressure boiler |
| HPE2 | High pressure economizer 2 |
| HPE3 | High pressure economizer 3 |
| HPS0 | High pressure superheater 0 |
| HPS1 | High pressure superheater 1 |
| HPS3 | High pressure superheater 3 |
| HRSG | Heat recovery steam generator |
| H ₂ O | Water |
| IP | Intermediate pressure |
| IPB | Intermediate pressure boiler |
| IPE2 | Intermediate pressure economizer |
| IPS1 | Intermediate pressure superheater 1 |
| IPS2 | Intermediate pressure superheater 2 |
| K _b | Bauman factor |
| K _t | Flow area coefficient |
| LAC | Lean amine cooler |
| L/G | Liquid to gas ratio [kg/kg] |
| LHV | Lower heating value |
| LP | Low pressure |
| LPB | Low pressure boiler |
| LPS | Low pressure superheater |
| LTE | Low temperature economizer |
| MAP | Mean absolute percentage error |
| MEA | Monoethanolamine |
| MPC | Model predictive control |
| MV | Manipulable variable |
| NGCC | Natural gas combined cycle |
| NO _x | Nitrogen oxides |
| N ₂ | Nitrogen |
| O ₂ | Oxygen |
| PCC | Post-combustion CO ₂ capture |
| reb | Reboiler |
| RH1 | Reheater 1 |
| RH3 | Reheater 3 |
| RGA | Relative gain array |
| s | Solvent |
| SIMC | Simplified internal mode 1 control |
| ST | Steam turbine |
| SO ₂ | Sulfur oxides |
| T | Temperature [K] |
| TET | Turbine exhaust temperature |
| TIT | Turbine inlet temperature |
| TPM | Throughput manipulator |
| VIGVs | Variable inlet guide vanes |
| wt | Weight percent [kg/kg] |
| x | Vapor quality [kg/kg] |
| X | Mass fraction [kg/kg] |
| 3PRH | Three-pressure reheat |
| <i>Greek symbols</i> | |
| η | Efficiency |
| ρ | Density [kg/m ³] |
| λ | Thermal conductivity [W/m K] |

low-carbon energy systems in different areas of the world. As concluded in Johnsson et al., (2014), conventional NGCC power plants are likely to be serious competitors to coal with CCS in the short to medium term. According to the International Energy Agency, the global average carbon intensity of power plants being operated today is around 530 kgCO₂/MWh, which is still far away from the 100 kg/MWh global average required in the power sector to be consistent with a 2 °C climate scenario by 2050 (IEA, 2016). Therefore, in the medium to long term, CCS might be required to enable the reduction of CO₂ emissions from NGCCs by retrofitting existing units and extending their lifetime or by implementing novel advanced process configuration concepts with higher levels of process integration.

The most promising near-term technology to implement post-combustion CO₂ capture from combined cycle power plants is that of chemical absorption with solvents (IEA, 2008). NGCC power plants with PCC can reach carbon intensities of below 50 kg/MWh (Adams and Mac Dowell, 2016). Chemical absorption with 30%wt aqueous monoethanolamine (MEA) is commonly used as the benchmark solvent for most of the academic work related to integrated studies of NGCC power plants with post-combustion CO₂ capture based on process simulation.

The increasing share of variable renewable energy sources in electricity generation changes the operating role of base load thermal power generating units (IEA, 2011; Brouwer et al., 2015). NGCC power plants will be operated as load-following, with an increased number of start-ups and shutdowns, and providing fast cycling capabilities (Genrup and Thern, 2013). That includes thermal power plants with

CCS (IEAGHG, 2012; IEAGHG, 2016). The Carbon Capture and Storage update 2014 concludes that the financial case for CCS requires that it operates in a flexible manner, and load-following ability is considered extremely important for the long-term economics (Boot-Handford et al., 2014).

A key aspect of the operational flexibility of power plants with post-combustion CO₂ capture using amines is the steady-state design and part-load off-design performance of the power plant. Recent simulation studies have analyzed the part-load performance of the NGCC plant integrated with post-combustion CO₂ capture for different process configurations and process integration concepts (Jordal et al., 2012). These concepts include exhaust gas recycle (EGR), partial reboiler integration in the heat recovery steam generator (HRSG) and the eco-reboiler concept (Jonshagen et al., 2010). A previous work (Jordal et al., 2012) suggested that understanding the dynamic interaction between the power plant and the PCC unit remains a key aspect for developing the NGCC PCC technology. In addition, it was concluded in Adams and Mac Dowell (2016) that a key area of future work should be the inclusion of detailed dynamic process models of the power plant when analyzing the transient performance of the PCC plant integrated with post-combustion CO₂ capture.

The transient or time-dependent behavior of the chemical absorption PCC process is characterized by being relatively slow, compared to that of the combined cycle power plant. Despite the increased interest in carrying out transient test campaigns in pilot chemical absorption plants to assess the transient performance and operational flexibility of

the chemical absorption process with MEA (Jordal et al., 2012; Faber et al., 2011), most of the work to assess transient plant performance and control has been based on dynamic process simulation (Bui et al., 2014). Recent work by Flø et al. (2016) carried out open-loop step responses on the plant via dynamic process simulation of validated models, where they characterized the transient response of several process variables (outputs) to step changes in main inputs to the plant, concluding that one can expect long dead times and relatively large settling times – in the order of hours.

A key area of research within the dynamic operation of the PCC process is the development and analysis of plant-wide control strategies for the post-combustion capture process (Panahi and Skogestad, 2011; Nittaya et al., 2014; Walters et al., 2016; Panahi and Skogestad, 2012). Most of the published work focuses on flue gas from a coal-based power plant (Bui et al., 2014). In these analyses the flue gas is considered a disturbance to the process, and the steam coming from the power plant to feed the reboiler duty required to regenerate the solvent is considered as a boundary condition, omitting dynamic interactions between the power plant and the post-combustion capture unit. A recent report from the IEAGHG includes a literature review and assessment of control strategies for the PCC process (IEAGHG, 2016). It concludes and recommends that future work should include detailed dynamic process models of the power plant with advanced dynamic process modeling tools. Some studies have assessed simulation of the NGCC process with post-combustion CO₂ capture, however these works do not implement detailed dynamic process models and controllers of the power plant (Mechleri et al., 2017; He and Ricardez-Sandoval, 2016). He and Ricardez-Sandoval mention to have included a dynamic process model of the power plant in Aspen Plus® for analysis of the integrated process, but details on the dynamic process model of the power plant were not

presented, and it is stated that to simplify their analysis, the off-design dynamic performance evaluation of the gas turbine and steam turbine under transient operations were not included. Their work concludes that future work in this research should aim at developing suitable control strategies for the integrated system and to study the dynamic operability of the closed-loop under changes in the power plant.

Due to the lack of operational experience of the commercial-scale integrated NGCC power plant with PCC, there is a need to assess its load-following capability via dynamic process simulation. Previous plant-wide control studies found in literature omitted the dynamic interactions between the power plant and the PCC systems. The aim of this work is to assess the transient performance of the NGCC with PCC during load changes, in order to gain understanding of the dynamic interaction between the power plant and the PCC unit. The study includes the identification and evaluation of suitable decentralized control structures for the integrated process. Firstly, we describe the power plant process configuration and design procedure, including PCC process scale-up. Secondly, the process models of the gas turbine (GT), steam cycle and PCC system are described, with an emphasis on the detailed dynamic process models of the steam cycle. The validation of the dynamic process models is assessed. Then, the performances of different control strategies for both the power plant and the PCC plant are discussed. Finally, we demonstrate and explain the transient load change of the NGCC with PCC and assess the performance of different decentralized control structures for the integrated process.

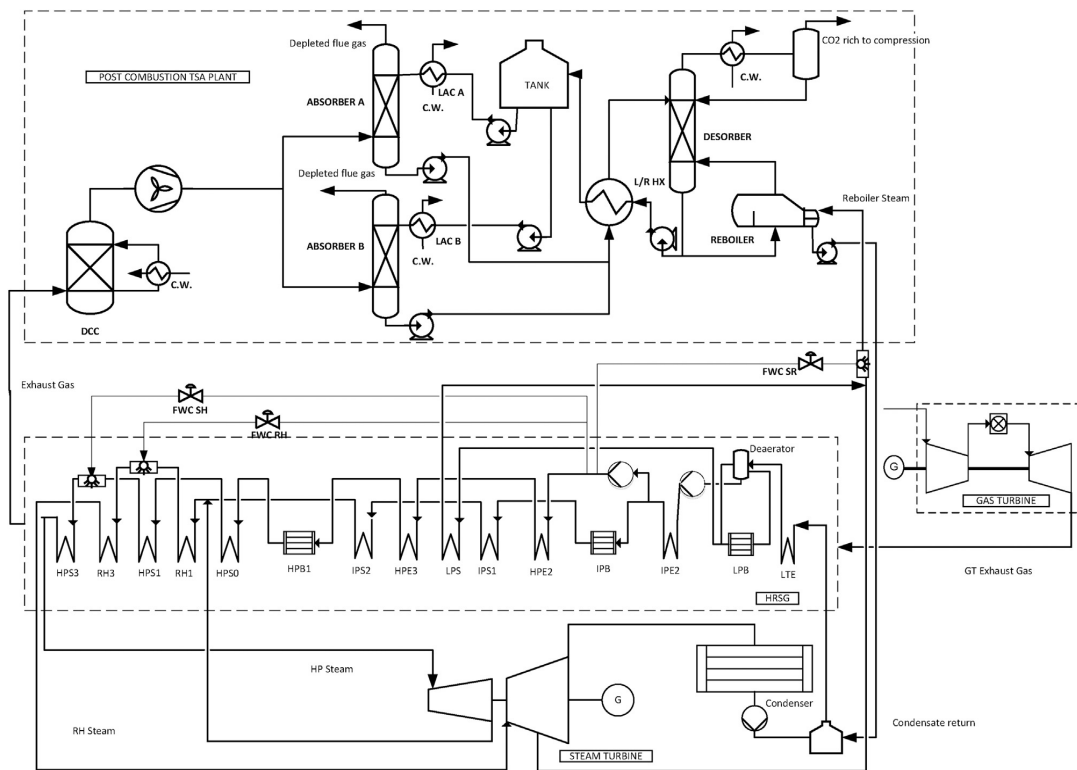


Fig. 1. Process flow diagram of the NGCC power plant integrated with post-combustion CO₂ capture.

2. Power plant description

2.1. Natural gas combined cycle power plant configuration

The NGCC power plant consisting of a 3PRH HRSG was designed by means of the process simulation software, ThermoFlow (ThermoFlow, 2014). As shown in Fig. 1, the NGCC has been designed considering the heat integration with the PCC plant. Steam extraction from the intermediate pressure (IP) and low pressure (LP) turbine crossover and steam from the LP superheater are mixed, de-superheated, and sent to the reboiler in order to feed the reboiler duty of the PCC system. The utilization of ThermoFlow (2014) allows detailed design data including main plant components' geometry, materials and process flowsheet to be obtained. In addition, it provides reliable steady-state full-load and part-load performance data of the plant, for both GT and steam cycle. These data reflect the current technology performance of the power plant and have been considered as a reliable source of plant performance under off-design loads in the literature (Jordal et al., 2012). Therefore, the performance data for off-design loads was used in this work as a reference for steady-state design and off-design validation of the dynamic process models of the combined cycle power plant configuration. In addition, detailed geometry, flowsheet and materials are required as inputs to parameterize the main dynamic process models of the steam cycle.

The key performance data at design load of the natural gas combined cycle power plant NGCC-PCC are shown in Table 1 including main steam cycle parameters. Fuel is assumed to be 100% CH₄, and the GT has a dry low NO_x combustor. The flue gas flow to the capture plant is assumed to be free of flue gas components SO₂ and NO_x.

2.2. Post-combustion CO₂ capture unit configuration

A post-combustion capture unit with 30% wt MEA as chemical solvent was designed with the commercial software, Aspen Plus[®] (A.T. Inc., 2014). The process configuration considered was the one with two absorbers and one stripper, as proposed by Jordal et al. (2012), following the methodology presented in Dutta et al. (2017). Modified process configurations, including absorber inter-cooling, solvent split flow or lean vapor recompression stripping, as studied by Amrollahi et al. (2011), were not considered in this paper. Therefore, no attempt was made to optimize the plant's steady-state performance.

The design point chosen for the post-combustion unit is 100% GT load under ISO conditions, which, for the Mitsubishi 701 JAC gas turbine, corresponds to flue gas with mass flow rate of 887.1 kg/s with 4.33 vol% CO₂ (wet). The design target CO₂ capture rate is 90% at 100% load operation. The flue gas from the HRSG is cooled from 126 °C down to 40 °C with a direct contact cooler (DCC) and fed to both absorbers (443.55 kg/s of flue gas per absorber at design conditions). Mellapak 350Y structured packing was selected for the absorbers and stripper. The diameter of the absorber columns was determined by setting 65% flooding limit for absorbers and 70% for stripper column, to be consistent with previous work in Jordal et al. (2012). Relevant input data for the simulations and scale-up of the PCC unit are shown in Table 2. Table 3 shows a list with main residence times and solvent hold-ups at design points in different parts of the PCC system. Residence times have been chosen according to data published in the literature (Flø, 2015).

2.3. Process integration

Two key integration aspects for this specific configuration of a NGCC-PCC plant are the exhaust gas from the HRSG stack sent to the chemical plant and the steam extraction from the steam turbine to feed the reboiler. Since CO₂ is captured from the GT exhaust gas, pressure drop will be imposed in the flue gas line by the HRSG recuperators and bypass-stack system with dampers, the DCC, the absorber column

packing and washer sections, and additional ducts and stacks. Most of this pressure drop is overcome by the GT. From an efficiency point of view, it is advantageous to let a fan, rather than the gas turbine, overcome this pressure drop. Therefore, a fan was included in the flue gas line after the DCC cooler to overcome the additional pressure drop imposed mainly by the absorber column.

A second important thermodynamic interface between the PCC process and the power plant is the steam extraction from the steam turbine to provide the heat required for solvent regeneration and to generate the stripping vapors flowing upwards through the stripper column. This integration aspect has been widely discussed in literature for both gas and coal-fired power plants with post-combustion CO₂ capture (Lucquiaud et al., 2009; Thern et al., 2014; Biyouki, 2014; Linnenberg et al., 2011). The most efficient method of providing that heat is to condense the steam extracted from the power plant. Due to solvent degradation problems, the temperature of the solvent in the reboiler should be limited within the range of 120–122 °C. Therefore, the supply temperature of the steam should at least be 130 °C at saturation, when considering a differential temperature approach to be at least 10 °C. This corresponds to a steam pressure of 2.7 bar. In addition, the process conditions for steam supply to the reboiler should be above these to overcome the piping pressure losses. In this work the integration methodology with steam extraction from the IP/LP crossover has been applied as presented in Biyouki (2014). The IP/LP crossover extraction option for reboiler heat integration has also been implemented in previous part-load performance studies for 3PRH power plant with post-combustion CO₂ capture with aqueous MEA as solvent (Rezazadeh et al., 2015). Steam extracted from the IP/LP crossover at 3.7 bar is mixed with steam from the LP superheater. The steam is de-superheated by water injection from the high pressure (HP) feedwater line of the HRSG (refer to FWC SR in Fig. 1). The HP water extraction is regulated by a throttling valve, with the objective of controlling the steam temperature of the superheated steam sent to the reboiler at 150 °C, with the purpose of preventing solvent degradation. Under design conditions, steam extracted from the IP/LP crossover, from the LP superheater and from the HP water extraction, represents, respectively, around 71%, 14%, and 15% of the total steam fed to the reboiler. Sufficient steam must be available at the extraction for solvent regeneration under part-load operation (Jordal et al., 2012). Steady-state off-design simulations conducted during this work revealed that enough steam is available at the extraction for part loads down to 60% GT load. The condensate from the reboiler is sent to a feedwater tank, where it is mixed with the feedwater coming from the steam turbine condenser. All feedwater is circulated to the low temperature economizer in the HRSG

Table 1
NGCC with PCC performance data summary.

| Gas Turbine | Mitsubishi 701 JAC |
|---|--------------------|
| GT Power Output [MW] | 451.8 |
| Fuel | CH ₄ |
| Fuel lower heating value [MJ/kg] | 50.047 |
| GT Exhaust mass flow [kg/s] | 887.1 |
| GT Exhaust temperature [°C] | 632 |
| HRSG efficiency [%] | 82.81 |
| Steam turbine gross power [MW] | 161.1 |
| Plant net LHV electrical efficiency [%] | 52.38% |
| HP pressure and temperature [bar/°C] | 145/591 |
| RH pressure and temperature [bar/°C] | 30/591 |
| LP pressure and temperature [bar/°C] | 3.69/290 |
| Crossover pressure [bar] | 3.69 |
| Condenser pressure and temperature [bar/°C] | 0.0483/32.25 |
| Cooling water temperature [°C] | 15 |
| HP/IP/LP dry section efficiencies [%] | 87.9/92.3/93.8 |
| HP turbine inlet flow [kg/s] | 111.15 |
| IP turbine inlet flow [kg/s] | 125.7 |
| LP steam generated in HRSG [kg/s] | 12.9 |
| LP turbine extraction flow [kg/s] | 3.7 |

Table 2

Absorber columns, heat exchanger and desorber design data (Jordal et al., 2012; Jilivero et al., 2014).

| Absorber columns | |
|--|---------------|
| Diameter [m] | 16.3 |
| Height [m] | 23.2 |
| Packing material | Mellapak 350Y |
| Design flooding limit [%] (Jordal et al., 2012) | 0.65 |
| Lean loading | 0.27 |
| Rich loading | 0.5 |
| Whole column pressure drop [bar] | 0.06 |
| Inlet gas velocity [m/s] | 1.9 |
| Pressure at top of column [bar] | 1.1 |
| Lean solvent inlet temperature [degC] | 40 |
| Stripper | |
| Diameter [m] | 9.7 |
| Height [m] | 10 |
| Packing Material | Mellapak 350Y |
| Pressure at top of column [bar] | 2 |
| Whole column pressure drop [bar] | 0.06 |
| Design flooding limit [%] (Jordal et al., 2012) | 0.7 |
| Heat Exchanger | |
| Average U-value [W/m ² K] (Jilivero et al., 2014) | 2000 |
| Lean-rich temperature approach [K] | 5 |
| Heat exchanger area [m ²] | 27855.3 |

Table 3

Residence time, volumetric flow and solvent hold-up at different parts of the PCC system, based on data from literature (Flo, 2015).

| | Residence time [min] | Volumetric flow solvent [m ³ /min] | Hold-up [m ³] |
|---------------------------------|----------------------|---|---------------------------|
| Absorber sump | 5 | 32.9 | 164.6 |
| Buffer tank | 16 | 68.8 | 1100.5 |
| Reboiler | 5 | | 353.2 |
| Desorber sump | 5 | 70.7 | 353.3 |
| Desorber sump and reboiler | 10 | 70.7 | 706.6 |
| Cross heat exchanger and piping | 26 | 66.8 | 1736.7 |
| Reboiler steam side | 1 | 5.9 | 5.9 |

(refer to Fig. 1).

Extracting steam from the steam turbine results in lower steam flow rate through the LP turbine and condenser and, hence, reduced turbine power output. The LP steam turbine has been sized for operation with the post-combustion system operating under full-load plant operation. This results in a smaller LP turbine, condenser and generator than if the LP turbine is designed for temporary CO₂ capture shutdown. Thern et al. (2014) discuss implications of temporary CO₂ capture shutdown for LP steam turbine design and performance. A recent study (Rezazadeh et al., 2015) discusses the impacts of non-capture operation on IP and LP turbine efficiency and condenser backpressure; it concludes that, if the NGCC plant is to be operated with an integrated post-combustion CO₂ capture scheme, it is not beneficial to operate it in a standalone mode (non-CO₂ capture operation), aside from inevitable situations such as CO₂ capture plant or compression train unit trip.

3. Dynamic process model description for power plant and post-combustion plant

3.1. Dynamic process models of the power plant

The dynamic process models in this work were developed with the open physical modeling language, Modelica (Modelica Association, 2017). The dynamic process models implemented in Modelica were obtained from the ThermalPower library (TPL) (Modeloon, 2015). The base models were utilized to build up the power plant model as

designed in Thermoflow (2014), by using the dynamic process-modeling environment, Dymola (Dassault Systems, 2017). Accumulation of energy and mass within process equipment is highly dependent on fluid inventories and equipment size. Therefore, dynamic process models from the ThermalPower library require design data of the equipment for model parameterization, obtained from Thermoflow (2014). Those data include equipment size, tube geometry, hold-up of vessels and residence times, wall materials, fluids' property packages, drum geometry and wall thickness.

3.1.1. Gas turbine model

It is a generalized approach in load-change transient modeling and simulation of combined cycles to omit the full dynamic process model of the GT (Dechamps, 1995; Dechamps, 1994). For transient applications, the GT is normally modeled with the block diagram approach to simulate its governor controls (Rowen, 1983; Can Gülen and Kim, 2013). In this work, a quasi-static approach is considered, in which the off-design performance of the GT exhaust's temperature and mass flow rate is implemented. Small variations in exhaust gas composition were disregarded, since those were found to be small for the operating window studied in this work. A common procedure is to simulate the steady-state off-design performance of the GT and include the key characteristics of the exhaust as a disturbance to the dynamic process model of the HRSG and turbine island. By assuming a ramp rate, a turbine exhaust time series can be tailor-made to simulate the GT load change; refer to Fig. 2. This method is justified because of the faster transient performance of the GT than that of the steam cycle due to the HRSG thermal inertia (Can Gülen and Kim, 2013). Hence, the GT exhaust characteristics for different loads were modeled as a disturbance to the HRSG gas-side process models. The exhaust gas from the gas turbine, consisting of a mixture of Ar, H₂O, O₂, N₂ and CO₂, is modeled with the ideal thermodynamic equation of state, and thermochemical properties are calculated using a seven-coefficient version of the NASA ideal gas properties.

A steady-state model in Thermoflow (2014) was used to obtain the validated part-load performance of this GT. Table 4 shows the main performance values of the GT at loads from 100% to 60%, for ISO ambient conditions. Fig. 2 includes the steady-state off-design loads' gas turbine characteristics in terms of exhaust temperature, mass flow rate and gross power. Fig. 3 shows the time-dependent exhaust temperature and mass flow for an event with load reduction from 100% GT load to 80% GT load, with a typical GT load reduction of 5%/min (Genrup and Thern, 2013). Load change rate from one load point to another would be typically 4–5% per min, for both load increase and load decrease, for a combined cycle (Genrup and Thern, 2013; Jordal et al., 2012).

3.1.2. Heat recovery steam generator, deaerator and condenser models

The heat recovery steam generator of this plant consists of

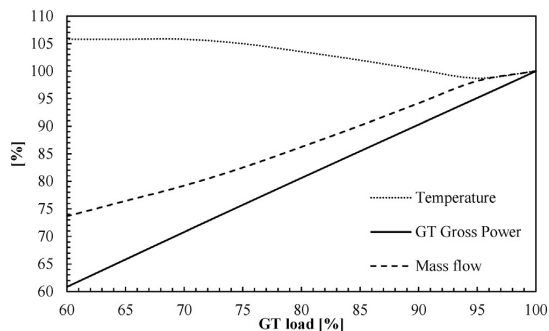


Fig. 2. GT exhaust characteristics at different steady-state off-design loads with ISO ambient conditions.

Table 4
Main performance values of the Mitsubishi 701 JAC for ISO ambient conditions, at different off-design loads.

| GT Load% | 100 | 95 | 90 | 85 | 80 | 75 | 70 |
|--|--------|--------|--------|-------|-------|-------|-------|
| GT gross power [MW] | 451.8 | 429.7 | 407.9 | 386.1 | 364.2 | 342.1 | 319.8 |
| GT fuel LHV chemical energy input (77F/25 °C) [MW] | 1081.5 | 1038.7 | 1002.1 | 965.2 | 927.5 | 889.1 | 849.2 |
| Turbine exhaust mass flow [kg/s] | 887.1 | 871.2 | 835.4 | 799.4 | 765.1 | 731.9 | 702.7 |
| Turbine exhaust temperature [C] | 632 | 623.8 | 633.8 | 644.5 | 654.3 | 663.4 | 668.5 |
| Exhaust gas N ₂ mole fraction [%] | 73.97 | 74.04 | 74.02 | 74 | 73.99 | 73.98 | 74 |
| Exhaust gas O ₂ mole fraction [%] | 11.25 | 11.46 | 11.4 | 11.34 | 11.3 | 11.28 | 11.33 |
| Exhaust gas CO ₂ mole fraction [%] | 4.33 | 4.23 | 4.26 | 4.29 | 4.30 | 4.31 | 4.29 |
| Exhaust gas H ₂ O mole fraction [%] | 9.56 | 9.38 | 9.43 | 9.48 | 9.52 | 9.53 | 9.49 |
| Exhaust gas Ar mole fraction [%] | 0.89 | 0.89 | 0.89 | 0.89 | 0.89 | 0.89 | 0.89 |

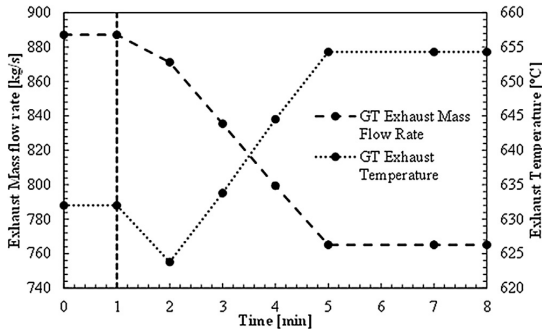


Fig. 3. Time-dependent tailor-made GT exhaust characteristic considering a quasi-static modeling approach. GT load reduction from 100% to 80% load. Transience starts at minute one.

horizontal three-pressure levels with reheat system. It has three drum systems with evaporator (LPB, IPB, HPB), including an integrated LP drum and deaerator system (LPB and DA). In addition, there are a total of 12 finned tube flue gas to water and steam recuperators. The recuperators consist of four economizers (LTE, IPE2, HPE2 and HPE3), six superheaters (LPS, IPS1, IPS2, HPSO, HPS1 and HPS3) and two reheaters (RH1 and RH3). Two inter-stage superheated steam temperature control systems are implemented: one between the last two superheaters and the other between the two reheaters. Such systems use high pressure water from the HP feedwater line upstream of the high pressure economizer, HPE2. The HP water is injected into the pipe between the superheating and reheating stages, and consequently the temperature is reduced by evaporative cooling. A valve implemented for the extraction is manipulated to change the HP water mass flow rate and hence control the temperature of the steam sent to HP and IP steam turbine intakes. The water and steam thermophysical property package is implemented by using the IAPWS-IF97 standard, with analytic derivatives (Wagner et al., 2000).

The heat exchanger recuperator model is built from base physical process components of hot side piping, conductive heat transfer wall and cold side piping. Both pipes and wall are discretized in the axial direction, and heat transfer equations are solved in a discretized manner. The process model configuration assumes counter-current flow, while the physical configuration is cross-flow. Note that, in a HRSG heat exchanger the entire metal mass has a specific geometry with bare tubes with serrated fins on them. As discussed in Dechamps (1994), for transient simulations, an important consideration is the wall temperature evolution over time. A typical approach is to consider the whole heat exchanger metal mass as a lumped metal cylinder, since in the exhaust flow gas path the tubes are quite close to each other and have a high density of fins; thus, the entire heat exchanger is substituted by a lumped cylinder with the same mass (volume and density) and external heat transfer surface area as the real heat exchanger (HX) (Can Gülen and Kim, 2013). The cylinder has a wall thickness equivalent to

that of a single tube and geometry (length and diameter) and is calculated so as to consider the overall heat transfer area and metal mass as the actual heat exchanger. Therefore, the hypothetical heat exchanger model is a 1-D counter-current model, which is then discretized in the axial direction in n volumes.

The dynamic discretized pipe models are implemented with a similar modeling approach for both gas and water/steam side. For the gas side, mass, mass fraction and energy balance equations are discretized by means of the finite volume method, with n the number of volume segments. For this work, static balances on the gas side have been considered, since such processes are relatively fast (Dechamps, 1995). A uniform velocity is assumed in the cross-section leading to a 1-D distributed parameter model. The state variables are mass fractions, n temperatures and a lumped pressure. The energy balance equation is written by assuming a uniform pressure distribution, and the pressure drop calculation is lumped at the piping outlet. Longitudinal heat transfer diffusion is neglected within the pipe.

For the water/steam side, the model allows for calculation of both fluid states with one-phase or two-phase mixture, and it uses the integrated mean density and lumped pressure approach. The model consists of dynamic mass and energy balances with static momentum balance; equations are discretized as well by means of the finite volume method, with n the number of volume segments.

Fluid flows in the pipes can exchange thermal power through the lateral heat surfaces, which are connected to the wall process model. This allows the calculation of convective heat transfer between the water/steam fluid bulk and the wall's inner surface, and between the gas bulk and the wall's outer surface. A wall model for transient conductive heat transfer, considering the capacity of the metal to store heat (thermal inertia) and the resistance for conductive heat transfer, is implemented in the HX model. The wall is discretized in n segments in the longitudinal direction. Longitudinal wall conductive heat transfer is neglected. For this application, a discretization of the wall model in the radial direction was not considered, but it would be possible to do so for thermal stress estimation applications, as presented by Benato et al. (2015).

The convective heat transfer coefficient for 1-phase gas flow over tube bundles is modeled continuously with a Nusselt correlation covering the entire flow region, and the flow is considered to be thermally and hydraulically developed. The heat transfer coefficient h_g is computed for each segment as in Eq. (1), where F_a is a tube arrangement factor, λ is the thermal conductivity of the gas and d_{hyd} is the hydraulic diameter of the pipe. The Nusselt number for each row is calculated by Reynolds-dependent correlations from (G.V.-G.V.u., 1997).

$$h_g = \frac{F_a Nu_0 \lambda}{d_{hyd}} \quad (1)$$

For the water side, a heat transfer correlation has been considered for estimating the convective heat transfer coefficient for superheaters, h_s , for 1-phase; see Eq. (2). A similar formulation is employed for economizers. The mean Nusselt number, Nu_m , is calculated by Reynolds-number-dependent correlations from (G.V.-G.V.u., 1997).

$$h_s = \frac{Nu_m \lambda}{d_{hyd}} \quad (2)$$

For the two-phase flow in the evaporators, a constant heat transfer coefficient of 120 kW/m²K for the cold side was considered. The pressure drop in both the cold and hot sides is computed with Colebrook’s equation, where the hydraulic friction coefficient *f* is specified by the nominal operating point (mass flow rate, pressure drop and density).

The main function of a drum in a subcritical HRSG is to separate the steam from the liquid water, at a given pressure level. Transient phenomena and dynamic modeling of drum boilers has been studied extensively (Åström and Bell, 2000). As described in Eborn (2001), one difficulty in power plant control is the drum-level control problem, due to the known shrink and swell effect. The drum model available in the ThermalPower library is capable of capturing pressure and drum-level dynamics and includes wall dynamics. The model describes the cylindrical drum of a drum boiler, where there is no thermodynamic equilibrium between the liquid and gas hold-ups. The drum and evaporator dynamic process model included in TPL (Modeloon, 2015) uses the formulation described in Francesco Casella (2003). The required parameterization of the model is mainly the equipment data (geometry and material properties). Natural circulation in the drum-evaporator system was implemented by means of an ideal height difference model with pressure head for modeling the downcomers and risers of the system.

In a steam power plant, the main function of the deaerator is the removal of non-condensable gases such as CO₂ and O₂. The objective is to avoid synergetic corrosion effects within the water tubes of the HRSG, which would reduce the lifetime of the plant considerably (Bolland, 2014). In this case, the deaerator model is simulated to consider the water/steam inventory under transient conditions. Therefore, the medium in the process model is water/steam. The dynamic process model assumes thermodynamic equilibrium between the liquid and vapor hold-ups (same temperature and pressure), and takes into account variable hold-ups (level and pressure must be controlled).

The condenser model is a model of a cylindrical condenser that assumes thermodynamic equilibrium between vapor and liquid hold-ups. In addition, a dynamic wall model accounting for transient wall effects is included in the model. The wall separates the condensing steam from the cooling media. The wall model considers the capacity of the tubes to store heat under transient conditions. The cooling liquid heat transfer uses a liquid correlation, valid for both laminar and turbulent flow. It uses a logarithmic average of the cooling inlet and cooling outlet temperatures as the driving temperature. A correlation for heat transfer condensation over tube bundles has been implemented for the water/steam side of the condenser (G.V.-G.V.u., 1997). The model includes a hotwell that collects the liquid hold-up. The level of water in the hotwell has been decided by considering the design inventory of water in the condenser, as defined in Thermoflow (Thermoflow, 2014). The cooling water inlet temperature and the mass-flow under part-load conditions are maintained as constant.

Table 5
Validation of the power plant model under off-design GT load operation.

| GT Load | ST gross power [MW] | | | HP admission pressure [bar] | | | RH admission pressure [bar] | | |
|---------|---------------------|--------|--------|-----------------------------|--------|--------|-----------------------------|--------|--------|
| | GT pro | Dymola | Error% | GT pro | Dymola | Error% | GT pro | Dymola | Error% |
| 100 | 161091 | 161444 | 0.22 | 145 | 145.3 | 0.20 | 30 | 30.4 | 1.23 |
| 95 | 154716 | 154767 | 0.03 | 139.2 | 139.9 | 0.55 | 28.9 | 29.2 | 0.98 |
| 90 | 153359 | 153260 | 0.06 | 137.3 | 137.3 | 0.02 | 28.5 | 28.8 | 1.11 |
| 85 | 151046 | 151020 | 0.02 | 133.8 | 133.6 | 0.17 | 28.2 | 28.5 | 1.08 |
| 80 | 148347 | 148373 | 0.02 | 130.2 | 129.7 | 0.37 | 27.8 | 28.2 | 1.19 |
| 75 | 145356 | 145343 | 0.01 | 126.5 | 125.8 | 0.58 | 27.3 | 27.6 | 0.99 |
| 70 | 141617 | 141501 | 0.08 | 122.5 | 121.6 | 0.74 | 26.6 | 26.9 | 0.96 |
| MAP | | | 0.06 | | | 0.38 | | | 1.08 |

3.1.3. Steam turbine models

For the range of part-load operation considered in this study (100–60% GT load), the steam cycle of the combined cycle plant is operated under sliding pressure operation mode (Kehlhofer et al., 2009). The steam turbine model is assumed as a quasi-static model. This is justified because the purpose of the transient model is to simulate the load-following transient event; therefore, the main thermal inertia of the system consists of the HRSG inertia (Dechamps, 1994). Effects of steam turbine rotor dynamics and steam turbine casing and rotor thermal inertia are not of interest here, since those are normally relatively fast. Therefore, dynamic interactions between the power grid and the steam cycle in terms of real-time frequency control-related transients are neglected, as those are outside the scope of this work. Steam turbine expansion is defined by the swallowing capacity and the isentropic efficiency. Stodola’s law of cones is used to define the swallowing capacity of the turbine (Eqs. (3)–(4)), where *K_t* is the flow area coefficient, based on the nominal flow conditions of pressure and density, subscript *n* stands for nominal conditions, *i* for inlet, *o* for outlet, and *F_t* for mass flow through the turbine.

$$K_t = \frac{\dot{F}_n}{\sqrt{p_{i,n} \rho_{i,n} \left(1 - \left(\frac{p_{o,n}}{p_{i,n}}\right)^2\right)}} \quad (3)$$

$$\dot{F}_t = K_t \sqrt{p_i \rho_i \left(1 - \left(\frac{p_o}{p_i}\right)^2\right)} \quad (4)$$

Turbine expansion was assumed to have constant isentropic efficiency under variable loads. For different loads, the steam turbine has approximately constant volumetric flow. This helps to keep the velocity triangles of the stages approximately constant, and therefore the efficiency remains approximately unchanged (Bolland, 2014). Dry isentropic efficiencies were assumed to be 0.88, 0.923, and 0.931, for the HP, IP and LP sections, respectively. In addition, the efficiency of the LP section of the steam turbine has been corrected for the moisture content, since the expansion crosses the Wilson line (Bolland, 2014). The dry efficiency degradation is a function of the steam quality and can be expressed by Bauman’s formula, Eq. (5). The Bauman’s coefficient *K_b* has been set to 0.8 (Bolland, 2014). A simplified generator model is included to account for mechanical shaft and generator losses, with a constant mechanical efficiency of 0.98.

$$\eta_{is} = \eta_{is,dry} \cdot (1 - K_b \cdot (1 - x_{mean})) \quad (5)$$

3.2. Dynamic process model of the post-combustion CO₂ capture plant

The dynamic process models for the main equipment of the PCC plant are implemented in the Modelica language. A library called Gas Liquid Contactors (Modeloon, 2017), containing dynamic process models of the main equipment of the PCC unit, has been utilized as a basis for this work. For a detailed description of the models and equations, the

reader should refer to Garðarsdóttir et al. (2015) and Pröhl et al. (2011). The Modelica models were calibrated to fit the design point data from the AspenPlus® design of the two-absorber and one-desorber scaled-up plant, as described in Table 2. Calibration included matching temperature profiles of the absorber and desorber columns, lean/rich loadings at the inlet and outlet of columns and absorption and desorption rates. The main calibration factor was the enhancement factor for chemical reactions.

4. Process model validation

The power plant dynamic process model has been validated against steady-state data for both design and off-design conditions by comparing the results obtained from Thermoflow (Thermoflow, 2014). Absolute percentage errors AP in Table 5 are calculated based on Eq. (6), while mean absolute percentage errors MAP are based on Eq. (7), where R_t is the reference value and S_t is the value from simulations.

$$AP = 100 \left| \frac{R_t - S_t}{R_t} \right| \tag{6}$$

$$MAP = \frac{100}{n} \sum_{i=1}^n \left| \frac{R_t - S_t}{R_t} \right| \tag{7}$$

The gas side HRSG’s temperature profile under design conditions was validated, and mean absolute error was found to be 0.16%, maximum absolute error being 0.62% (not shown). Table 5 includes validation results of the steam turbine gross power, HP and RH steam admission pressures for different GT loads.

The transient performance in terms of steam turbine power output showed correct behavior in respect of 99% settling time for load changes with a 5%/min GT load ramp rate. Note that, by settling time, we mean here the time required for the response curve to reach and stay within a range of 1% of the final value. These settling times were similar to those reported in Thermoflow software (Thermoflow, 2014). In addition, a similar modeling methodology for predicting transient performance of NGCCs has been utilized in literature (Benato et al., 2015), resulting in similar settling times of 6–9 min. This means that the dynamic process model of the power plant is also capable of

capturing the process dynamics with high fidelity. Therefore, it can be concluded that the power plant dynamic process model is capable of predicting proper steady-state performance under different loads to an appropriate level of accuracy, required for the analysis, and predicts transient trends under load change transient event driven by the GT load reduction.

The models of the post-combustion capture plant were validated in a recent work by Montañés et al. (2017). That work uses large-scale steady-state and transient data from an amine pilot plant with flue gas from a natural gas-fired power plant at CO₂ Technology Center Mongstad (2017).

5. Proposal of different control structures

The day-to-day operation of thermal plants can be handled by closed-loop control (Kehlhofer et al., 2009). The main objective of the control system is to provide load control and frequency response. Frequency response is utilized when sudden increases or decreases in electrical power load are required (Montañés et al., 2016) and is normally provided by the gas turbine and by the steam turbine if it is designed to do so. The load of the combined cycle is controlled by means of the GT load reduction/increase. The steam cycle will follow the GT load change by providing power with the available steam generated in the HRSG. Once a GT load change is applied, the steam turbine load will adjust automatically with a time delay of about 10–15 min (Kehlhofer et al., 2009), normally defined by the thermal inertia added by the HRSG. In this regard, the GT load change can be seen as a disturbance to the steam cycle. In addition, from the PCC plant’s perspective, the exhaust gas coming from the NGCC power plant is a disturbance to the process; thus, the control system of the PCC plant must be capable of handling this disturbance under load changes.

The control system of a process plant is typically designed in a hierarchical manner, with different tasks assigned to different control layers. As described in the literature (Kehlhofer et al., 2009; Skogestad and Postlethwaite, 2005), the control layer of a chemical and a power plant can be divided into two main layers: the regulatory control layer (“base control”) and the supervisory control layer (“advanced control”).

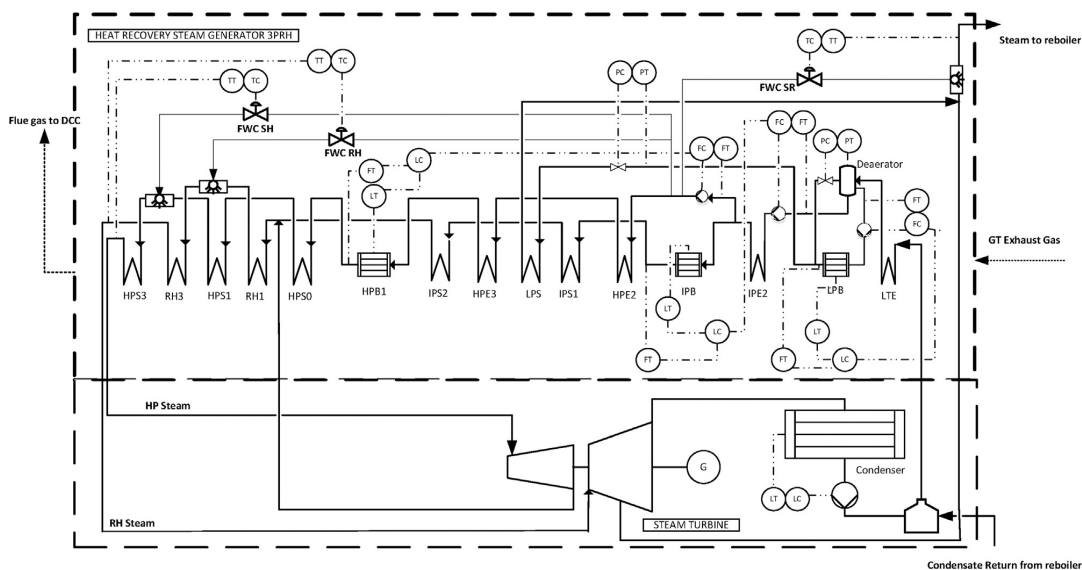


Fig. 4. Power plant control layers. For controllers, the first letter stands for temperature (T), pressure (P), level (L) or flow rate (F), while the second letter stands for controller (C) or transmitter (T).

- Regulatory control layer: The main task of the regulatory control layer is to stabilize the plant's drifting variables under fast disturbances and keep these variables close to the set-points in the fast timescale. Stabilization here means that the process does not drift away from acceptable operating conditions under disturbances. This normally implies controlling temperatures, pressures and levels, and having a consistent inventory control structure (Aske and Skogestad, 2009).
- Supervisory control layer: The supervisory control layer is used to control variables that are more important from an overall point of view, i.e., in a longer timescale. It is the slower upper layer that acts on the set-points of the regulatory control layer or remaining degrees of freedom. This layer will be in charge of supervising load changes.

In the following, the control structures implemented in the dynamic process models are presented. Functions related to logic on start-up/shut-down and safety systems of the plant were not included in this work.

5.1. Control layers for combined cycle

The gas turbine in a combined cycle is normally provided with a standardized control system and therefore the gas turbine supplier provides an engine that is already automatized for operation. The gas turbine load is controlled by the combination of variable inlet guide vanes (VIGVs) and fuel mass flow rate (Kehlhofer et al., 2009). VIGVs allow modification of the air mass flow rate input to the gas turbine. The main objective during part-load operation is to keep high turbine inlet temperatures (TIT) and turbine exhaust temperatures (TET) under part loads, since that will allow highly efficient part-load operation of the steam cycle. TIT is normally controlled by a combination of fuel flow input and the position of the VIGVs; this keeps high levels of both TIT and exhaust gas temperature at part loads. In modern gas turbines, this strategy can be utilized down to about 40% GT load, from which the VIGVs saturate and air mass flow rate cannot be further reduced. Lower loads can be achieved by further reducing fuel input flow rate,

but the TIT cannot be kept at high values. In this work the GT model is a quasi-static model. To control the steam production in the HRSG at part loads, a strategy called sliding pressure operation is normally implemented. With sliding pressure operation mode, the steam turbine inlet control valves are fully open, so that the admittance pressure is sliding or floating. This allows high levels of efficiency to be maintained in the steam cycle, compared with strategies in which the HRSG steam pressures are controlled by valve throttling, partial arc admission or hybrid configurations (Jonshagen, 2011). Sliding pressure operation is normally applied down to approximately 50% live-steam pressure, from which a control strategy based on pressure control via valve throttling is applied (Kehlhofer et al., 2009). Valve throttling will be required under normal operation to provide a fast frequency response, if the steam cycle is designed to do so.

Fig. 4 shows the regulatory control layer implemented in the steam cycle. It includes the essential control loops that are required in order to ensure stable steam cycle operating conditions in the combined cycle power plant under stable operation and for load changes driven by GT load changes. The controllers were implemented in the dynamic process models and are described as follows:

- Live-steam temperature control (FWC-SH, FWC-RH and FWC-SR): The temperature of the live steam (superheated, reheated and steam sent to reboiler) must be controlled to limit the temperature peaks that occur during off-design operation. High pressure feedwater is injected in between the superheaters and reheaters into the live steam to cool it down. In this work, proportional and integral (PI) controllers on control valves were implemented. The superheated steam sent to the reboiler must come at suitable temperatures required for the proper operation of the reboiler. Therefore, it was controlled by injecting high-pressure feedwater from the HRSG with a PI controller on a control valve.
- Drum level control: A three-element controller was applied for the three drums (LP, IP and HP) in the process. Drum level, feedwater and live-steam flows are measured. These signals were processed in a cascading manner (Basu and Debnath, 2015) so that the controllers decide on the feedwater valves' opening.

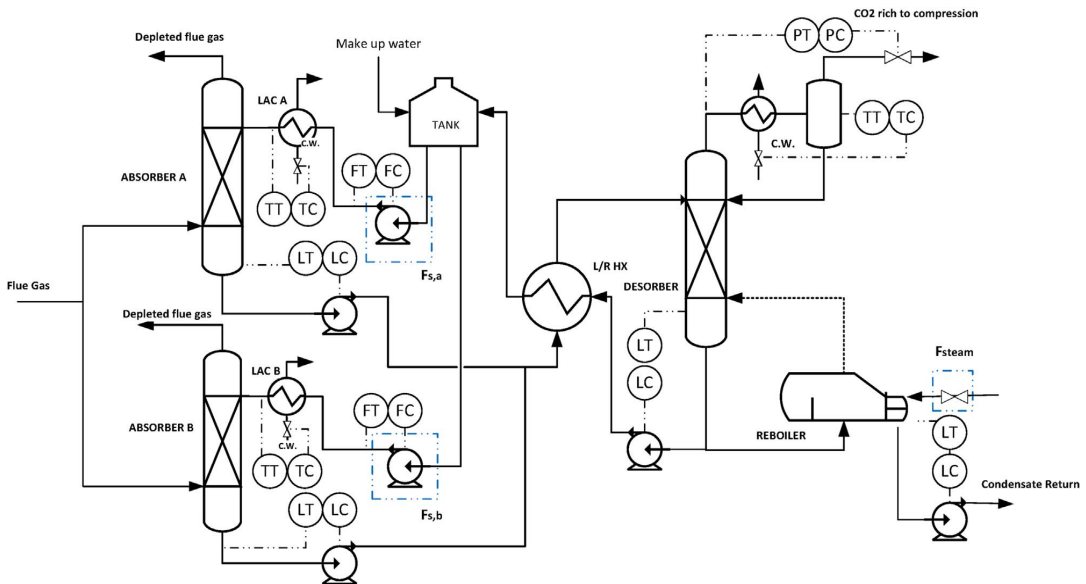


Fig. 5. Control layer of the post-combustion capture system. $F_{s,a}$, $F_{s,b}$ and F_{steam} are the main degrees of freedom of the plant. For controllers, the first letter stands for temperature (T), pressure (P), level (L) or flow rate (F), while the second letter stands for controller (C) or transmitter (T).

- The pressure of the LP drum and that of the deaerator are controlled; refer to Fig. 4.
- A level controller was applied to the condenser howtwell; refer to Fig. 4.

5.2. Control layers of the post-combustion plant

Rules for consistent inventory control were followed (Aske and Skogestad, 2009) in order to design the regulatory control layer of the PCC system. An important decision is to select the location of the throughput manipulator for the amine/water solvent circulation, i.e., the mass flow rate of the recycled solvent circulating through absorber and stripper. For this configuration with two absorbers in parallel, there are two throughput manipulators (TPMs). Those two have been located at the inlet of the absorber; therefore, the TPMs are the solvent flow rates at the inlet of the absorbers $F_{s,a}$ and $F_{s,b}$. This defines the direction of the level controllers for absorber sumps and stripper sump. For this process configuration, the main drifting variables that need to be controlled to ensure stable operation of the PCC plant are:

- Rich solvent temperatures at the inlet of the absorbers.
- Absorber sumps and stripper sump levels.
- Stripper pressure.
- Condenser temperature.
- Reboiler steam/water side level.
- Make-up water.

The “pairings” or inputs utilized to control the above-mentioned drifting variables are shown in Fig. 5. During pilot plant operation, MEA concentration is manually monitored onsite by periodic lab samples. MEA concentration is adjusted to (30 wt%) by the addition or extraction of water (Bui et al., 2016). For practical implementation in the dynamic process model, the water injected/rejected from the PCC plant is the amount required to have a water mass balance of the overall PCC plant; water is added/rejected in the surge tank based on the measured water flow rate inlet to the absorbers, outlet to the absorbers and outlet to stack. MEA make-up was not introduced because the process model assumes that MEA is non-volatile and does not leave the plant through the absorber.

The supervisory control layer of the PCC plant for this process configuration has three degrees of freedom, consisting of lean solvent flow rates to the absorber $F_{s,a}$ and $F_{s,b}$ and steam mass flow rate to the reboiler F_{steam} . These degrees of freedom will be used to control different process variables, depending on the operational strategy and objectives of the plant. Based on a literature study, five decentralized control structures were studied for load-change operation of the full power plant with PCC; refer to Table 6. Choosing appropriate tuning rules is of importance. Controller tuning was carried out based on simplified internal model control (SIMC) tuning rules, which are analytically derived and are well-suited for processes with large dead times and long stabilization times (Skogestad and Grimholt, 2012).

Panahi and Skogestad (2011, 2012) carried out a plant-wide control procedure for the post-combustion capture process with flue gas from a coal-fired power plant source, based on self-optimizing control theory (Skogestad and Postlethwaite, 2005). Their study concluded that the two main self-optimizing control variables (CVs) are the CO₂ capture rate Cap at the outlet of the absorber and the temperature of a tray within the stripper (T_{str}). They evaluated four decentralized control

structures based on different pairings of the above mentioned manipulable variables (MVs) and CVs and different regions of operation of the plant. They also evaluated a model predictive control scheme (MPC), concluding that MPC might not be required for base-load operation. Nittaya et al. (2014) evaluated three different control structures under disturbances from coal-fired power plants with absorber-desorber PCC system; they studied different control structures based on a static relative gain array (Chinen et al., 2016) analysis and heuristic approaches. The control structures were evaluated under different scenarios, including CO₂ capture rate set-point change and changes in flue gas flow rate. Their study concludes that decentralized control structures A and B (see Table 6) showed the best performance in respect of disturbances and set-point tracking, considering different operational objectives. Control structures A and B have CO₂ capture rate at top of absorber columns as CVs, see Table 6, and were selected for further study with the integrated dynamic process model of the power plant. The results are presented in Scenario 2 Case 1, in Section 6.2.1.

In addition, control structures in which the CO₂ capture rate is not a constraint or operational objective were studied. Since changes in solvent circulation rate can result in large dead times and total stabilization times of the main process variables of the plant (Flø et al., 2016), control structure C with constant solvent circulation rates was studied. In addition, ratio control on solvent circulation rate to keep constant liquid to gas (L/G) ratio in the absorber at part-load operation was considered, with T_{reb} controlled by F_{steam} (structure D) and ratio control on F_{steam} (structure E), as proposed in Ceccarelli et al. (2014). The results are presented in Scenario 2 Case 2, in Section 6.2.2.

6. Results and discussion

6.1. Scenario 1: performance of the NGCC-PCC during load change

The transient performance of the integrated power plant during load change driven by GT load reduction was studied for different ramp rates. These simulations represent the operation of the plant when following a scheduled power output change established in a day-ahead power market (Montañés et al., 2016). The plant operator will change the power plant load set-point, and the transience will be driven by GT load change. In this study we consider load change from 100% GT load to 85% GT load. The ramp rates are chosen to represent a slow change of 2%/min GT load; a typical load change in NGCC power plant operation is 5%/min GT load reduction (Genrup and Thern, 2013; Jordal et al., 2012), and a more aggressive load change of 10%/min GT load is utilized in modern fast cycling combined cycle power plants (Genrup and Thern, 2013). For this scenario, the PCC unit is operated with control structure A, according to Table 6. The transient gross power output of the gas turbine, steam turbine and combined cycle plant is presented in Fig. 6. Fig. 7 shows the HP and IP pressures at the steam turbine intake during load change. Table 7 shows 100% rise times and 99.9% settling times for GT power output and steam turbine (ST) power output for different GT ramp rates. Rise time is a measure on how fast the response of the process variable to load change is in the short timescales of 10⁰–10¹ min, characteristic of the transient operation of NGCC power plant during load change (Benato et al., 2015). Here, rise time means the time required for the response changing from 0% to 100% of its final value. In addition, the settling time is a good indicator of the long total stabilization time of the process variables, which propagate to the longer timescales, 10¹–10² min, normally observed in

Table 6
Control structures for the PCC plant studied in this work.

| Structure | A | | | B | | | C | | | D | | | E | | |
|-----------|-----------|-----------|-------------|-----------|-----------|-------------|-----------|-----------|-------------|-----------|-----------|-------------|-----------|-----------|---------------------|
| MV | $F_{s,a}$ | $F_{s,b}$ | F_{steam} | $F_{s,a}$ | $F_{s,b}$ | F_{steam} | $F_{s,a}$ | $F_{s,b}$ | F_{steam} | $F_{s,a}$ | $F_{s,b}$ | F_{steam} | $F_{s,a}$ | $F_{s,b}$ | F_{steam} |
| CV | Cap_a | Cap_b | T_{reb} | T_{reb} | T_{reb} | Cap_a | $F_{s,a}$ | $F_{s,b}$ | T_{reb} | L/G_a | L/G_b | T_{reb} | L/G_a | L/G_b | $F_{steam}/F_{s,a}$ |

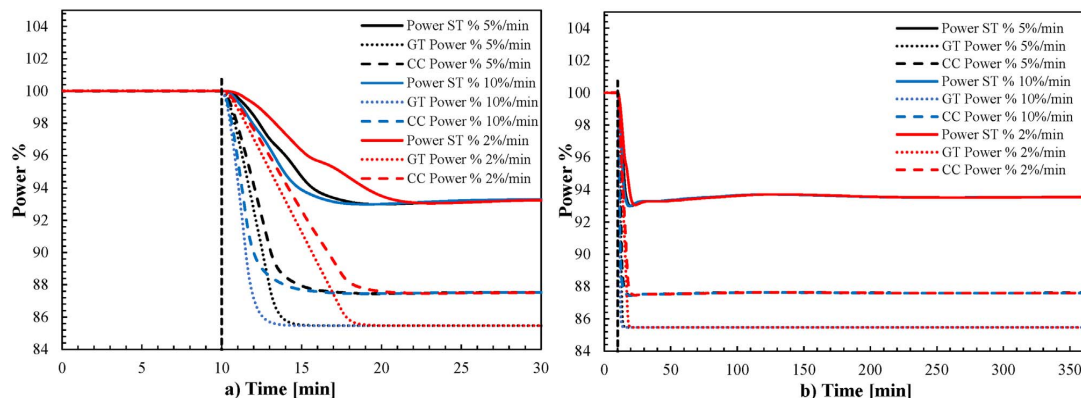


Fig. 6. Scenario 1: Percentage of power output with respect to nominal values for steam turbine (ST), gas turbine (GT) and the total combined cycle (CC). Three scenarios for load change driven by GT load reduction (100% to 85%) at three different ramp rates are: conservative (2%/min), typical for modern NGCCs (5%/min) and modern NGCCs with fast cycling concepts (10%/min). The vertical dotted line shows when the load change begins. Note that the only change in the figure a to b is on the timescale and range (axis-of-abscissas).

PCC process load change transient operation (Flø et al., 2016). Settling times refer to the time required for the response curve to reach and stay within a range of 0.1% of the final value.

Fig. 6a shows that, after a GT load reduction, the ST power output is reduced with a longer rise time, in the range of 4–9 min instead of the 2–8 min of the GT, see Table 7. This shows the effect of the mass and energy storage of the HRSG and other components of the power plant on the transient response of the steam cycle. The faster the GT load change ramp rate, the faster the change in ST and total CC power output of the power plant. In addition, with faster ramp rate, the difference between the GT and ST rise times will be larger. Fig. 6b shows slow oscillations with small amplitude (< 1%) in the ST transient response. Slow here means in the order of 160 min, clearly within the timescales of chemical plant operation. This is explained by the fact that the steam mass flow rate extraction for different GT load ramp rates is presented in Fig. 8e and f. It should be mentioned here that the contribution made by the GT to total CC power output is 74.8% at 100% GT load and 71.9% at 85% GT load. This proportion is larger than for combined cycles without post-combustion capture (around 2/3 GT power at high GT loads), since the steam extraction from the IP/LP turbine represents around 50% of the total steam mass flow rate through the LP turbine. This means that the highest contribution to

Table 7

Rise times and settling times for main power plant and PCC unit process variables.

| Variable | 2%/min | | 5%/min | | 10%/min | |
|------------------------------|------------|---------------|------------|---------------|------------|---------------|
| | Rise time | Settling time | Rise time | Settling time | Rise time | Settling time |
| | 100% [min] | 99.9% [min] | 100% [min] | 99.9% [min] | 100% [min] | 99.9% [min] |
| GT Power | 7.5 | 7.4 | 3 | 2.9 | 1.5 | 1.4 |
| ST Power | 9.9 | 160 | 6.5 | 160 | 3.7 | 160 |
| HP Pressure | 13.2 | 13.2 | 8.9 | 8.9 | 7.6 | 7.6 |
| IP Pressure | 11.0 | 21.2 | 7.7 | 20 | 6.9 | 18 |
| Steam Extraction to reboiler | 73.3 | 301.15 | 73.3 | 301.5 | 70 | 301.5 |
| Product CO ₂ flow | 78.33 | 292.9 | 9.5 | 292.9 | 8.6 | 292.9 |

total power output of the power plant is provided by the GT. Hence, the ST's slower stabilization time loses importance when compared with the total power output of the power plant.

The sliding pressure operation mode of the HRSG is demonstrated in Fig. 7, where it is shown that the ST intake pressures vary over time for different GT load change ramp rates. The transient response of ST intake pressures varies for different GT load ramp rates, there being faster rise time and settling time for faster GT ramp rates. This transient

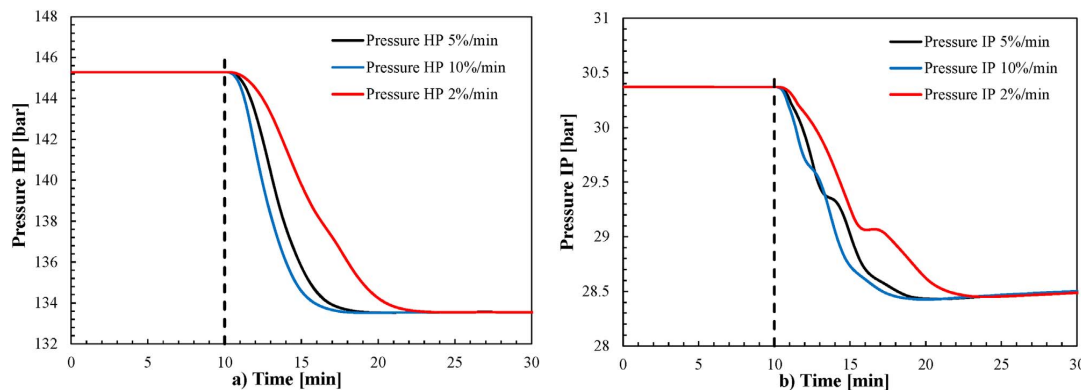


Fig. 7. Scenario 1: HP and IP pressures at steam turbine intakes during load change driven by GT load reduction, for three different ramp rates (2%/min, 5%/min and 10%/min).

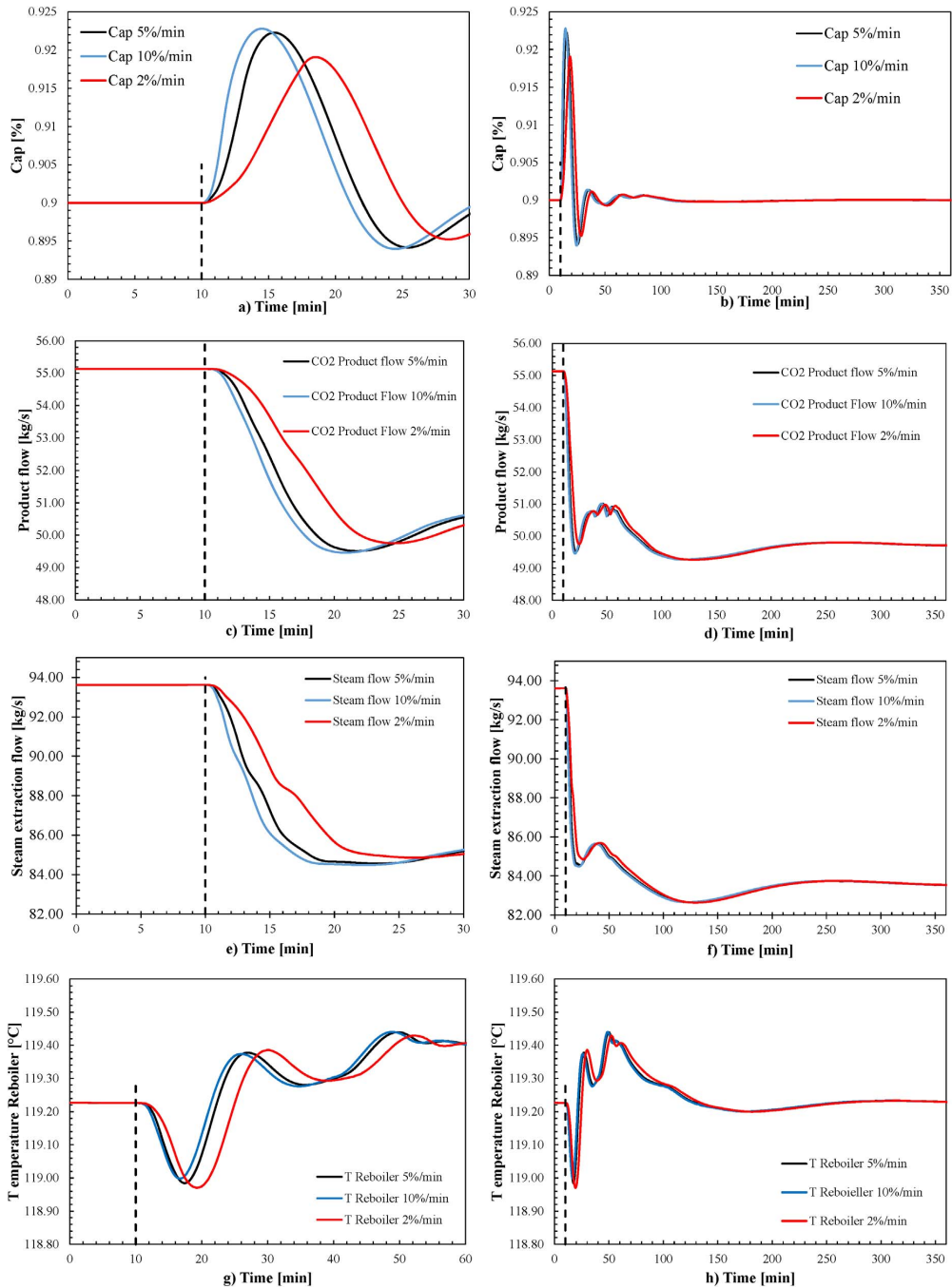


Fig. 8. Scenario 1: Main process variables of the post-combustion capture system during load change driven by GT load reduction for different GT ramp rates. For these simulations, control structure A was implemented, refer to Table 6. Left figures include timescales on thermal power plant operation, while right figures show timescales for interest on post-combustion capture system operation. Note the differences on the timescale and range (axis-of-abscissas).

response can be explained by the HRSG thermal inertia, added mainly by mass and energy storage phenomena in large lumped metal mass walls and fluids within the drum boilers and recuperators. In addition, the rise time and settling time for HP and IP pressures remain within the

timescale for power plant operation; see Table 7. Consequently, for these main process variables in the power plant, it can be said that there is no interaction between the power plant and the PCC unit.

Fig. 8 shows the transient performance of the main process variables

of the PCC unit during the GT driven load change. The CO₂ capture rate measured at the top of the absorbers, as in Eq. (8), is shown in Fig. 8a (short timescale) and Fig. 8b (long timescale). It can be seen that the power plant load change has a strong effect on the PCC unit's load change, mainly through the fast reduction of GT exhaust mass flow rate that propagates towards the HRSG, fan, DCCs and absorber columns. Hence, the GT load change imposes the load change of the PCC unit within the timescales of power plant operation (10⁰–10¹ min). The CO₂ capture rate depend on the ramp rates. The faster the ramp rate, the larger the amplitude of oscillations in the CO₂ capture rate in the short timescales (Fig. 8a), while a similar amplitude of oscillations is found in the longer timescales (Fig. 8b). A similar trend is found in the uncontrolled CO₂ rich product mass flow rate and in the steam extraction mass flow rate; refer to Fig. 8c–f. The reboiler solvent temperature, shown in Fig. 8g–h, is properly controlled within reasonable limits, so no excessive solvent thermal degradation can be expected under transient load change.

$$Cap = \frac{\dot{F}_{abs,in} \cdot X_{in,CO_2} - \dot{F}_{abs,out} \cdot X_{out,CO_2}}{\dot{F}_{abs,in} \cdot X_{in,CO_2}} \quad (8)$$

6.2. Scenario 2: performance of different PCC plant control structures under power plant load change

6.2.1. Case 1: CO₂ capture rate to 90% as a control objective

In this case the CVs, *Cap_a*, *Cap_b* and *T_{reb}*, are to be controlled by means of the remaining degrees of freedom or MVs, those being *F_{s,a}*, *F_{s,b}* and *F_{steam}*. As shown in Table 6, control structure A pairs solvent

circulation flows with capture rates at the top of the absorber and *F_{steam}* with *T_{reb}*, whereas control structure B pairs solvent circulation flow rates with *T_{reb}* and *F_{steam}* with capture rate *Cap*. The transient performance of the power plant integrated with PCC for these two control structures is tested for a typical GT load change with a ramp rate of 5%/min down and up, of the range of 100% GT load to 75% GT load; refer to Figs. 9–11. Rise times and settling times for the transient events are presented in Table 8.

Steam turbine power output is shown in Fig. 9a and b. It can be observed that the five different decentralized control structures show similar responses in terms of steam turbine power output transient performance in the short timescales (10⁰–10¹), with similar rise times. This means that, in the shorter timescale, the response of the power plant is similar from a dynamic perspective for the different control structures. However, steam turbine power output settling times are larger for structures A and B, where *Cap_a* and *Cap_b* are controlled to the set value of 90%. In addition, a slow response in terms of CO₂ product mass flow rate is observed for both control structures A and B.

Total stabilization times for this process variable range from around 3–4 h for structure A and around 7–10 h for structure B. When utilizing control structure A, the CO₂ product mass flow rate rise time remains within the shorter timescales of thermal power plant operation, being faster than for structure B (Fig. 9c–d).

Fig. 10 shows the input usage required to operate the PCC unit during transient load change, i.e. solvent circulation mass flow rates for each of the absorbers and steam circulation flow rate. The stabilization of input usage process variables or MVs is clearly slower when CO₂ capture is an objective for plant operation, structure B being slower; see

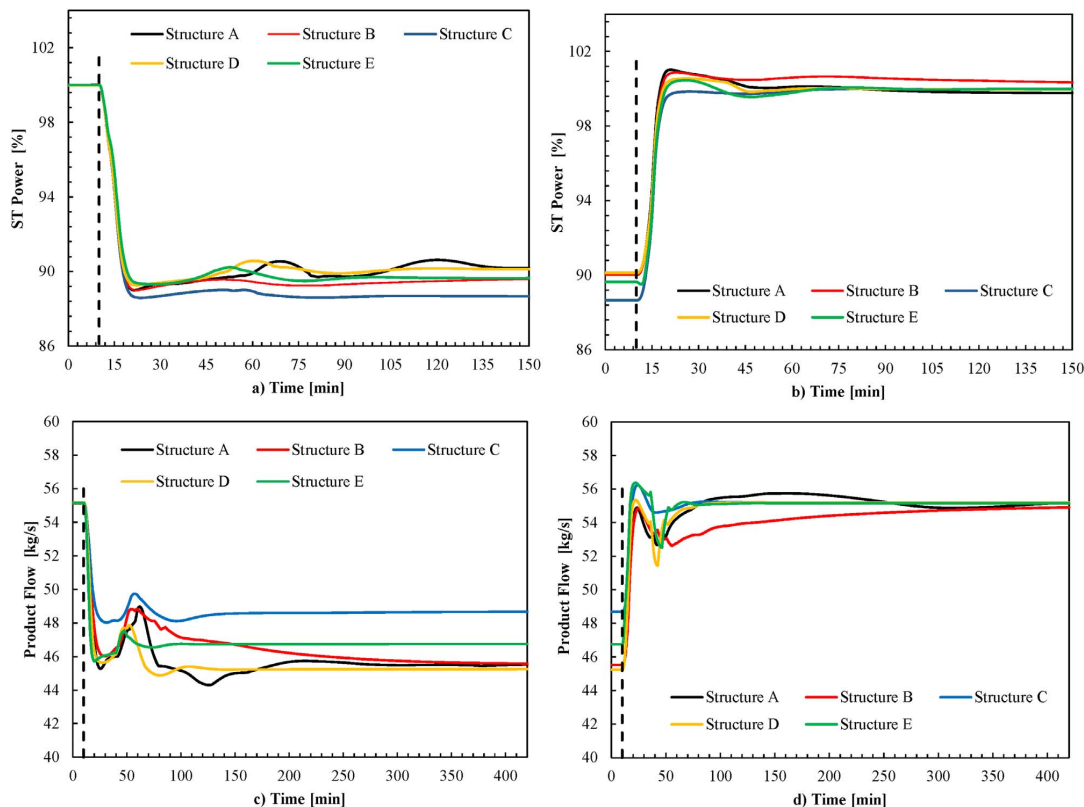


Fig. 9. Scenario 2: Transient response of different control structures to GT load change with 5%/min ramp rate reduction and increase. Steam turbine power output [%] (a) and (b), and CO₂ product flow [kg/s] (c) and (d). Note the difference in timescale in the axis-of-abcissas.

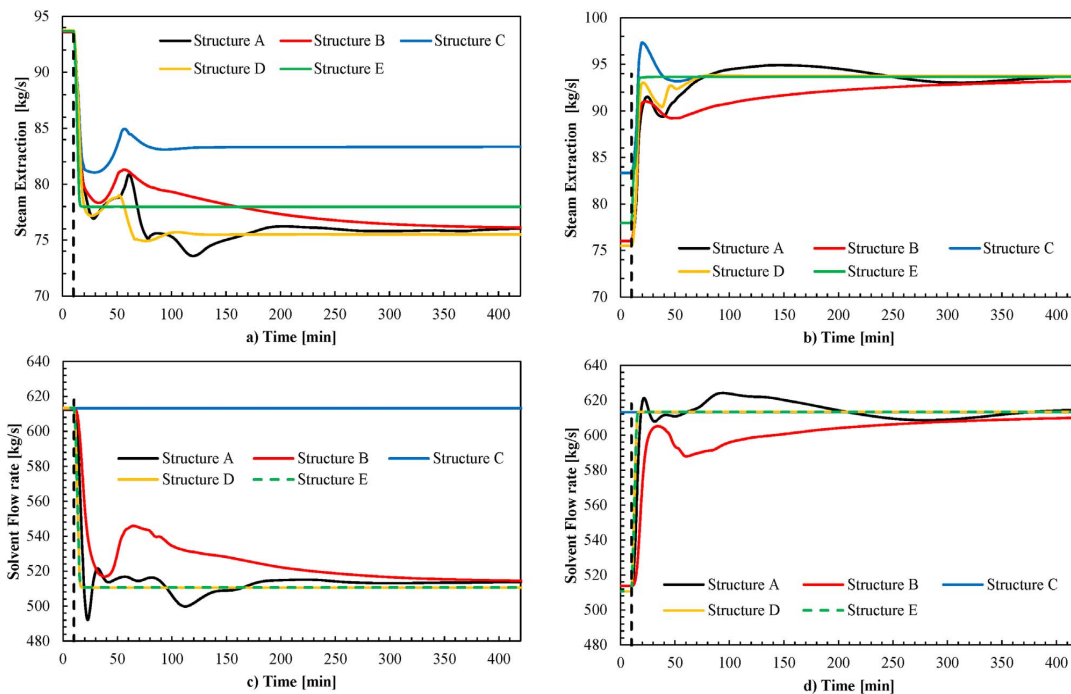


Fig. 10. Scenario 2: Steam turbine extraction flow rate [kg/s] (a) and (b), and solvent flow rate [kg/s] (c) and (d). Transient response of different control structures to a 5%/min ramp rate GT load reduction (a) and (c) and increase (b) and (d).

also Table 8. This might explain the slower response of steam turbine power output due to slower steam extraction mass flow rate stabilization time. In addition, Fig. 11 shows the controlled variables, Cap_a , Cap_b and T_{reb} , for the different control structures. It can be seen how structure A shows superior performance, when comparing the CO_2 capture rate response to a disturbance driven by GT load change, and it can be said that structure A would lead to more efficient operation during transient load change. The faster response of the main plant process variables to GT load change when implementing control structure A can be explained by that structure A has faster closed feedback control loops. This means that the paired MVs and CVs are physically closer, which results in tight control when compared with control structure B. It can be observed in Fig. 10 that the manipulated variables, $F_{s,a}$, $F_{s,b}$ and F_{steam} , reach faster stabilization for control structure A than for control structure B; also refer to rise times and settling times for steam extraction mass flow rate presented in Table 8.

6.2.2. Case 2: CO_2 capture rate to 90% is not a control objective

In this case the CVs, Cap_a and Cap_b , at the top of the absorbers are not a control objective, leading the remaining degrees of freedom or MVs for control of another process variable.

Studies consisting of the plant’s open-loop response to step changes in solvent circulation rate have shown that the main process variables of the PCC plant have long stabilization times, mainly due to the large residence times in components that contain large inventories of solvent and long dead times within piping and process hold-ups (Flø et al., 2016). In addition, the dynamic interaction between the absorber and reboiler operation might lead to large total stabilization times. Hence, slow stabilization of the plant are expected when the liquid solvent flow network is disturbed. This can explain why the utilization of the solvent circulation rate, as a MV to regulate a control variable in feedforward (ratio) or closed-loop feedback control, might lead to large total stabilization times of the PCC unit’s main process variables. Therefore, it can

be reasonable to believe that leaving the MVs’ solvent circulation rates at the top of the absorber in flow control mode might lead to a faster plant (keeping circulation flow rate constant as in Fig. 9 c) and with control structure C). However, even if the plant stabilizes relatively quickly when keeping the solvent flow network unaltered, the plant is operated in a less efficient manner under off-design loads. This is shown in Figs. 9–11, where it can be seen that, for the steady-state off-design conditions of 75% GT load, lower steam turbine power output is obtained, in addition to larger steam extraction mass flow rate (and reboiler duty) and therefore large CO_2 capture rate of around 97%. It must be said that, for structure C, it is not possible to keep the reboiler temperature at set-point, since the steam valve stem saturates and no further steam can be sent to the reboiler at the part-load operation point of 75% GT load. At part load operating conditions, less steam was available for the extraction from the ST. In addition, a large solvent circulation flow rate (large L/G ratio) was obtained when solvent circulation $F_{s,a}$ and $F_{s,b}$ were kept constant. That lead to relatively larger steam extraction and reboiler duty required for operation of the process, as observed in control structure C, refer to Fig. 10. In addition, control structure E showed faster stabilization response to the disturbance than control structures A and B, see Table 8. However, control structure E lead to relatively larger L/G ratio in the absorber columns when compared to A, B and D, and therefore a sub-optimal operation of the process with a larger steam extraction required and resulting capture rate.

Structure D utilizes solvent flow rates on L/G ratio control mode (feedforward). The mass based L/G ratio in the absorber columns is kept constant at off-design loads by using the lean solvent flow rates’ MVs. This results in the fast change and stabilization of solvent circulation rate, as shown in Fig. 10, that follows the exhaust gas mass flow rate reduction of the GT. In addition, this also leads to faster stabilization of steam extraction F_{steam} than for control structures A and B; refer to rise times and settling times in Table 8. By looking at the steady-

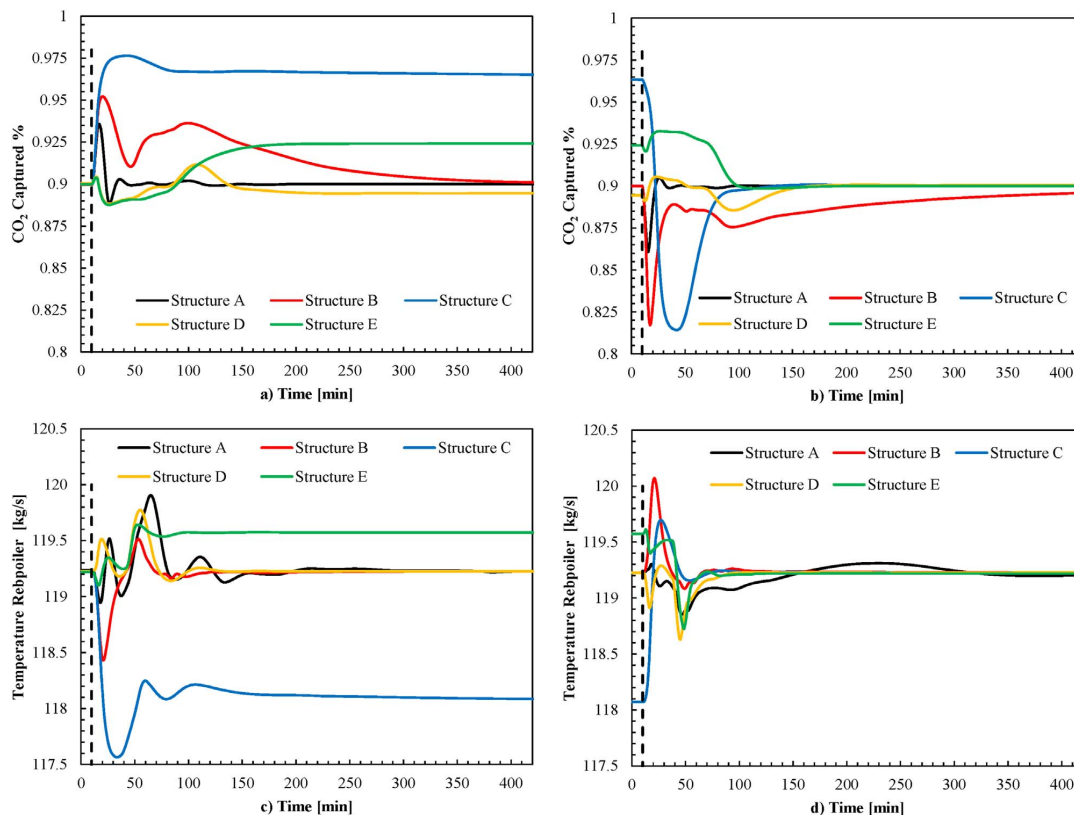


Fig. 11. Scenario 2: CO₂ capture rate [%] (a) and (b), and solvent temperature in reboiler [°C] (c) and (d). Transient response of different control structures to a 5%/min ramp rate GT load reduction (a) and (c) and increase (b) and (d).

state off-design performance of the PCC unit when operated with GT load of 75%, it can be seen that the CO₂ capture rate is kept almost constant when the L/G ratio is kept constant. In steady-state terms, the plant's main process variables have a similar steady-state value but significantly faster stabilization of CO₂ product flow rate and steam extraction flow rate; however, the CO₂ capture rate is slower than when compared with CO₂ capture controlled as in structure A. Therefore, the L/G ratio control, as in structure D, can be considered as a good option if relatively fast stabilization times in CO₂ product flow rate and steam turbine power output are required simultaneously, while keeping the CO₂ capture rate close to 90% at part-load operation.

Control structure E uses feedforward ratio control for both steam mass flow rate and solvent circulation mass flow rate, by keeping constant the mass based L/G ratio in the absorber and the ratio of steam extraction mass flow rate to solvent circulation mass flow rate at the inlet of the absorbers; see Table 6. Fig. 10 shows that the MVs quickly follow the change in exhaust gas mass flow rate imposed by GT load change. CO₂ product mass flow rate and steam turbine power output have similar settling times and transient trajectories for structures D and E. However, structure D leads to a more efficient steady-state part-load operation, since structure E results in higher steam extraction flow rate – and hence more CO₂ being stripped from the solvent – and a larger CO₂ product flow rate. It seems that control structure D results in better performance than structure E under transient load change.

It should be mentioned that there is a significant difference between the trajectories, rise times and settling times of most process variables for a given control structure when ramping down (100% GT load to

75% GT load) and when ramping up (75% GT load to 100% GT load). This highlights the fact that the dynamic process system is highly non-linear.

7. Conclusions

Understanding the dynamic interaction between the NGCC power plant and the PCC unit remains a key aspect when developing the NGCC with PCC technology. This work simulates real-like operation of a 3PRH natural gas combined cycle power plant with post combustion capture during load change transient event with closed-loop controllers. In addition, this work includes detailed dynamic process models of the power plant to the same level of detail as in the chemical absorption and desorption plant.

The performance of the integrated NGCC power plant with PCC for different GT load change ramp rates was demonstrated and assessed via dynamic process model simulations. When the steam extraction mass flow rate is regulated by a throttle valve, which is used as a MV to control a CV of the PCC unit, dynamic interaction is found between the power plant and the PCC unit in the longer timescales, 10¹–10² min. Slow oscillations with relatively small amplitude are found in the power production from the steam turbine. These oscillations in the long timescales are within (< 1%) of total ST power output. In addition, the GT load change imposes the load change of the PCC unit within the timescales of power plant transient operation of 10⁰–10¹ min, due to the fast reduction of exhaust mass flow rate from the GT during load change. Faster GT ramp rates cause faster rise times in the power plant process variables. For different GT ramp rates, different trajectories of

Table 8

Rise times and settling times for different process variables with different control structures of the integrated power plant with PCC for GT load change at 5%/min ramp rate. GT load decrease from 100% to 75% and GT load increase from 75% to 100%. Times in min.

| Variable | | ST Power | CO ₂ capture rate | Steam Extraction to reboiler | Product CO ₂ flow |
|---------------------------|------|----------|------------------------------|------------------------------|------------------------------|
| Structure A | | | | | |
| Rise time 100% [min] | Down | 7.9 | | 63.4 | 12.9 |
| | Up | 7.7 | | 67.26 | 72.1 |
| Settling time 99.9% [min] | Down | 164.7 | | 484.7 | 175.6 |
| | Up | 321.5 | | 530.7 | 242.9 |
| Structure B | | | | | |
| Rise time 100% [min] | Down | 8 | | 148.3 | 412.5 |
| | Up | 8.1 | | 658 | 658.1 |
| Settling time 99.9% [min] | Down | 278 | | 435.9 | 412.5 |
| | Up | 356 | | 658 | 658.1 |
| Structure C | | | | | |
| Rise time 100% [min] | Down | 11.3 | 9.3 | 6.8 | 12.1 |
| | Up | 19 | 12.3 | 6.3 | 9.3 |
| Settling time 99.9% [min] | Down | 54.7 | 381.8 | 11.5 | 317.2 |
| | Up | 50.4 | 114.3 | 81.3 | 61.4 |
| Structure D | | | | | |
| Rise time 100% [min] | Down | 8.1 | 8.4 | 53.9 | 120.3 |
| | Up | 8.6 | 7.2 | 65.3 | 104.4 |
| Settling time 99.9% [min] | Down | 61.4 | 45 | 108.4 | 251.7 |
| | Up | 40.1 | 153.3 | 65.3 | 79.2 |
| Structure E | | | | | |
| Rise time 100% [min] | Down | 10.1 | 274.1 | 9.4 | 6.7 |
| | Up | 9.23 | 89.55 | 11.51 | 27.4 |
| Settling time 99.9% [min] | Down | 55.3 | 274.1 | 9.4 | 48 |
| | Up | 53.4 | 89.55 | 9.4 | 92.05 |

the main process variables of the PCC unit are found within the time-scales of power plant transient operation. Nevertheless, within the longer timescales of 10^1 – 10^2 , the transient performance of the PCC unit is similar for different GT ramp rates. Based on these simulations, it can be concluded that the addition of the PCC unit to the NGCC plant should not impose any constraint on, or problem for, stable power plant operation under scheduled load changes, nevertheless inefficient transient operation of the PCC unit can be expected in the long timescales.

The transient performance of five different decentralized PCC plant control structures under power plant load change was assessed. It is observed that the control structures display similar performance in terms of steam turbine power output in the short timescales (10^0 – 10^1), with similar rise times, while, in the longer timescales, the steam turbine power output differs for different control structures. This means that, within shorter timescales, the response of the power plant is similar from a dynamic perspective for the different control structures. When controlling the CO₂ capture rate, the power plant performs in a more efficient manner at steady-state off-design loads; however, the time-dependent response of the PCC plant is slower, leading to long stabilization times in the main process variables. The control structure where L/G ratio is kept constant and reboiler temperature is controlled by the steam throttle valve, has shown similar part-load off-design performance as that found in control structures with constant capture rate as CVs. In addition, this control structure results in relatively fast total stabilization time of the steam turbine power output and CO₂ product flow rate. It is recommended to apply control structure D, with L/G ratio control, if controlling CO₂ capture rate is not an operational constraint.

Acknowledgements

This work has been financially supported by the Department of Energy and Process Engineering at the NTNU – Norwegian University of Science and Technology. The authors also acknowledge the Chalmers Energy Initiative, the Swedish Energy Agency and Landsvirkjun Energy Research Fund for funding parts of this project.

References

- Åström, K.J., Bell, R.D., 2000. Drum-boiler dynamics. *Automatica* 36, 363–378.
- A.T. Inc., Aspen Plus V8.6. (2014).
- Adams, T., Mac Dowell, N., 2016. Off-design point modelling of a 420 MW CCGT power plant integrated with an amine-based post-combustion CO₂ capture and compression process. *Appl. Energy* 178, 681–702.
- Amrollahi, Z., Ertesvåg, I.S., Bolland, O., 2011. Optimized process configurations of post-combustion CO₂ capture for natural-gas-fired power plant—exergy analysis. *Int. J. Greenh. Gas Control* 5, 1393–1405.
- Aske, E.M.B., Skogestad, S., 2009. Consistent inventory control. *Ind. Eng. Chem. Res.* 48, 10892–10902.
- Basu, S., Debnath, A.K., 2015. Chapter VIII – boiler control system. *Power Plant Instrumentation and Control Handbook*. Academic Press, Boston, pp. 585–694.
- Benato, A., Stoppato, A., Mirandola, A., 2015. Dynamic behaviour analysis of a three pressure level heat recovery steam generator during transient operation. *Energy* 90 (Part 2), 1595–1605.
- Biyouki, Z.A., 2014. Thermodynamic Analysis of CO₂ Capture Processes for Power Plants. Energy and Process Engineering, Norwegian University of Science and Technology.
- Bolland, O., 2014. Compendium – Thermal Power Generation.
- Boot-Handford, M.E., Abanades, J.C., Anthony, E.J., Blunt, M.J., Brandani, S., Mac Dowell, N., Fernandez, J.R., Ferrari, M.-C., Gross, R., Hallett, J.P., Haszeldine, R.S., Heptonstall, P., Lyngfelt, A., Makuch, Z., Mangano, E., Porter, R.T.J., Pourkashanian, M., Rochelle, G.T., Shah, N., Yao, J.G., Fennell, P.S., 2014. Carbon capture and storage update. *Energy Environ. Sci.* 7, 130–189.
- Brouwer, A.S., van den Broek, M., Seebregts, A., Faaij, A., 2015. Operational flexibility and economics of power plants in future low-carbon power systems. *Appl. Energy* 156, 107–128.
- Bui, M., Gunawan, I., Verheyen, V., Feron, P., Meuleman, E., Adeloju, S., 2014. Dynamic modelling and optimisation of flexible operation in post-combustion CO₂ capture plants—a review. *Comput. Chem. Eng.* 61, 245–265.
- Bui, M., Gunawan, I., Verheyen, V., Feron, P., Meuleman, E., 2016. Flexible operation of CSIRO's post-combustion CO₂ capture pilot plant at the AGL Loy Yang power station. *Int. J. Greenh. Gas Control* 48, 188–203.
- CO₂ Technology Center Mongstad.
- Can Gülen, S., Kim, K., 2013. Gas turbine combined cycle dynamic simulation: a physics based simple approach. *J. Eng. Gas Turbines Power* 136 011601–011601.
- Ceccarelli, N., van Leeuwen, M., Wolf, T., van Leeuwen, P., van der Vaart, R., Maas, W., Ramos, A., 2014. Flexibility of low-CO₂ gas power plants: integration of the CO₂ capture unit with CCGT operation. *Energy Procedia* 63, 1703–1726.
- Chinen, A.S., Morgan, J.C., Omell, B.P., Bhattacharyya, D., Miller, D.C., 2016. Dynamic data reconciliation and model validation of a MEA-based CO₂ capture system using pilot plant data. 11th IFAC Symposium on Dynamics and Control of Process Systems, Including Biosystems.
- Dassault Systems, Dymola, <http://www.3ds.com/products-services/catia/products/dymola>.
- Dechamps, P.J., 1994. Modeling the transient behaviour of combined cycle plants. *ASME Paper* 94-GT-238.
- Dechamps, P.J., 1995. Modelling the transient behaviour of heat recovery steam generators, proceedings of the institution of mechanical engineers, part a. *J. Power Energy* 209, 265–273.
- Dixon, T., Herzog, H., Twinning, S., Ceccarelli, N., van Leeuwen, T., van Leeuwen, P., van der Vaart, R., Maas, W., Ramos, A., 2014. 12th international conference on greenhouse gas control technologies, GHGT-12 Flexibility of low-CO₂ gas power plants: integration of the CO₂ capture unit with CCGT operation. *Energy Procedia* 63, 1703–1726.
- Dutta, R., Nord, L.O., Bolland, O., 2017. Selection and design of post-combustion CO₂ capture process for 600 MW natural gas fueled thermal power plant based on operability. *Energy* 121, 643–656.
- Eborn, J., 2001. On model libraries for thermo-hydraulic applications. Department of Automatic Control, Lund Institute of Technology (LTH), Lund.
- Faber, R., Köpcke, M., Biede, O., Knudsen, J.N., Andersen, J., 2011. Open-loop step responses for the MEA post-combustion capture process: experimental results from the Esbjerg pilot plant. *Energy Procedia* 4, 1427–1434.
- Flo, N.E., Kvamsdal, H.M., Hillestad, M., Mejdell, T., 2016. Dominating dynamics of the post-combustion CO₂ absorption process. *Comput. Chem. Eng.* 86, 171–183.
- Flo, N.E., 2015. Post-Combustion Absorption-Based CO₂ Capture: Modeling, Validation and Analysis of Process Dynamics. Chemical Engineering Department, Norwegian University of Science and Technology, Trondheim.
- Francesco Casella, A.L., 2003. Modelica open library for power plant simulation: design and experimental validation. In: Fritzon, P. (Ed.), 3rd International Modelica Conference, Modelica Association. Linköping (Sweden), pp. 41–50.
- G.V.-G.V.u., 1997. Chemieingenieur-wesen, VDI-Wärmeatlas (VDI-Buch) (German Edition), 9th edition.
- GarDarsdóttir, S.Ó., Normann, F., Andersson, K., Pröhl, K., Emilsdóttir, S., Johnsson, F.,

2015. Post-combustion CO₂ capture applied to a state-of-the-art coal-fired power plant—the influence of dynamic process conditions. *Int. J. Greenh. Gas Control* 33, 51–62.
- M. Genrup, M. Thern, Ny gasturbinteknik 2012–2014: Gas Turbine Developments. Report 2012., in, ELFORSK, March 2013.
- He, Z., Ricardez-Sandoval, L.A., 2016. Dynamic modelling of a commercial-scale CO₂ capture plant integrated with a natural gas combined cycle (NGCC) power plant. *Int. J. Greenh. Gas Control* 55, 23–35.
- IEA, 2008. CO₂ capture and storage: a key carbon abatement option. Energy Technology Analysis. International Energy Agency.
- IEA, 2011. Harnessing Variable Renewables: A Guide to the Balancing Challenge. International Energy Agency.
- IEA, 2015. World Energy Outlook. OECD Publishing.
- IEA, 2016. World Energy Investment.
- IEAGHG, 2012. Operating Flexibility of Power Plants with CCS. IEAGHG June.
- IEAGHG, Evaluation of process control strategies for normal, flexible, and upset operation conditions of CO₂ post combustion capture processes. 2016/07, in, IEAGHG, September 2016.
- IPCC, Climate Change, 2013. The Physical Science Basis. Contribution of Working Group I to the Fifth Assessment Report of the Intergovernmental Panel on Climate Change. Cambridge University Press, Cambridge, United Kingdom and New York, NY, USA.
- IPCC, Climate Change, 2014. Synthesis Report. Contribution of Working Groups I, II and III to the Fifth Assessment Report of the Intergovernmental Panel on Climate Change. IPCC, Geneva, Switzerland 151 pp.
- Jilvero, H., Mathisen, A., Eldrup, N.-H., Normann, F., Johnsson, F., Müller, G.I., Melaan, M.C., 2014. Techno-economic analysis of carbon capture at an aluminum production plant – comparison of post-combustion capture using MEA and ammonia. *Energy Procedia* 63, 6590–6601.
- Johnsson, F., Odenberger, M., Göransson, L., 2014. Challenges to integrate CCS into low carbon electricity markets. *Energy Procedia* 63, 7485–7493.
- Jonshagen, K., Sipócz, N., Genrup, M., 2010. A novel approach of retrofitting a combined cycle with post combustion CO₂ capture. *J. Eng. Gas Turbines Power* 133 011703–011703.
- Jonshagen, K., 2011. Modern thermal power plants. Aspects of modeling and evaluation. Division of Thermal Power Engineering. Department of Energy Science, Lund University, Lund.
- Jordal, K., Ystad, P.A.M., Anantharaman, R., Chikukwa, A., Bolland, O., 2012. Design-point and part-load considerations for natural gas combined cycle plants with post combustion capture. *Int. J. Greenh. Gas Control* 11, 271–282.
- Kehlhofer, R., Rukes, B., Hannemann, F., Stirnimann, F., 2009. Combined-Cycle Gas and Steam Turbine Power Plants, 3rd edition. PennWell.
- Linnenberg, S., Liebenhal, U., Oexmann, J., Kather, A., 2011. Derivation of power loss factors to evaluate the impact of postcombustion CO₂ capture processes on steam power plant performance. *Energy Procedia* 4, 1385–1394.
- Lucquiaud, M., Chalmers, H., Gibbins, J., 2009. Capture-ready supercritical coal-fired power plants and flexible post-combustion CO₂ capture. *Energy Procedia* 1, 1411–1418.
- Möller, B.F., Genrup, M., Assadi, M., 2007. On the off-design of a natural gas-fired combined cycle with CO₂ capture. *Energy* 32, 353–359.
- Mechleri, E., Lawal, A., Ramos, A., Davison, J., Dowell, N.M., 2017. Process control strategies for flexible operation of post-combustion CO₂ capture plants. *Int. J. Greenh. Gas Control* 57, 14–25.
- Modelica Association, <https://www.modelica.org/>.
- Modelon, Post-combustion capture with amine solutions. <http://www.modelon.com/industries/energy-process/carbon-capture-and-sequestration/>.
- Modeloon, 2015. ThermalPower Library.
- Montañés, R.M., Korpás, M., Nord, L.O., Jaehnert, S., 2016. Identifying operational requirements for flexible CCS power plant in future energy systems. *Energy Procedia* 86, 22–31.
- Montañés, R.M., Flo, N.E., Dutta, R., Nord, L.O., Bolland, O., 2017. Dynamic process model development and validation with transient plant data collected from an MEA test campaign at CO₂ Technology Center Mongstad. *Energy Procedia* in press.
- Nittaya, T., Douglas, P.L., Croiset, E., Ricardez-Sandoval, L.A., 2014. Dynamic modelling and control of MEA absorption processes for CO₂ capture from power plants. *Fluid* 116, 672–691.
- Panahi, M., Skogestad, S., 2011. Economically efficient operation of CO₂ capturing process part I: self-optimizing procedure for selecting the best controlled variables. *Chem. Eng. Process. Process Intensif.* 50, 247–253.
- Panahi, M., Skogestad, S., 2012. Economically efficient operation of CO₂ capturing process. Part II. Design of control layer. *Chem. Eng. Process. Process Intensif.* 52, 112–124.
- Pröls, K., Tummescheit, H., Velut, S., Åkesson, J., 2011. Dynamic model of a post-combustion absorption unit for use in a non-linear model predictive control scheme. *Energy Procedia* 4, 2620–2627.
- Rezazadeh, F., Gale, W.F., Hughes, K.J., Pourkashanian, M., 2015. Performance viability of a natural gas fired combined cycle power plant integrated with post-combustion CO₂ capture at part-load and temporary non-capture operations. *Int. J. Greenh. Gas Control* 39, 397–406.
- Rowen, W.I., 1983. Simplified mathematical representations of heavy-duty gas turbines. *J. Eng. Power* 105, 865–869.
- Skogestad, S., Grimholt, C., 2012. The SIMC method for smooth PID controller tuning. In: Vilanova, R., Visioli, A. (Eds.), *PID Control in the Third Millennium: Lessons Learned and New Approaches*. Springer, London, London, pp. 147–175.
- Skogestad, S., Postlethwaite, I., 2005. *Multivariable Feedback Control: Analysis and Design*. John Wiley & Sons.
- Thermoflow, 2014. GT Pro 24.0. Thermoflow Inc.
- Thern, M., Jordal, K., Genrup, M., 2014. Temporary CO₂ capture shut down: implications on low pressure steam turbine design and efficiency. *Energy Procedia* 51, 14–23.
- Wagner, W., Cooper, J.R., Dittmann, A., Kijima, J., Kretschmar, H.J., Kruse, A., Mareš, R., Oguchi, K., Sato, H., Stöcker, I., Šifner, O., Takaishi, Y., Tanishita, I., Trübenbach, J., Willkommen, T., 2000. The IAPWS industrial formulation 1997 for the thermodynamic properties of water and steam. *J. Eng. Gas Turbines Power* 122, 150–184.
- Walters, M.S., Edgar, T.F., Rochelle, G.T., 2016. Regulatory control of amine scrubbing for CO₂ capture from power plants. *Ind. Eng. Chem. Res.* 55, 4646–4657.
- World, G.T., 2016. Performance specs. *Gas Turbine World*, 32nd edition. Pequot Publishing Inc., Fairfield, USA pp. 48.